UNIVERSITY OF CAPE TOWN

Development of the Small Punch Test Platform to Evaluate the Embrittlement of Power Plant Materials

Masters of Science: Materials Engineering

Student name	**Lavhelesani Oliet Tshamano**
Student number	**TSHLAV001**
Supervisor(s)	**Prof Bernhard Sonderegger & Prof Rob Knutsen**
Co-Supervisor	**Dr T Becker**
Address	**32 Charing Crescent Road Parklands North, 7441**
Contacts	**Cell: 076 149 5538 Telephone: 021 522 2255 (Work) Email: oliet.tshamano@eskom.co.za**

8/21/2017

Declaration

I declare that this thesis is my own, unaided work. It is being submitted for the Degree of Master of Science in the University of Cape Town. I have not copied the whole or any part from any source whatsoever, and where I have copied, verbatim or otherwise, I have acknowledged the source so utilised. I further understand that if I am suspected of plagiarism or any other form of cheating, disciplinary proceedings will be instituted against me. This in turn may result in me being expelled from this institution. This work has not been previously submitted for any degree or examination in any other university.

Signed by candidate

Signature Removed

(Signature of student)

17 _____day of _____20_____

ABSTRACT

Life assessment of critical components and piping is performed in the electrical power plants in order to prevent structural/component failure and prolong safe operation of the equipment. In the event that these components fail, the consequences can be very costly since this may result in power supply disruptions, component replacements, environmental damages and the loss of human life. Regulations, standards and codes are designed to ensure the safe operation of the power plants. However, on their own, they are not adequate to account for aging power plants that have been in service for more than half of their originally designed lifespans, since failures have been experienced due to in-service aging mechanisms (i.e. temper embrittlement, creep, etc.) and poor engineering and maintenance practises.

Mechanical, metallurgical and non-destructive techniques are used to evaluate the condition of the in-service materials in order to aid in these life assessments. The structural integrity assessments utilise material toughness properties as determined through fracture toughness testing, which requires a significant quantity of material, and is therefore cumbersome and expensive. Consequently, several other material property testing techniques are used to aid in structural integrity assessments, such as impact energy, tensile and hardness testing. Through empirical correlations, these test results are used to estimate fracture toughness properties and, consequently, the error bands are expected to be as high as 50%. Due to its small size, the small punch test (SPT) technique can be regarded as a quasi-non-destructive test, and is therefore a preferred method for determining the fracture toughness in aid of structural assessment. The SPT technique involves a compression load from the punch to a sample (ϕ8mm x 0.5mm thick) clamped between clamping and receiving dies.

This study aims to develop a test rig that will be used to perform the SPT in order to quantify the level of embrittlement on the ex-service, low-pressure steam turbine material (NiCrMoV steel). The data results acquired from the SPT technique are the reaction load of the punch and the deformed displacement of the sample performed at a constant displacement rate according to CWA 15627:2007. Two SPT rigs were designed, manufactured and commissioned. These two were commissioned using FEM and tensile test results for validations. The steel was subjected to three different conditions: as received (AR), de-embrittled (DE) and hardened (HD). The three types of steel illustrated that the SPT can quantify embrittlement levels through the correlation of tensile, Charpy impact energy and fracture toughness testing.

ACKNOWLEDGEMENTS

I would like to thank my employer and sponsor Eskom (EPPEI) for affording me the time to study and further my career development. I would also like to thank my family and friends for their patience and understanding towards my studies and my academic mentors, Professor Robert Knutsen from the University of Cape Town (UCT) and Professor Bernhard Sonderegger from Graz University of Technology. My special thanks goes to the UCT technical staff (mechanical workshop staff and electrical staff); Dr Thorsten Becker from the University of Stellenbosch for his advice, thesis review and guidance on fracture mechanics and finite element modelling (FEM); industrial mentors Phillip Doubell, Kobus Smit and Jacques Calitz for discussion, guidance and advice on the mechanical testing techniques; Hellmut Bowles from FEAS for FEM advice; Victor Balden for advanced FEM guidance and advice; Alex Becker for assisting with fracture toughness testing and the Centre of Materials Engineering (CME) technical and administration staff and fellow students.

TABLE OF CONTENTS

LIST OF FIGURES

LIST OF TABLES

LIST OF EQUATIONS

NOMENCLATURE

Δa	Crack length
ε_f	Fracture strain
AR	As-received: identification for a material sample that was not heat treated
CVN	Charpy V-Notch
D	Power law hardening constant for Ramberg-Osgood model
DBTT	Ductile to brittle transition temperature
DE	De-embrittled: identification for a material sample that was heat treated to remove temper embrittlement
ε	Strain
E	Young's modulus
FATT	Fracture appearance transition temperature
FEA	Finite element analysis
FEM	Finite element model
HD	Hardened: identification for a material sample that was heat treated to introduce damage in the material
HRC	Rockwell C hardness
HV	Vickers hardness
J_{IC}	Plane stress fracture toughness (ductile fracture toughness test)
K_{IC}	Plane strain fracture toughness (brittle fracture toughness test)
kJ or J	kilo Joules or Joules
kN or N	kilo Newton or Newton
LDC	Load displacement curve
LDC_{EXP}	Experimental load displacement curve
LDC_{FEM}	Modelled load displacement curve

LSE	Lower shelf energy
MPa or Pa	Mega Pascal or Pascal
n	Strength coefficient and exponent for Ramberg-Osgood model
NDT/E	Non-destructive testing/examination
NiCrMoV	Low alloy steel used mostly for turbine material with main alloy of Nickel, Chromium, Molybdenum and Vanadium
OEM	Operating equipment manufacturer
SPT	Small punch test
QADP	Quality Assurance Data Package
Quasi-NDT	Refers to SPT sampling process to power plant components that the technique is almost non-destructive if applied correctly
σ_y	Yield strength
TEM	Transmission electron microscopy
T_{SP}	Small punch transition temperature
USE	Upper shelf energy
UTS	Ultimate tensile strength
W_{CT}	Strain energy density for compact tension specimen
W_{SP}	Strain energy density for small punch test specimen

CHAPTER 1: INTRODUCTION

1.1 Background

Protecting the structural integrity of critical components from catastrophic failures due to fracture is very important in the power plant industry, especially with regards to fracture in the primary systems of nuclear power plants where the consequences can affect public health and employees, plant and economic safety. Codes, standards and regulations have been developed to ensure that the plants are operated and maintained within safety margins; however, these safety tools do not guarantee a fracture-free environment within power plants. Fracture is the separation of a body into two or more pieces caused by stresses and/or temperature, and can be referred to as ductile fracture (creep) or brittle fracture (embrittlement). This study will investigate the brittle fracture behaviour, which is known as embrittlement, using a small punch test (SPT) technique.

The risk of catastrophic failure of an operating component or system in a power plant is related to the tolerable size of a flaw or defect, which is directly and quantitatively proportional to the material fracture toughness, KIC or JIC [1]. The parameter, KIC or JIC is used to estimate the remaining life of power plant components. Conventional mechanical tests are required to determine fracture toughness. However, it is impractical to obtain the large material specimens required from the in-service components at a location that has been identified as at risk of failure. The influence of weld repair on performance of components or materials that were possibly damaged during sampling, as well as the challenges of plant configuration that limit accessibility, can result in costly time delays [2].

Established in South Africa in 1923, Eskom is the only utility and largest electric power producer in Africa. Eskom supplies a total of just over 45% of Africa's electricity and 95% of South Africa's electricity [3]. South Africa is a newly reformed developing country that has a population of approximately 55 million people. According to the Southern Africa power pool [4] (2013), Eskom has installed a capacity 44,170 MW, with an available net output of 41,074 MW and a forecasted demand of 42,416 MW. There was a 3% shortfall of power demand, which resulted in power plants being operated at a higher capacity than normal. This practice causes unplanned and unavoidable maintenance on failing components. Life management of critical components is increasing and more advanced and cost-effective technologies are required because of the aged power plants that are beyond their design-life.

The SPT technique is the testing method preferred by most utilities that are using it as a life assessment technique, as compared to standard mechanical test technique(s), because of the small specimens required to perform the test. The SPT can supply direct fracture toughness measurements to aid Eskom's existing life management techniques, which are aligned to world best techniques. The SPT is fairly easy to perform but requires significant attention in its data analysis as there can be a marked scatter within the data. In addition, techniques such as numerical models, finite element modelling (FEM) and empirical correlation are necessary. The technique is cost effective and can reduce and/or avoid unplanned shutdowns in cases where specimens can be extracted without shutting down a component or system.

Embrittlement is defined by EPRI [2] as "phenomena whereby materials suffer a marked decrease in the ability to deform (loss of ductility) and the ability to absorb energy during fracture (loss of toughness), with the little change in other mechanical properties, such as strength and hardness."

It can be evaluated by using either mechanical testing techniques (tensile, Charpy V-notch, compact tension and hardness testing, etc.) and/or metallurgical techniques (optical metallography: grain size measurement, assessment of phosphorus segregation, phase identification; electron microscopy: scanning electron microscopy for fractographic examination; and auger electron microscopy for composition analysis). Critical components such as turbine material are susceptible to temper embrittlement, which occurs during the service life or slow cooling following heat treatment during the manufacturing of large components such as low pressure steam turbine rotors [2], [5].

Temper embrittlement is a major cause of degradation of fracture toughness especially in ferritic steel, while neutron irradiation embrittlement affects the reactor core pressure vessel [2], [6], [7]. Ensuring the integrity of these critical components is very costly and planned shutdowns or outages are used to assess these components. Charpy transition temperature, also referred to as ductile to brittle transition temperature (DBTT) or fracture appearance transition temperature, is also used to assess embrittlement mostly on low alloy steels [5]. The transition is known to occur at 50% of upper shelf energy (USE) and lower shelf energy (LSE) and it is expected that power plant steels will experience a reduction in impact energy, which will result in a decrease of fracture toughness when the steel is embrittled [2].

In nuclear power plants, the level of embrittlement caused by radiation damage to pressure vessels is monitored using surveillance capsules consisting of small Charpy V-Notched

(CVN) specimens of pressure vessel and weld metal of the beltline of the pressure vessel, which is placed closer to the fuel core [8]. These specimens are removed periodically for testing over a wide range of temperatures to evaluate if there is: (1) a decrease in upper shelf toughness and (2) a shift in reference temperature, RTNDT (refer to Figure 1-1 below) [8]. In the case where embrittlement starts to affect the nuclear reactor pressure vessel, limitation specified by regulators and the American Society of Mechanical Engineers (ASME) Section XI, Appendix G, requires the power plant owner or operator to operate, heat up and cool down within the operating window in terms of both temperature and pressure, as shown in Figure 1-2 below [7].

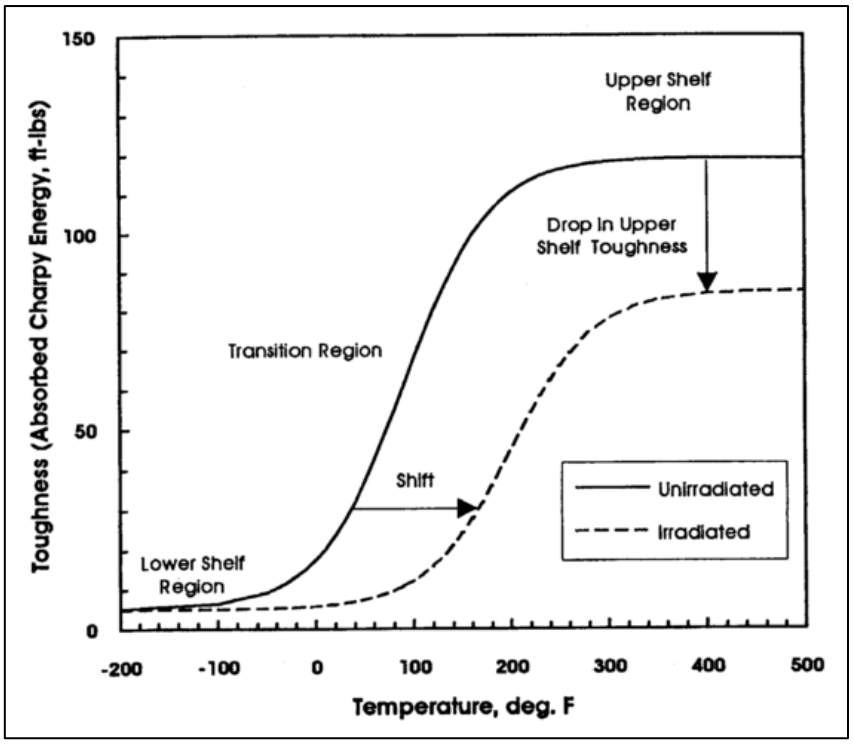

Figure 1-1: Brittle to ductile fracture toughness transition showing increase in ΔFATT [8]**.**

There are many other types and causes of embrittlement that are discussed in Chapter 2: Literature Review. The SPT, which is a mechanical testing technique, will be used to evaluate embrittlement of power plant materials in this research. The SPT technique is preferred due to its cost effectiveness as compared to traditional mechanical testing. This technique allows for the avoidance of premature replacement, which is normally made based on contracted design life, and its use of small specimens is regarded as quasi-non-destructive-testing. Traditional life assessment philosophies are usually used to assess turbine material in power plants.

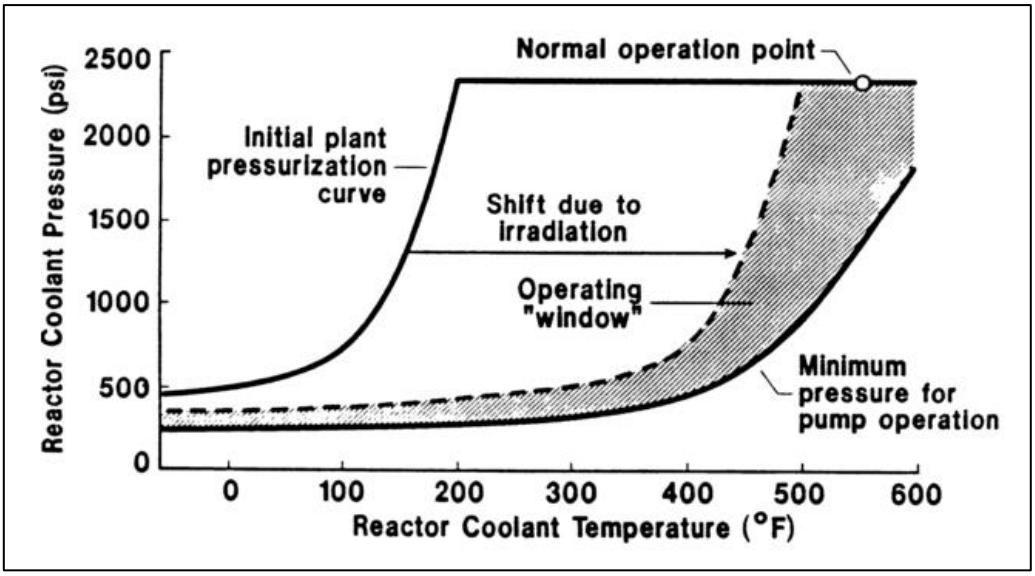

Figure 1-2: Effects of irradiation on pressure-temperature limit curve [7]**.**

1.2 Life assessment philosophies

Critical components such as turbine material, reactor pressure vessels, steam generators/boilers etc. are assessed prior to and during service life and at the end of design life in order to prevent catastrophic failure. Philosophies that are used to assess turbine materials (rotor and discs) are discussed below.

1.2.1 End of life criteria

Failure criteria requires an understanding of several factors such as the technical, financial, safety and risk tolerances associated with the hardware [9]. There are three criteria used to assess the turbine materials and Table 1-1 shows the summarised characteristics of these three end of life criteria.

Table 1-1: Summary of end of life criteria [9]**.**

History-based end of life criteria	Performance-based criteria	Inspection-based criteria
Design life of 30-40 years has elapsed	Severe loss of efficiency due to component degradation	Non-destructive examination shows crack initiation, large crack formation and microscopic damage
Prior failure experience and statistical data indicate impending failure	Vibration problems that are unable to be corrected by normal procedures	Severe dimensional change such as rotor bending (may be caused by water

History-based end of life criteria	Performance-based criteria	Inspection-based criteria
		induction or rubbing)
Calculation indicate life exhaustion	High frequency of repairs renders continued operation uneconomical	Mechanical or metallurgical testing of small samples indicate material property degradation
	Catastrophic failure	

Each criterion listed above depends on the collection of data at specific interval(s). It is essential to determine the correct inspection interval based on one of the three criteria above.

1.2.1.1 Inspection definition interval

Turbine rotors and discs are large components which are assessed using crack initiation and propagation [9]. Detection of the crack initiation, for which NDE techniques are used, can be challenging [10]. Predicting when the crack will initiate to a critical crack (for K_{IC}) requires the establishment of safe re-inspection intervals, which conduct the integrity and remaining life assessment of rotor and disc [9]. The inspection intervals need to be established in order to detect cracks, which may form and grow during service life before reaching critical crack size where catastrophic failure can become imminent (refer to Figure 1-3) [9].

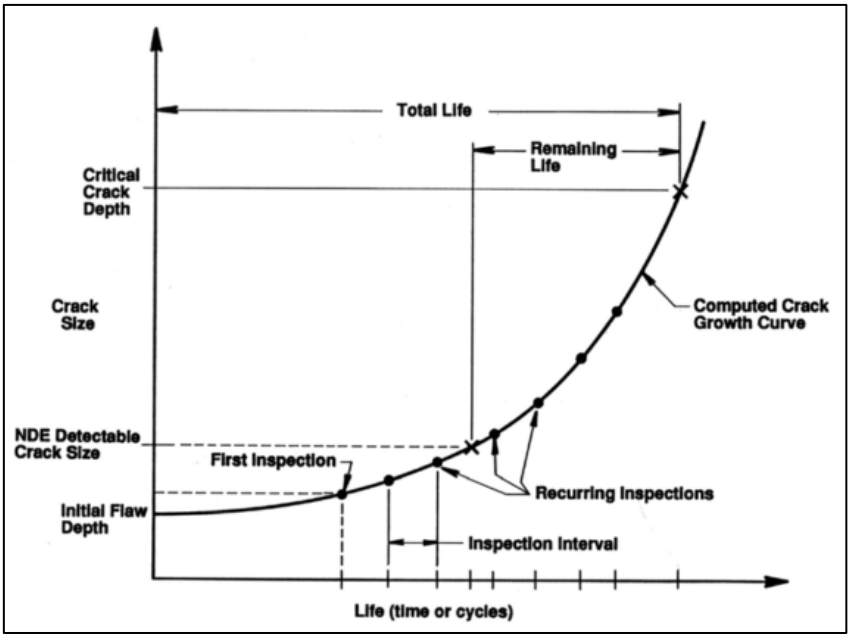

Figure 1-3: Schematic plot showing the relationship between non-destructive examination detectable crack size, life of the rotor, and re-inspection intervals [9]**.**

The EPRI paper [9] has developed three levels of life assessment that are linked to inspection intervals. Thus, the higher the level, the shorter the period of inspection intervals. Refer to the levels of life assessment below with the minimum requirements for each level.

1.2.1.2 The three-level life assessment approach

The three options/levels that turbine operators can use to assess the integrity and remaining life of turbine components depend on vintage, service condition (operating stresses and temperatures) and environment (corrosive environment, etc.) [9].

Table 1-2: Elements of the three-level life assessment approach [9]**.**

Data needed	Level I	Level II	Level III
Failure history	Plant records	Plant records	Plant records
Dimensions	Design/nominal	Measured/nominal	Measured or original drawings
Inspection (NDE)	Records or minimum detectable flaw/crack size	Limited inspection and analysis	Detailed inspection and data reduction
Operational data review	Minimum review /design condition	Average/medium	In-depth review
Operational data (temperature, pressure, rpm, load, etc.)	Design/nominal	Simple calculations	Detailed analysis/actual data-acquisition
Stresses and metal temperature	Design/nominal and simulations	Simple calculations	Detailed analysis(FEM)
Material properties	Specifications/lower bound data	Minimum/literature data/correlation	Sample removal and testing
Material sample needed?	No	No	Yes

1.3 Hypothesis

Embrittlement causes a decrease in ductility and toughness and traditional evaluation methods are destructive mechanical tests. The SPT technique is a quasi-non-destructive mechanical test that can be used as a direct fracture toughness test. The main aim of this research is to design, manufacture and commission/validate the SPT rig. The commissioning

of the rig is undertaken by a validation method of comparing the SPT test data with conventional mechanical test data through correlation. The SPT technique will be employed to evaluate embrittlement through assessing the ductility and energy absorbed from the SPT data results.

1.4 Research motivation

Power utilities experience many component failures as they age and different conventional mechanical testing techniques are used when possible to assess the structural integrity of critical components. Traditionally, a large amount of material for specimens is required, followed by weld repairs, which can further damage the material that has already been identified as at risk of failure. The traditional mechanical tests require that the component or system be shut down prior to testing, an unfavourable decision for the utilities that are already struggling to meet consumers' power demands. The SPT technique will enable utilities to perform certain tests without shutting down the components or systems (for instance static components such as pressure vessels, piping, casings, etc.). Prior to testing, specimens can be extracted on-line (when accessible), and due to the small amount of material and non-intrusive nature of sampling, shutdown times can be minimised.

Most Eskom power plants have been in operation for more than half of their design lives (and some are beyond their design lives). The SPT technique is relatively cheap to perform and is an option that will guarantee the following:

- quasi-non-destructive testing that provides a range of mechanical and fracture properties that can be used during the life assessment of plant components;
- the minimisation of premature replacement by knowing fracture toughness properties of critical components, such as turbines, steam piping, boilers, heat exchangers, etc., based on designed life.

1.5 Research objectives

- Literature review of life management techniques on components operating under embrittlement conditions in the power plant industry.
- Identification of components susceptible to embrittlement.
- Design and manufacture equipment required to perform the SPT.
- Validate SPT rig(s).
- Develop the SPT procedure for the application of testing and interpreting the test data.

- Evaluate embrittlement using the SPT technique by means of correlating the SPT data to standard mechanical test data through:
    - Charpy transition temperature (*FATT*) with estimated SPT transition temperature, $T_{SP.}$
    - Tensile properties using developed approach
    - Fracture toughness using developed approach
- Application of the SPT data to remaining life assessment of component/material (e.g. estimated fracture toughness).

CHAPTER 2: LITERATURE REVIEW

2.1 Embrittlement of power plant steels

Embrittlement has been defined in the Introduction. The premature failure of power plant equipment is often traced to low ductility caused by cyclic operation stresses and temperatures [2]. Failures occurring in critical components like turbine materials, high energy piping and pressure vessels can result in high costs, extended downtime, loss of life and the revoking of operating licences by power plant regulators. Common factors that affect embrittlement are summarised below.

2.1.1 Factors affecting embrittlement of power plant steels

Embrittlement results in brittle failure behaviour caused by the following internal and external factors [2], [5], [9]:

- Manufacturing processes during steel-making (e.g. chemical composition, heat treatment, cooling methods, etc.)
- Operating procedures used by utilities which include the following:
    - Operating stresses and temperatures – these are specified in designs and are tested in accordance with design codes and/or standards;
    - Microstructural phase change – this occurs during the service exposure (ageing) of the material and results in changes in grain size, second particles etc.;
    - The presence of surface notch or cracks – this mostly occurs in high stress zones and serves as a fracture criterion prior to material failure;
    - Maintenance practices – these are implemented through engineering programmes that provide condition monitoring methods and best maintenance practises on power plant components;
    - Increasing rate of application of load – this often occurs when the maximum load is applied to meet consumer power demands.
- Environmental influenced embrittlement such as corrosive environment which can degrade materials from an external reaction with gases on the atmosphere and react with chemistry processes used to remove corrosive elements in the power plant systems.

- Failure mechanisms of embrittlement in power plant steels are listed in Appendix-3 under Table A3-1, which describes the types, causes and typical components affected.

The degree of embrittlement in power plant components is evaluated through either metallurgical (microstructural change) or mechanical techniques (uniaxial tensile, CVN, K_{IC}, etc.). The uniaxial tensile test has illustrated how the material behaves in plastic deformation as shown in Figure 2-1. A loss of ductility is expected while the elasticity region shows insignificant change. CVN can also assess embrittlement by means of evaluating the change in energy transition temperature (loss of toughness and increase in $\Delta FATT$), as shown in Figure 1-1 in Chapter 1.

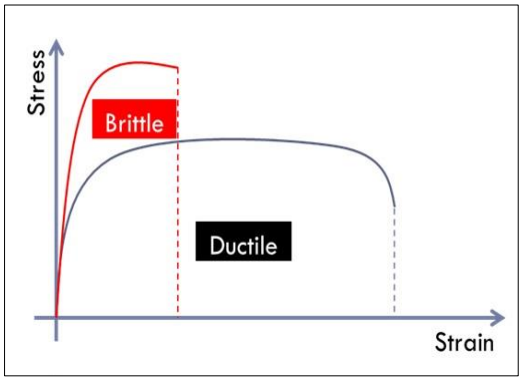

Figure 2-1: Mechanical test showing power plant steel affected by embrittlement resulting in loss of ductility.

It is important to note that it is not always possible to say that a material is ductile or brittle because the fracture behaviour depends on the exposure to service conditions. Figure 2-2 illustrates the brittle fracture of a steel pressure vessel that normally operated at elevated temperatures and failed during hydro testing with cold water.

Figure 2-2: Pressure vessel failed by brittle fracture during hydrostatic test using cold water [2]**.**

This study focuses on testing low pressure steam turbine rotor material; EPRI [9] has developed an assessment approach towards turbine material.

2.1.2 Embrittlement in turbine materials

Steam turbine materials such as low alloy steel and stainless steel are selected based on operating temperature and allowable stresses [9]. These steels have designation based on the chemical composition with the main alloying of these elements, nickel (Ni), chromium (Cr), molybdenum (Mo) and vanadium (V) [9]. A typical high pressure (HP) and high pressure to intermediate pressure (HP-IP) steam turbine rotor and disc for high temperature creep resistance will have about 1% chromium content, 1% molybdenum and 0.25% vanadium, referred to as 1CrMoV steel [9]. Low pressure steam turbine materials that operate below 399°C are normally referred to as NiCrMoV steel [9].

Embrittlement in power plant materials is commonly caused by service exposure and in the case of turbine materials, HP-IP turbine materials are the most affected by temper embrittlement while LP turbine materials are more susceptible to stress corrosion cracking [14], [17- 19]. Figure 2-3 illustrates the three main factors that degrade the HP-IP rotor material during service life and that are evaluated during life assessment of these materials. Temper embrittlement is the major fracture toughness degradation in ferritic steel and can occur during manufacturing heat treatment or life operation between 345-540°C [2], [9]. Some of the traditional mechanical tests which are used to evaluate embrittlement are discussed below.

2.1.3 Traditional mechanical testing of embrittlement of power plant steels

Structural designs are made based on tensile strength (UTS) and tensile strain (percentage elongation) of the material. Allowable or applied stresses are determined based on yield stress or UTS using safety factors and this approach is called the strength of materials approach (refer to Figure 2-4(a)) [12]. This approach can prevent failure of the materials against brittle fracture but can fail to do so during ductile fracture that can be caused by the formation of voids.

Unlike the strength of materials that consist of two variables, fracture mechanics consist of three variables, namely: applied stress, flaw size and fracture toughness. These three variables serve as minimum operating requirement conditions for materials in order to avoid fracture during operation (see Figure 2-4(b)).

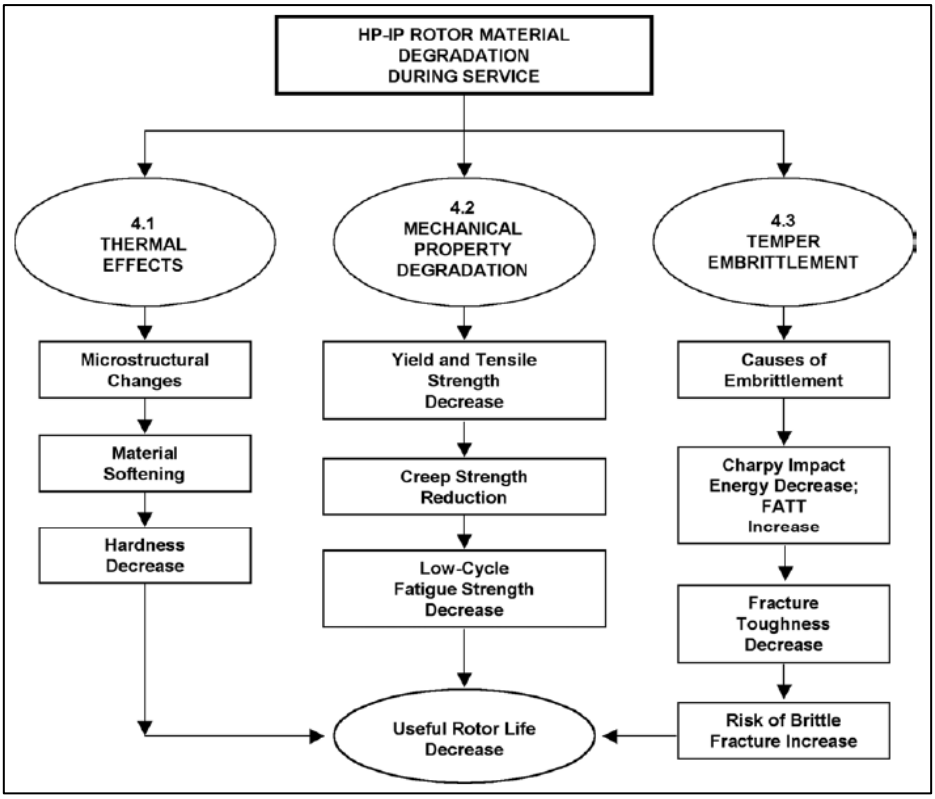

Figure 2-3: 1CrMoV HP-IP rotor material degradation and effects on properties [9]**.**

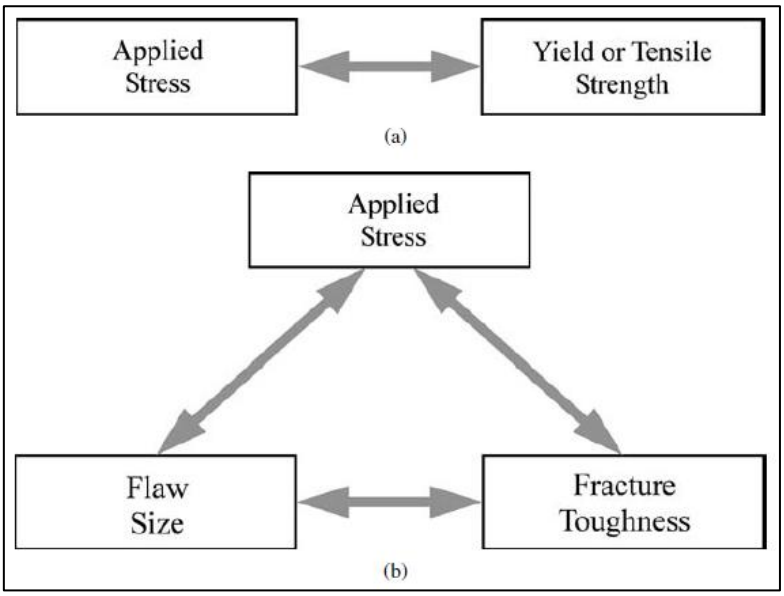

Figure 2-4: Material design approaches: (a) strength of materials approach and (b) fracture mechanics approach [12]**.**

Embrittlement is evaluated using one of the following common standard mechanical tests, which are also used to assess structural integrity of materials during component life assessment: the American Society for Testing Materials (ASTM), the European Standards (EN), the International Organisations for Standardisation (ISO), etc.

2.1.3.1 Uniaxial tensile test

Callister and Williams [13] define the uniaxial tensile test as a test during which "a specimen is deformed, usually to fracture, with a gradually increasing tensile load that is applied uniaxially along the long axis of a specimen." The test normally uses circular cross section specimens, but rectangular specimens can also be used. The tension test evaluates the strength and ductility of the materials under tensile stress [14]. Properties such as ultimate tensile strength (UTS), reduction in area (%) and elongation are directly extractable from this test. Yield stress, Poisson's ratio, Young's modulus and strain hardening can be determined. As such, the test provides information that may be used for material selection, alloy development, quality control and design [14]. It is noted that the tensile test cannot extrapolate the fracture properties due to the low loading rate used to perform the test [13]. Some ductile material shows little plastic deformation in the high loading rate test and, therefore, the performance of a high loading test to investigate fracture characteristics is required.

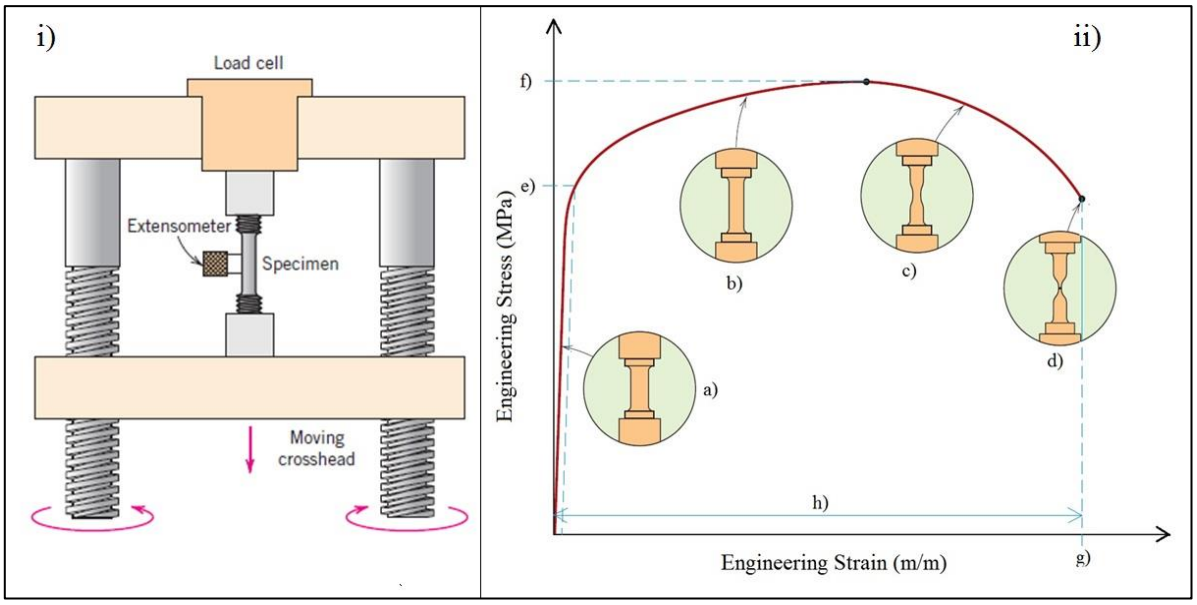

Figure 2-5: Mechanical tensile test of isotropic material: i) equipment and ii) results [13].

Figure 2-5 illustrates the engineering tensile test results: a) yielded specimen showing no deformation in geometry dimension (material elasticity) up to yield strength, b) specimen deformed through material plasticity (hardening) up to ultimate tensile strength, c) specimen necking due to micro cracks within the material, d) specimen fracture or fail due to multiple cracks, e) 0.2% offset yield stress, f) UTS, g) fracture point corresponding to fracture strain

and stress and h) total elongation representing ductility of the material up to fracture point. Ductility is expected to decrease with insignificant changes to strength and hardening and it is measured using the change in dimensions (length or area) per original dimensions (length or area) in percentage (see Figure 2-1).

2.1.3.2 Charpy V-Notch (CVN) test

The CVN test uses a notched sample (refer to Figure 2-6) that undergoes a high loading rate in order to fracture the sample. CVN characterises the material fracture behaviour by means of assessing the following parameters: 1) deformation at a relative low temperature, 2) a high strain rate (rate of deformation) and 3) triaxial stress state (maybe introduced by notch) [13]. It is the most used mechanical test to assess the material ability to absorb energy and ductile to brittle or fracture appearance transition temperature (*DBTT*/*FATT*). This test is fairly easy to perform and can be used together with known tensile parameters to estimate fracture toughness by means of established correlation methods, which will be discussed later in this chapter.

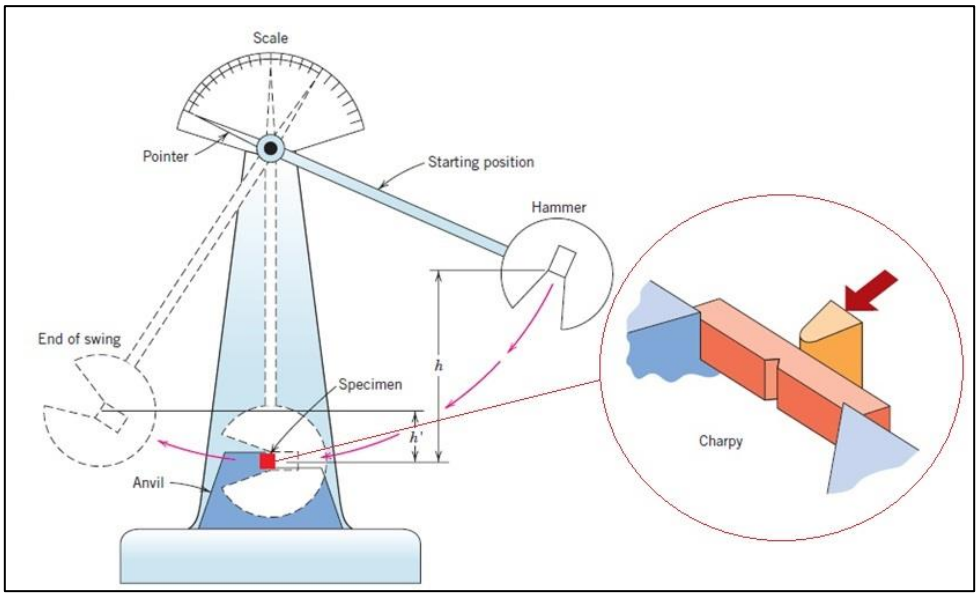

Figure 2-6: CVN test equipment [13]**.**

Typical data that CVN test analyses provide include (refer to Figure 2-7):

- Region I: Lower shelf energy region– this region is related to the brittle fracture region at low temperature.
- Region II: Transition temperature region – this region has both brittle and ductile fracture regions. 50% *FATT* is noted at 50% brittle shear fracture and 50% ductile

shear fracture (at some cases it is 50% absorbed energy, which is known as *DBTT*) and test temperature T2. Fracture toughness is found within this region by means of selecting fracture energy (e.g. E1 corresponding to T1) which is based on service performance or other tests [2].

- Region III: Upper shelf energy region – this region is a ductile region and is up to 100% shear fracture or maximum absorbed energy at test temperature. T3 is the lowest temperature that represents 100% ductile shear fracture [2].

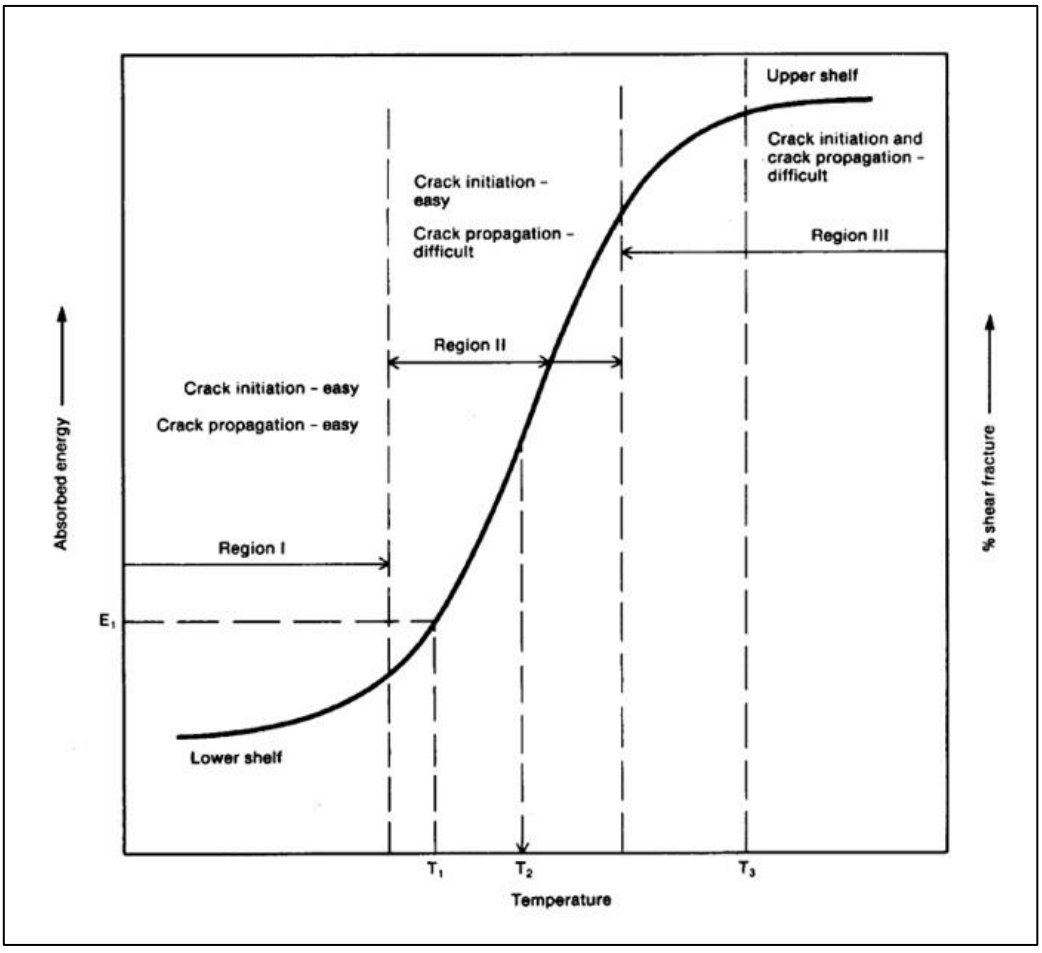

Figure 2-7: CVN absorbed energy vs test temperature diagram [2]**.**

When absorbed energy or % shear fracture decrease and/or increase T2, brittle fracture can be expected to occur at a high temperature. This process normally occurs after service exposure of steel and is known as embrittlement.

2.1.3.3 Fracture toughness test (K_{IC})

Power plant steels are designed and manufactured as ductile materials to meet the plant operation conditions. The fracture toughness test measures the resistance of material to a

crack extension [12]. Any of these fracture toughness parameters such as K (Stress Intensity), J (J-Integral) or CTOD (Crack-Tip Opening Displacement) can be plotted on a resistance curve (R-curve) to determine fracture toughness [15]. Organisations of standards (ASME, ISO, etc.) have developed standards for fracture toughness for elastic and elastic-plastic materials with three different modes of testing as shown in Figure 2-8 below. The three cracking separation modes are namely, Mode I: tensile stress mode, also known as opening mode, is normally applied to the plane of the crack and its fracture toughness is referred to as 'plane strain fracture toughness'; Mode II: shear stress is applied by means of a sliding load acting in parallel to the plane of the crack and perpendicular to the front face of the crack; and Mode III: shear stress is applied in parallel to both the front of the crack and the plane of the crack, and is also referred to as 'tearing stress' [16].

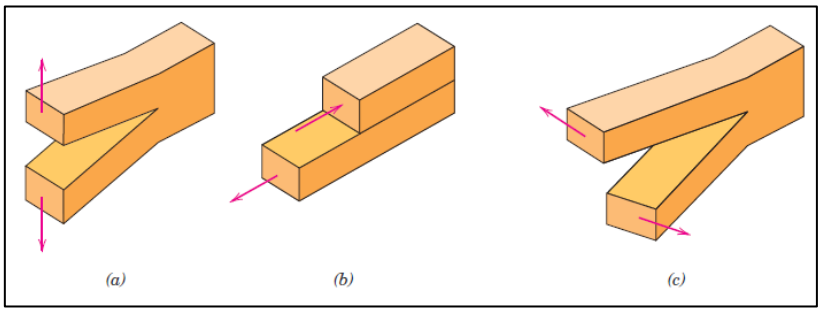

Figure 2-8: The three modes of crack surface displacement: (a) Mode I, (b) Mode II and (c) Mode III [13]**.**

ASTM standards are widely used to assess both linear elastic fracture mechanics (LEFM – ASTM E399) and elastic-plastic fracture mechanics (EPFM – ASTM E1820). In this study, EPFM is applicable as the steel behaves in an elastic-plastic manner. It is important to note that the two standards are similar and only differ in terms of how the test load shall be carried out as well as the analytic procedure of the test data. Below is the general consideration when the fracture toughness test is carried out. The following fracture toughness information is based on the two above standards [15], [17] and Anderson's work [12].

2.1.3.3.1 Specimen configuration

ASTM standards entail five different specimen configurations; none of the other standards cover all five specimen configurations. These specimens may differ in geometric sizes but allowable tolerances are clearly noted. Specimens are designed with crack notch for crack initiation and crack growth. Figure 2-9 illustrates the compact (CT) specimen during fatigue crack growth.

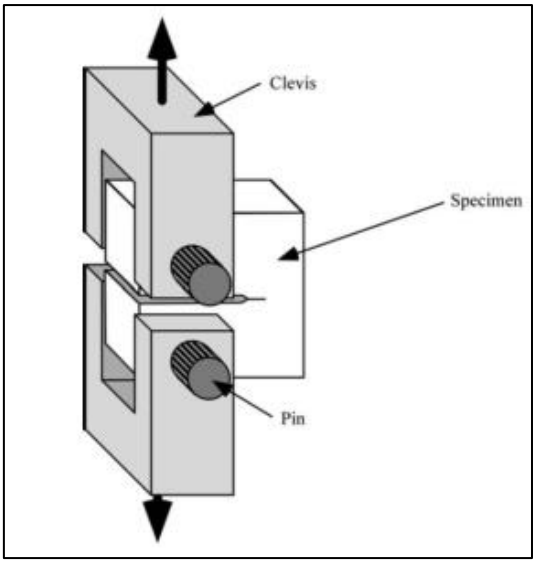

Figure 2-9: Compact specimen during fatigue loading [12]**.**

2.1.3.3.2 Specimen orientation

It is important to note the orientation of the specimen in order to realise that mechanical properties are sensitive to microstructures that contain planes of weakness, that in turn allow for easy propagation of the crack.

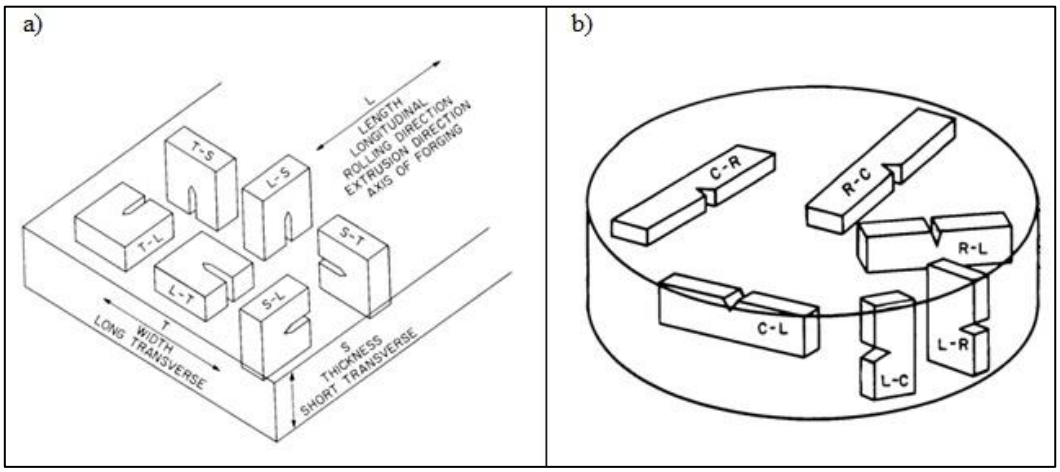

Figure 2-10: Fracture toughness specimen orientation for: a) rolled plates and forgings and b) cylindrical tubes and bars [12].

2.1.3.3.3 J-Integral testing of steel

J-Integral testing is used on EPFM guided by ASTM 1820. However, it is advisable to carry out the fracture toughness test using ASTM E399 and evaluate for test compliance (only if there are no constraints for material and time). There are two methods to test for J-Integral (refer to Figure 2-11 and Figure 2-12):

a) An extrapolating method without crack growth measurement

The method consists of experimental equations that are detailed based on ASTM E1820 and does not require crack growth to be measured. The disadvantage of the method is that it is a trial and error method and requires few tests to be carried out in order to generate the J-R curve that complies to the standard. J_Q represents J_{IC} (ductile fracture toughness) once the compliance is met in accordance with ASTM E1820. Refer to Figure 2-11 for how J_Q is determined from a 0.2mm offset of a small crack, Δa.

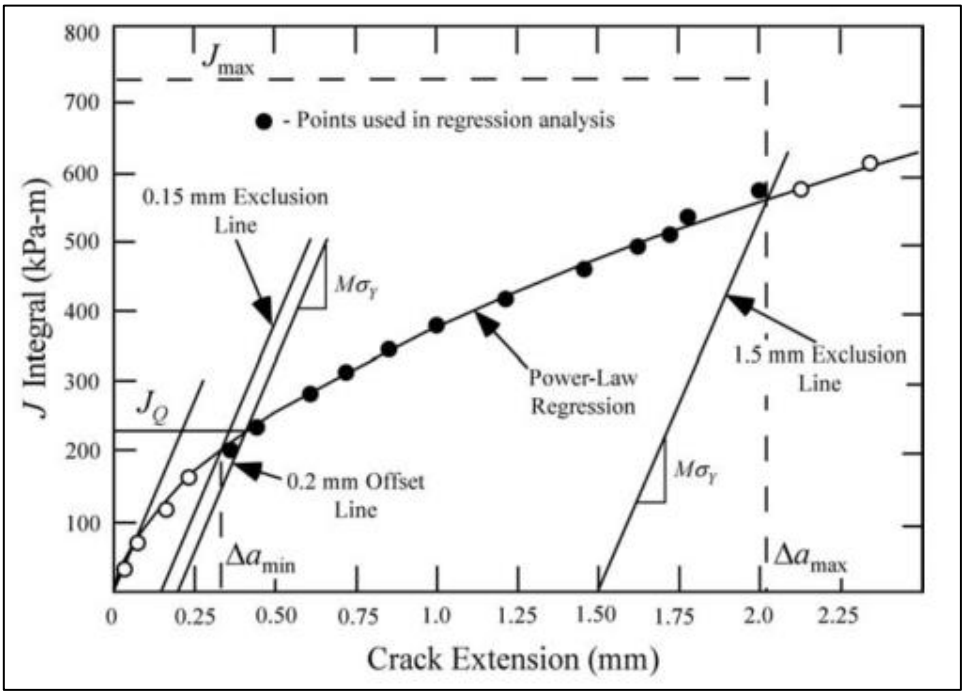

Figure 2-11: J_Q plotted against Δa for J_{IC} measurement [12]**.**

b) A J-R curve with monitoring crack growth

This method requires monitoring of the crack growth, which means that additional instrumentation is required. A J-R curve can be obtained from a single specimen; however, the test has unloading compliance requirements as shown in Figure 2-12. The details of how the compliance is achieved are included in the ASTM E1820. The CTOD method is another option to achieve the J-R curve, which can be applied to determine the fracture toughness and is also in the ASTM E1820.

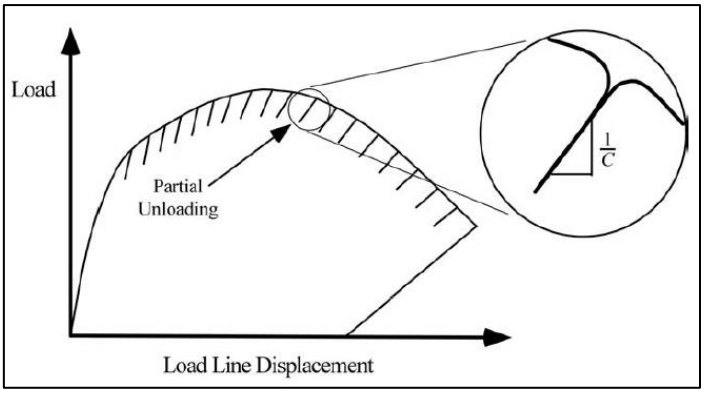

Figure 2-12: Load displacement curve [12]**.**

2.2 Introduction and background study of the small punch test (SPT)

The miniature disk-bend test that is commonly referred to as the 'small punch test' (SPT) has been used to characterise mechanical properties of materials from as early as the 1980's [18], [19]. The SPT uses a circular specimen of 3 to 10 mm in diameter and 0.1 to 0.75 mm thick or a square specimen of 10 mm x 10 mm [20]. The SPT is normally carried out on a specimen clamped between an upper and lower die but it can also be carried out on an unclamped specimen [19]. The details of the SPT working principle, including the test conditions, are explained in Section 2.2.1.

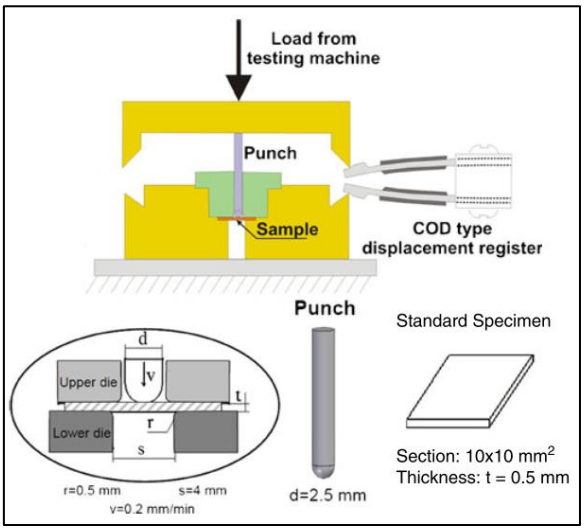

Figure 2-13: SPT test equipment [21]**.**

2.2.1 Working principle

A load is applied at a constant displacement rate/load to a fixed/clamped specimen between an upper/clamping and lower/receiving die, or sometimes to a non-fixed/unclamped (no upper die required) specimen up to a fracture point. The setup may also depend on what the

user's interest(s) is/are during the SPT. For example, a constant load may be applied to investigate creep and stress rupture strength properties (time dependent behaviour), while a constant displacement rate will be applied to investigate mechanical properties for time independent behaviour such as: i) Fracture Appearance Transition Temperature (*FATT*), ii) Ductile to Brittle Transition Temperature (*DBTT*), iii) tensile properties (stress-strain curves) and iv) fracture toughness on both metallic and non-metallic materials [19]. A load displacement curve (LDC) is the conventional output data resulting from the SPT experiment that investigates time independent behaviour of the material, such as in this study (refer to Figure 2-14 below).

The tests are carried out in a controlled environment, e.g. liquid nitrogen coolant is used when embrittlement tests are carried out at a constant displacement, and heating furnaces are used to elevate temperature at a constant load. Correlation methods are used to evaluate test data, which include advanced material modelling for material assessment.

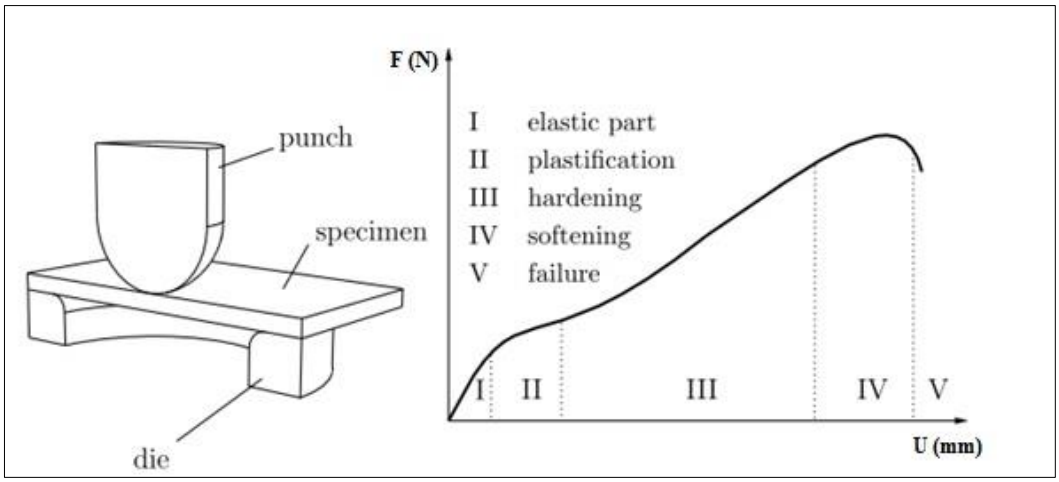

Figure 2-14: SPT setup (left) and experiment output (right) of unclamped specimen [22]**.**

Figure 2-15 shows a typical SPT equipment setup used for *DBTT* and other mechanical time independent behaviour parameters. The LDC consists of five stages that can be clearly seen in Figure 2-14 above: Stage I - elastic bending represented by a linear curve; Stage II - plastic deformation; Stage III - hardening occurring during membrane stretching; Stage IV - softening occurring up to a peak load and Stage V - load drop during failure or fracture. The LDC, as shown in Figure 2-14, is true for elastic-plastic materials, i.e. elastic modulus, yield stress and hardening coefficient materials [24]. A summary of the history and current developments of the SPT technique are discussed in 2.2.2.

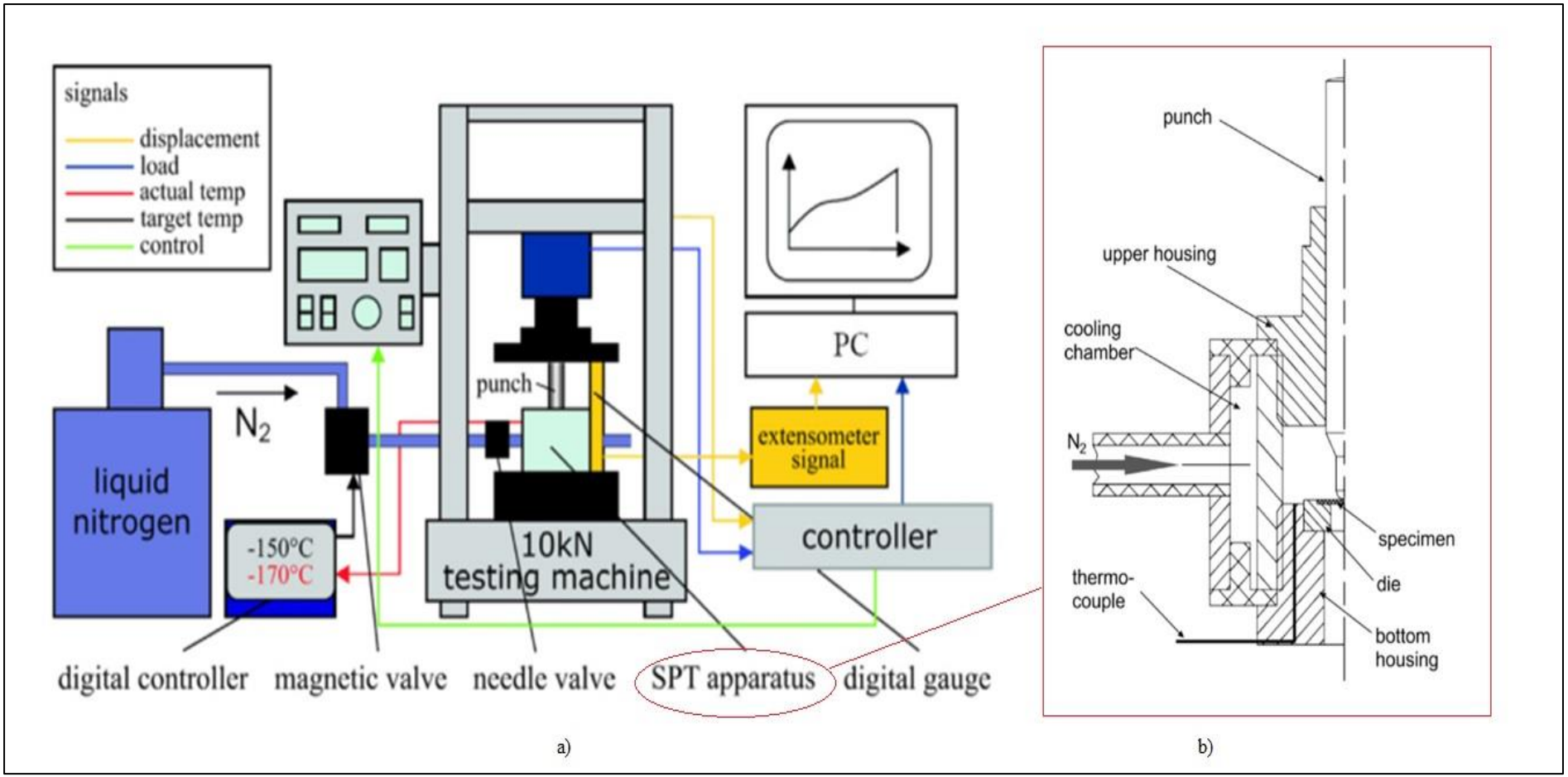

Figure 2-15: SPT equipment showing: a) test equipment setup and b) cross-section of environmental chamber [23]**.**

2.2.2 History of SPT

This sub-section is based on Foulds et al [1] and EPRI [11], [19], [20], [25].

The small punch test was introduced by Westinghouse Hanford researchers in the early 1980's during the transmission electron microscopy (TEM) test of a reactor pressure vessel in the United States of America. At the time, the ductility assessment of the vessel structure was carried out to determine the level of irradiation embrittlement. A typical 3 mm diameter x 0.25 mm thick specimen, which was meant for TEM, was also used to characterise mechanical ductility. Westinghouse Hanford researchers continued to develop a method of interpreting stress-strain behaviour based on FEM at the Massachusetts Institute of Technology (MIT).

More developments were done in Japan by Mao, Saito and Takahashi [1], [11], and this led to the first attempt at standardising the SPT technique by the Japanese Atomic Energy Research Institute (JAERI) in 1988. The draft recommended a TEM specimen disk, 3 mm in diameter x 0.25 mm thick, a much larger specimen of 10mm x 10 mm square x 0.25 or 0.5 mm thick, and provided guidance for determining *DBTT*, equivalent fracture strain, ε_{qf}, and fracture toughness, J_{IC}. The draft was based on work by Mao et al. and Misawa et al. [19], [20], and did not include the determination of stress-strain behaviour.

In 1988, the Electric Power Research Institute (EPRI) researched the properties of: i) *FATT*, ii) tensile stress-strain behaviour and iii) fracture toughness of the power plant turbine rotor steels. EPRI also improved the irradiation embrittlement method of using FEM. In 1990, the SPT technique was extensively studied in Europe, where creep testing was developed and a European guideline, CWA 15627:2007, for the SPT was first published in 2006 and revised in December 2007. Today, the SPT technique is arguably the most effective mechanical testing technique for small specimens, but it still needs to be standardised once all of the uncertainty of using correlation is resolved.

2.2.3 Developments on small punch test

This sub-section is a summary of the development of the SPT technique (explained in Section 2.2.2) from its beginning to current developments. Some of the main contributors are mentioned in Figure 2-16, which reads from left to right (years ascend from left to right).

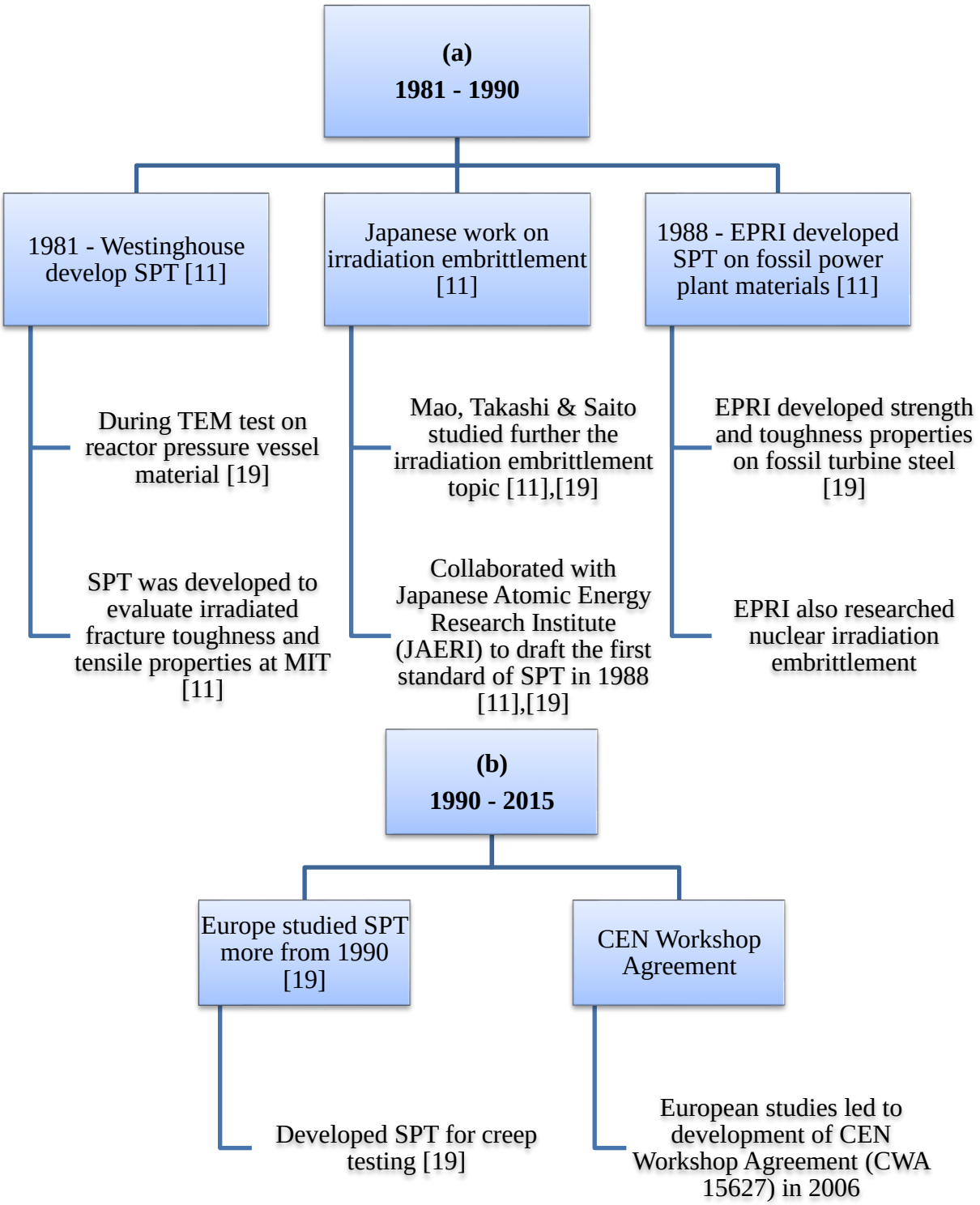

Figure 2-16 Development of the SPT between year (a) 1981-1990 and (b) 1990-2007.

2.2.4 Application of code of practice CWA 15627 [18]

In 2006, the CEN Workshop Agreement (CWA 15627) was developed to provide guidance on the design of the SPT test rig and test requirements. The agreement was revised in December 2007.

2.2.4.1 Design of the SPT test rig

The minimum requirements specified in the CWA 15627 only apply to the working part of the rig, namely dies and punch [18]. Figure 2-17 below was extracted from the code of practice in order to identify the prescribed requirements:

- U_1 and U_2 are displacement for punch and specimen respectively,
- F is load applied (constant for time dependent behaviour),
- V is velocity (constant for time independent behaviour, 0.2 to 2 mm/min),
- h is specimen thickness (0.5 mm is recommended but it can range from 0.1 to 0.75 mm),
- *l* is the chamfering length (0.2 mm at 45° is recommended),
- d_1 is the diameter of the specimen (8 mm is recommended but it can also range from 3 to 10 mm and can be a square shaped specimen of 10 x 10 mm^2),
- r is the punch radius (range from 1 to 1.25 mm),
- d_2 is the receiving die hole (4 mm in diameter is recommended)

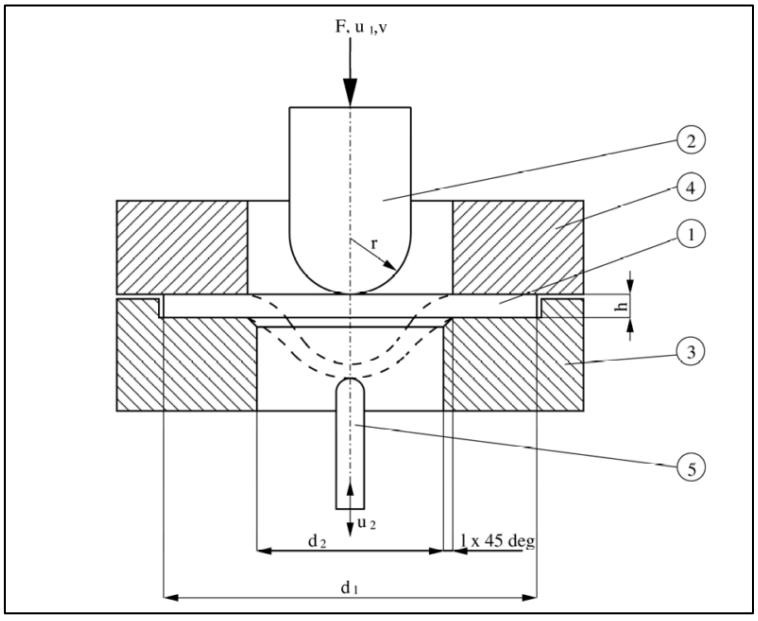

Figure 2-17: Cross–sectional scheme of the testing apparatus (1 – specimen, 2 – punch, 3 – receiving die, 4 – clamping die, 5 – deflection measurement rod) [18].

Hardness of 55 HRC or higher is recommended on both dies (item 3 and 4, from Figure 2-17) and punch (item 2 from Figure 2-17) as not to be deformed during experimental testing. The clamping contact surface area must have minimum of the third of the total specimen area.

2.2.4.2 Sampling and preparation

A scoop cutter sampler (see Figure 2-19) that has a hemispherical cutter plated with cubic boron nitride (CBN) grit as an abrasive, spins about its axis of symmetry and is slowly advances perpendicularly to a base material [18]. Coolant is used to cool and clear the cutting path and sample depths of 3-4 mm are normally cut with ranging diameter (e.g. 25 mm) depending on the scoop cutter size [18].

Figure 2-18: Sample removed by the scoop system with the SPT specimens cut using EDM [18]**.**

The SPT specimen wire is cut to a thickness of 0.55 mm or 0.7 to 0.8 mm and is lapped to a final thickness of 0.5 mm using the metallurgical lapping grit paper size of FEPA P1200 [18], [26]. The allowable tolerance for thickness at four points positioned at 90° is ±0.5%, and ±1% for diameter at two points positioned at 90° [18].

Eskom, in collaboration with the Nelson Mandela Metropolitan University, has developed a sampling method called ‘core sampling and friction taper stud welding’ (FTSW)[27]. The method was applied on a high pressure (HP) turbine disc by coring the sample with a minimum diameter of 7 mm, and maximum diameter of 23 mm, tapered at 20° [27]. Following the coring of the sample, a friction weld using the same grade of consumable metal to that of the base material is used to repair it, see Figure 2-20 below [27].

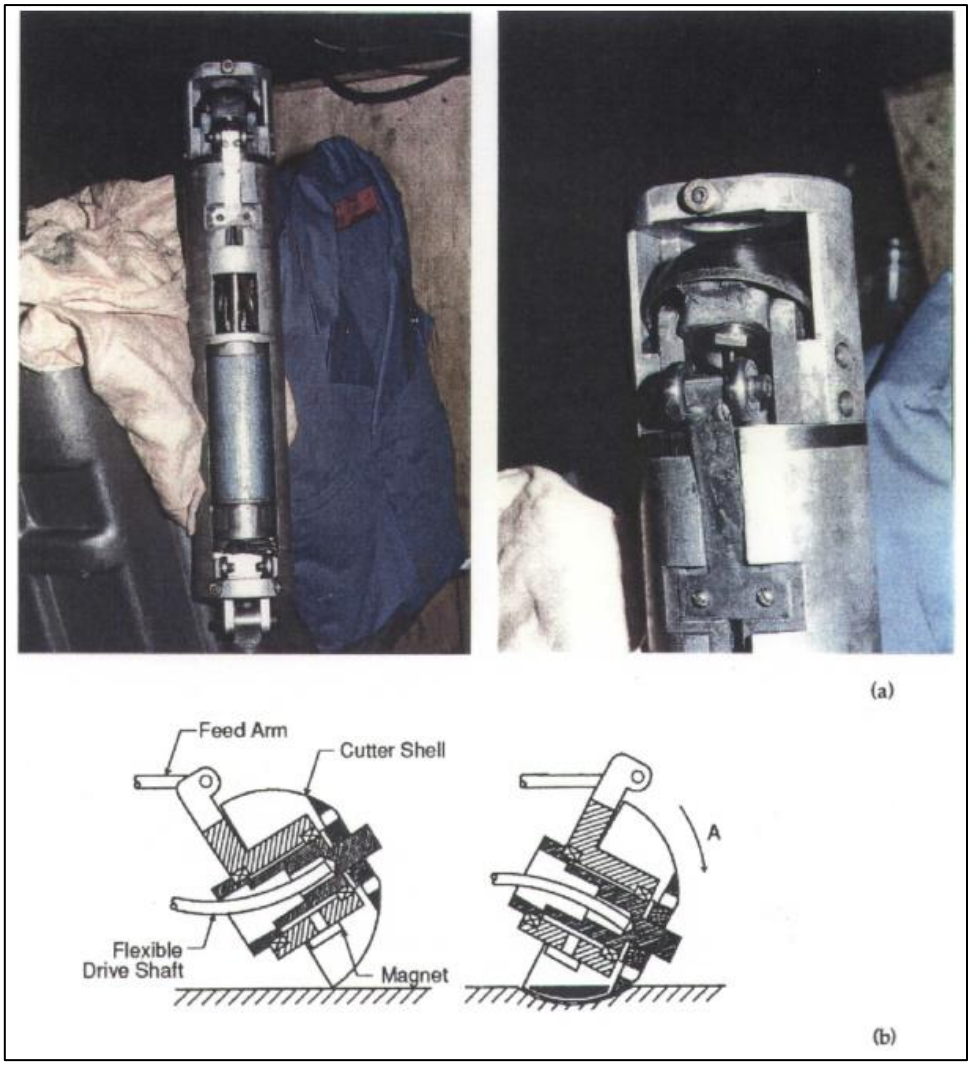

Figure 2-19: Scoop cutter sampler showing: a) photograph and b) schematic [18]**.**

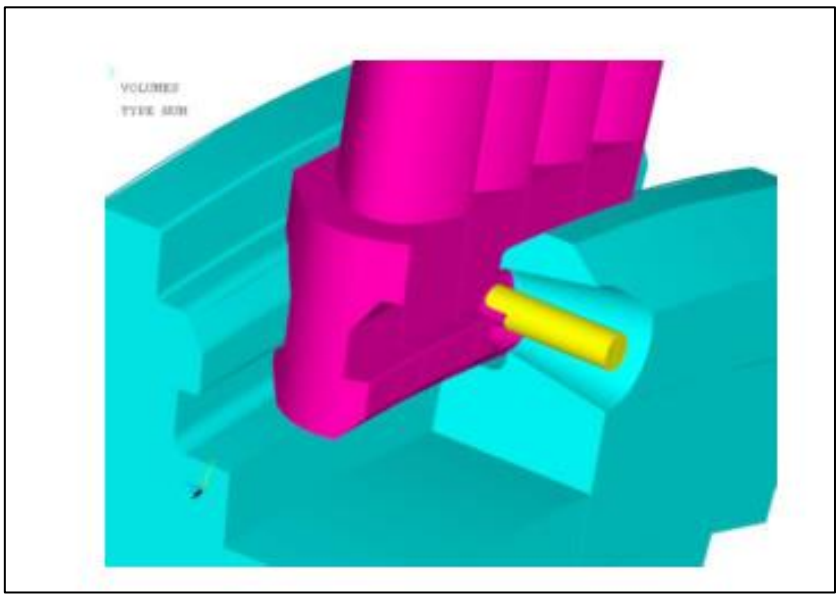

Figure 2-20: Sectional view of core sample hole [27]**.**

2.2.4.3 Testing requirements according to CWA 15627 [18]

The information in this section was extracted from EN CWA 15627: 2007. The mechanical properties of a material are used to assess the integrity of its remaining life on both time dependent and time independent behaviour. Table 2-1 summarises the mechanical properties that can be derived from the SPT with a minimum number of tests required.

Table 2-1: Summary of damage/failure mode and the relevant the SPT derived properties and specimen needs [18]**.**

Damage or failure mode	SPT derived properties	Minimum number of SPT specimens/test	Loading method	Comments
Overload, yielding and plastic collapse	Yield strength and tensile strength	2	Constant displacement rate (0.2 to 2 mm/min)	Properties are used to estimate other properties (J_{IC} / K_{IC})
Creep/creep rupture	Rupture strength	5	Constant load	Acceleration method are used for standard test specimen
Time independent fracture	FATT or DBTT	7	Constant displacement rate (0.2 to 2 mm/min)	Applicable to carbon and low alloy steels (BCC)
	Fracture initiation toughness, J_{IC} or K_{IC}	2	Constant displacement rate (0.2 to 2 mm/min)	Tests at desired temperatures using empirical correlation

2.2.4.3.1 Loading system

A screw-driven tensile testing machine is equipped with the SPT rig that has a load and displacement measuring system. A load/force measurement must not have a percentage error that exceeds ±1% and must comply with EN 10002 and be calibrated once per annum.

2.2.4.3.2 Displacement and deflection measurement system

Any method of measuring displacement or deflection may be used and a displacement indicator shall monitor the punch movement with an accuracy of ±1% of the specimen thickness.

2.2.4.3.3 Heating and cooling system

Uniform temperature across the specimen must be maintained within the range of ±3 K of the designated test temperature. Thermocouples of the correct type must be applied and calibrated in accordance with the EN 10002 standard

2.2.4.3.4 Data recording

Hardware and software should be provided and record the test parameters automatically with a resolution that matches the hardware. ±1% of full scale deflection should be maintained and preferably be within ±1% of the measured signal.

2.2.4.4 SPT rig compliance

There are no standard methods for determining the compliance of the SPT rig because of the use of different universal tensile machines that use different data acquisition software. It is preferable to use the existing tensile machine software to avoid the programming or coding of independent data acquisition software.

2.2.4.4.1 Modelling experimental LDC

The rig is manufactured to not deform during testing of the SPT, especially when testing embrittled material that can be hard, it is expected to reproduce the same experimental LDC (LDC_{EXP}). Once the rig can reproduce the same experimental LDC, the comparison of the experimental LDC with FEM LDC (LDC_{FEM}) can be done. LDC_{FEM} is produced by modelling a complete rig and by defining all parts of the rig to have elastic material behaviour except for the sample, which is to be defined as elastic-plastic material behaviour. Figure 2-21 shows the compliance of the apparatus by means of superimposing the measured curve (LDC_{EXP}) and corrected curve (LDC_{FEM}) developed by means of FEM.

2.2.4.4.2 Determine elastic behaviour of the material

EPRI [19] has tested the test setup compliance by testing a 5 mm thick sample with a punch that has no ball. The test is run for the elastic stage of the LDC and Young's modulus is determined using the contact area of the punch, the thickness of the sample and the load within the elastic region.

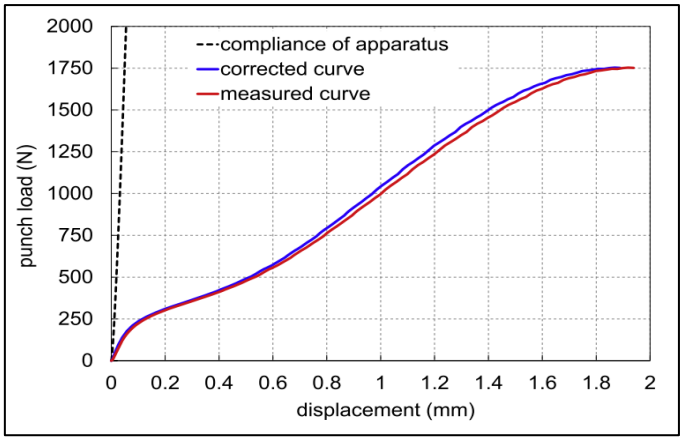

Figure 2-21: LDC showing compliance of apparatus [23]**.**

$$\sigma_{x1} = \frac{F_{x1}}{A_c}$$

Equation 2-1: Stress at displacement, x_1.

Where: σ_{x1} is stress at displacement x_1, F_{x1} is load at displacement x_1 and A_c is a contact area of the punch head face.

$$\varepsilon_{x1} = ln\frac{t_o}{t_{x1}}$$

Equation 2-2: Strain at displacement, x_1.

Where: ε_{x1} is strain at displacement x_1, t_o is original thickness and t_{x1} is thickness at displacement x_1.

Using a known point of the elastic gradient curve, Young's modulus can be determined as follows:

$$E = \frac{\sigma_{x1}}{\varepsilon_{x1}}$$

Equation 2-3: Young's modulus.

However, it is not easy to estimate t_{x1} and, therefore, it is recommended to compare/superimpose the determined elastic curve with an existing validated curve of the same material. Validation can be done by LDC_{FEM} using uniaxial tensile properties.

2.2.5 Risks associated with the SPT

The SPT risks and uncertainties are listed in Table 2-2 and have consequences if ignored during testing.

Table 2-2: Types of risks associated with the SPT [7]**.**

Types of risk	Definition	Consequences
Safety	The SPT is not yet standardised and can be questioned as to whether it can satisfy design code requirements (ASME code) especially when dealing with critical components such as a nuclear reactor pressure vessel (RPV)	Public health and human safety Plant component safety
Technical	Conversion of small specimen data to large specimens is a technical risk that has data scatter. The technique has been widely researched and improvements have been made over the years yet the approach differs when predicting material fracture toughness	Plant component safety
Regulatory	Correlation of data to estimate material fracture toughness may not be enough to satisfy regulatory bodies (NNR, NRC etc.) as a prevention method to brittle fracture especially in a component like nuclear RPV	Licence issues to resolve
Economical	Safety, technical and regulatory risk will require mitigation in order to minimise all these risks, which can be costly. It may, however, look as if the SPT benefits are cancelled out by mitigation cost.	Mitigation cost can be high especially with a technology or technique that is not formally standardised since the data can be interpreted differently

2.2.6 The SPT rig designs

The following designs are adopted from the SPT draft paper [18], Foulds and EPRI old [1], [16] and current designs from EPRI [28], Rasche and Kuna [23] and Omacht [29].

2.2.6.1 Past designs

Foulds and EPRI [1], [19] have used a design that uses a digital camera mounted on the bulge surface of the sample as shown in Figure 2-23 below. Omacht from Material and

Metallurgical Research Ltd. in the Czech Republic has worked with EPRI in developing the SPT rigs and Figure 2-23 shows the sketch and photograph of the design from the collaboration of the two organisations.

2.2.6.2 Current designs

The focus was around the design that is suitable to perform the *DBTT* experiment and elevated temperature up to 100°C. The current designs work from normal/room temperature to LN_2 temperatures. EPRI has improved its design and replaced the camera with acoustic emission sensors that detect crack initiation as shown in Figure 2-24. Rasche & Kuna [23] have developed the SPT rig design that was used for the *DBTT* experiment as well, refer to Figure 2-25

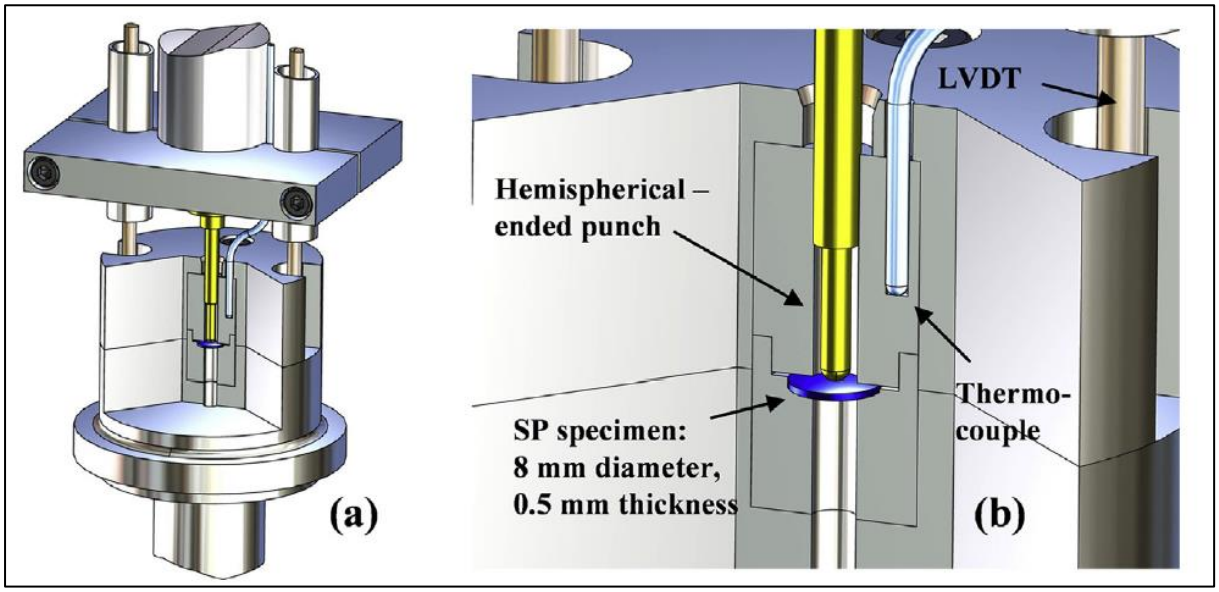

Figure 2-22 SPT apparatus for DBTT testing by Turba, Hurst and Hahner [30]**.**

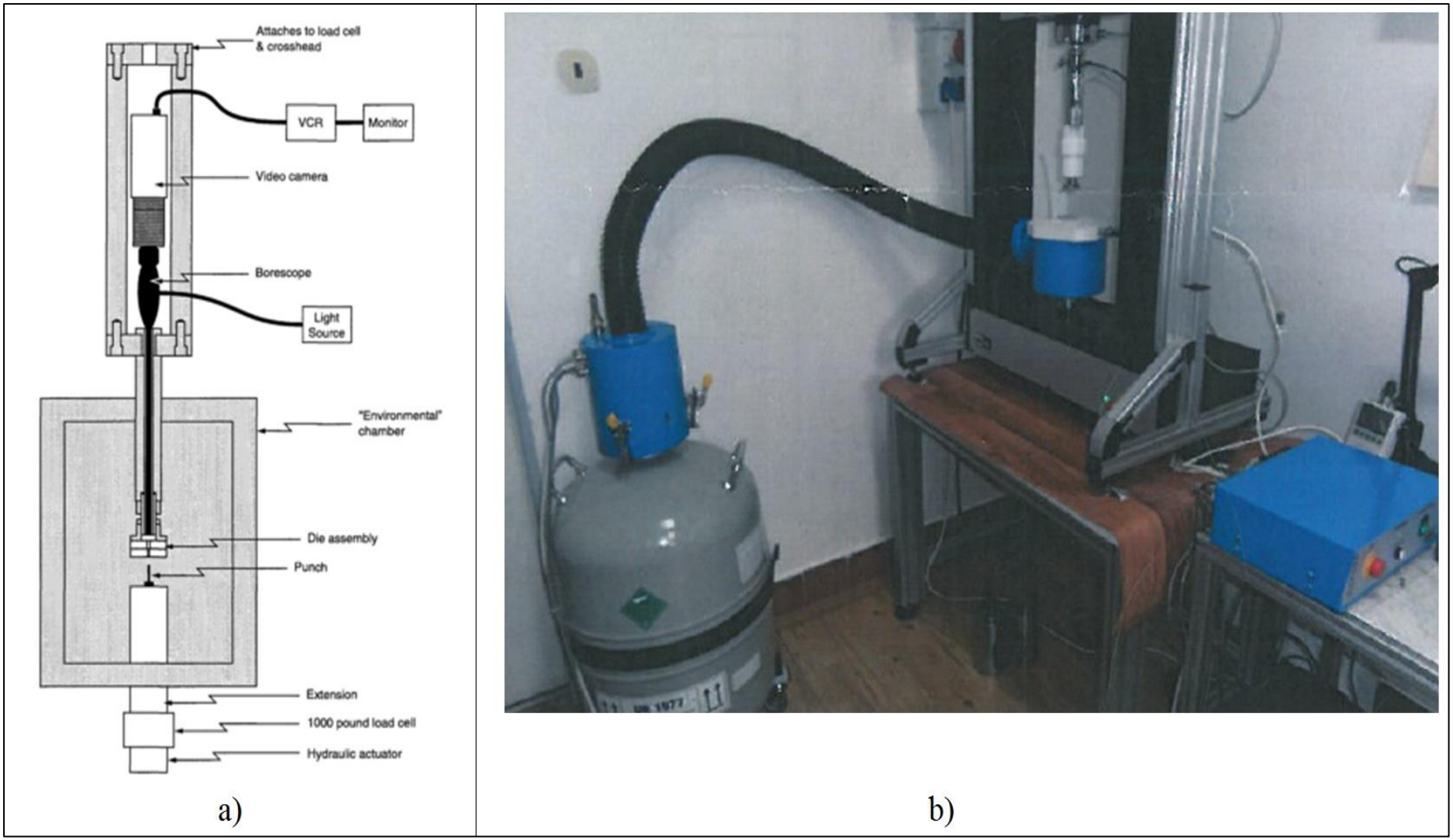

Figure 2-23: DBTT SPT setup: a) schematic [1] **and b) photograph by EPRI and Omacht** [29]**.**

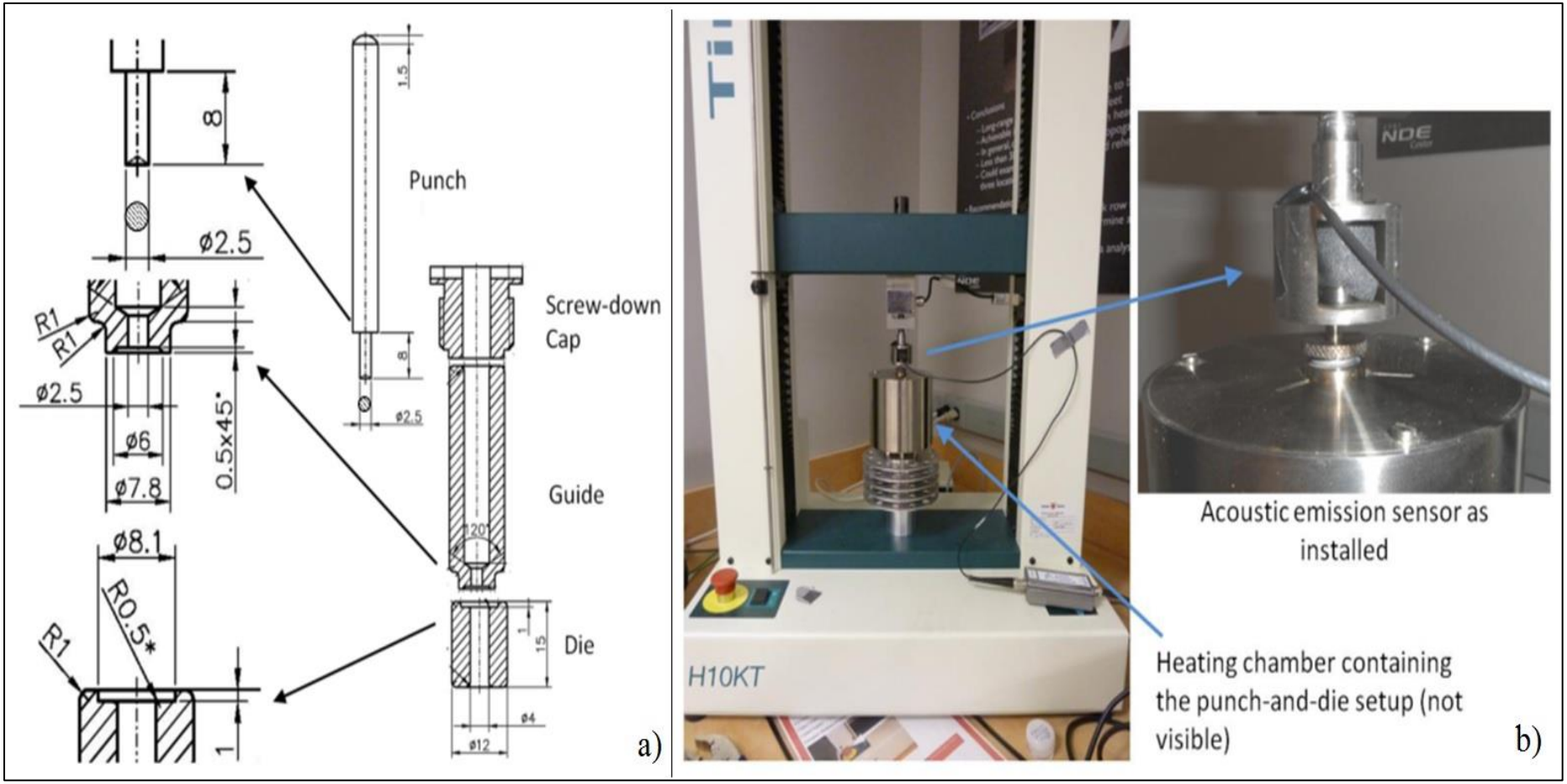

Figure 2-24: a) schematic and b) photograph of EPRI SPT setup with acoustic emission sensor [28]

.

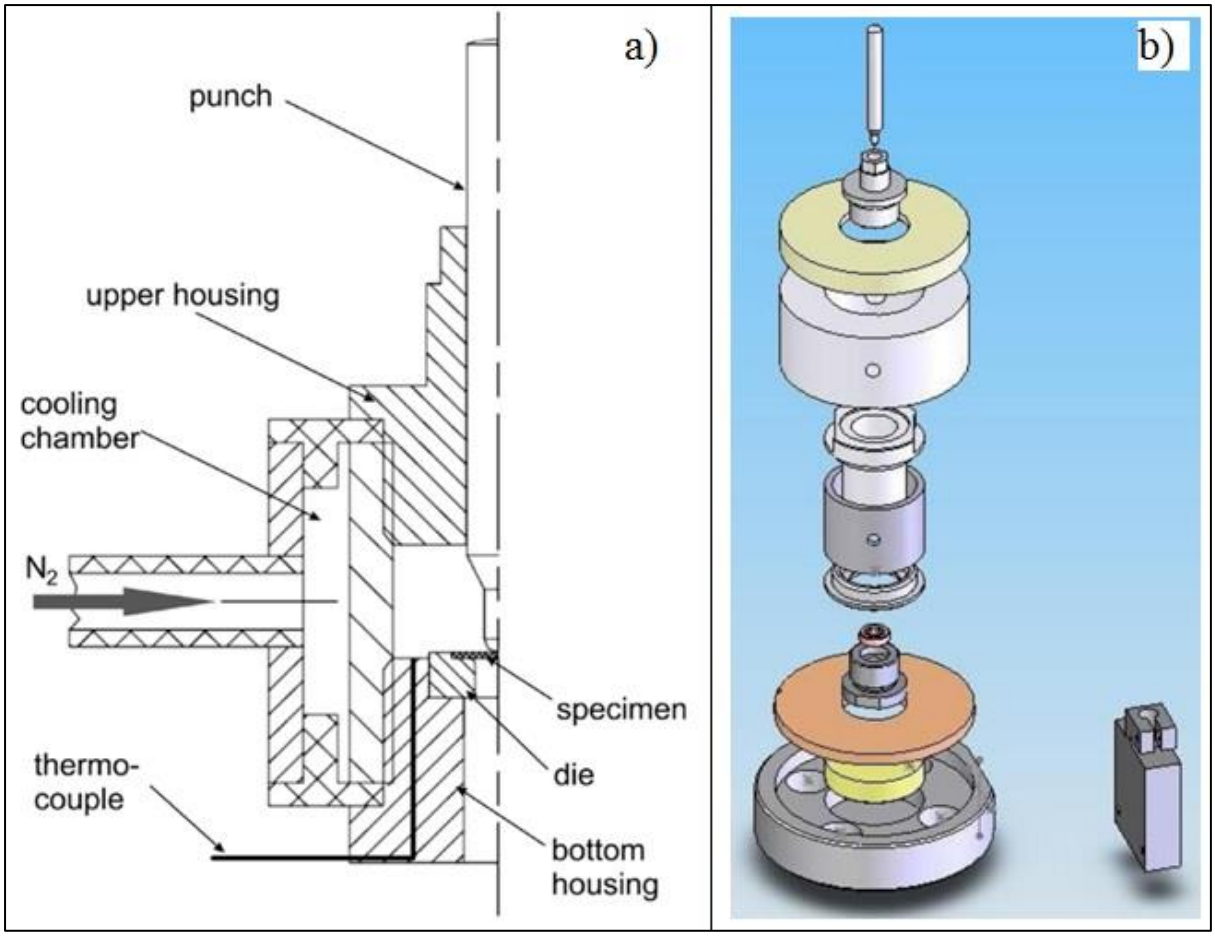

Figure 2-25:SPT apparatus for DBTT: a) schematic and b) 3D exploded view model by Rasche and Kuna [23].

2.2.7 Application of the SPT on power plant materials

The technique is a life assessment tool for structural integrity and therefore can be used to estimate any of the mechanical properties below.

- Fracture toughness properties
  - Either J_{IC} or K_{IC} as a criterion for life assessment of power plant materials or components
  - This includes critical crack length or critical flaw dimension estimation
- Transition temperature and energy absorbed
  - *DBTT* or Charpy *FATT* (embrittlement)
  - Energy absorbed at fracture
- Uniaxial tensile properties
  - Yield stress and tensile strength
  - Tensile elongation

- Fracture strain

- Creep properties

These properties listed above are estimated using empirical correlation, which requires extensive testing.

Table 2-3: Summary of the SPT application on power plant materials.

Material/Component		Description of application
Critical components		
	Boiler & its components	Structural integrity, embrittlement, creep, uniaxial tensile parameters and remaining life assessment
	Steam generator (nuclear plant)	Structural integrity, uniaxial tensile parameters and remaining life assessment
	Reactor pressure vessel	Irradiation embrittlement, structural integrity, uniaxial tensile parameters, DBTT and remaining life assessment
	Turbine & its components	Structural integrity, embrittlement, creep, uniaxial tensile parameters, DBTT and remaining life assessment
	Main supply steam pipes	Structural integrity, embrittlement, creep, uniaxial tensile parameters and remaining life assessment
	Primary water piping (nuclear plant)	Structural integrity, embrittlement, uniaxial tensile parameters and remaining life assessment
Non-critical systems (secondary systems)		
	Low alloy carbon steel piping	Uniaxial tensile parameters
	Re-heaters pressure vessel	Structural integrity and uniaxial tensile parameters
	Condenser water boxes	Structural integrity and uniaxial tensile parameters
	Heat exchangers	Structural integrity and uniaxial tensile parameters
Big mechanical components		
	Pumps, fans, etc. casings	Structural integrity and uniaxial tensile parameters
Auxiliary & back-up systems		Structural integrity and uniaxial tensile parameters

Material/Component		Description of application
	Auxiliary boiler components in the nuclear power plant	Structural integrity and uniaxial tensile parameters
	Ash plant components in the coal power plant	Structural integrity and uniaxial tensile parameters

2.2.8 Advantages and disadvantages of the SPT technique

This sub-section is summarised in Table 2-4, which describes the advantages and disadvantages of SPT as compared to the conventional methods of mechanical testing that were summarised in the Literature Review.

Table 2-4: Advantages of the SPT technique and comparison to conventional mechanical testing techniques [1], [26], [28], [30-34]**.**

Property estimation	Advantages of the SPT technique	Disadvantages/comparison to conventional mechanical testing
Charpy FATT	Less test material required than CVN specimens test	It is material dependent but a group of similar materials can be expected to have similar empirical constants (e.g. CrMoV steels)
	Fracture energy is determined during the estimation of FATT	The data can be scattered and empirical constants can be affected by this scatter
	No prior knowledge is required to correlate T_{SP}-FATT	T_{SP} can be very challenging to correlate, especially if it is at significantly low temperatures, below -196°C. The specimen is normally cooled using LN_2
Uniaxial tensile stress-strain parameters	A single test of ϕ8 mm x 0.5 mm thick specimen can be used to estimate required stress-strain parameters. Quasi non-destructive test.	Elastic-plastic materials require more than one model to estimate less than 1% error of these parameters. For example, using Gurson models for more ductile material and a Weibull model for brittle material or a Ramberg-Osgood model. ±5-10% error margin is to be expected for predicted parameters if one model is used

Property estimation	Advantages of the SPT technique	Disadvantages/comparison to conventional mechanical testing
		to characterise both elastic and plastic regions on the stress-strain curve.
Fracture toughness, K_{IC}	Single test required to estimate K_{IC} (8 mm diameter x 0.5 mm thick) specimen. Quasi non-destructive test	Correlation has ±25% error band as compared to 10% error band for CTOD specimen
	Direct fracture toughness test, eliminates the estimation of K_{IC} from lower bound K_{IC}-FATT correlation from traditional CVN test	Based on the interpretation of the SPT data from EPRI approach and there is no standard that can be adopted
Test condition	Test can be carried out at an interested condition such as determining stress-strain parameters at certain temperature	Not always possible to test at any temperature when performing a normal mechanical test
	Tests can be carried out on a live system (with limitations) such as turbine casings and pipes with large wall thickness (non-destructive)	Not possible to test on a live system when performing normal mechanical testing. A large amount of test material is required and it is therefore destructive.
Economic benefit	Test is easy to carry out and is relatively low cost	Conventional mechanical testing requires weld repair after extraction of test samples, and the repair incurs labour and requalification (radiographic testing) costs.
Safety	It is fairly safe to carry out the SPT and it is also safe for the components or materials that are tested. There is a low risk of compromising the structural integrity of the component.	Mechanical testing is normally destructive and damaging to the components or materials that are tested.

2.3 Evaluation of embrittlement using the SPT technique

Embrittlement can be evaluated by using mechanical testing (loss of ductility and toughness) or metallurgical testing (microstructural change). In this research, mechanical testing techniques such as uniaxial tensile, CVN and fracture toughness testing are used to correlate the SPT results as a means of quantifying embrittlement.

Table 2-5: Mechanical test technique to evaluate embrittlement.

Mechanical test	Parameters evaluate	Sign of embrittlement
Uniaxial tensile test	Yield stress, UTS, elongation	Reduction in ductility (elongation)
CVN	Absorbed energy DBTT or FATT	Reduction in absorbed energy and increase in change of FATT or DBTT
Fracture toughness	K_{IC}	Reduction in fracture toughness
SPT	Yield stress, UTS, elongation, absorbed energy, DBTT or FATT and K_{IC}	Decrease in all parameters except for FATT or DBTT, increase in transition temperature is expected

2.3.1 Adopted approaches to evaluate embrittlement

This research adopted two approaches, namely, the *FATT*/*DBTT* approach based on work from authors in papers [9–12] and the EPRI approach of the SPT from technical reports [1],[13–15]. The two approaches (*FATT* and EPRI) can be used to estimate the mechanical parameters mentioned in Table 2-5.

2.3.2 FATT approach to estimate K_{IC}

The SPT are carried out at different testing temperatures, normally from room temperature to liquid nitrogen temperature (-196°C), in order to determine the SPT transition temperature, T_{SP} [6], [24]. Each test (out of seven tests as per CWA 15627) will consist of a load displacement curve (LDC), with a decrease in ductility as the test temperature decreases. The integral of LDC is energy absorbed (SPT energy, E_{SP}) by sample up to a fracture point as seen in Figure 2-26 [1], [26], [20], [31]. The fracture point is located by a 10% drop in load past the peak load, as recommended by EPRI [19], and is normally determined using FEM. The CWA 15627 recommends the fracture point to occur at a 20% drop past the peak load

[18]. It is important to note that T_{SP} is material dependent and can be empirically correlated to Charpy *FATT* and K_{IC} [6]. T_{SP} is expected to occur at very low temperatures as compared to Charpy *FATT*. There are a few reasons for this behaviour, namely: i) the size effect of the SPT specimen being smaller than the Charpy specimen, ii) the slower strain rate (almost static) used on the SPT as compared to the quick CVN test and iii) possibly the notching on the CVN that is absent on the SPT specimen [35]. *FATT* as a parameter has been used to limit significant component operating stresses to always be at temperatures above the *FATT*, in order to minimise the potential for brittle fracture [36]. Since the $\Delta FATT$ is directly proportional to embrittlement and it tends to increase as the specimen degrades due aging, it is desirable to have the *FATT* as low as possible [23], [31] for steels that operate above room temperature.

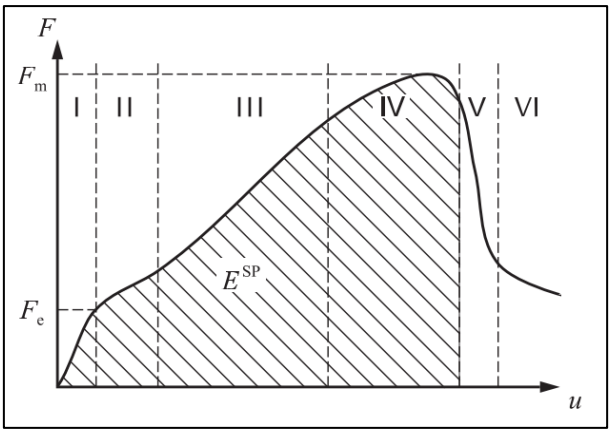

Figure 2-26: E_{SP} – Small punch energy, area under LDC [23]**.**

FATT becomes unknown as soon as the material is thermally exposed and it can be monitored by observing the flaw tolerance through empirical correlation [26]. Through the flaw tolerance, the empirical correlation to find fracture toughness can be obtained [26]. According to EPRI [1], there are two sources of material properties uncertainty that contribute to the level of operating conservatism that may be excessive and prohibitively costly:

- The material *FATT* is unknown because (1) original material test records are not available, (2) it was never tested, (3) there was embrittlement of the mechanism in-service, such as temper embrittlement, or (4) *FATT* at a concern area cannot be reliably estimated due to unknown spatial variation of *FATT*.
- The empirical correlation between *FATT* and fracture toughness, K_{IC}, is uncertain and is therefore interpreted conservatively.

2.3.2.1 Correlating T_{SP} with charpy FATT using small punch energy

T_{SP} is correlated with Charpy *FATT* to determine the fracture toughness (K_{IC}). This is done through extensive laboratory experimental tests that are carried out between -196°C and room temperature (see Figure 2-27). T_{SP} is determined using the code of practice CWA 15627:2007 [18], and Charpy *FATT* is determined using ASTM E23 [37] and is correlated by the following general equations.

$$T_{SP} = \alpha \cdot FATT$$

Equation 2-4: Coefficient of transition temperature for T_{SP} correlated to charpy FATT [20]**.**

Where α is a coefficient variable which is material dependent ($0 < \alpha < 1$). Coefficient $\alpha = 0.4$ for ferritic steel as has been found by Mao and Kameda, however Cheon and Kim prove that the coefficient lies between 0.36 and 0.59 [24].

$$T_{SP} = A + B \cdot FATT$$

Equation 2-5: T_{SP} correlated to charpy FATT [2]**.**

Foulds and Viswanathan [20] have offered T_{SP}-*FATT* correlations for low alloy steels, given in Table 2-6.

Table 2-6: T_{SP}-FATT correlation for low alloy steam turbine steel [20]**.**

Steel type	Correlation
CrMoV steam turbine rotor	FATT (°C) = 457.61 + 2.536T_{SP} (°C)
Low alloy NiCrMoV	FATT (°C) = 363.80 + 2.312T_{SP} (°C)
CrMo (1Cr ½Mo, 2 ¼Cr 1Mo)	FATT (°C) = 506.96 + 2.857T_{SP} (°C)

T_{SP}-*FATT* correlation has a linear relationship as shown above in Table 2-6 and Figure 2-27. There are other mechanical properties such as uniaxial stress strain properties that can also be estimated when using this *FATT* approach prior to predicting fracture toughness. T_{SP} and *DBTT* are correlated by plotting mean energy per upper shelf energy in percentages against each test temperature. A 50% *DBTT* line can be drawn to cut both the SPT and CVN transition temperature curves. The following limitation of estimating *FATT* using the SPT technique have been noted in the paper of Foulds et al [1]:

- The scatter in the correlation can be large enough to make the choice of the lower bound *FATT* estimate potentially conservative.

- This approach relies on an empirical correlation that is material dependent; this means that the application is limited to the alloys or class of alloys for which the correlation has been developed.
- Conservatism can be introduced into flaw tolerance-based integrity assessment when estimating K_{IC}.

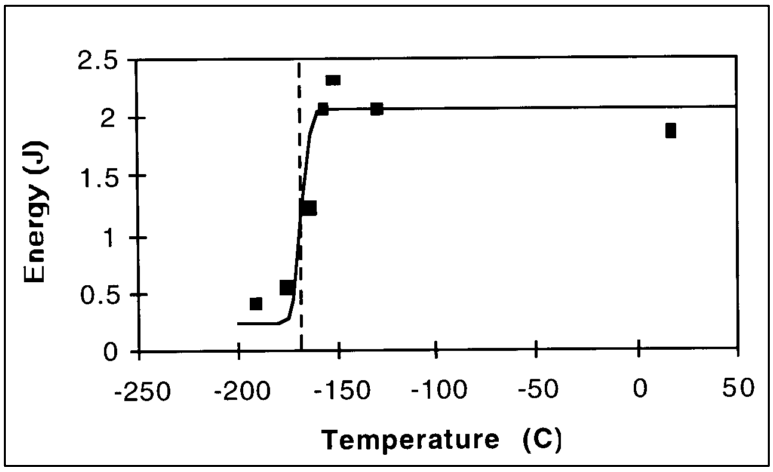

Figure 2-27: T_{SP} for unirradiated Beaver Valley plate A533B [6]**.**

2.3.2.2 Uniaxial stress-strain parameters using FATT approach

With reference to Figure 2-26 and Figure 2-28, the LDC can be used to extract uniaxial tensile properties as shown in the work of Rodriguez [24]. Figure 2-26 illustrates a yield point on LDC whereby the yield strength of the SPT can be calculated using Equation 2-6 and UTS can be calculated using peak load by applying the same linear relation that is expected for low carbon steel materials.

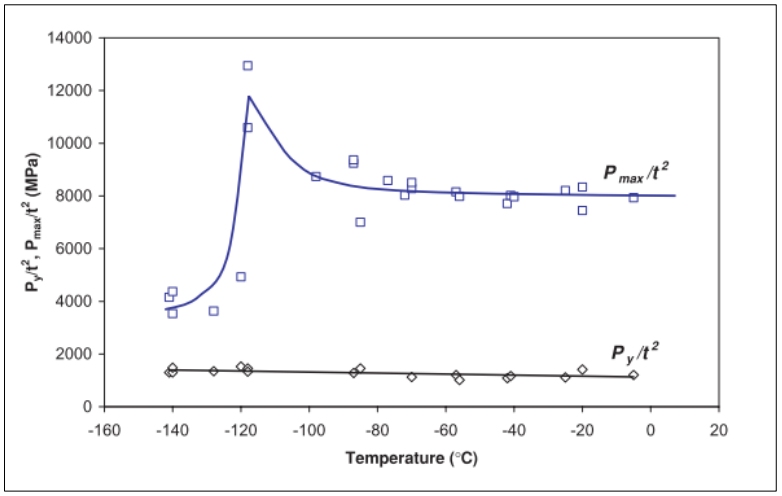

Figure 2-28: Variation of SPT (σ_y and σ_u) with temperature AE460 [24]**.**

$$\sigma_y = \alpha_1 + \alpha_2 \cdot \left(\frac{p_y}{t^2}\right)$$

Equation 2-6: SPT yield stress [24]**.**

Where σ_y = yield stress, α_1 and α_2 are empirical constants that are material dependent, $P_y = F_e$ load at yielding and lastly, t = specimen original thickness.

$$\sigma_u = \beta_1 + \beta_2 \cdot \left(\frac{p_m}{t^2}\right)$$

Equation 2-7: SPT ultimate tensile strength [24]**.**

Where σ_u = yield stress, β_1 and β_2 are empirical constants that are material dependent, p_m = maximum load and lastly, t = specimen original thickness. Tensile elongation can be found by using displacement at maximum load, d_{max}, displacement at fracture, d_f. fracture strain, ε_f is given as: Where t = original thickness and t_f = thickness at final fracture

$$\varepsilon_f = ln(t/t_f)$$

Equation 2-8: Fracture strain [24]**.**

Figure 2-28 shows a typical uniaxial tensile property graph that is achieved at a range of testing temperatures. It also shows the linear relationship that is expected as well as unstable crack growth ($\left(\frac{p_{max}}{t^2}\right)$ graph) at low temperature (below -180°C) at which the material has become brittle.

2.3.2.3 Estimating K_{IC} using FATT approach

T_{SP} can be obtained by carrying out the SPT at a wide range of test temperature. Applying the correlated equation between T_{SP} and *FATT* shown in Table 2-6, *FATT* can be estimated with its impact energy by using energy curves of the SPT. The advantage of this approach is that it gives ductile to brittle transition parameters, i.e. temperature, E_{SP} (small punch fracture energy), estimated impact energy and K_{IC} value correlated from impact energy.

Researchers in the past have developed empirical approaches to correlate Charpy impact energy (*FATT*) with plane strain fracture toughness K_{IC} [2]. The ASTM standards (other equivalent standard techniques can also be used), ASTM E23 for notched bar impact test and ASTM E399 for fracture toughness were used to develop these empirical correlations in Table 2-7 [2].

This approach allows a quantitative assessment of the critical flaw size and permissible stress and give, necessary toughness information related to operating conditions [2]:

- Transient conditions (Lower shelf energy related to brittle fracture)
- Operating conditions (Upper shelf energy related to ductile fracture)

Table 2-7: Correlation of impact energy/transition temperature and fracture toughness [2]**.**

Correlation	Comments
Barsom-Rolf	
$K_{IC}^2/E = 2(CVN)^{3/2}$	σy = 269 to 1696MPa static test
$K_{IC}^2/E = 0.22(CVN)^{3/2}$ [38]	CVN energy = 3 to 82J
$K_{IC}^2/E = 2(PCVN)$	Pre-cracked Charpy test
Sailors-Corten	
$K_{IC}^2/E = 8(CVN)\ or\ K_{IC} = 15.5(CVN)^{1/2}$	Static test
$K_{Id} = 15.873(CVN)^{3/8}$	Dynamic test (high strain-rate)
$K_{IC} = 14.6(CVN)^{1/2}$ [38]	7 to 68J
Marandet-Sanz	
$K_{IC} = 20(CVN)^{1/2}$	$T_{K_{IC}} at\ K_{IC} = 100MPa\sqrt{m}$
$T_{K_{IC}} = 16.2 + 1.37T_{28}$	$T_{28} at\ CVN = 28J$
Begley-Logsdon	
$K_{IC}\ at\ FATT = {}^1/_2\,(K_{IC}\ from\ Rolf - Novak\ relationship + 0.5\sigma_y)$	$\sigma_y = 269\ to\ 1696MPa$
Lwadate-Watanabe-Tanaka	
$K_{IC}/K_{IC-US} = 0.0807 + 1.962\exp[0.0287(T - FATT)]$	For -40°C > (T-FATT)
$K_{IC}/K_{IC-US} = 0.623 + 0.406\exp[-0.00286(T - FATT)]$	For 350°C > (T-FATT) > -40°C

Table 2-8 can be used as an important aid to component assessment for operating condition, which is normally in the upper shelf energy parameters (permissible stresses and ductile fracture) [2].

Table 2-8: Correlation between upper shelf impact properties (ductile condition) and fracture toughness [2]**.**

Correlation	Comments
Rolf-Novak	
$\left({}^{K_{IC}}/_{\sigma_y}\right)^2 = 5[(CVN/\sigma_y) - 0.05]$	σ_y = 269 to 1696MPa static test
Wullaert-Server	
$K_{Jd} = 20(DVN)^{1/2}$	σ_y = 345 to 483MPa
$K_{JC} = 2.1(\sigma_y \cdot CVN)^{1/2}$ or $\left(K_{JC}/\sigma_y\right)^2 = 4.41(CVN/\sigma_y)$	Dynamic J-integral initiation All loading rates with appropriate σ_y
Lawrence Livermore Laboratory	
$\left(K_{JC}/E\right)^2 = CVN(9.66 + 0.04\sigma_y)$	$K_{JC} = (E \cdot J_{IC})^{1/2}$ or $K_{JC} = (E \cdot J_{Id})^{1/2}$
Ault-Wald-Bertolo	
$\left(K_{IC}/\sigma_y\right)^2 = 1.37\left(CVN/\sigma_y\right) - 0045$	High strength, low toughness steels
Lwadate-Karushi-Watanabe	
$\left(K_{IC}/\sigma_y\right)^2 = 0.6478(CVN/\sigma_y - 0098)$	Pressure vessels steel

2.3.3 EPRI approach to estimate K_{IC}

The Electric Power Research Institute (EPRI) is an American institute that researches industrial challenges that are faced by power plants worldwide. EPRI developed an approach to quantify direct fracture toughness using the SPT in the mid-1990s. EPRI's approach for K_{IC} estimation was adopted from a summarised continuum fracture toughness concept by researchers from the US Naval Research Laboratory [1].

The concept was developed to estimate the fracture initiation toughness by making use of strain energy density, also referred to as 'critical strain energy density', W_C, as a fracture

criterion to determine fracture toughness. This fracture criterion occurs at a crack initiation and can be identified using a high magnification video camera or acoustic emission sensors. Figure 2-29 illustrates identified points of crack initiation on a load displacement curve (LDC) of the SPT.

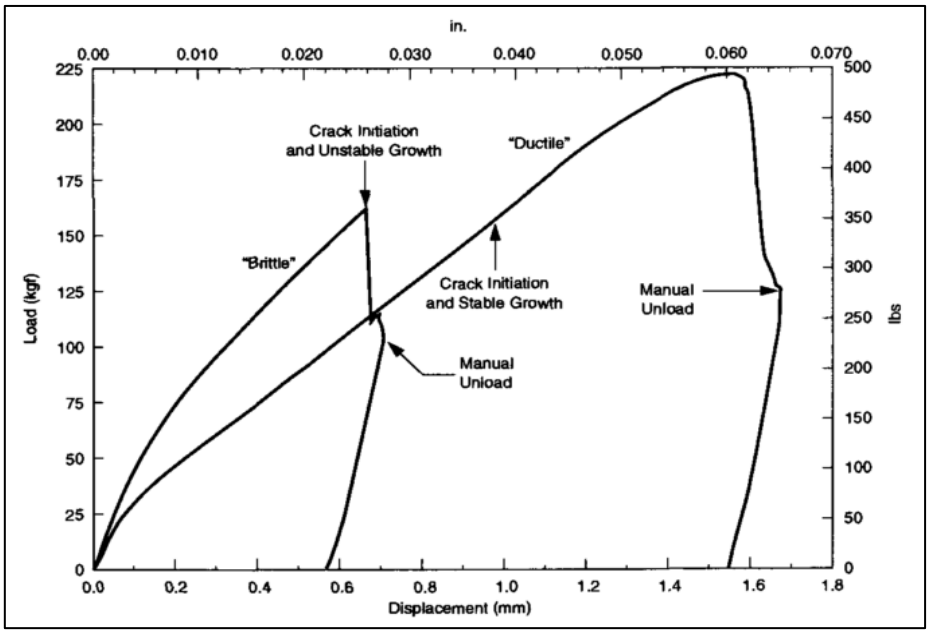

Figure 2-29: Examples of small punch load-displacement curves for macroscopically ductile and brittle behaviour; note point of crack initiation [26]**.**

$$W_c = \sum_{i,j} \int_0^{(\varepsilon_{ij})_c} \sigma_{ij} d\varepsilon_{ij}$$

Equation 2-9: Strain energy density [1]**.**

Where σ_{ij} and ε_{ij} are stress and strain, $(\varepsilon_{ij})_c$ is a critical fracture condition, the summation indicates that the energy density, which is energy per unit volume is the sum of integrals of all stress–strain components.

According to a report by EPRI [1], this concept resolved the limitation that the previous developed approaches had at the time (in 1989), such as: (a) mathematical prediction of stress at crack tip, strain and strain energy density associated with J-integral as a failure criterion, (b) failure criterion which is not limited by the local deformation prior to fracture when dealing with a material with a large strain and (c) measurements of conventional fracture parameters or criteria require that a crack is present in the test specimen.

The EPRI approach ia a model that is developed in the following stages [1]:

- Stage I: perform the SPT to obtain LDC,
- Stage II: estimate uniaxial tensile stress-strain parameters (e.g. yield stress, etc.),
- Stage III: compute strain energy density at crack initiation of the SPT specimen,
- Stage IV: model compact tension specimen to compute strain energy density at crack tip open noted and equate it to the noted/computed strain energy density from Stage III, i.e. $W_{SP} = W_{CT,}$
- Stage V: determine the load that corresponds to W_{CT} and
- Stage VI: determine fracture toughness, J_{IC} and K_{IC} the load found in Stage V.

These stages are explained below in details with figures generated to aid the explanation, Figure 2-30 illustrates how the EPRI approach/model works in determining the fracture toughness from a single SPT specimen. This approach is reasonably accurate, with an error band of ±5% of stress at given strain and a ±25% error bounding line of estimated K_{IC} as compared to the ±50% error bounding line of estimated K_{IC} when using the *FATT* approach [1],[34].

2.3.3.1 EPRI approach to estimate uniaxial tensile stress-strain parameters

A constitutive model used in the EPRI approach is a modified Ramberg-Osgood model that accommodates dual yielding [34]. This model is used to describe the plastic mechanical behaviour of the material and it consists of four parameters: E, D, n and ε_{py}. The model is mostly used in low alloy steels and is proven to be a good tool to estimate the stress-strain parameters using the SPT LDC. The model is defined by the following behaviour:

$$\sigma = \varepsilon \cdot E \qquad \text{for} \qquad \varepsilon < \varepsilon_{ey}$$

Equation 2-10: Ramberg-Osgood for perfect elastic material [1]**.**

$$\sigma = \sigma_y \qquad \text{for} \qquad \varepsilon_{ey} \leq \varepsilon \leq \varepsilon_{ey} + \varepsilon_{py}$$

Equation 2-11: Ramberg-Osgood for elastic-plastic material [1]**.**

$$\sigma = D(\varepsilon - \varepsilon_e)^{1/n} \qquad \text{for} \qquad \varepsilon \geq \varepsilon_{ey} + \varepsilon_{py}$$

Equation 2-12: Modified Ramberg-Osgood for elastic-plastic dual yielding material [1]**.**

Where:

- ε is the total strain, ε_e is elastic strain, ε_{ey} is strain at yield point and ε_{py} is plastic strain accumulated during dual yielding,

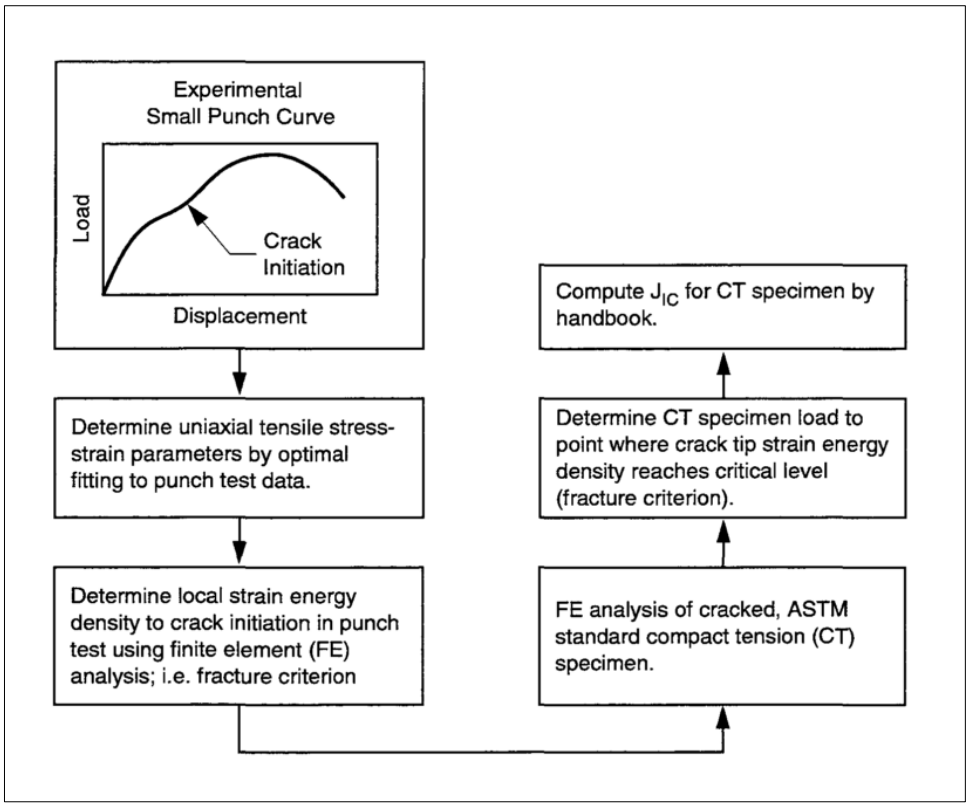

Figure 2-30: EPRI approach to determine fracture toughness from a single test [1]**.**

- σ is stress and σ_y is stress at yield point,
- D is power law hardening constant,
- n is strength coefficient and exponent

Numerical parameters *D* and *n* are expected to change with ageing of the material, i.e. both parameters will increase with ageing of the material (a sign of hardening in the material and possible embrittlement forming). A set of database LDCs of the same alloy steels (exposed to different temperatures, stresses and ageing) can be generated with different parameters, *D* and *n*, as shown in Figure 2-31. Figure 2-31 above illustrates how the experimental LDC is fitted and compared to the already correlated database curves. Each of the curves shows different parameters, the *D* value that is the power law hardening constant and the *n* value that is the strength coefficient and exponent. The closest two matching curves that the experimental curve fits in between are chosen. These two curves are then used through the optimisation to model a new best fitting the SPT LDC, as shown in Figure 2-32. The optimisation is done by interpolating between the database curves by attempting to reduce the number of squares of residuals using Powell's Algorithm [1]. The procedure attempts to minimise the function of (observed and matching loads curves), F(X) [1]:

$$F(X) = \sum_{i=1}^{n_p} w_i [P(\delta_i, X) - T(\delta_i)]^2$$

Equation 2-13: Optimisation procedure for observed and matching LDC [1]**.**

Where:

- X is the vector of tensile stress-strain, constitutive parameters to be estimated; D, n in this instance (ε_{py} has been taken to 0.01 and 0.02 for the dual and continuous yield cases)
- P is the predicted load at each point of observed displacement, δ_i
- T is the observed (measured) load at each δ_i and
- n_p and w_i are the numbers of discrete points and associated weights used for the procedure

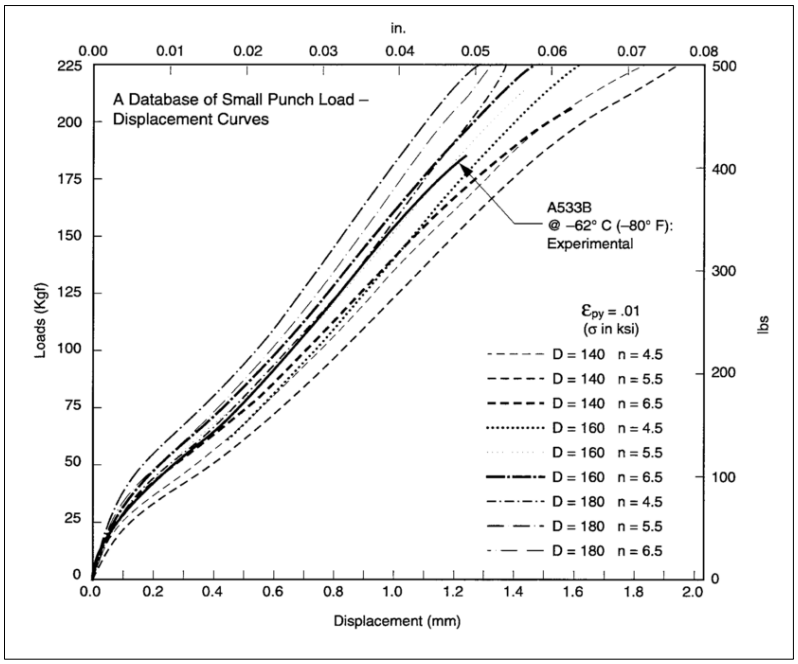

Figure 2-31: Set of the SPT LDC database [1]**.**

This procedure was developed by Failure Analysis Associates Inc. and was used to determine the Mooney-Rivlin coefficient for rubber materials and for the relaxation of moduli and characteristics times of viscoelastic materials [1]. The procedure uses a sequential unconstrained minimisation technique known as the Augmented Lagrange Multiplier Method which can handle equality and inequality constraints [1]. The SPT does not include these constraints.

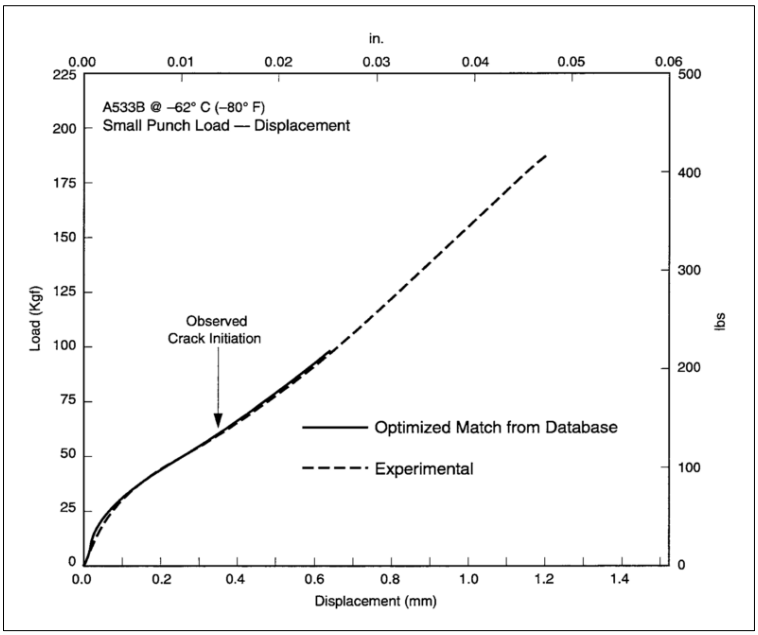

Figure 2-32: Optimised SPT LDC [1]**.**

Once the SPT experimental LDC matches the optimised database LDC, the tensile uniaxial stress-strain parameters can be called out using FEM. and Figure 2-33 below is an example of predicted tensile stress-strain parameters.

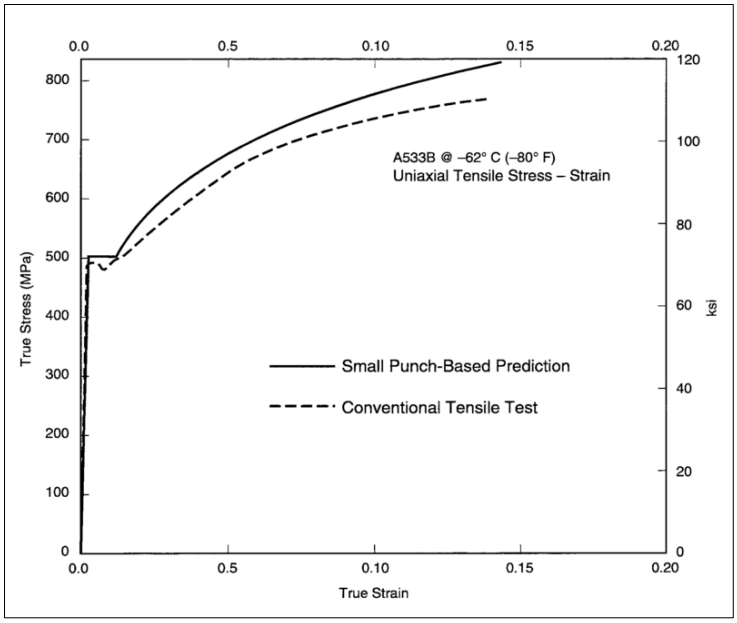

Figure 2-33: Correlation of modelled SPT stress-strain with conventional tensile test [1]**.**

2.3.3.2 Estimating K_{IC} using EPRI approach

Plane strain fracture toughness, K_{IC}, is estimated using stress-strain fracture toughness, J_{IC}, using the critical strain energy density, W_{SP}, of the SPT as a fracture criterion. W_{SP} is then

equated to modelled energy density at the crack tip of a compact tension specimen test, W_{CT}), that complies (by geometry) to the ASTM standard [1]. The load is computed at the strain energy density at the crack tip of the FEM CT specimen that equate to the strain energy density that was computed from the SPT. The procedure is explained in detail below.

2.3.3.2.1 Computing critical strain energy density (W_{SP}) from predicted the SPT true stress – true strain curve using FEM

The uniaxial tensile true stress-true strain curve is used to compute strain energy density (using FEM) up to a point of observed crack initiation in the SPT (i.e. the area under the graph of true stress-true strain curve up to a point where the crack initiates). The strain energy density computed is then termed 'critical strain energy density', W_{SP} [1]. The procedure of identifying the crack initiation is applied using a video camera mounted on the bulge surface of the specimen; the video is started simultaneously with the SPT. The crack is identified when the video is watched and marked on the LDC using the time at which the crack initiated from the start of the SPT, see Figure 2-34 below that shows crack initiation extracted from a video recorded during the SPT. It is recommended to use a video camera that is capable of 30X magnification or more [1].

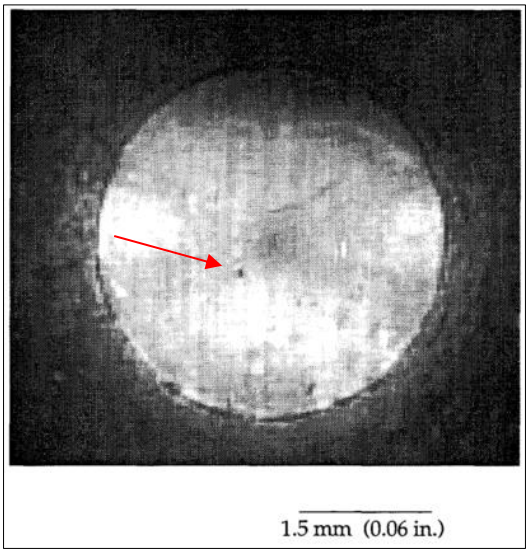

Figure 2-34: SPT specimen showing crack initiation at 1.5 mm away from centre [1]**.**

A 2D axisymmetric FEM which is displacement driven is used to compute W_{SP} at crack initiation and below is an example of the SPT FEM extracted from an EPRI paper [1].

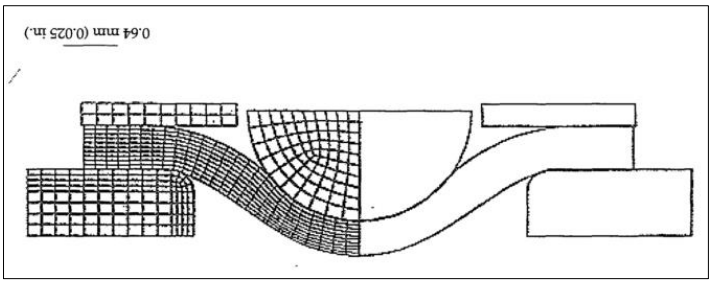

Figure 2-35: SPT FEM [1]**.**

2.3.3.2.2 Determining J_{IC} from W_{SP} fracture criterion

CT FEM with a geometry based on the ASTM E399 is used to determine fracture toughness, J_{IC}. The CT specimen's geometry is: B = 25.4 mm, W = 50.8 mm, crack length a, a/W = 0.5 mm and crack tip radius is assumed to be 0.025 mm [1]. This model is 2D plane strain and below is an example of how the model looks.

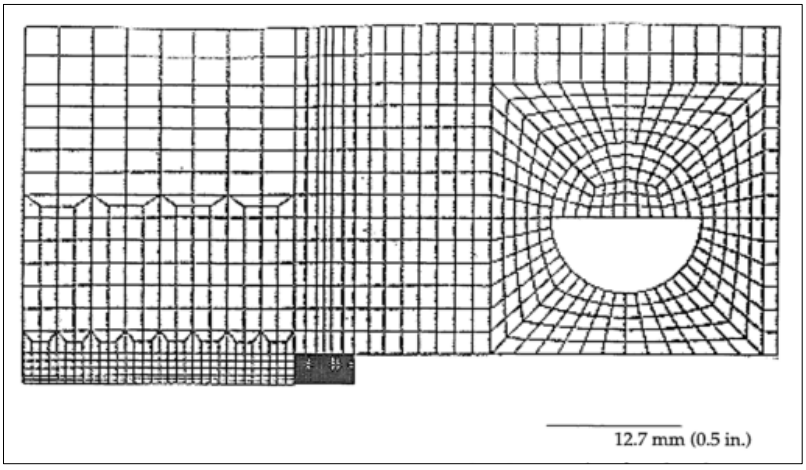

Figure 2-36: CT FEM [1]**.**

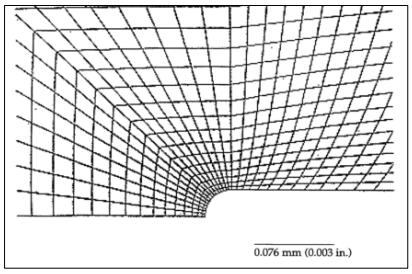

Figure 2-37: CT FEM showing tip radius of 0.025mm [1]**.**

The strain energy density is averaged over some expectedly material-dependent distance, x, ahead of the crack tip and it is denoted as W_{CT}. J_{IC} is determined directly from the load level

at which $W_{CT} = W_{SP}$ and it has also been recommended that the material dependent distance is x = 0.7Δa (Δa is a crack length) for low alloy steel.

$$K_{IC} = \sqrt{\left(\frac{E \cdot J_{IC}}{(1 - v^2)}\right)}$$

Equation 2-14: Brittle fracture toughness.

Where: E is Young's modulus, J_{IC} is the ductile fracture toughness and v is Poisson ratio.

2.3.4 Finite Element Modelling (FEM)

Finite element analysis (FEA) software packages use numerical techniques to solve complex scientific and engineering questions. FEA, which is also referred to as FEM, estimates an approximate solution by minimising error using variation methods from calculus variation [39]. FEM software packages, such as Abaqus and Ansys, have built-in popular models like the Ramberg-Osgood model, which is used when plastic deformation of metals is analysed under small displacement. Abaqus version 6.14 consists of three main analysis products: Abaqus/standard, Abaqus/Explicit and Abaqus/CFD [39].

According to Abaqus documentation [39], Abaqus/standard is a "general-purpose analysis product used for linear/non-linear problems involving the static, dynamic, thermal and electrical response of components." Abaqus/explicit is a special-purpose analysis product that uses an explicit dynamic finite element formulation and it is suitable for impact and blast problems, especially for highly nonlinear problems [39]. Abaqus/CFD, which stands for Computational Fluid Dynamics, is suitable for incompressible flow problems. Abaqus/CAE, which stands for Complete Abaqus Environment, is an interactive and graphical for Abaqus analysis [39]. Abaqus/CAE allows users to create models that can be decomposed to required meshes and assign material properties. Geometries can be imported from compatible CAD software, and load and boundary conditions are also assigned by the user. When the 'job' or analysis is completed, the user can export the required results. The results can differ slightly depending on the complexity of the model and element type used to mesh the geometry part(s), refer to Figure 2-38. Figure 2-38 shows a 2D continuum element with a full and reduced integration. Linear element CPS4 mean continuum element for plane stress analysis with four nodes and four integration points within the element and one integration point for reduced

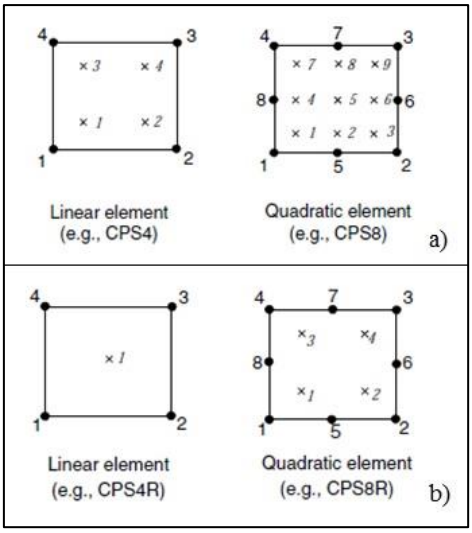

Figure 2-38: a) Fully and b) reduced integration point for linear and quadratic element.

integration (CPS4R). More integration points can improve the accuracy of the results. CPS8 is a quadratic element that doubles the nodes and integration points of the linear element type and is, therefore, more sensitive on the results than the linear element type. This study makes use of reduced integration for computational efficiency while it is known that full integration is better for crack type investigation. However, J-Integral can be used to overcome the issue of using full integration.

2.3.5 Comparison of two approaches

Table 2-9 is compiled based on two approaches. Summary of the accuracy and parameters that can be extracted from each approach are shown in the table.

Table 2-9: Comparison of research approaches [1]**,**[20]**.**

Characteristic	EPRI's approach	FATT's approach
Number of specimens required	Two specimens/temperature test and prediction can be done	Seven specimens/temperature test for a full DBTT curve (requires many specimens)
K_{IC}	Direct estimation using modelled compact tension specimen	Indirect estimation (empirical correlation using FATT parameter)
Output parameters	Uniaxial tensile stress-strain, modelled compact tension and fracture toughness properties	Uniaxial tensile stress-strain, Charpy transition temperature and fracture toughness properties

Characteristic	EPRI's approach	FATT's approach
Accuracy of estimated conventional mechanical tests	Uniaxial tensile stress-strain (within ±5-10% error margins) Fracture toughness (within ±25% bounding line)	Uniaxial tensile stress-strain (within ±10-20% error margins) Fracture toughness (within ±50% bounding line)
Limitation	Material independent, therefore no prior knowledge is required. However, the database of set of curves for similar group of material is required (for stress-strain curve estimation).	A material dependant T_{sp} FATT correlations required before prediction can be done

2.4 Guide to evaluate in-service material using SPT

EPRI [28] has developed three stages of assessing the turbine-generator material. The guide entails decision trees that analyse the benefits and risks of sampling and testing. This sub-chapter summarises the EPRI [28] guide to evaluating turbine-generator material.

2.4.1 Step 1: The preliminary benefits analysis

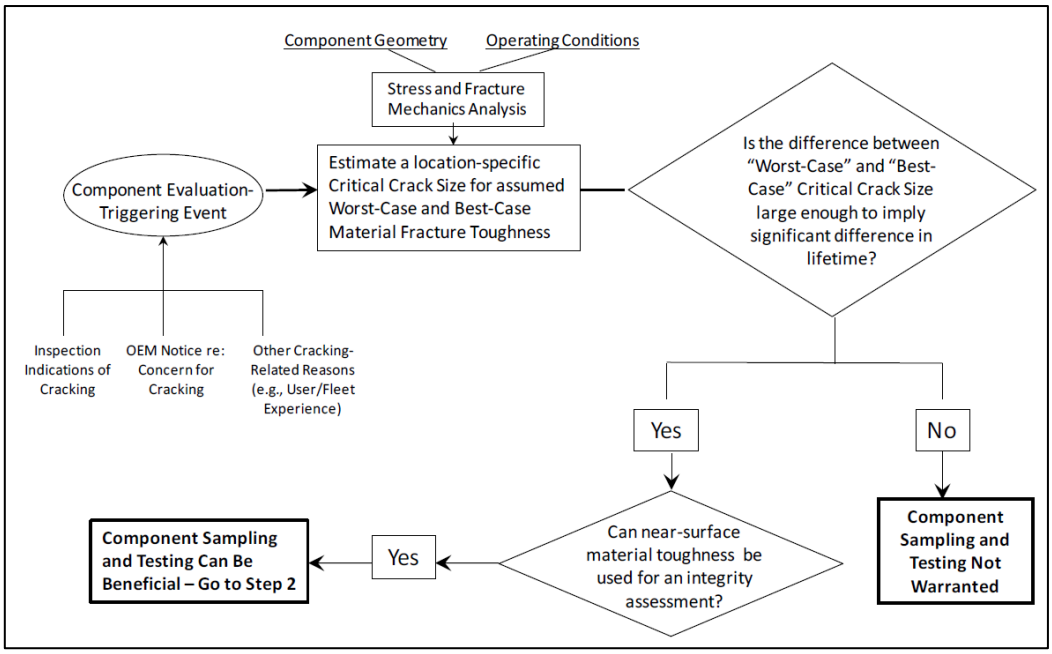

Figure 2-39: The preliminary benefits analysis (Step 1) of the roadmap of general guide to SPT of steam turbine-generator components [28].

Step 1 considers the following before removing the sample from the suspected component (component evaluation triggering event):

- Inspection indications of cracking – it will be discovered during component life assessment that is normally carried out using NDE, the NDE results can be used to determine what repairs/replacement/operation window will be or future inspection intervals. Assumptions based on the crack growth estimated from operating stresses and temperature can be used to estimate when critical crack size will be reached.
- Operating equipment manufacturer (OEM) monitors the critical components and notifies the utility/power plant owner of any crack growth of concern. The crack growth is associated with lower fracture toughness than the design fracture toughness. OEM suggests replacement such as retro fit replacement of major overhaul based on the risk of crack growth reaching critical crack size.
- Operating Experience (OE) of the plant owner which is quantified in terms of inspections data (NDEs) collected over a long period to monitor component integrity. OE will precede any consideration of sample removal.

Once these three considerations are assessed, the sample removal can be decided on based upon on the decision tree/road map as shown in Figure 2-39 which will lead to Step 2.

2.4.2 Step 2: Component sampling

Sampling is supposed to be beneficial after it is done, however, there are negative factors that can be introduced to the component. The following factors are to be evaluated when sampling:

- Accessibility – areas of interest are generally not accessible or are too risky to be sampled. LP turbine and generator rotors are known to not be affected by thermal in-service exposure on properties and therefore it would not matter where the sample was removed. Properties will, however, differ based on chemistry, microstructure and the inside to outside of the large surface of forgings. Cracking in the bore can be done by sampling near bore areas if accessible. If not, measured properties from an accessible area can be extrapolated to the area of interest.
- Sample removal effect on future integrity – it is important to note that the removal of sample may introduce local geometry-related stress intensification. If the sample removal imposes a stress condition like compressive from peening, such a condition may affect the future integrity of the component.

- Sample removal effects on future inspections – once the sample is removed where surface inspection such as ultrasonic testing (UT) is used for evaluation, UT may be ineffective and pick up flaws at sampled areas (UT at sampled turbine rotor bore). Penetrant test (PT) or magnetic test (MT) may be used as a substitute.
- Removal plan – it considers the number of samples required based on the properties that are being evaluated (e.g. Charpy *FATT* or $K_{IC=}$). Refer to Table 2-1 for the required minimum number of samples for different mechanical properties.

Refer to Figure 2-40 for more details on how the sampling should be carried out, considering risks involved and offering solutions/mitigations for such risks.

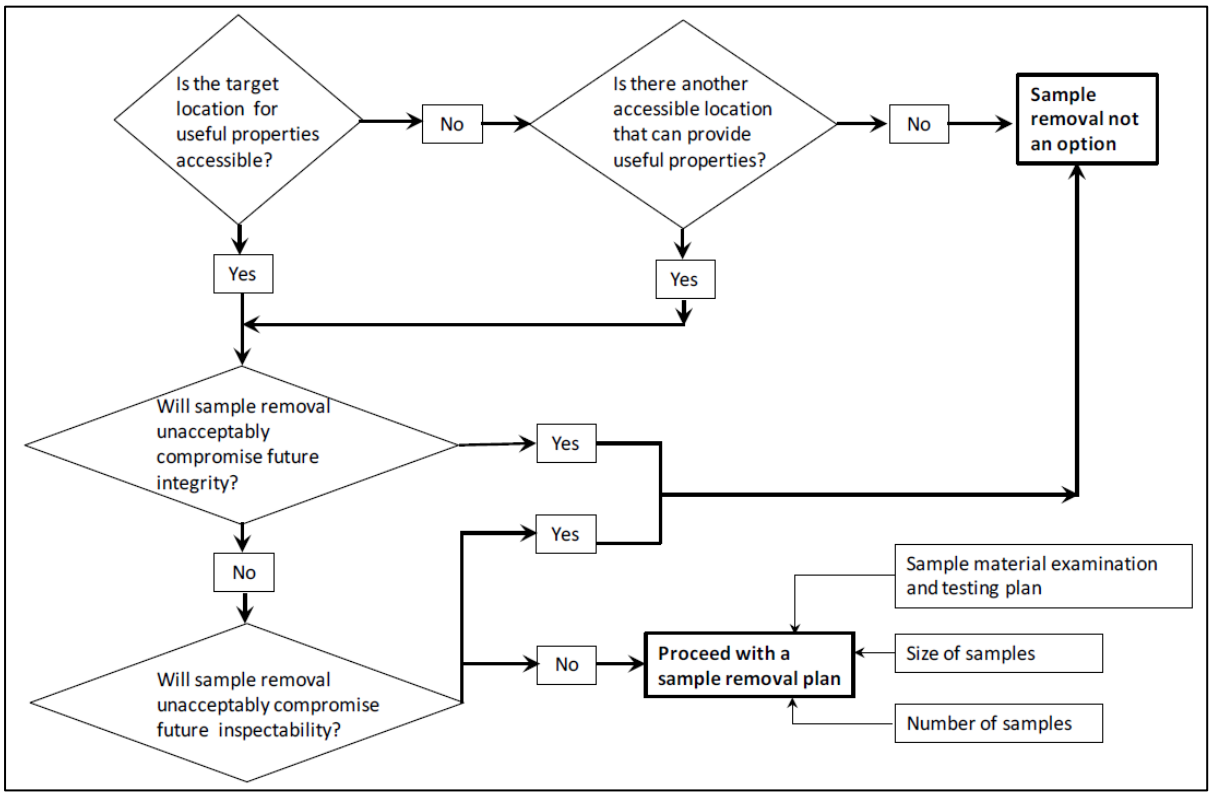

Figure 2-40: Component sampling (Step 2) of the roadmap of a general guide to SPT of turbine-generator components [28]**.**

2.4.3 Step 3: Material testing and evaluation

This stage is where the actual test is carried out and depending on what the user's interests are, both mechanical and metallurgical properties can be evaluated using sampled material. Figure 2-41 summarises the SPT outputs that can be correlated to mechanical properties.

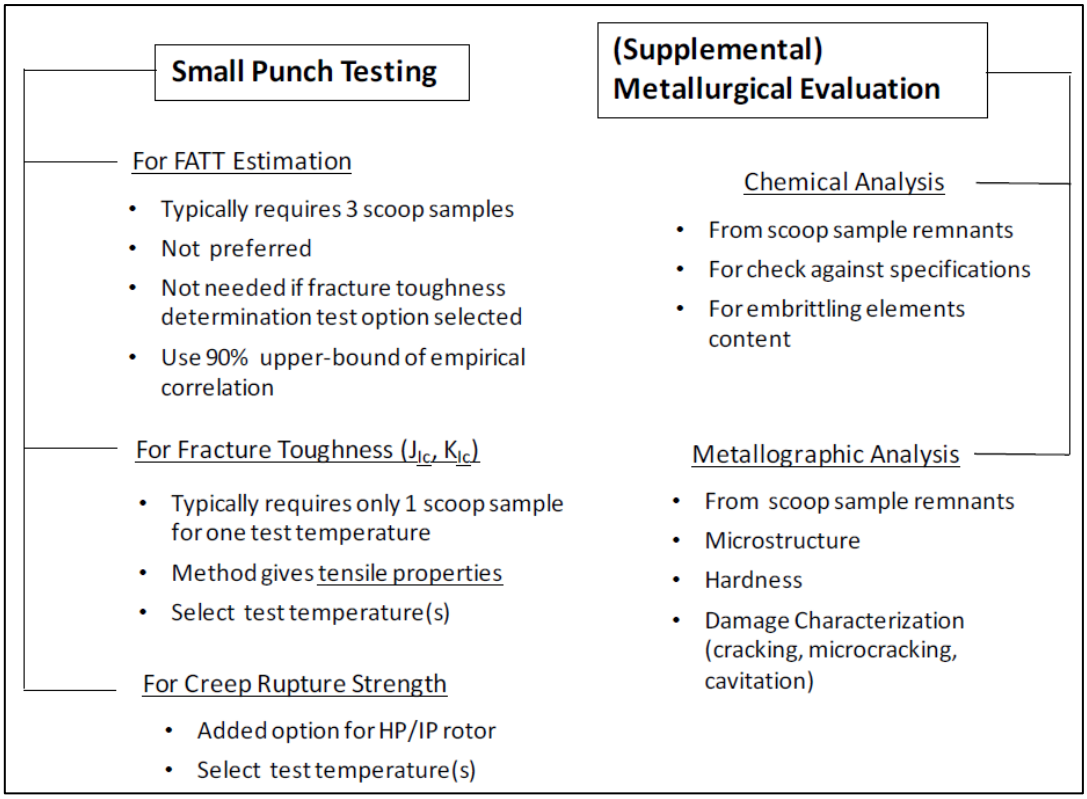

Figure 2-41: Material testing and evaluation (step 3) of the roadmap of general guide to SPT of steam turbine-generator components [28]**.**

CHAPTER 3: SMALL PUNCH TESTING EQUIPMENT

This chapter is an overview of choices made for the final concept of the SPT design. This was achieved through the literature review of old and current designs. It is, however, noted that details of these designs were limited in the literature. The most important part of the design is the working parts (covered in Chapter 2), which consist of dies and punches. These parts are supposed to have insignificant friction during testing for the sake of recording the accurate test data.

3.1 Design of the SPT rig

3.1.1 Design scope

- Design the SPT rig to be used to evaluate embrittlement of power plant steel
- Supply detailed manufacturing drawings
- Select suitable material to be used for manufacturing

3.1.2 Design user's requirements

- The SPT rig to be fitted on 5kN Instron or 200kN Zwick tensile tester,
- The SPT rig to test between LN_2 and room temperature,
- The SPT rig to comply to CWA 15627 guide,
- The SPT rig to evaluate embrittlement of power plant steels
- Easy user interface

3.1.3 Design specifications

- Comply to CWA 15627: 2007,
    - Sample dimensions (8 mm (±1%) diameter x 0.5 mm (0.5%) thickness),
    - Load-displacement data to be within 1% of error band,
    - Test temperature tolerance is ±0.25% of test temperature,
    - Constant displacement rate of 0.2-2 mm/min,
    - Receiving die to have 4 mm through hole chamfered 0.2 mm at 45° angle,
    - Working parts to be hardened at or above 55 HRC,
    - Receiving die shoulder height (i.e. 0.4 mm) to be 20% shorter than the sample height to allow for sufficient clamping,
    - Punch to have ball bearing or hemispherical head of 2-2.5 mm in diameter.

3.1.4 Design constraints

- Budget limit not to exceed R50,000.00,
- Material availability for manufacturing of the designs which will be non-corrosive and can be hardened to minimum 55 HRC,
- Time constraint was limited to less than 24 months including commissioning and testing for embrittlement.

3.1.5 Electronic hardware and software

A 6V DC supplied Linear Variable Differential Transformer (LVDT – stainless steel) was intended to be used to log the linear displacement. The LVDT consists of a stainless-steel casing that is mounted with magnetic coils and a sliding core, which induces voltage between itself and the coil in the casing. The LVDT used in this project had an analog output data in a format of induced voltage. The NI USB-6009 data acquisition card was connected to the LVDT to acquire displacement data. This card has eight single-ended analog input (AI) channels, two analog output (AO) channels, 12 digital input/output (DIO) channels, and a 32-bit counter with a full-speed USB interface (refer to Figure 3-1 and Figure 3-2).

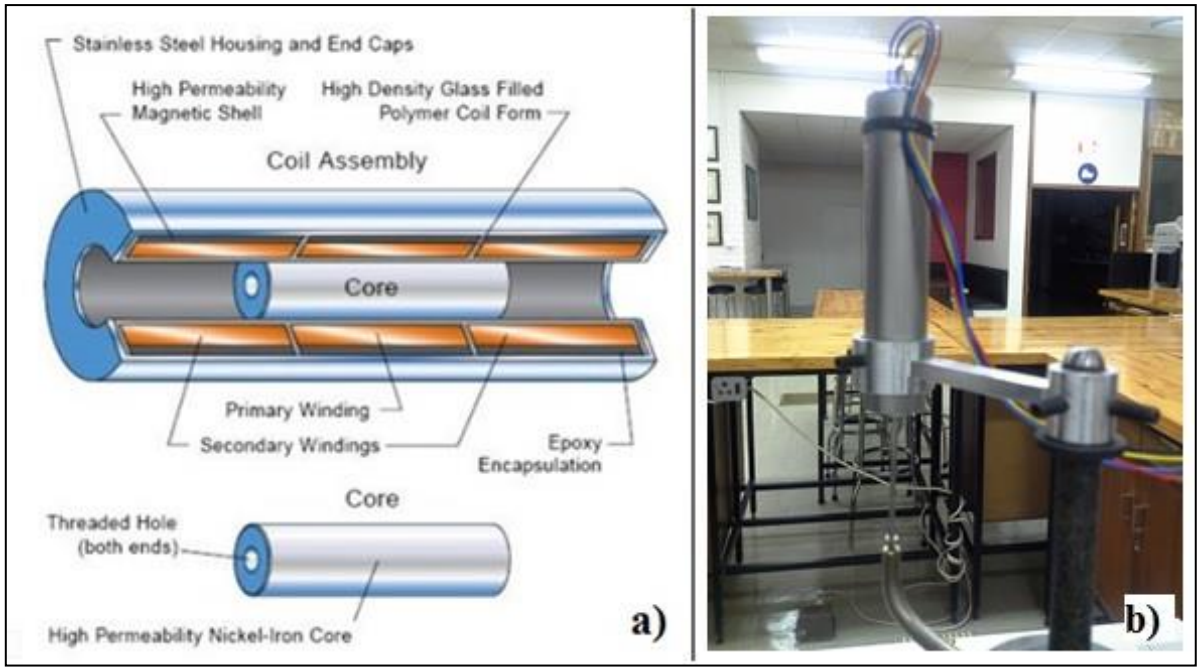

Figure 3-1: LVDT device showing: a) 3D CAD drawing [40] **and b) photograph.**

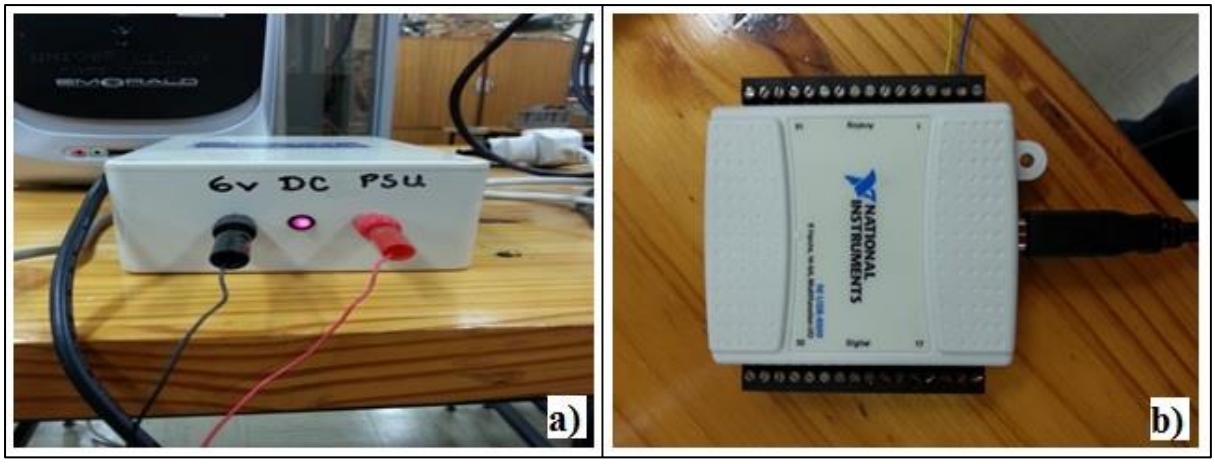

Figure 3-2: a) 6V DC supplier and b) NI USB-6009 data card.

3.2 Concept designs

The SPT design concepts were based on the reviewed designs from the literature and the CWA 15627 workshop guide. The purpose of the design concepts was to run trial experimental tests in order to improve or design a final concept based on the experience obtained from trials.

3.2.1 Concept 1: Room temperature design

This design was to be used with a Zwick 1484 200kN tensile tester machine. The rig was designed to the final dimensions as shown in Figure 3-3. The size of this rig design was concluded based on the physical size of the Zwick 1484. The purpose of this design was to determine the critical design factors that influence the SPT experimental data (compliance of the SPT rig), such as friction between moving parts, deformation experienced by the rig during test, repeatability of the SPT test results, etc.

Figure 3-3 consisted of a 3 mm deflection rod, made from round stainless steel (316L) stock bar. This rod was cut into a two-section threaded couple as shown in Figure 3-5. The deflection rod is located below the sample while remaining in contact with the sample; it is supported by a spring at the bottom and has an LVDT core rod connected at the bottom side.

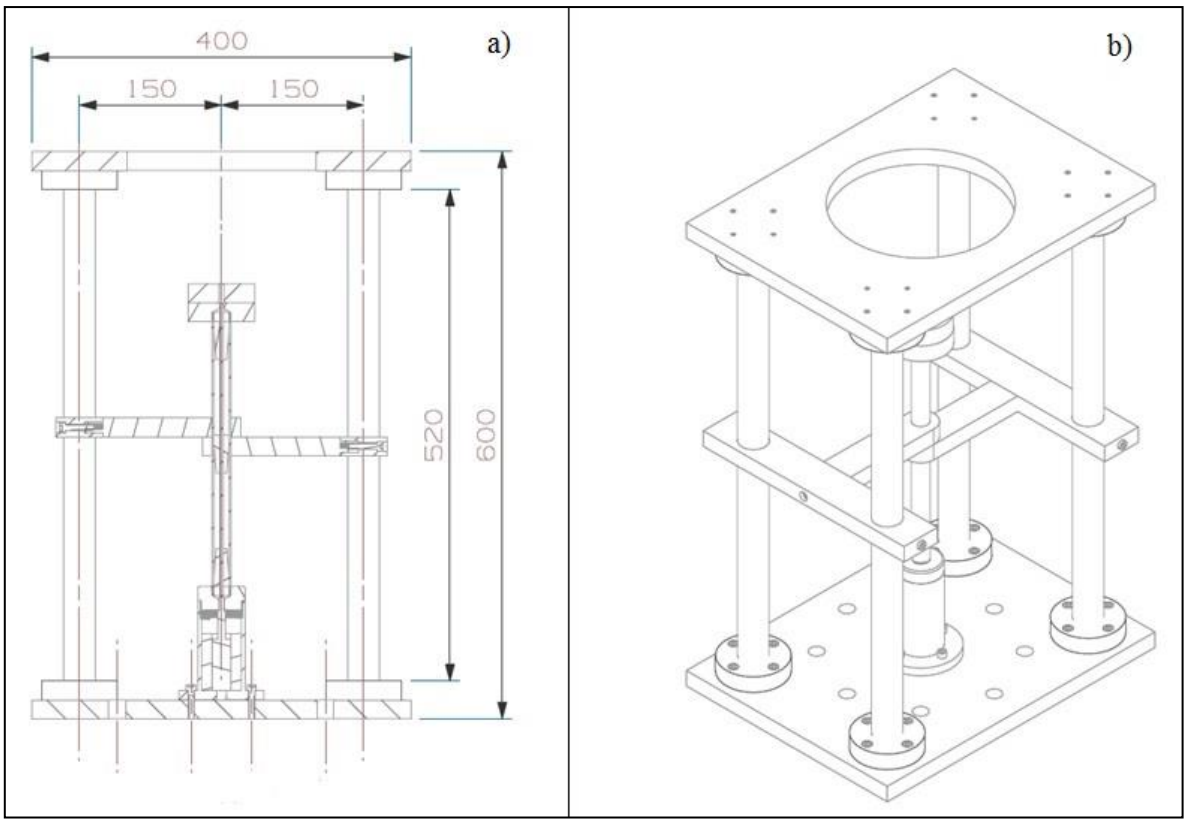

Figure 3-3: Concept-1 design: a) section-view sketch and b) 3D CAD drawing.

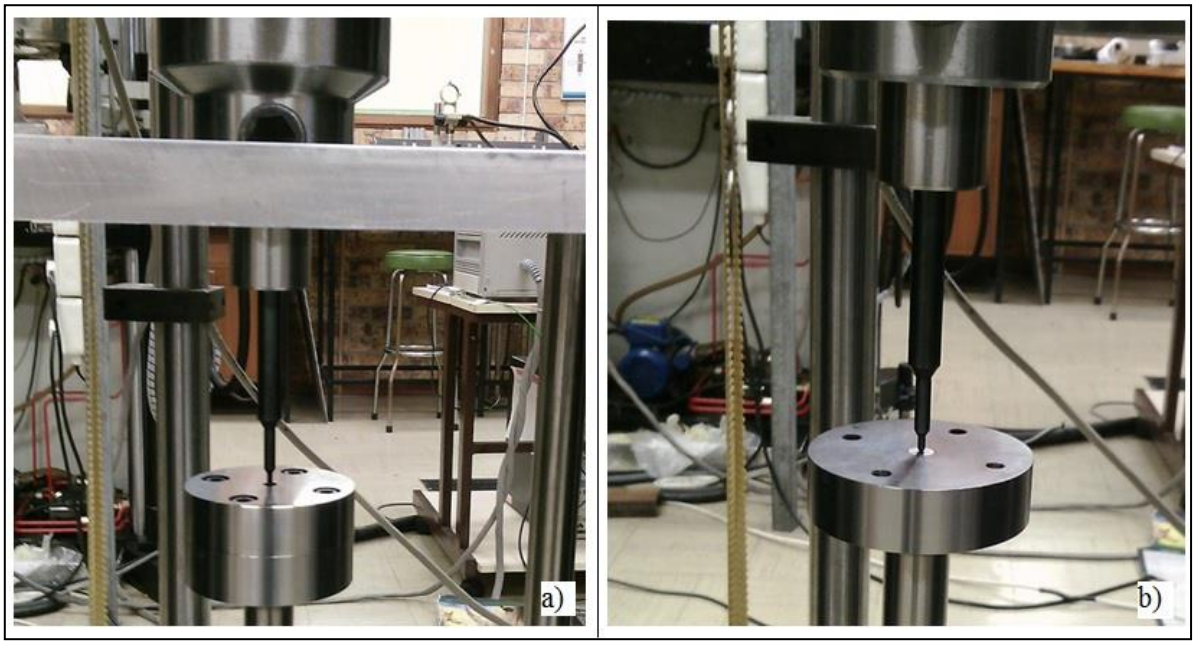

Figure 3-4: Photographs showing: a) setup during test and b) calibration of displacement.

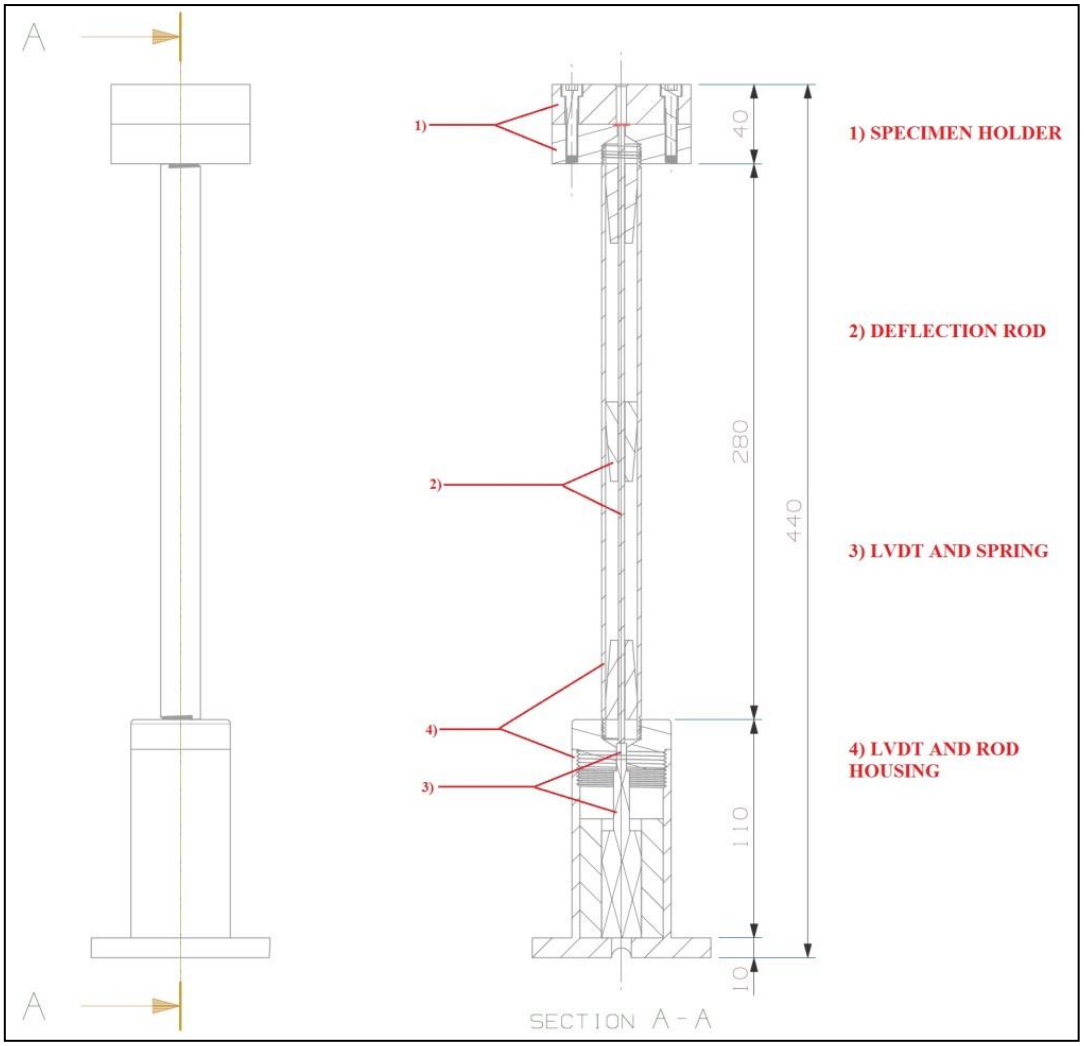

Figure 3-5: SPT sketch showing the LVDT configuration on design Concept 1.

3.2.1.1 Experimental tests

Experimental testing was carried out to validate the SPT rig for design Concept 1. The validation of the rig was done so as to identify the critical factors as discussed above. This process included the evaluation of the repeatability of tests performed and results are as shown below for the tested material.

3.2.1.1.1 Material used for validation

Aluminium and a commercial bohler steel, grade M300, were used. The bohlerM300 steel was heat treated to differentiate the plastic behaviour on untreated and treated steel. Table 3-1 illustratse the material type, grade and chemical compositions.

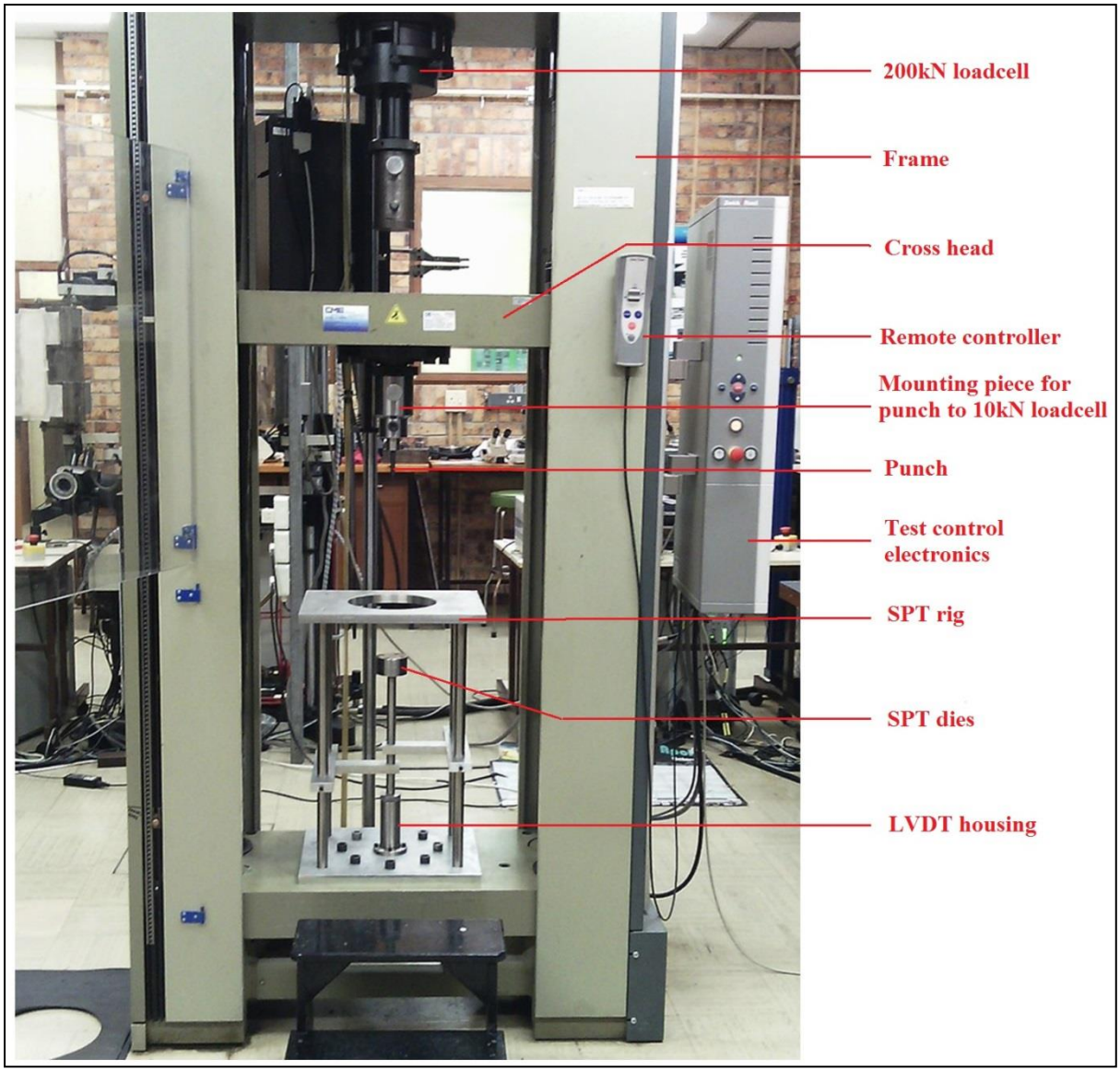

Figure 3-6: SPT rig setup for design Concept 1 (photograph).

Table 3-1: Material tested for design Concept 1.

Material type	**Chemical composition**								
Bohler M300	C	Si	Mn	Cr	Mo	Ni	Fe	-	-
	0.38	0.40	0.65	16	1	0.80	bal	-	-
Aluminium 1050	Al	Si	Mn	Cu	Mg	Fe	Zn	Ti	Other
	99.5	0.25	0.05	0.05	0.05	0.07	0.40	0.07	bal

3.2.1.1.2 Material identification

Four samples for each condition (heat treated or as received/untreated) were identified as 'sample n', n – number 1, 2, 3 and 4. Table 3-2 gives details about the heat treatment conditions of the samples tested.

Table 3-2: Material identification for design Concept 1.

Material identification	Heat treatment	Number of samples
Aluminium	-	4
Bohler M300 - tempered	650°C for 45min, vacuum cooled @20°C/h to 300°C then air cooled	8
Bohler M300 - hardened	1000°C for 1hour and quenched in oil	4

3.2.1.1.3 Specimen preparation

Specimens were machined to cylinders of 8 mm diameter and sliced using wire cut method to a final thickness of 0.7 to 0.8 mm. Polishing of samples/specimens followed in accordance to the CWA 15627 workshop guide.

3.2.1.1.4 Specimen polishing

This method required the following tools: aluminium holders, a specimen picker, a micrometre, an aluminium holder picker, crystal bond, a hot plate burner, acetone and a small specimen. This method required the aluminium holders to be heated to a temperature at which the crystal bond melts. Small specimens were placed on melted crystal bond and the hot plate burner was switched off to allow the small specimen to bond with aluminium holders (see Figure 3-6). It is important to note that this method has a success rate of 60-70% of useful polished specimens.

3.2.1.1.5 Test results

The SPT experimental tests were carried out at room temperature and each test was repeated four times, which was twice the time of the minimum required tests in accordance with the CWA 15627 guide. Each test was carried out at a constant displacement rate of 0.2 mm/min or 2 mm/min and it is specified on the results title.

Figure 3-7: Polishing tools.

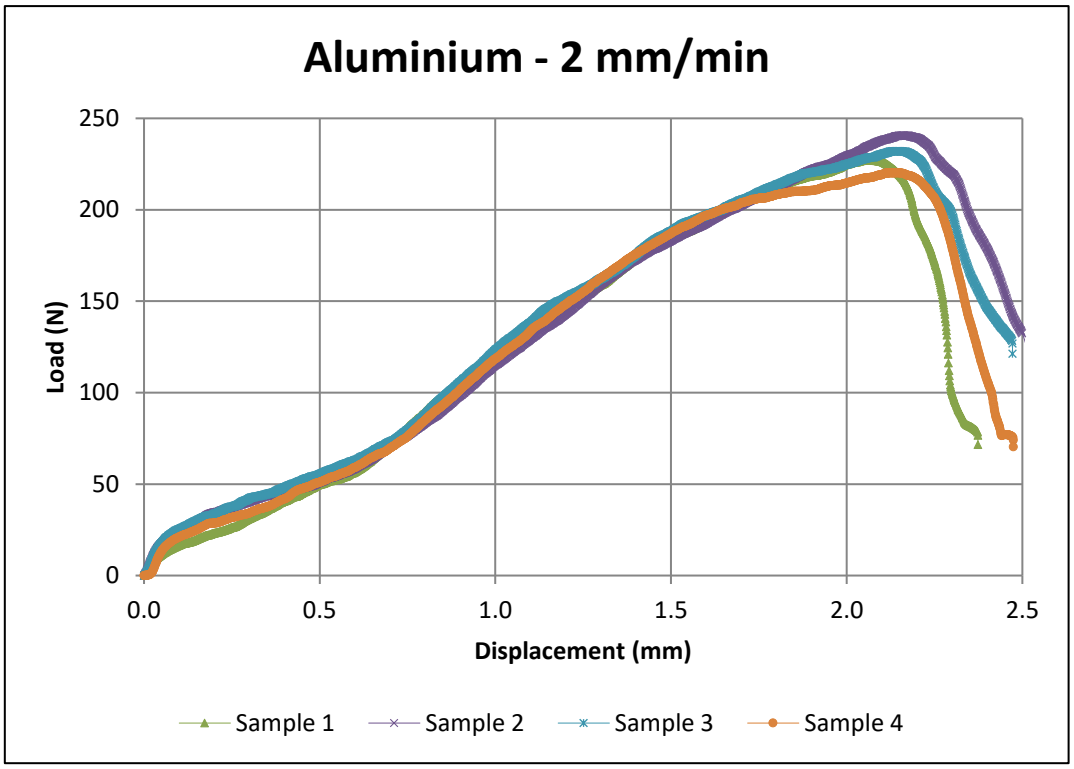

Figure 3-8: SPT LDC_{EXP} at 23°C for aluminium – 2 mm/min.

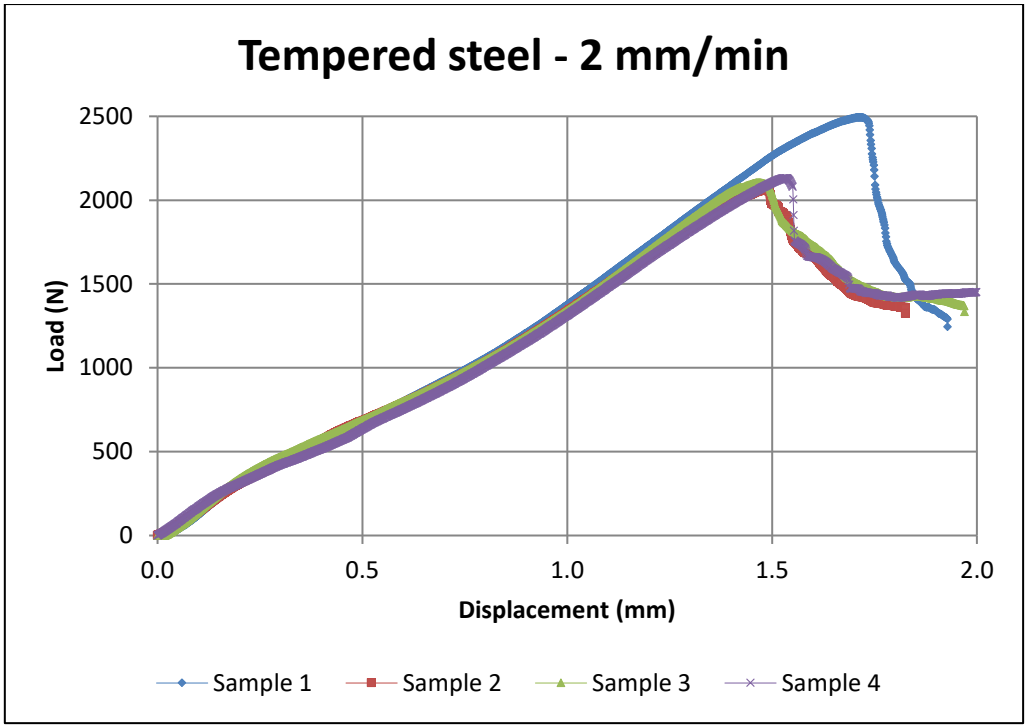

Figure 3-9: SPT LDC_{EXP} at 23°C for tempered steel – 2 mm/min.

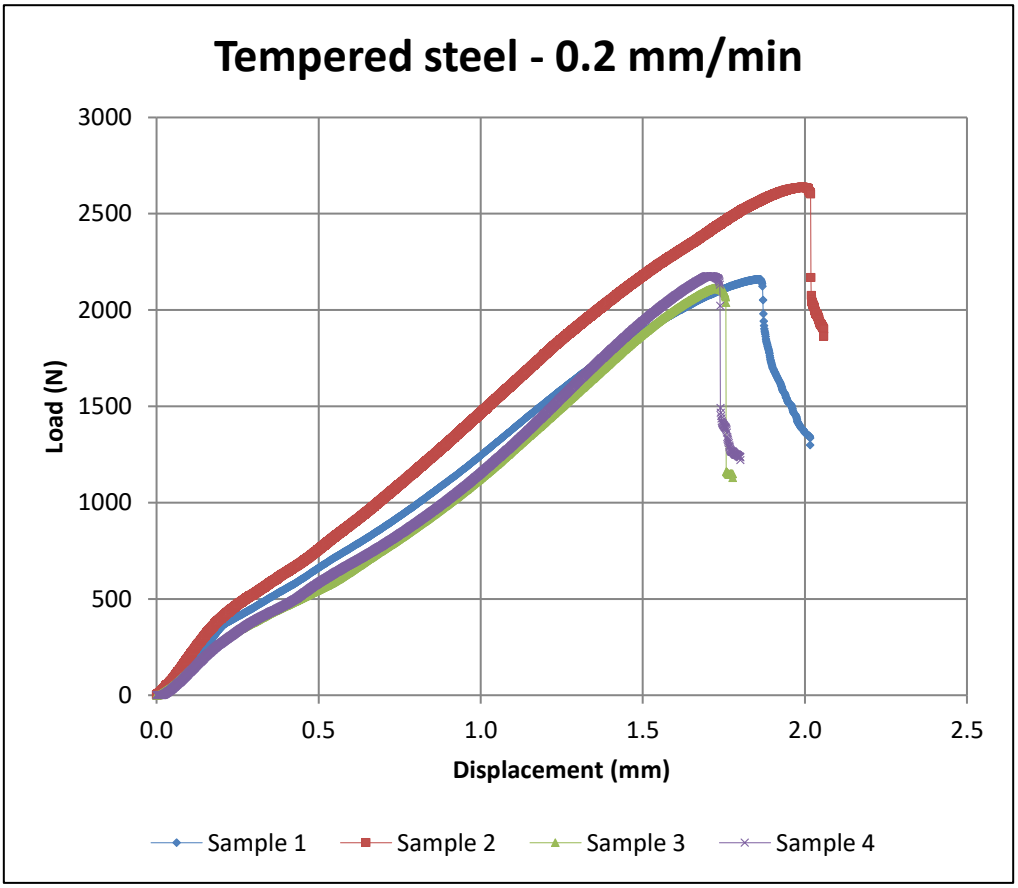

Figure 3-10: SPT LDC_{EXP} at 23°C for tempered steel – 0.2 mm/min.

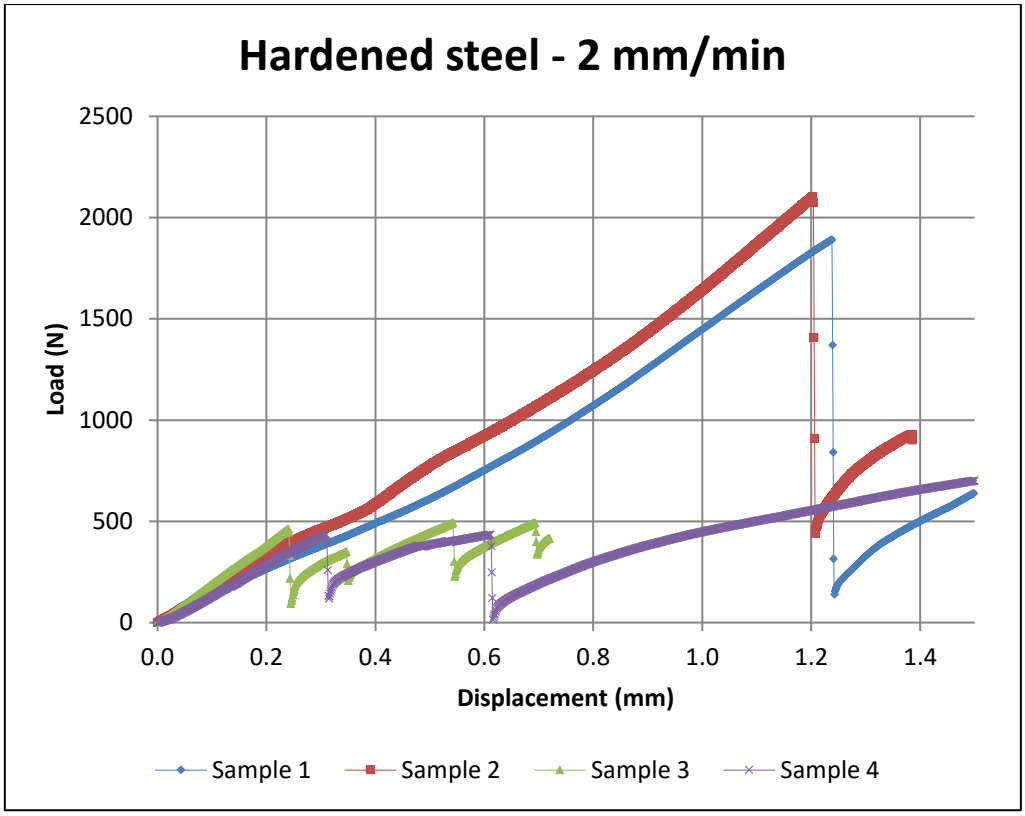

Figure 3-11: SPT LDC_{EXP} at 23°C for hardened steel – 2 mm/min.

3.2.1.1.6 Discussion of the results

The purpose of this experiment was to determine the SPT rig compliance and identify the critical factors that affect the compliance. Each of the factors and the relevant results are discussed below:

a) Compliance of elastic-region behaviour

This method of evaluating the compliance is adopted from literature review and it is expected of material to behave the same on first stage (i.e. elastic region) of the SPT LDC.

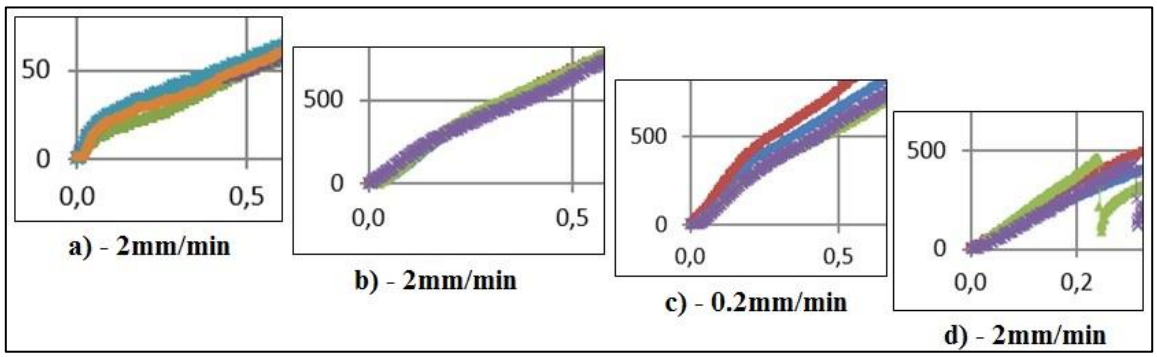

Figure 3-12: Snap shot of the elastic region: a) aluminium, b) & c) tempered steel and d) hardened steel tested at specified displacement rate.

When referring to Figure 3-12, it is evident that the SPT rig for design Concept 1 did not comply. The LDCs were supposed to coincide with each other, not as seen as in Figure 3-12 (linear curves deviated from each other).

b) Compliance of test repeatability

The SPT LDCs were not repeatable as can be seen in the test results under Section 3.2 (see Figure 3-8, to Figure 3-11). The rig was not in compliance with the CWA 15627.

3.2.1.1.7 Conclusion on test results

The test results obtained were not satisfactory and valid as per the CWA 15627 and the rig compliance test. The following factors were the contributors to error incurred during testing.

a) Punch

The punch was fixed to a 10kN load cell and experienced minor misalignment during the test. The problem of fixing the punch to the load cell resulted in the punch rubbing against the side of the clamping die.

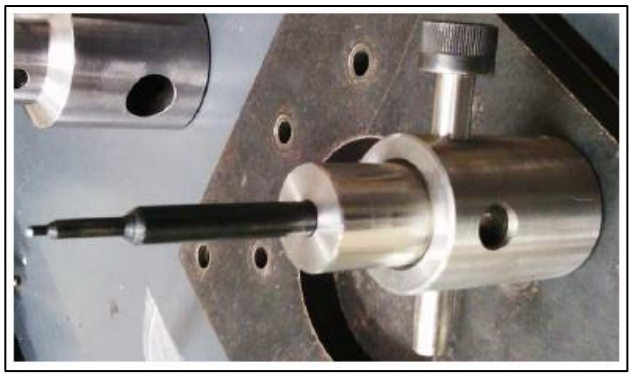

Figure 3-13: Punch mounted to load cell piece.

b) Rig size

The SPT experimental data is in micro scale data, specifically the displacement measured against the load. This means that the percentage error factor (e.g. 0.1% of 200 kN is 200 N) on both load cell and linear displacement on the tensile tester has a higher margin and cannot be used without supplementary hardware such as an external LVDT or strain gauge. The rig size was designed to suit the 200 kN tensile tester machine size. Thus, it was bigger and therefore compromised both the load and displacement acquired data as there was a higher probability of the rig deforming during testing because of the height.

c) Working parts material

CWA 15627 recommends the working material to be hardened to a minimum of 55 HRC, and it is important to know the hardness of the material (hard materials and those that are suspected to be embrittled) being tested.

3.2.2 Concept 2: Low & elevated temperature design

Concept 2 consists of a design that has eight thermoelectric coolers (TEC), also referred to as Peltier devices. The TEC device operates like an evaporator and condenser at the same time; it absorbs heat from the cold side and deposits the heat on its opposite side [41], refer to Figure 3-15 below for details. The TEC device operates at a maximum temperature of 90°C for longer periods while it operates for shorter periods at 135°C, with maximum change in temperature (ΔT) of 60-65°C [41]. These devices can be stacked on top of one another to achieve ΔT of up to 120°C [41].

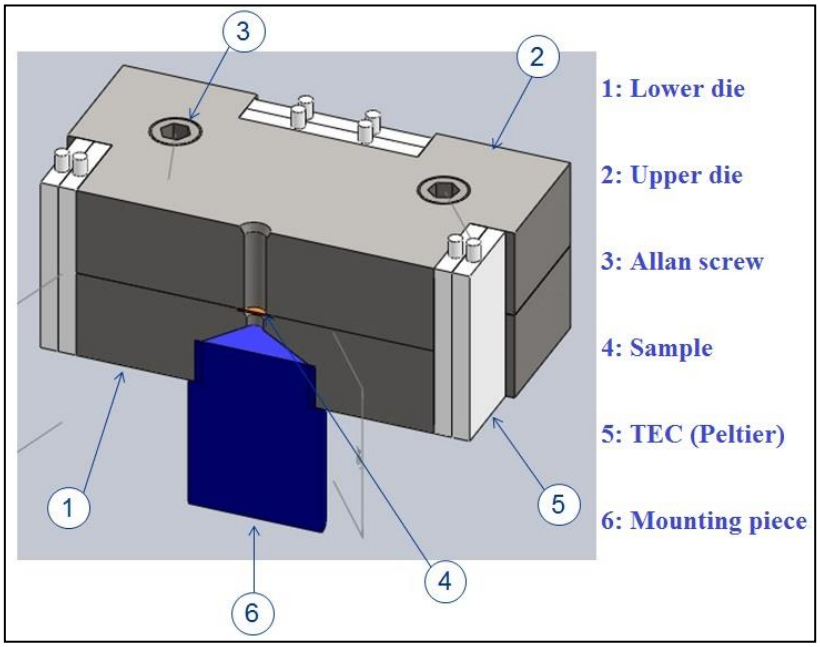

Figure 3-14: SPT design Concept 2 with TEC devices.

Figure 3-14 illustrates design Concept 2 that uses TEC devices. After purchasing two of the TEC devices, tests were conducted to evaluate if these devices could be applied to the SPT design Concept 2. The results of the conducted tests indicated the following with regard to the application of TEC devices to design Concept 2:

- Temperature varies with varied current; however, the varying of current reduces the TEC device design life,

- The heat sink fans are required for more effective ΔT (as shown in Figure 3-15),
- It is not clear how long TEC devices can last when stacked, especially when there will be switched on and off for every test at an average of 20 minutes per test.

It was concluded that this design would not be tried as the time constraints and uncertainties with the TEC devices were challenging.

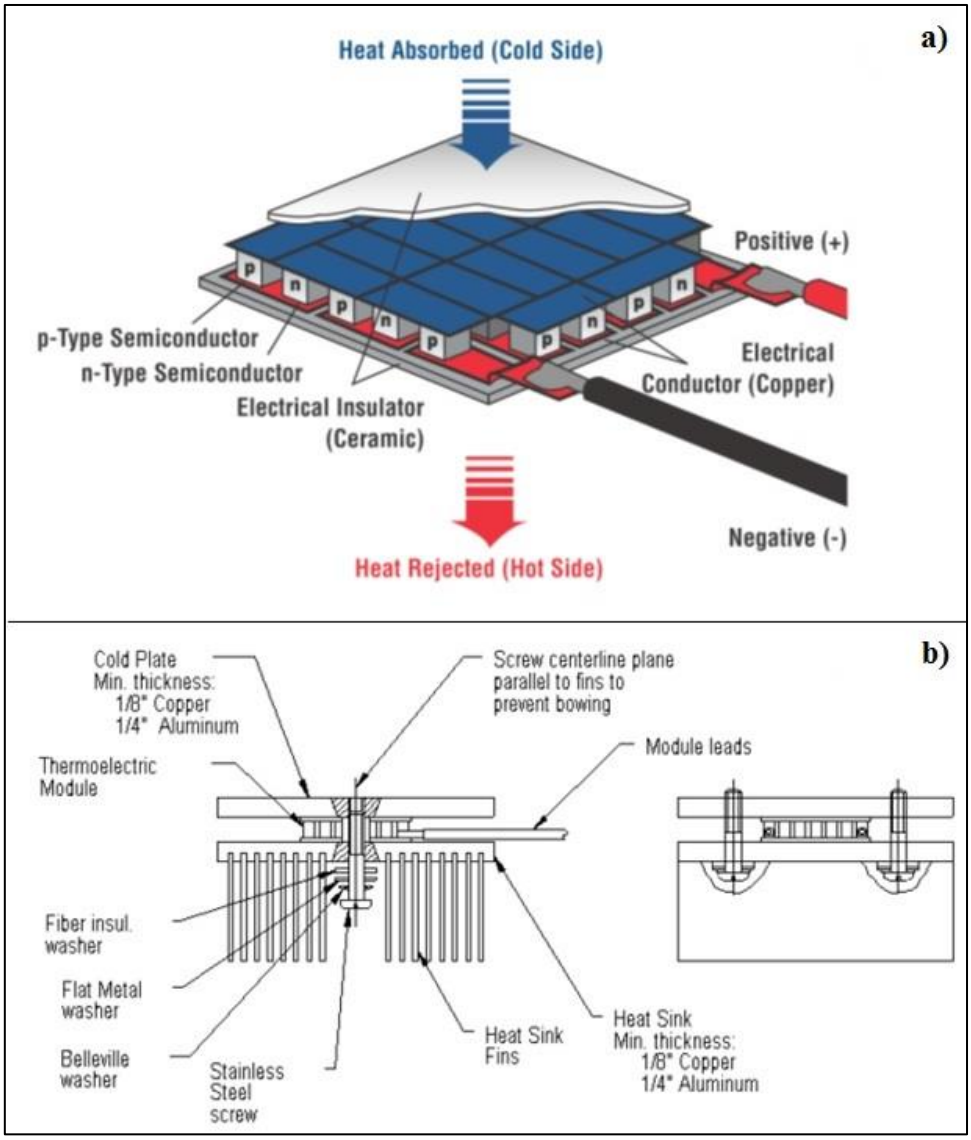

Figure 3-15: a) TEC 3D CAD and b) assembled TEC to heat sink fan for effective heat transfer [41]**.**

3.3 Lessons learnt from concept designs

This sub-chapter summarises the important lessons learnt from the tests carried out and what the critical factors were of the design. These factors are mentioned below and are incorporated in the new final concept design.

- Rig size – when the rig is smaller, it is easier to eliminate unaccounted deformation of the steel structure during the test. It is also easier to mount and align measuring devices closer.
- Tensile testing machine – Using a smaller tensile testing machine of a 5 to 25 kN frame reduces the load and displacement error factor (e.g. 0.1% of 2 kN is 2 N, which is insignificant).
- LN2 or dry CO2 is to be used as a cooling medium and, therefore, the design has to include a small cooling chamber (a smaller chamber will ensure effective heat transfer from cooling medium to sample).
- Punch – friction load experienced between the punch and clamping die could not be quantified and affected the test results. The punch head was a hemispherical head and small dents were noted that confirmed minor deformation of the head. The punch design was changed to be independent from the load cell and the head was changed to be flat (φ2.5 mm steel 'bearing' ball was used together with the punch).
- LVDT – the accuracy of the displacement measured with the LVDT could not be verified as the LVDT was housed in a closed casing. The synchronising of the LVDT with the load cell was not possible and the tensile machine used recommended same brand accessories to be plugged in. The LVDT mounting design was changed to be fixed in parallel to punch and allowed the LVDT core to move together with punch.
- Load cell – a small load cell (5 kN) was recommended after evaluating the percentage error factor, which affected the acquired load data. Synchronising of displacement and load data could not be met because the LVDT was not compatible with the tensile test machine's software. It was decided that a 1000kgf load cell would be purchased and used separately with the LVDT.
- Linear displacement measuring devices, which were compatible with the tensile test machine, were not affordable in accordance with the project's budget and the existing LVDT was used.

3.4 Final concept design

The final concept design was developed based on the literature review and experience gained from the trials with the concept designs. Lessons learnt from 3.3 were applied during the designing of these two final concepts, namely, the SPT rig for: a) *DBTT* testing (low temperature) and b) elevated temperature. Detail design drawings for manufacturing are

attached as Appendix-1. The LVDT was later replaced with a magnetic sensor as it was not acquiring reliable data, refer to Figure 3-16 for test result acquired at room temperature testing the LP rotor material. More details about the replacement of the LVDTs are discussed under Section 3.5. A number of the SPT FEM LDCs were developed using FEM packages, as explained in 3.7.1 and in full details in Appendix-2.

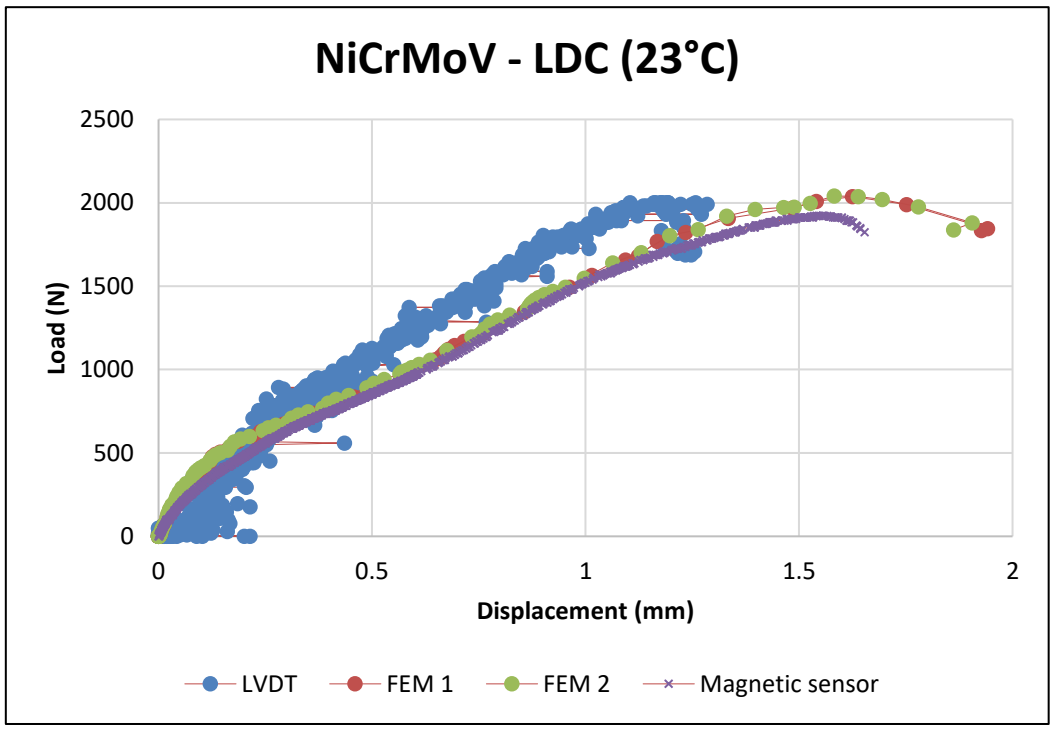

Figure 3-16: SPT LDC comparison between LVDT and magnetic sensor.

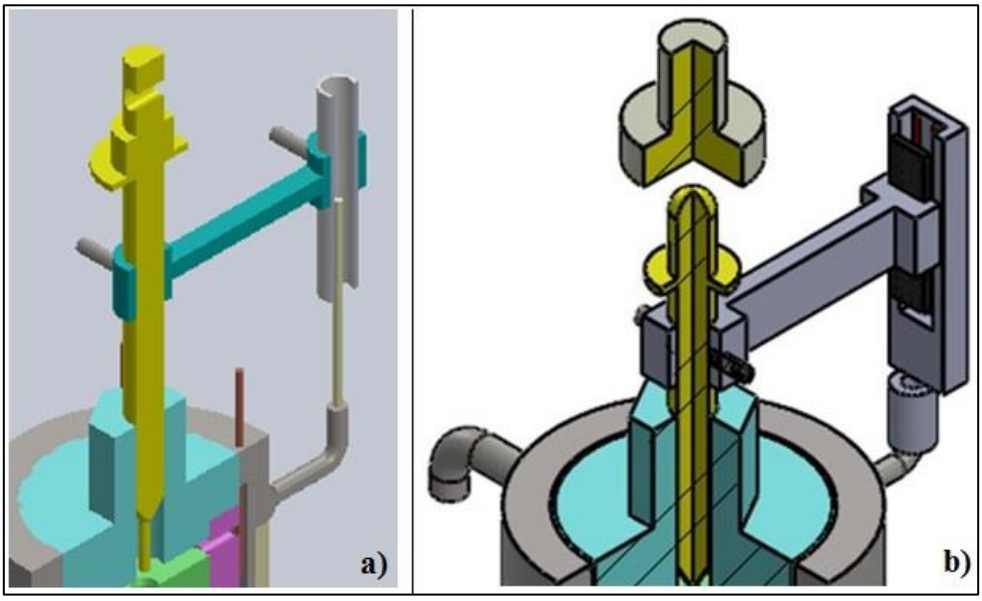

Figure 3-17: SPT design with: a) LVDT and b) magnetic sensor.

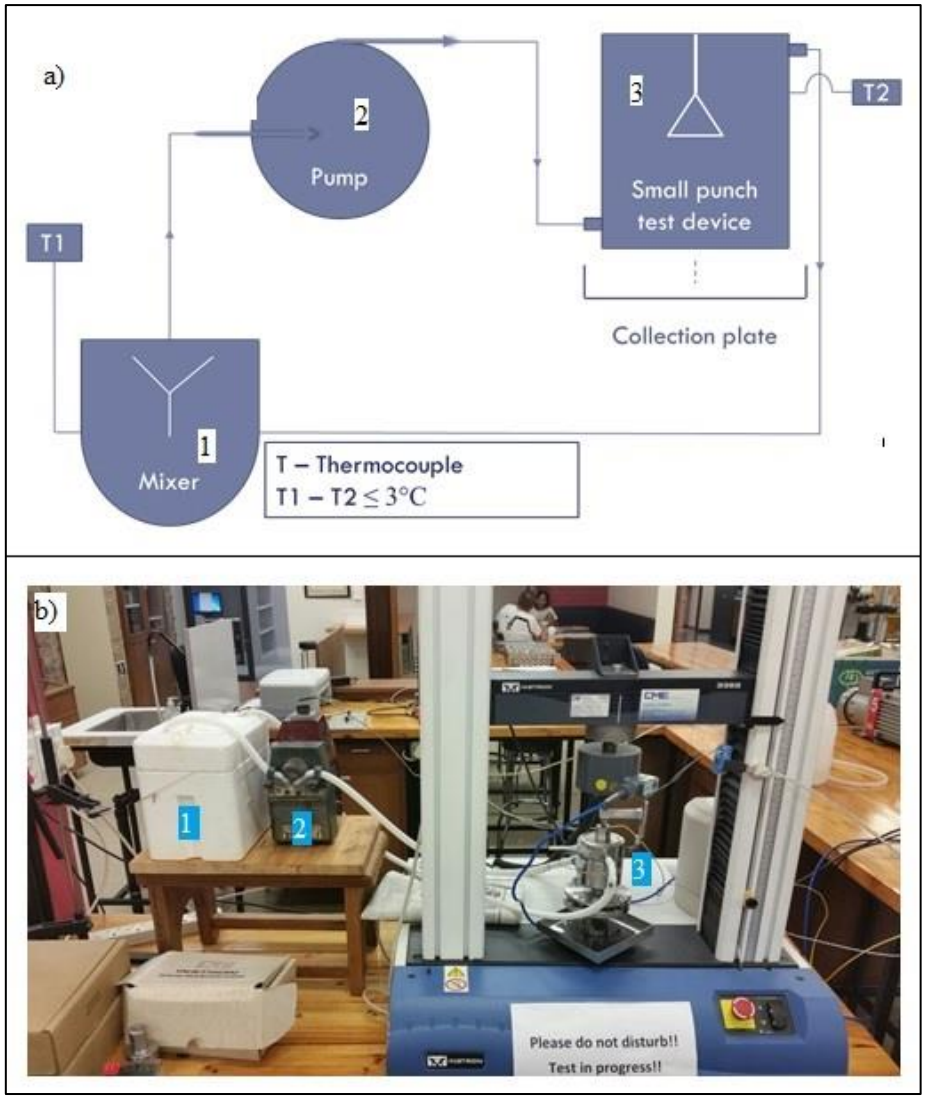

Figure 3-18: SPT setup for DBTT test: a) schematic and b) photograph.

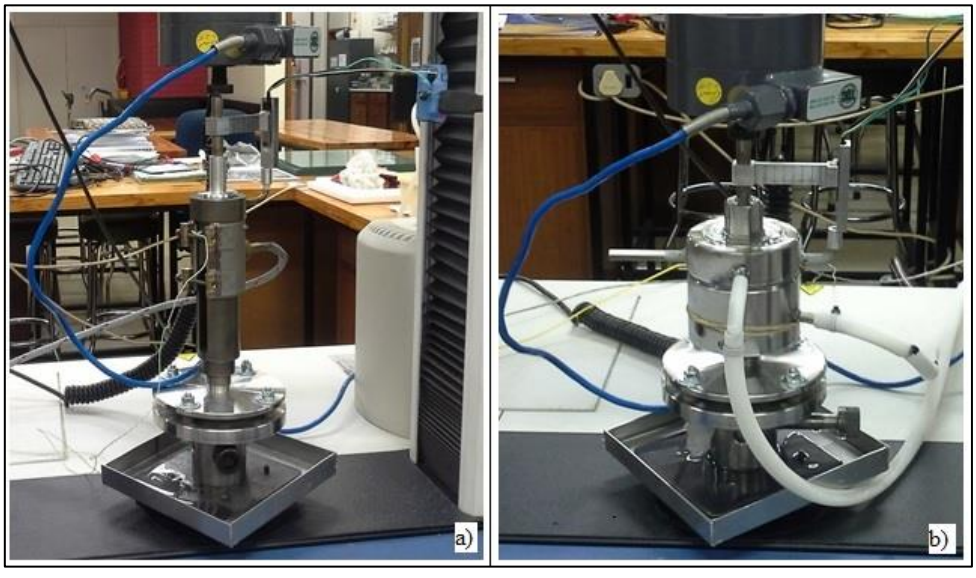

Figure 3-19: SPT rig for: a) elevated temperature and b) DBTT during testing.

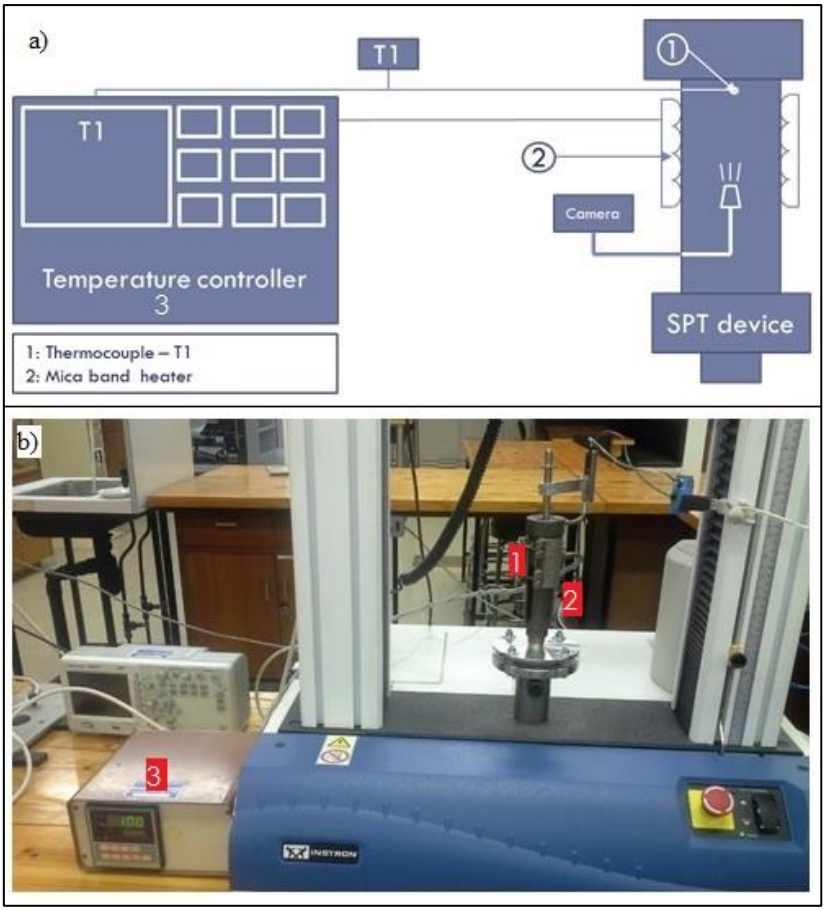

Figure 3-20 SPT rig for elevated temperature: a) schematic and b) photograph.

In Figure 3-18, Figure 3-19 and Figure 3-20 are the fully manufactured SPT rigs for both *DBTT* and elevated temperature experimental tests. Two rigs were designed and manufactured using tool steel (bohler K110) and stainless steel (SS 304) for the purpose of performing experiments at room temperature (SS 304) and at elevated temperatures (bohler steel). The rig manufactured from bohler k110 steel was hardened using a vacuum hardening furnace at 1020°C and held for a ½ hour, followed by quenching in oil in order to obtain a minimum hardness of 55 HRC (as per the manufacturer's hardening instructions). Detailed manufacturing drawings are attached under Appendix-1. The SPT rigs were operated attached on a 5 kN Instron 3365 universal testing machine; refer to Figure 4-18 for the detailed SPT rig setup.

The SPT rig for *DBTT* consisted of a mixer polystyrene box, a squeeze tube pump, rubber tubes for low temperature application, cable ties, two type K thermocouples and the SPT rig, see Figure 3-18 for details. The SPT rig for elevated temperature consisted of a 250 W mica-band heater, one type K thermocouple, a temperature controller and the SPT rig. See Figure 3-20 for details.

The SPT equipment test setup is detailed in Chapter 4. A 5 kN Instron tensile testing machine was used for both SPT rigs.

3.5 SPT data logging hardware

There are two sets of output data that are logged from the SPT, which are load and displacement. Hence, a load displacement curve is obtained from the test.

3.5.1 Load and displacement hardware

The test frame used is Instron 3365 (maximum load cell of 5 kN) and it is advisable to utilise Instron hardware (a strain gauge or LVDT) that can read displacement from the strain output sockets. However, it was costly to do so in this research as the computer software required an upgrading for it to allow for strain attachment. The plan to make use of the LVDT and independent load cell was evaluated and worked but unfortunately the LVDT had an analogue data output that had an error in its raw data. The reason to make use of an independent load cell was to allow synchronisation between itself and the LVDT.

The LVDT was replaced with an NSE-5310 magnetic sensor that has a digital output with a minimum capability of reading a linear scale of 4,8 µm. A 10 kN load cell was mounted in series with a 5 kN load cell of Instron. The 5 kN load cell was used as a safety limit to not overload the testing machine frame, since 10 kN was independently controlled.

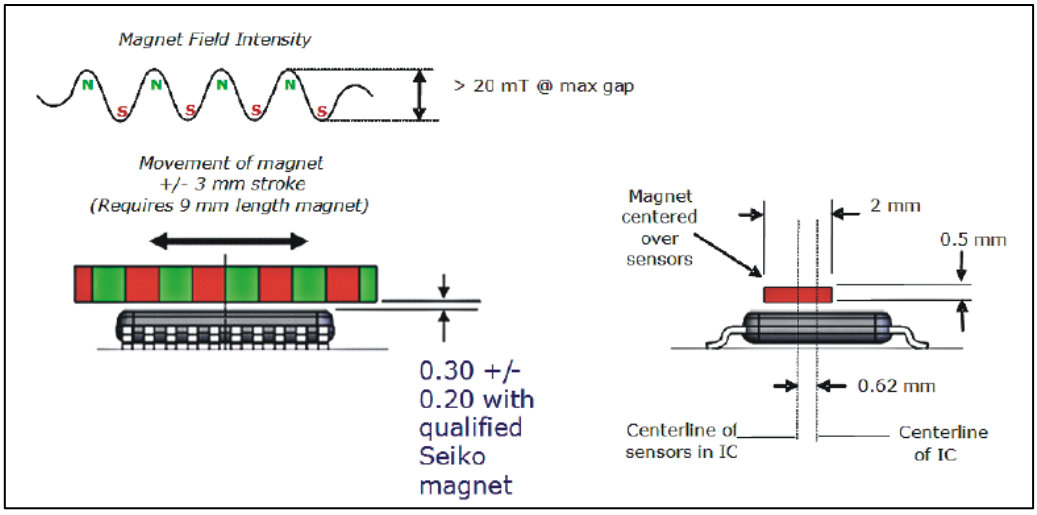

Figure 3-21: Magnetic sensor alignment [42]**.**

Figure 3-21 illustrates how the magnetic strip of 2 mm segments should be aligned in order to correctly record the output raw data. Figure 3-22 shows the assembled magnetic sensor unit with a built USB converter that was used to record linear displacement during the SPT.

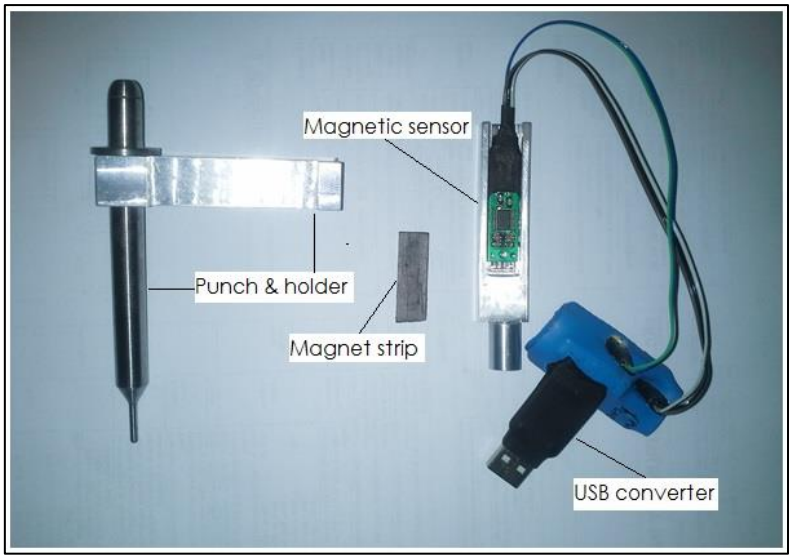

Figure 3-22: Magnetic sensor unit with aluminium holders and punch.

The 1000 kgf ULP load cell and TDC/I/0550 load cell digital transmitter were used to log the load for the LDC. As seen in Figure 3-23(a) below, the TDC supplied ULP load cell was connected with a threaded reducer to a 5 kN Instron load cell and the hardened stub was connected to the opposite side of the ULP load cell. The TDC load cell and transmitter were supplied connected and calibrated with the calibration certificate supplied. The RS232 serial to USB cable connector was connected to the load cell transmitter and the transmitter was programmed to allow digital output from the serial output to the computer USB input port in accordance with the supplied manual [43].

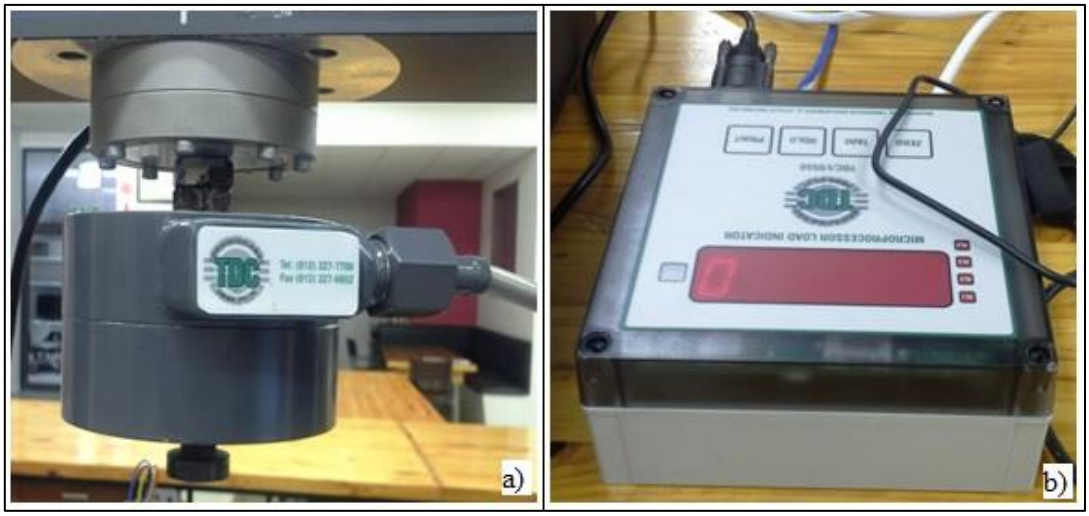

Figure 3-23: TDC: a) ULP load cell connected to 5 kN Instron load cell with a hardened stub and b) load cell TDC/I/0550 digital transmitter.

The magnetic sensor was calibrated using a depth gauge of 2 µm. The magnetic sensor calibration was run over 5 mm and it was found to be 100% accurate. During the calibration, the Instron LVDT for frame was evaluated for accuracy. Below are Figure 3-24 and Figure 3-25, showing the setup of the depth gauge and correlation for the magnetic sensor and Instron LVDT.

3.5.2 Thermocouple data logging hardware

Two type K thermocouples were used to measure temperature, one placed in the polystyrene mixer box and one placed inside the SPT chamber of the *DBTT* rig. These two thermocouples were connected to thermocouple data logger TC-08, which was connected to the computer using a USB cable. TC-08 has 8 input channels for thermocouples and is capable of reading 8 different types of thermocouple [44]. PicoLog data acquisition software, which made it easy to read and record temperatures during testing, was used as shown in Figure 3-26 below. The consideration of accuracy of temperature read, which is ±0.2% and ±0.5°C, was met [45].

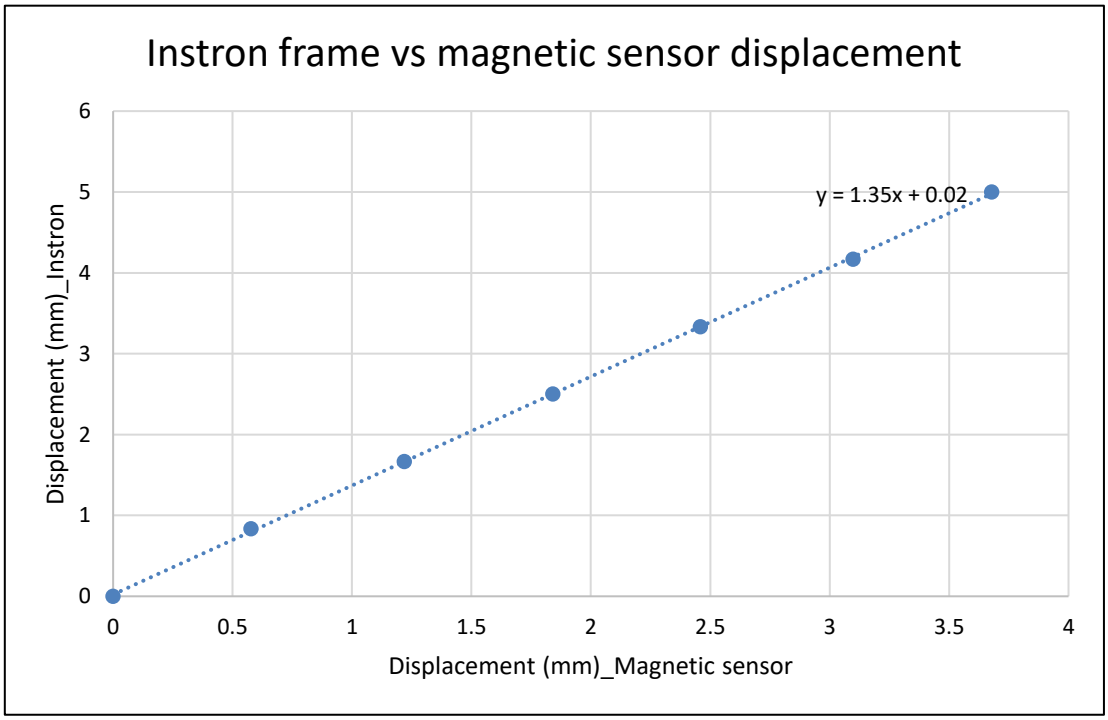

Figure 3-24: Instron LVDT vs magnetic sensor displacement.

Figure 3-25: Magnetic sensor calibration using depth gauge.

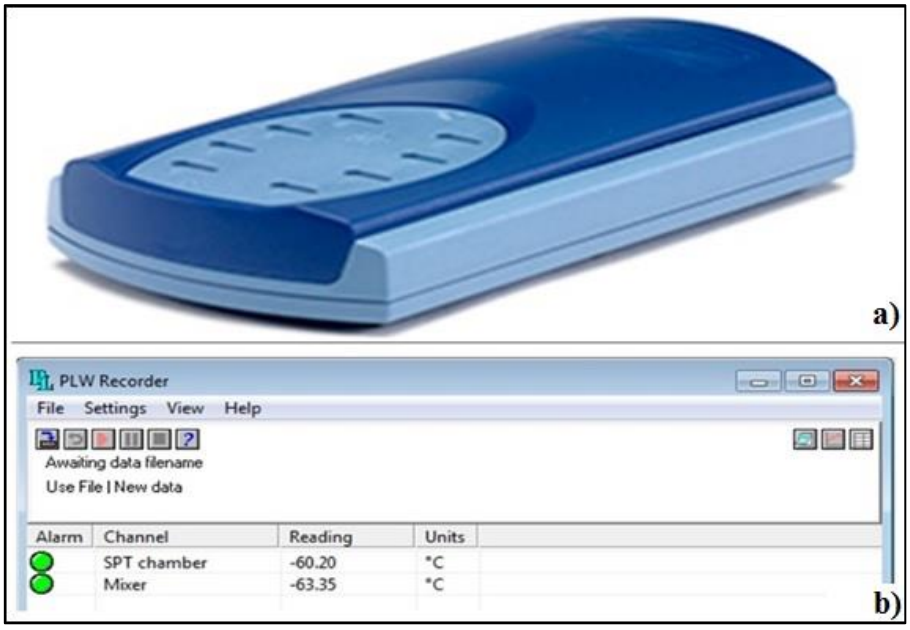

Figure 3-26: a) Thermocouple data logger TC-08 [44] **and b) PicoLog data logger software.**

3.5.3 Borescope camera

A borescope camera model WRS-108C was used as a device that would record a video in real time during the SPT. The video was then reviewed after each SPT to identify the crack initiation time and the location (distance away from the bulge surface centre). These two parameters were supposed to be synchronised with the SPT raw data and be applied to the

SPT FEM in order to determine the strain energy density for SPT (W_{SP}) in the SPT FEM. Unfortunately, the camera specification (pixel size) was not sufficient to identify these two parameters and an alternative method (fracture toughness test at room temperature to correlate with the SPT data and identify the two required parameters) was used to identify these parameters, which is covered in Chapter 4. Table 3-3 shows the camera specifications.

Table 3-3: Borescope camera WRS-108C [46]**.**

Specification	Camera	Monitor
Model no	GB8803	GB7303
Total pixel (PAL)	704 x 576	640 x 480
Power supply/waterproof	4 x AA batteries/IP67	2 hours and 3 hours to charge
Operating time/temperature	As per batteries/-10 to 50°C	2 hours/

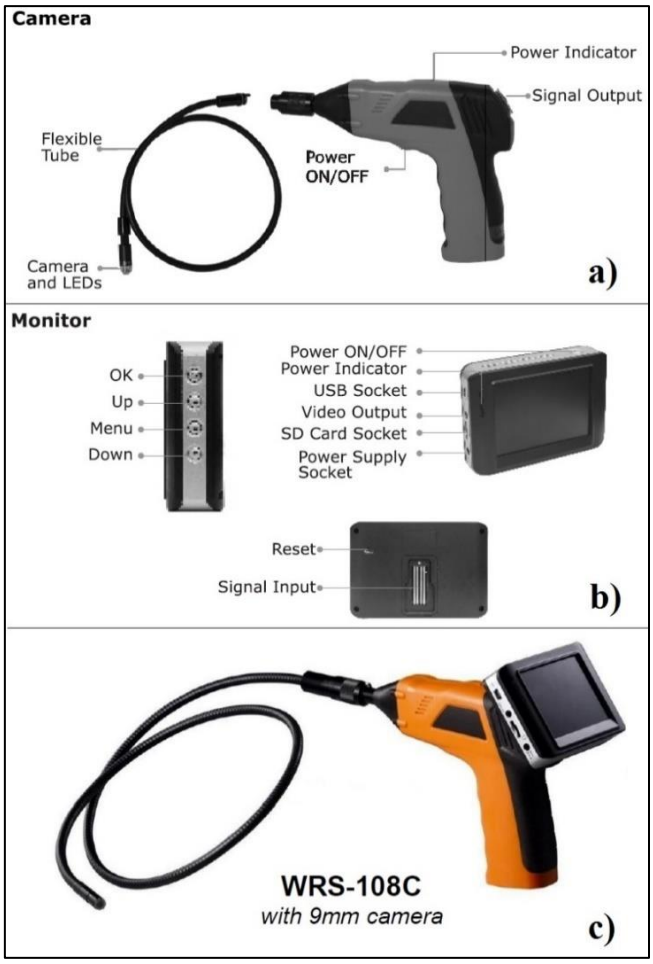

Figure 3-27: Borescope camera showing: a) camera, b) monitor and c) assembled unit [46]**.**

3.5.4 Mica band heater

A customised Mica band heater of 250W and 230V supplied was used as a heating method for samples performed above room temperature up to 100°C. A temperature controller (with 3-points plug input of 220/230V), as well as a type K thermocouple input, was built by the UCT Electrical Engineering Department and was used as input voltage to a Mica band heater. The temperature controller allows the user to program the temperature output of the Mica band heater by monitoring the temperature using the thermocouple (type K). This is achieved by varying the heat of the heater to maintain the required output temperature. The thermocouple was mounted directly to the SPT sample (as required by CWA 15627) at 50 and 100°C. Refer to Figure 3-28 below for details.

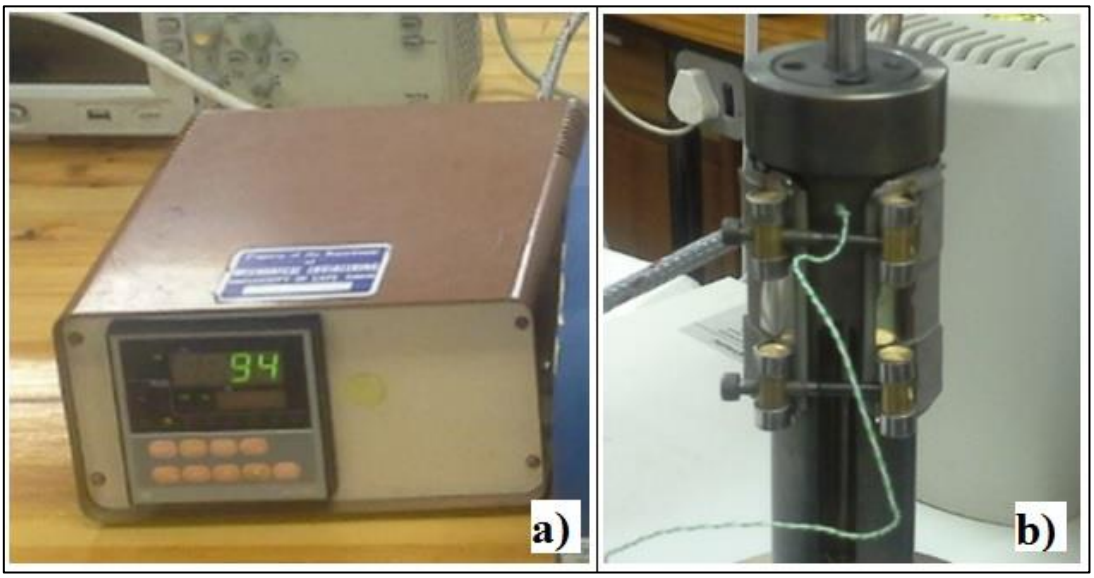

Figure 3-28: a) Temperature controller and b) Mica band heater with type K thermocouple.

3.5.5 Data logging software and data synchronisation

The LabVIEW system design software of 2014 was used to log the load data from load cell through the load cell transmitter and linear displacement data through magnetic sensor. The software allows the user to design, create or code with visualisation of engineering and science design system symbols [47]. This software has been in existence for a few decades and, with its graphical programming syntax, it is one of the few unmatched softwares used by engineers and scientists [47]. LabVIEW consists of a block diagram where all graphical programming codes are written and a front panel or user interface that displays the main data that is being logged.

LabVIEW software is a National Instruments (NI) product and, therefore, is supported by all NI devices as well as other engineering and scientific devices. LabVIEW software is easier and better to use to code than the traditional text based programming software because of its graphical programming. Figure 3-29 shows two split block diagrams made to fit in a page.

Figure 3-30 illustrates the designed user interface. Two load cell output wave charts and a magnetic sensor output wave chart were placed on the front panel with digital readings next to each wave chart. Calibration and alignment keys were also placed on the front panel in order to ensure accuracy in data logging.

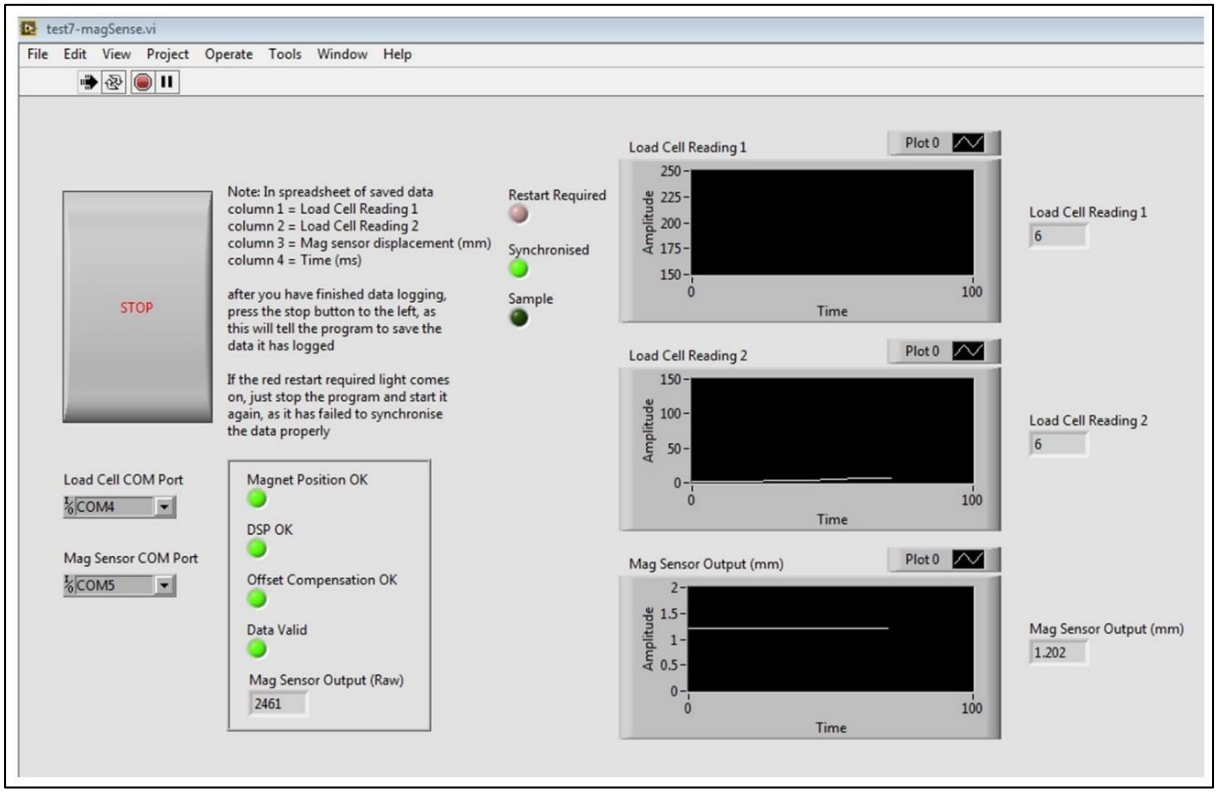

Figure 3-29: LabVIEW designed user interface.

3.6 Determining SPT equipment compliance

There are two methods discussed in the Literature Review that are used to test for the SPT equipment compliance. The hardness tests of the material used for both final designs were heat treated to meet the minimum requirement hardness as prescribed in the CWA 15627.

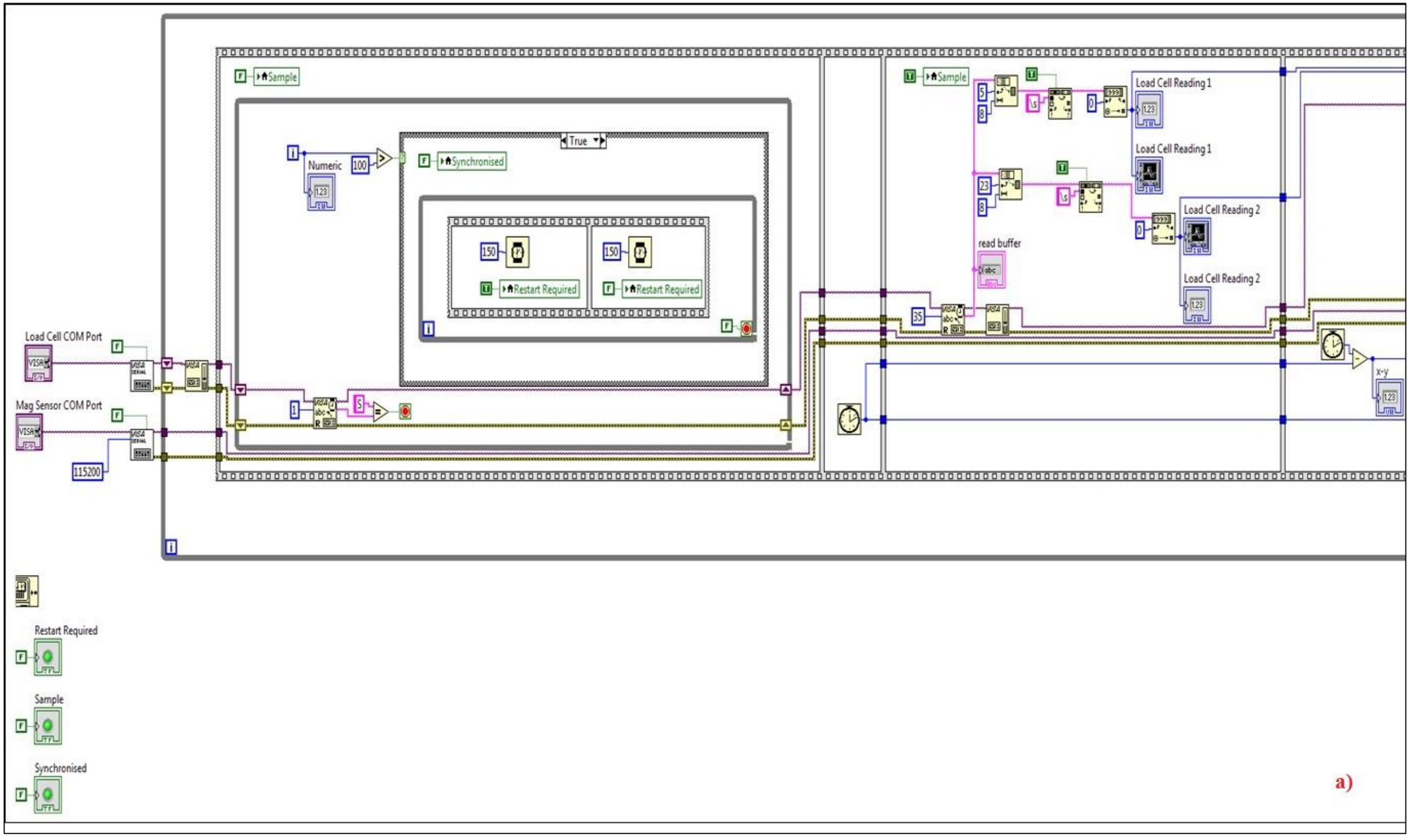
Sample
Numeric
100
True
Synchronised
150
Restart Required
150
Restart Required
Load Cell COM Port
Mag Sensor COM Port
115200
Sample
Load Cell Reading 1
Load Cell Reading 1
Load Cell Reading 2
Load Cell Reading 2
read buffer
35
x-y
Restart Required
Sample
Synchronised
a)

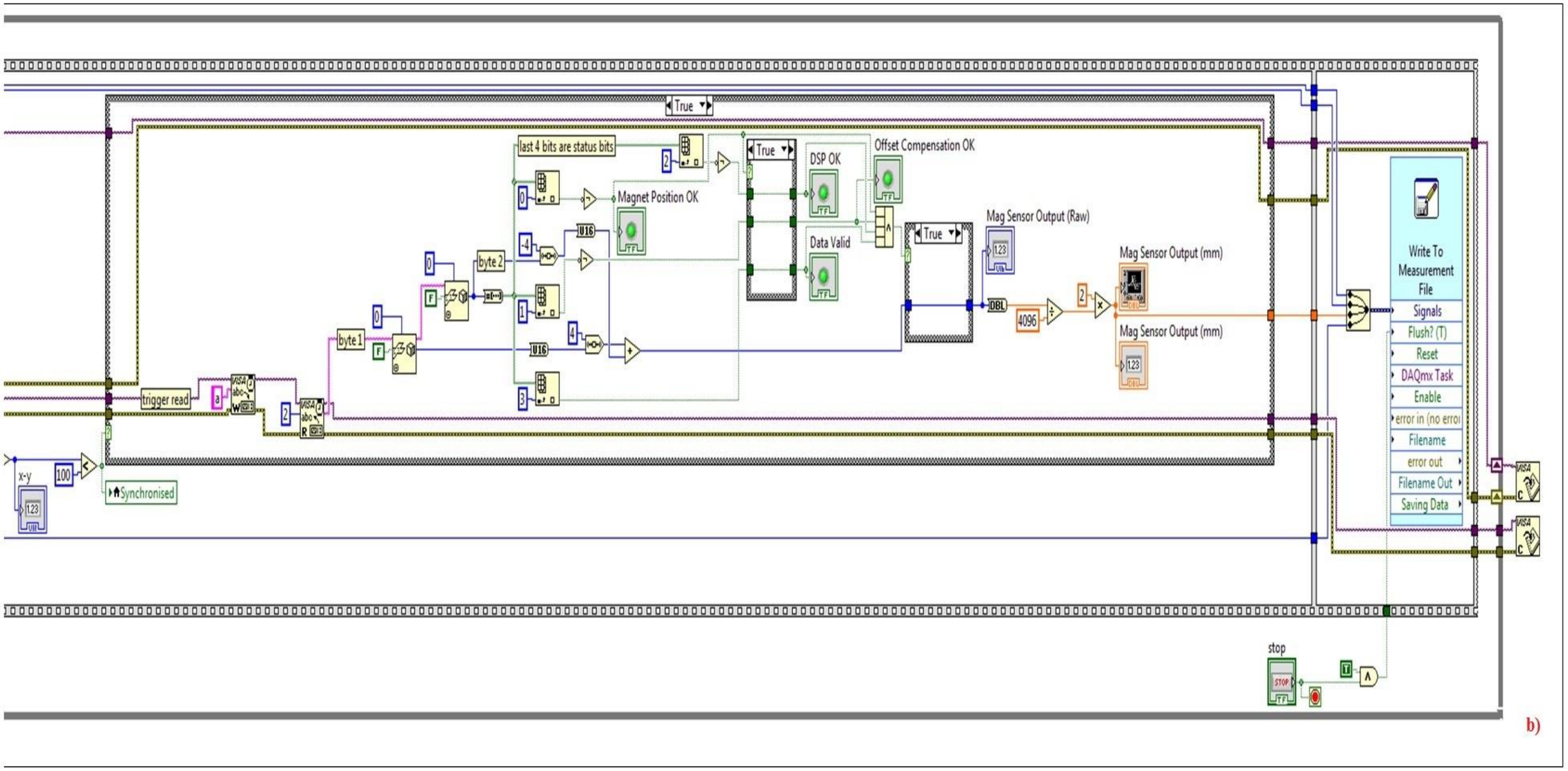

Figure 3-30: LabVIEW block-diagram: a) first half and b) second half.

3.6.1 Hardness test

Three SPT parts (the punch and the upper and lower dies) and a pressing stub, which is connected to the load cell, were hardened to Vickers hardness of above 596 HV (or 55 HRC). A hardness test was also performed on the rotor steel to evaluate for the possible change in hardness over the service life exposure. Brinell hardness of 244-256 HB (256-269 HV) was reported on a commissioning report [48] of prior service life. Vickers hardness test was carried out on ex-service rotor material and no change was noted, 256 HV.

3.6.1.1 Hardness test setup equipment

A hardness test was carried out at the Centre of Materials Engineering (CME) at UCT. This test was carried out for compliance with the SPT requirements as specified in the CWA 15627: 2007. Working parts (i.e. punch, upper and lower die and pushing stub which pushes the punch) were hardened to a minimum of 55 HRC to ensure no deformation of these parts during testing. Zwick Roell ZHV, which tests at various loads ranging from 0.2 to 30 kgf was used to perform Vickers hardness (HV) test. The test was performed in accordance with the ASTM E 92 standard. Refer to Figure 3-32 for details on the Vickers hardness testing machine.

3.6.1.2 Hardness test results

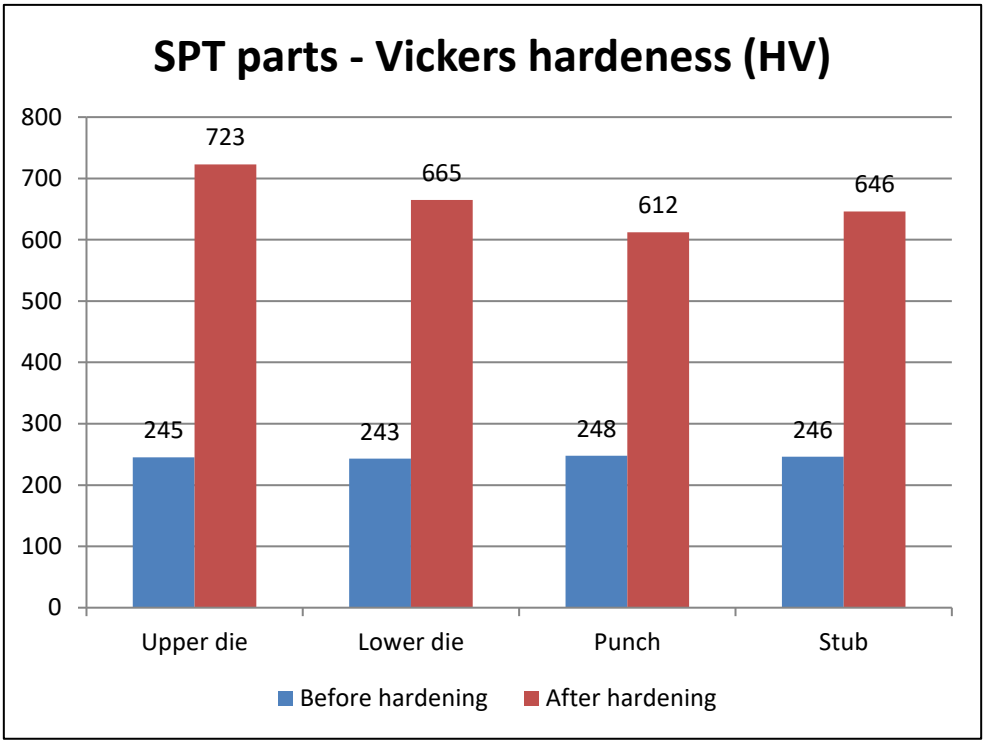

Figure 3-31: Hardened SPT parts.

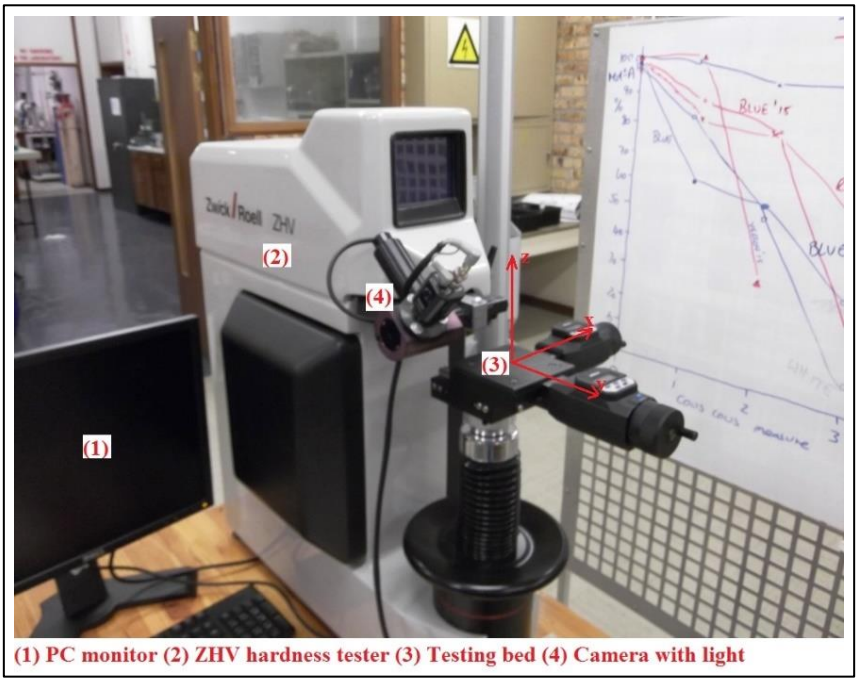

Figure 3-32: Hardness test machine – Zwick Roell ZHV.

3.6.2 Modelling the experimental LDC

An LDC_{FEM} using tensile properties of the steel investigated gets compared to an LDC_{EXP}. It is not expected for the curve to fit/match 100%; less than or equal to 5% error margin is expected and the rig is supposed to reproduce the same LDC_{EXP}. Figure 2-21 illustrates the LDC_{FEM} compared to the LDC_{EXP} with the percentage error between the two LDCs. The rig did reproduce an acceptable LDC_{EXP} with a slight 5% error margin in the plasticity region; refer to the SPT LDC_{EXP} results in Figure 3-33.

3.6.3 Determining Young's modulus

This method was explained in detail in Section 2.2.4.4.2 of the Literature Review. The method entails investigation of rig compliance by making use of a thicker sample of 5 mm to determine the elastic slope or Young's modulus. There are two ways this method can be achieved: firstly, the slope can be expected to fit 100% elastic region of the SPT LDC_{FEM} or, secondly, stress can be determined using load and contact area of punch and strain can be estimated using FEM. Below is Figure 3-33, showing the compliance of the two rigs. The three graphs are offset by 0.002 m to illustrate the parallelism in all three curves up to ~150 N.

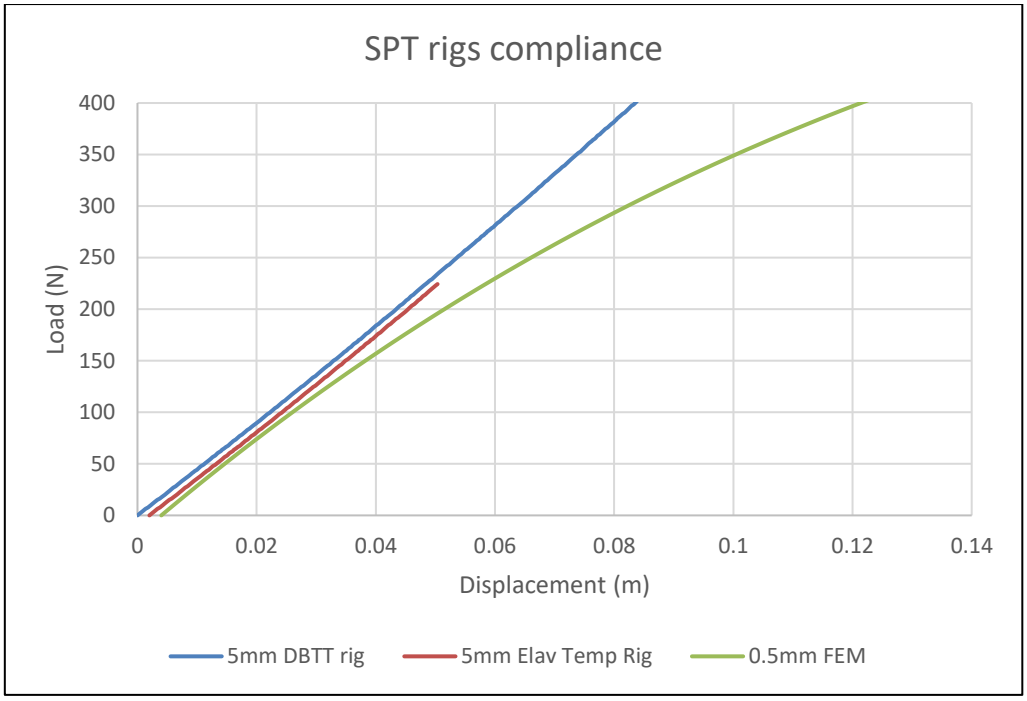

Figure 3-33: SPT rigs compliance.

3.7 Analytic procedure for SPT results

The procedure developed was used in both the *FATT* and EPRI approach for estimating K_{IC}, which were both explained in detail in Chapter 2.

3.7.1 Finite Element Modelling (FEM) software package

The FEA software package used in this research was Abaqus version 6.14-1. The analytic model is a 2D-axisymmetric model. Three parts (the punch and the clamping and receiving dies) are deformable and elastic with no plasticity defined in the model. The sample is a deformable elastic-plastic material that is loaded using a punch displacement of 3 mm in total. Figure 3-34 shows the 2D axisymmetric SPT FEM used to estimate the fracture properties and mechanical properties. Please refer to Appendix-2 for the FEM instructions and model validation used in this research.

3.7.2 Ramberg-Osgood model

The model used to describe the elastic-plastic mechanical behaviour of the material is the Ramberg-Osgood model, which was also explained in Chapter 2. The numerical values of *D* and *n* were determined using uniaxial tensile true stress and true strain raw data of the plastic region of the curve.

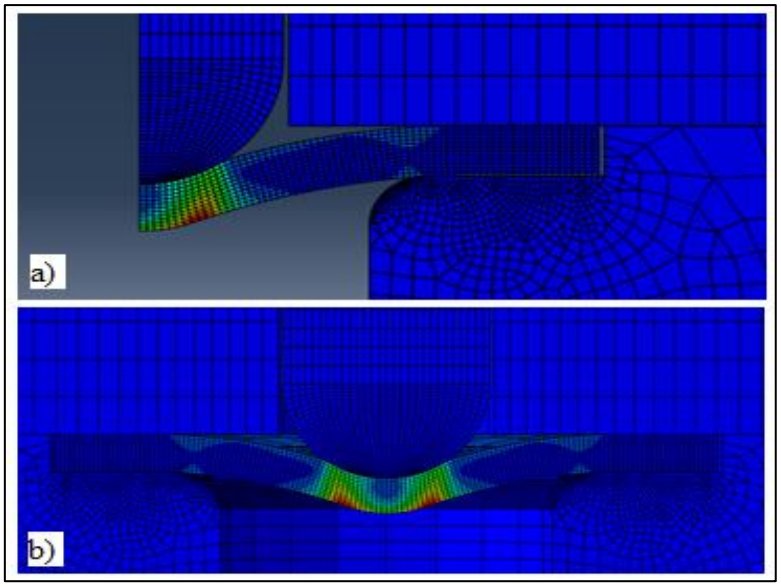

Figure 3-34: a) 2D axisymmetric and b) 2D revolved SPT FEM.

The true stress is plotted against true strain and a power trend line is used to predict the numerical values of *D* and *n*. Figure 3-35 is an example used to illustrate how parameters *D* and *n* are determined.

$\sigma = D(\varepsilon - \varepsilon_e)^{1/n}$

$\sigma = D(\varepsilon_{py})^{1/n}$

D = 1202.64MPa and n = 1/0.11728018 = 8.5

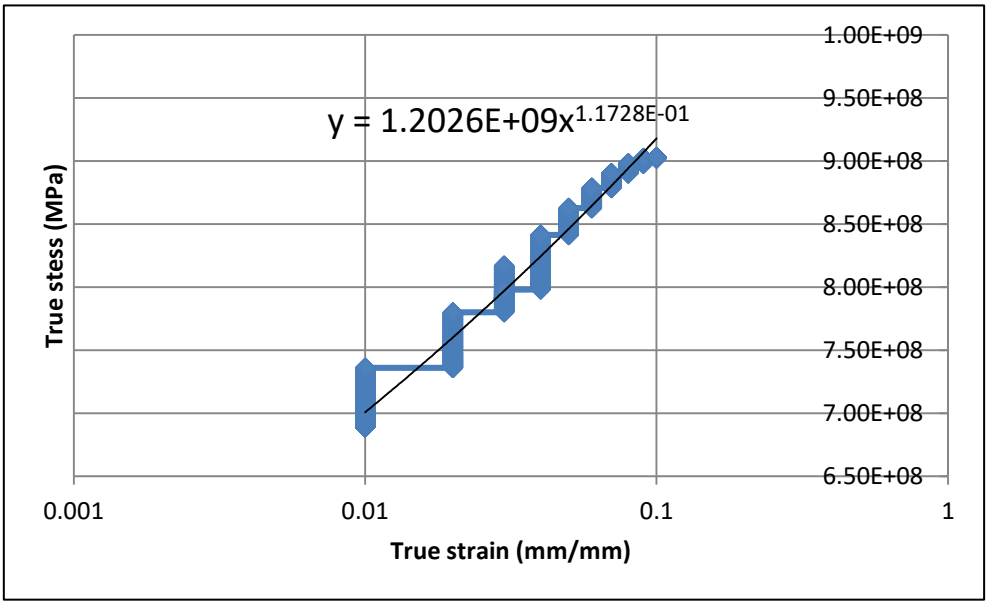

Figure 3-35: NiCrMoV LP rotor steel showing true stress – true strain.

CHAPTER 4: EXPERIMENTAL METHODOLOGY

4.1 Research approach

A research approach was developed based on the two adopted models, namely, the EPRI and the *FATT*. The two approaches were used as a guide and provided the required mechanical test data for validation and correlation purposes. Figure 4-1 illustrates the basic approach used in this research. The approach consists of three stages and four mechanical testing techniques, namely: the uniaxial tensile test, the CVN, the fracture toughness and the SPT. Each mechanical test is explained in terms of the research approach, as given in Figure 4-1.

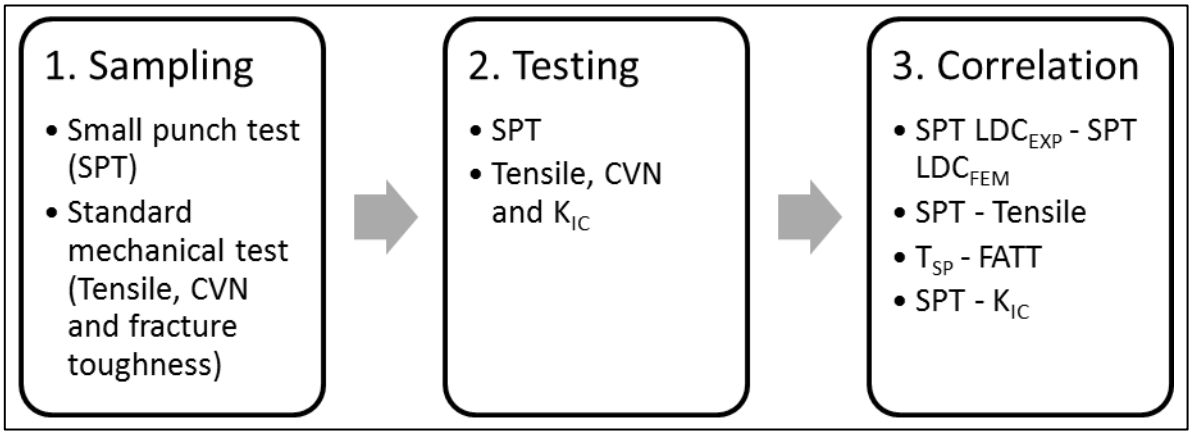

Figure 4-1: Basic research approach.

4.1.1 Stage 1: Sampling

Stage 1 is the sampling process for all four mechanical tests. It details the requirements of preparing each test sample in accordance with applicable ASTM or BS EN standards. Table 4-3 shows the samples' geometry and their applicable mechanical standards.

4.1.2 Stage 2: Testing

The four tests are performed in accordance with ASTM (fracture toughness and CVN tests) and BS EN (tensile and SPT) standards. This stage summarises the required test data from each standard mechanical test. These output data are either used as input for the SPT FEM or for correlation **(Stage 3: Correlation)** between the SPT and mechanical tests.

The material description and characteristics are detailed in the next section.

4.2 Material investigated

A series of the SPTs on the ex-service low alloy steels of a low pressure (LP) steam turbine rotor (see Figure 4-2 below) were conducted to evaluate embrittlement, tensile properties and fracture toughness. The materials' composition and identification are given in the tables below.

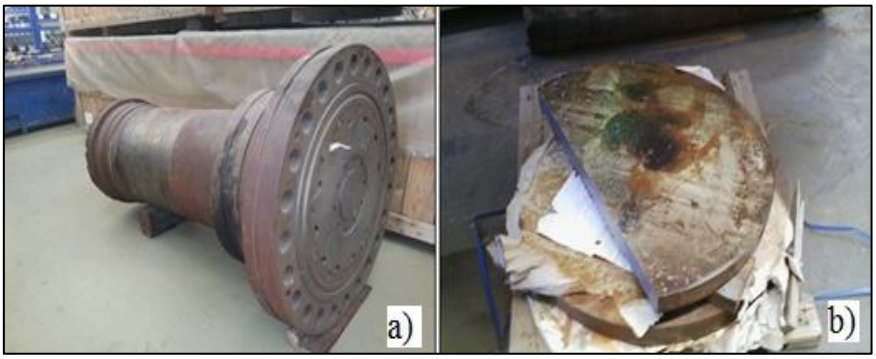

Figure 4-2: NiCrMoV rotor steel showing: a) rotor stub and b) sliced rotor.

Table 4-1: Chemical composition of alloy steel [48]**.**

Chemical composition									
Type/Element	C	S	P	Si	Mn	Ni	Cr	Mo	V
NiCrMoV LP rotor	0.249	0.007	0.009	0.100-0.110	0.335	2.93	1.61	0.435	0.060

Specimens were identified as 'as-received' or 'heat treated'. Heat treatment at the temperatures stated in Table 4-2 were performed to remove any susceptible temper embrittlement in the LP rotor steel (de-embrittling), as described by Shekhter [38], and were hardened to introduce material damage to the LP rotor steel (i.e. changing material mechanical properties).

Table 4-2: Material identification.

Material – ID	**Component**	**Alloy grade**	**Heat treatment**	**Exposure in hours**	**Tests carried out**
As Received (AR)	LP steam turbine rotor	NiCrMoV	As received	Exposed for 26 years for 1527743 hours	Tensile, CVN, CT test and SPT
De-	LP steam	NiCrMoV	600°C/1,5hours		Tensile,

Material – ID	Component	Alloy grade	Heat treatment	Exposure in hours	Tests carried out
Embrittled (DE)	turbine rotor		and quenched in water		CVN, CT test and SPT
Hardened (HD)	LP steam turbine rotor	NiCrMoV	700°C/0,5hours and quenched in water		Tensile, CVN, CT test and SPT

Specimens were prepared in accordance with the standard(s) given in Table 4-3 below and each process of preparing the samples is explained in each test sub-section below.

Table 4-3: Mechanical tests geometry size.

Test name	Standard compliance	Specimen type	Specimen size (mm)	Crack plane identification
Tensile test	BS EN 10002: 2001 Part 1 and 5	Round bar	D = 8, L = 30	L-R
Fracture toughness test	ASTM E399-09	Compact tension type	W = 25, B = 12.5	L-R
CVN test	ASTM E23-12c	Type A	T = 10, W = 10, L = 55	L-R
SPT	CWA 15627:2007	Round specimen	D = 8, T = 0.5	Not applicable

*** BS EN 1002: D – Diameter, L – Gauge Length, ASTM E399: W – Width, B – Thickness, ASTM E23: T – Thickness, W – Width and L – Length***

4.3 Experimental matrix

Specimens were tested in accordance with standards (in Table 4-3) at the following testing conditions. The SPT matrix for certain test temperatures was not completed as required by the code of practice. Table 4-4 illustrates the number of specimens required to be tested and the actual number of specimen that were tested.

Table 4-4: Experimental matrix.

Test name		Test temperature (°C)										
		-80	**-65**	**-60**	**-40**	**-30**	**-20**	**-10**	**0**	**23**	**50**	**100**
Tensile	Specimen required/tested	x	x	x	x	x	x	x	x	2/2	2/2	2/2
K_{IC}		x	x	x	x	x	x	x	x	2/3	x	X
CVN		3/3	x	3/3	3/3	3/3	3/3	3/3	3/3	3/3	3/3	3/3
SPT		x	7/4	x	x	7/4	7/4	7/7	7/5	7/7	7/7	7/7

4.4 Uniaxial tensile test

Figure 4-3 is an approach used to acquire tensile test data for the SPT correlation.

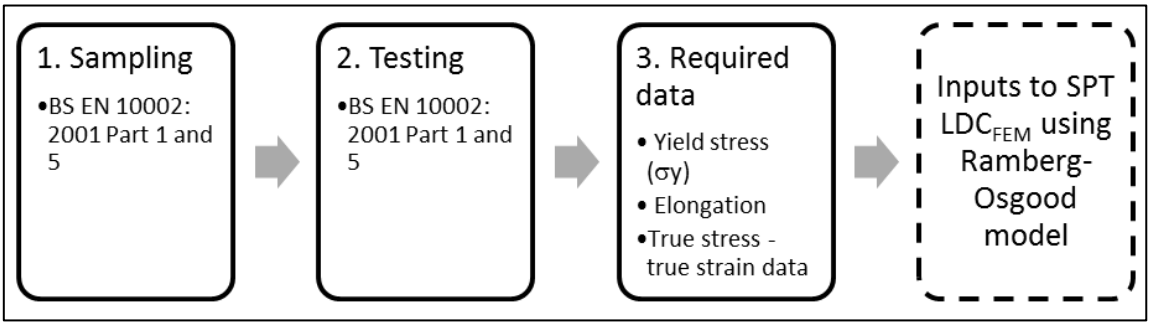

Figure 4-3: Tensile test approach SPT LDC_{FEM}.

4.4.1 Tensile test specimen preparation

The specimens were prepared as per the BS EN standard shown in Table 4-3 above. Part 1 of the standard was applied for specimen geometry tested at room temperature and Part 5 was applied for specimen geometry tested at elevated temperatures.

4.4.2 Uniaxial tensile test setup and equipment

The tensile test was carried out at Eskom's Research, Testing and Development (Eskom RT&D) laboratory. The equipment used to perform the uniaxial tensile test was the Instron 5582 screw driven tensile testing machine with a maximum load cell of 100 kN. Specimen gauge lengths were punched on each specimen. A strain gauge (up to approximately 3,5% of total strain) was attached to each test specimen to monitor changes in gauge length and served as an accurate method in determining Young's modulus. Figure 4-5 illustrates the strain gauge fit up for both room and elevated temperature with the heating furnace in place.

4-4: Photograph of the tensile specimens for elevated temperature (D = 8 mm) and room temperature (D = 6 mm).

Figure 4-6 shows the test setup for the tensile test at the Eskom RT&D laboratory.

Figure 4-5: Strain gauge attached during: a) room and b) elevated temperature test.

4.5 Charpy V-Notch (CVN) test

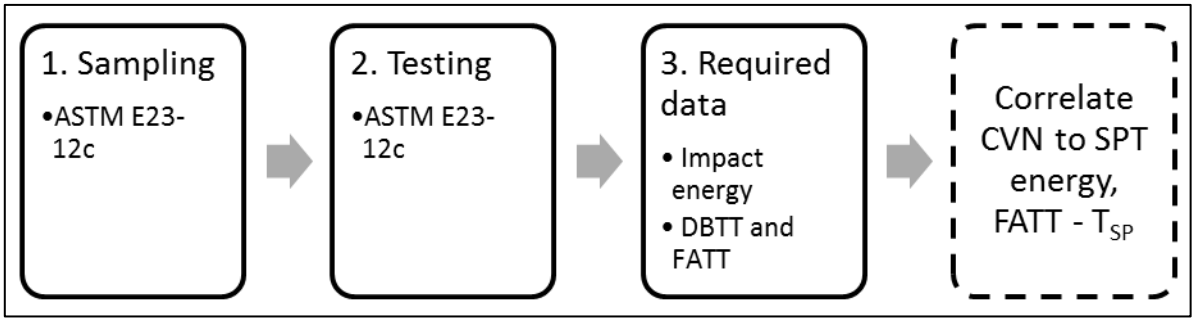

Figure 4-6: CVN FATT approach to SPT transition (T_{SP}) temperature.

(1) Cross head, (2) Temperature controller, (3) Remote control
(4) Clamp/Chunk with loadcell, (5) Heating furnace
(6) Computer and (7) Test frame

Figure 4-7: Instron 5582 tensile testing machine.

4.5.1 CVN specimen preparation

Specimens were machined using a milling machine and surface grinder to the geometry size given in Table 4-3 and Figure 4-8. The ASTM standard for notched bar was applied during preparation and the notch cutter of 2 mm with an inclusive angle of 45° was used to cut the notch (see Figure 4-8 below).

4.5.2 CVN test setup and equipment

The CVN test was carried out at the Eskom RT&D laboratory. The equipment used to perform the CVN test was the Instron SI series motorised pendulum impact testing machine,

Figure 4-8: Photograph of CVN specimens.

model SI-1M, with a maximum energy of 450 joules. The CVN specimens were placed in the testing position using a specimen holder (centring tong) that ensures that the specimen notch is positioned in the centre with reference to the applied load. The CVN testing temperature ranged from room temperature to -80°C and specimens tested below room temperature were soaked in thermal H5 oil or dry CO2 mixed with methanol and held for a minimum of a ½ hour. The notches of the samples were cut using a notch cutter, as shown below in Figure 4-9. Figure 4-13 shows the universal testing machine for the CVN test below.

Figure 4-9: Cutting machine for V-Notch for CVN specimen.

4.6 Fracture toughness test

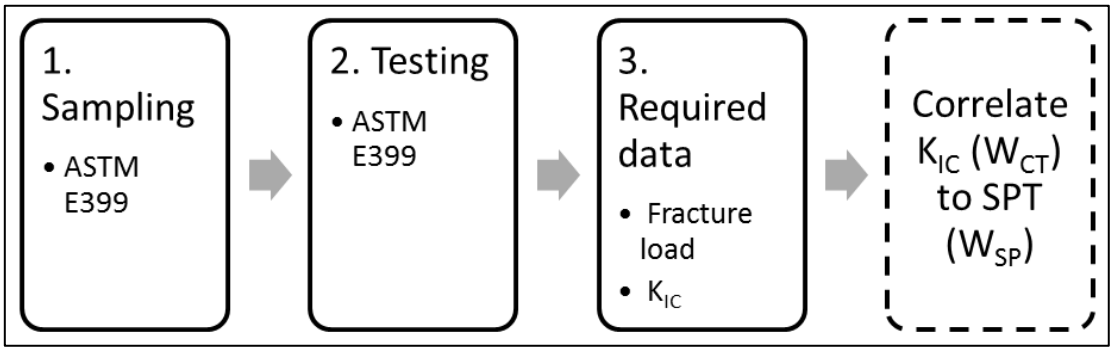

Figure 4-10: K_{IC} approach to correlate modelled compact tension (CT_{FEM}) using W_{SP} - W_{CT}.

4.6.1 Fracture toughness specimen preparation

CT specimens were machined to size using an electro discharge machine (EDM) method called wire cutting. The process was used to save the minimum material that was present. The specimens were marked with 1 mm gaps with reference to the notch. Refer to Figure 4-11.

Figure 4-11: ASTM CT specimen (with 1 mm gap marks from the notch).

4.6.2 Fracture toughness test equipment setup

The fracture toughness test was carried out at the Centre of Materials Engineering (CME) at UCT. The fracture toughness test was performed using an ESH testing machine with a maximum load cell of 45kN that uses Instron data acquiring software. The crack was grown to crack length that complies with the recommended length specified in the standards presented in Table 4-3. Applied fatigue load of 8-10kN was used to grow a fairly straight crack prior to strain gauge attachment. Figure 4-12 shows the equipment used to perform the fracture toughness and specimen setup prior to testing.

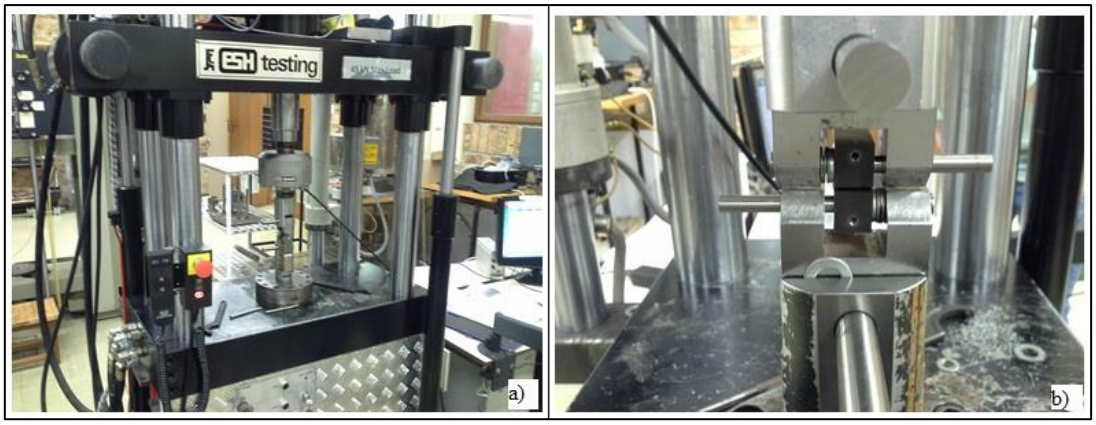

Figure 4-12: Fracture toughness: a) 45 kN ESH testing machine and b) setup with specimen prior to fatigue.

(1) Safety glass/door, (2) Swinging hammer, (3) Computer, (4) Sample holder and (5) Cooling bath using H5 thermal oil

Figure 4-13: Instron SI-1M for CVN test.

4.7 Small punch test (SPT)

4.7.1 SPT specimen preparation

The SPT specimens were prepared in accordance with the CWA 15627 as explained in Section 2.2.4.2 of the Literature Review and Figure 4-14, which addresses the risks involved when sampling the SPT samples.

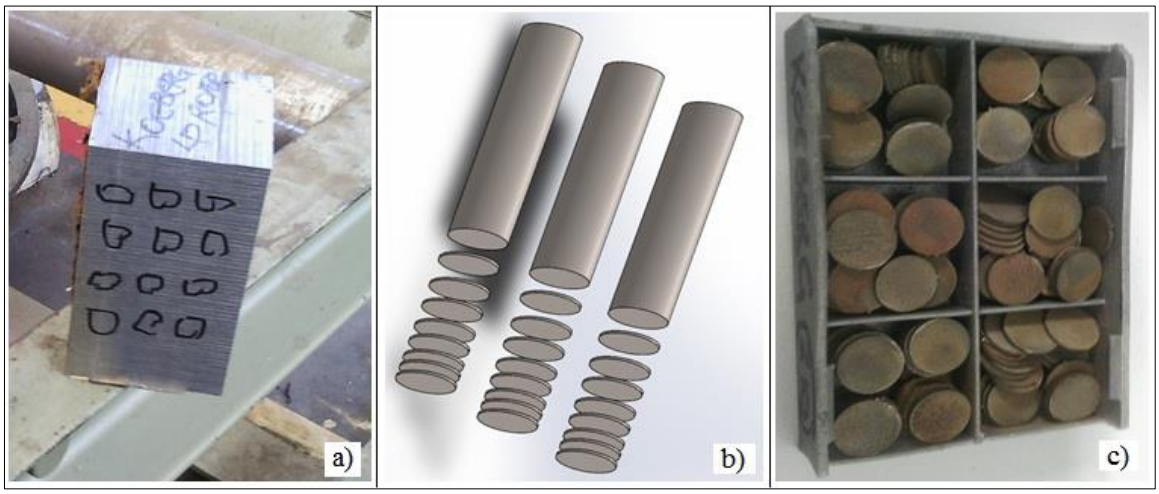

Figure 4-14: SPT sampling for LP rotor steel showing: a) the big sample before wire cutting, b) 3D CAD round bars wire cut to ϕ8 mm x 0.8 mm thick and c) unpolished samples.

Specimens were required to be lapped using metallographic lapping or grit paper. The sequence of lapping/grinding and polishing is shown in **Error! Reference source not found.** below. A new method of lapping/grinding was developed to improve the success rate of polishing the sample and is explained below.

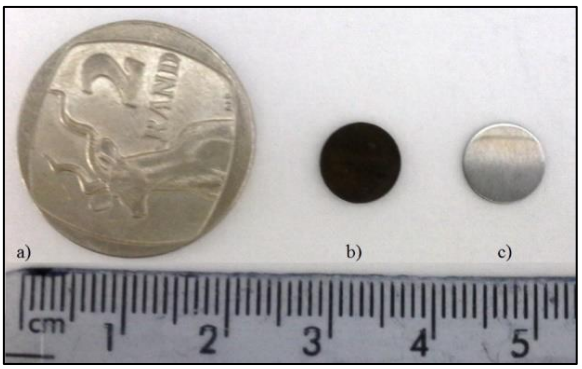

Figure 4-15: Comparison of size factor of: a) R2 coin, b) unpolished specimen (ϕ8 mm x 0.8 mm) and c) polished sample (ϕ8 mm x 0.5 mm).

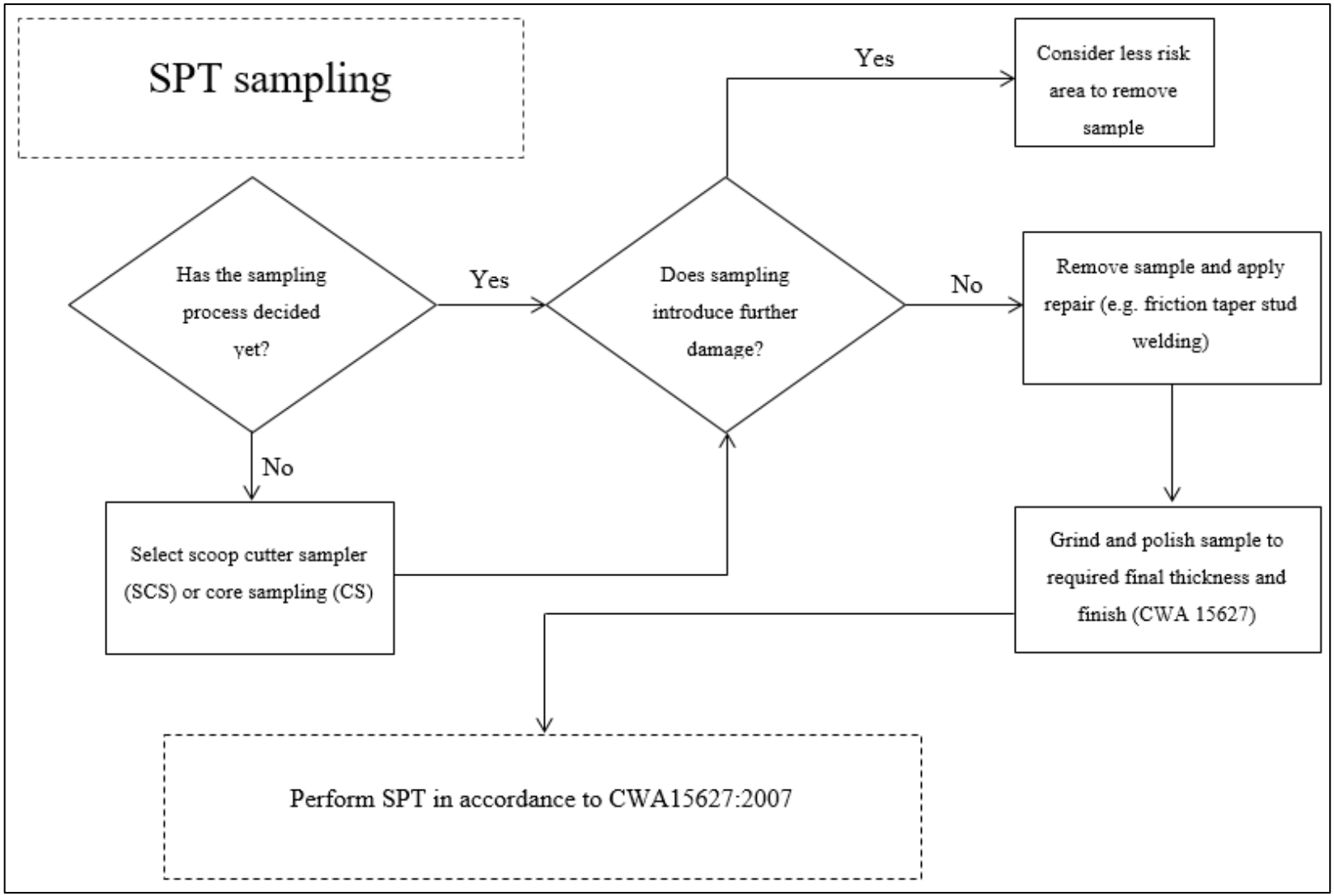

Figure 4-16: SPT sampling risk analysis.

4.7.1.1 Manufactured specimen holder and specimen

A sampling holder was designed and manufactured using 316L grade stainless steel. The sampling holder was made to minimise the time taken to lap samples and improve the success rate of the useful sample from 60-70% to 95%. The specimen holder has a 1 mm deep seat that allows the 0.8 mm wire cut disc to sit securely. The locked nut is used to adjust the height of the sample, which is to be grinded/lapped until the required height is obtained.

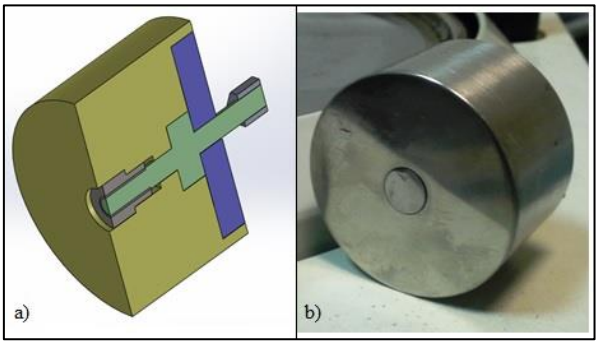

Figure 4-17: Specimen holder showing: a) sectional CAD drawing and b) photograph.

4.7.2 SPT setup and equipment

Testing equipment used to carry out mechanical tests was calibrated and in compliance with the standards mentioned in Table 4-3. These tests were carried out at the Eskom RT&D laboratory and UCT's Materials Engineering Laboratory.

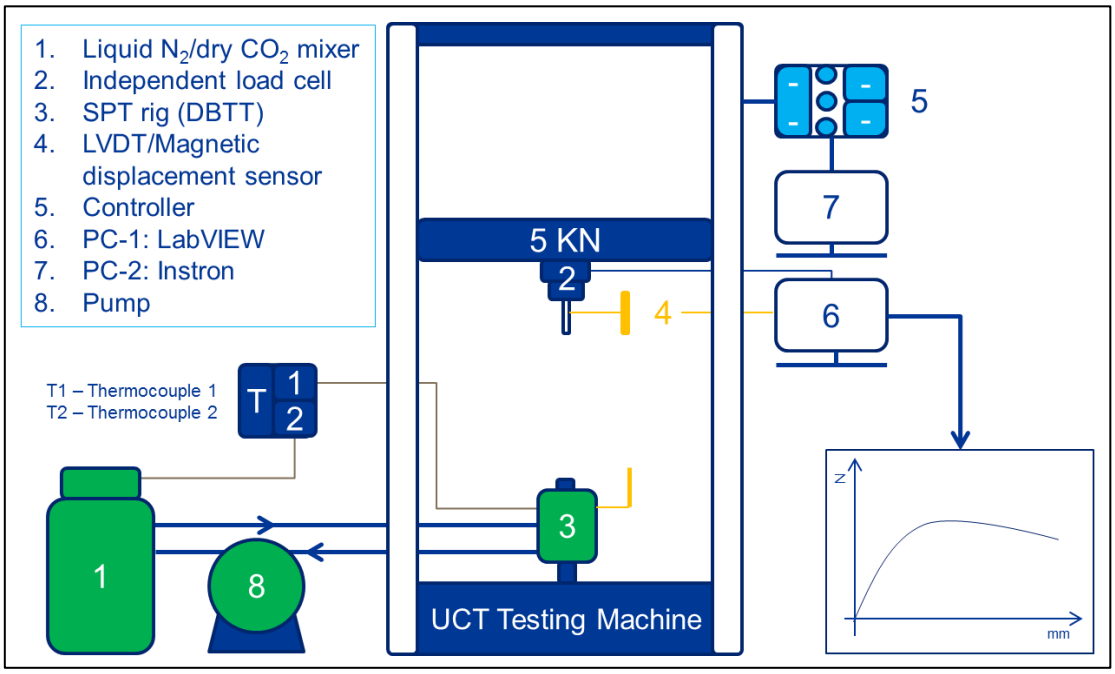

Figure 4-18: Schematic UCT SPT rig setup.

Figure 4-18 illustrates the SPT rig setup for both *DBTT* and elevated temperature. When elevated temperature experiment tests are carried out, items 1 and 8 are not required. The rig is exchanged with the relevant type as shown in Figure 3-18, Figure 3-19 and Figure 3-20 in Chapter 3. Items 5 and 7 are the control and the PC is connected to the testing machines. These items (5 and 7) are used to control the cross bar at the required constant displacement and the data that have been acquired through the Instron software can be used as raw test data.

4.8 Test required data for correlation

Standard mechanical tests are performed to validate the SPT_{FEM} and the SPT rigs and correlate with the SPT experimental data. Comments in Table 4-5 correspond to the same letter numbering i.e. comment a) and b) correspond to test data a) and b), respectively.

Table 4-5: Mechanical test data for correlation.

Type of standard mechanical test	**Test required data for SPT validation/correlation**		**Comment for correlation**	
Uniaxial tensile	a) Yield stress (σ_Y) and %Elongation	b) Raw true stress and strain (σ_{TRUE}; ε_{TRUE})	a) elasticity and ductility properties	b) SPT_{FEM} input data for Ramberg-Osgood model
CVN	a) Transition temperature (DBTT/FATT) and absorbed energy at transition temperature (E_{TT})	b) Raw absorbed energies (E_X) and corresponding test temperatures (T)	a) Material transition temperature properties (E_{CVN} and E_{SP} vs DBTT/FATT and T_{SP})	b) SPT energy (E_{SP}) at test temperature are plotted in %energy with CVN energy (E_{CVN}) graph (i.e. LSE to USE) to obtain SPT transition temperature (T_{SP})
Fracture toughness	Fracture load (P_Q), crack length (a_i or Δa) and fracture toughness (K_{IC})		SPT_{FEM} determines strain energy density (W_{SP}). W_{SP} is applied to CT_{FEM} to	

Type of standard mechanical test	Test required data for SPT validation/correlation	Comment for correlation
		determine strain energy density ($W_{CT} = W_{SP}$). P_Q at W_{CT} determines K_{IC} (ASTME E399) or J-Integral at W_{CT} determines J_{IC}

4.8.1 SPT procedure

The mechanical tests were performed in accordance with the applicable standards as shown in Table 4-3. The SPT test was carried out as per the instructions detailed below.

The procedure entails the pre-testing procedure requirements, testing instructions and end of test instructions. The procedure is developed for both the SPT rigs and the instructions that are not applicable are noted for each SPT rig.

4.8.1.1 Pre-testing setup instructions

1. Fit up the required SPT rig (DBTT or elevated temperature rig) in position and lock it using the sliding pin.

2. Ensure the SPT rig is secured, fixed and not moveable.

3. Connect the magnetic USB converter to the USB extension cable.

4. Fit the magnetic strip onto the punch and fix it at the required height using grab screws.

5. Fit the polished sample on the receiving die.

6. Fit and tighten the upper die using Allan screws to hold the sample in place (please note that if performing room or elevated temperature experiments, skip steps7 and 13).

7. Close and tighten the upper housing casing if it was removed (it is not necessary to remove this part to insert or replace the sample).

8. Insert the hardened ball into the upper die self-centring hole.

9. Insert and tighten the guide nut until it is flush with the face of the upper housing casing.

10. Connect tubes from/to the mixer and from/to the SPT casing via the pump and tighten with cable ties.

11. Insert the thermocouple in the SPT rig and seal with thread tape, and another thermocouple in mixer.

12. Connect the thermocouples to the TC-08 card.

13. Open the PicoLog software to monitor temperatures.

14. Insert the punch and ensure it is resting on top of the ball (for an elevated temperature SPT rig, bond the ball to the punch tip using crystal bond chemical prior testing).

15. Insert the camera in its designated slot (only applicable to the SPT rig of room/elevated temperature).

16. Start-up Instron Bluehill software from the PC on the left and the LabVIEW file named 'test 7'.

17. From the Bluehill software, setup a compression method with a displacement rate of 0.2 mm/min under test and activate limits (Load = 4 kN and displacement = 4 mm) and press save (note: the Instron 5 kN load cell has to be connected in series with the ULP load cell for safety limits to work).

18. From the LabVIEW 'test 7' file, ensure all lights are green from the front panel (note: the magnetic strip and sensor are allowed to be in contact or leave a small gap. The magnetic position light will turn red if these two are misaligned).

19. From the Bluehill software, open the test and select the setup compression method and name the test.

4.8.1.2 **Test instructions**

1. Manually move the crossbar downward until there is a clearance gap of approximately 0.5 mm between the stub connected to the ULP load cell and punch head.

2. Using the reset keys, zero the load and displacement.

3. From the LabVIEW front panel, click the white arrow positioned under the file tab and name the test excel file.

4. Press ok from the LabVIEW pop-out window and start the Bluehill software simultaneously.

5. Start the video camera recording 10 seconds after starting the test (ensure the recording is in real time)).

4.8.1.3 **End test instructions**

1. Observe the LDC from the Bluehill software.

2. Stop the test on both the video camera and LabVIEW simultaneously when the peak load drops.

3. Press stop test on Bluehill and move the crossbar upward with a clearance of approximately 200-250 mm for sample replacement.

4. The excel format LDC raw data (with real time as additional raw data on the third column) will save after stopping the LabVIEW front panel.

5. Determine the total time taken to run the test from the excel time recorded.

Watch the video and estimate the position of the punch displacement and crack initiation (consider the delayed 10 seconds).

4.9 Correlation

The correlation between the standard uniaxial tensile, CVN and fracture toughness with the SPT is carried out using FEM. Details of FEM instructions, comments and correlations are attached in Appendix-2 and in Table 4-5. Figure 4-19 and Figure 4-20 are the detailed research approach and correlation procedure between the SPT and tensile and Charpy impact energy.

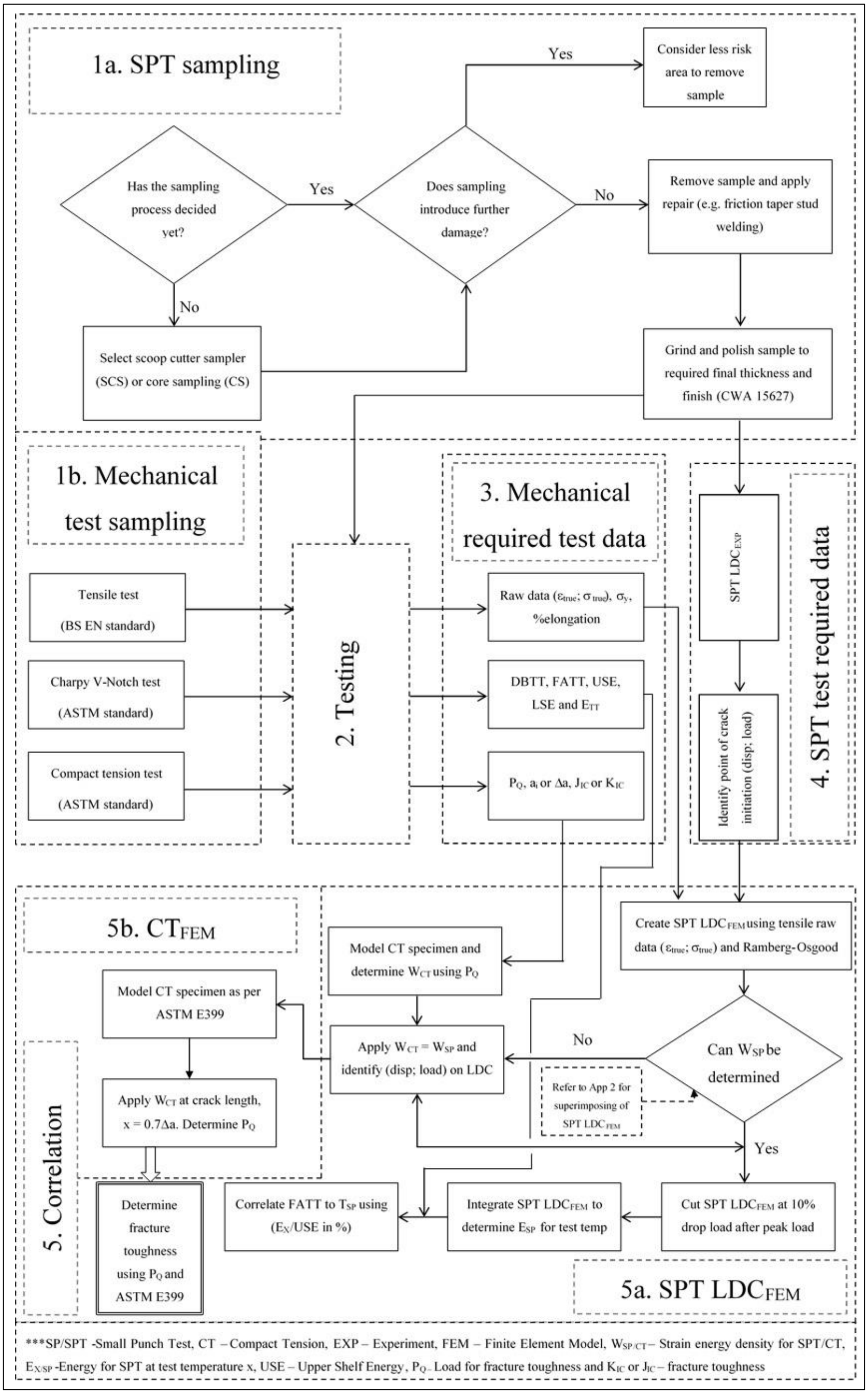

Figure 4-19: Detailed research approach.

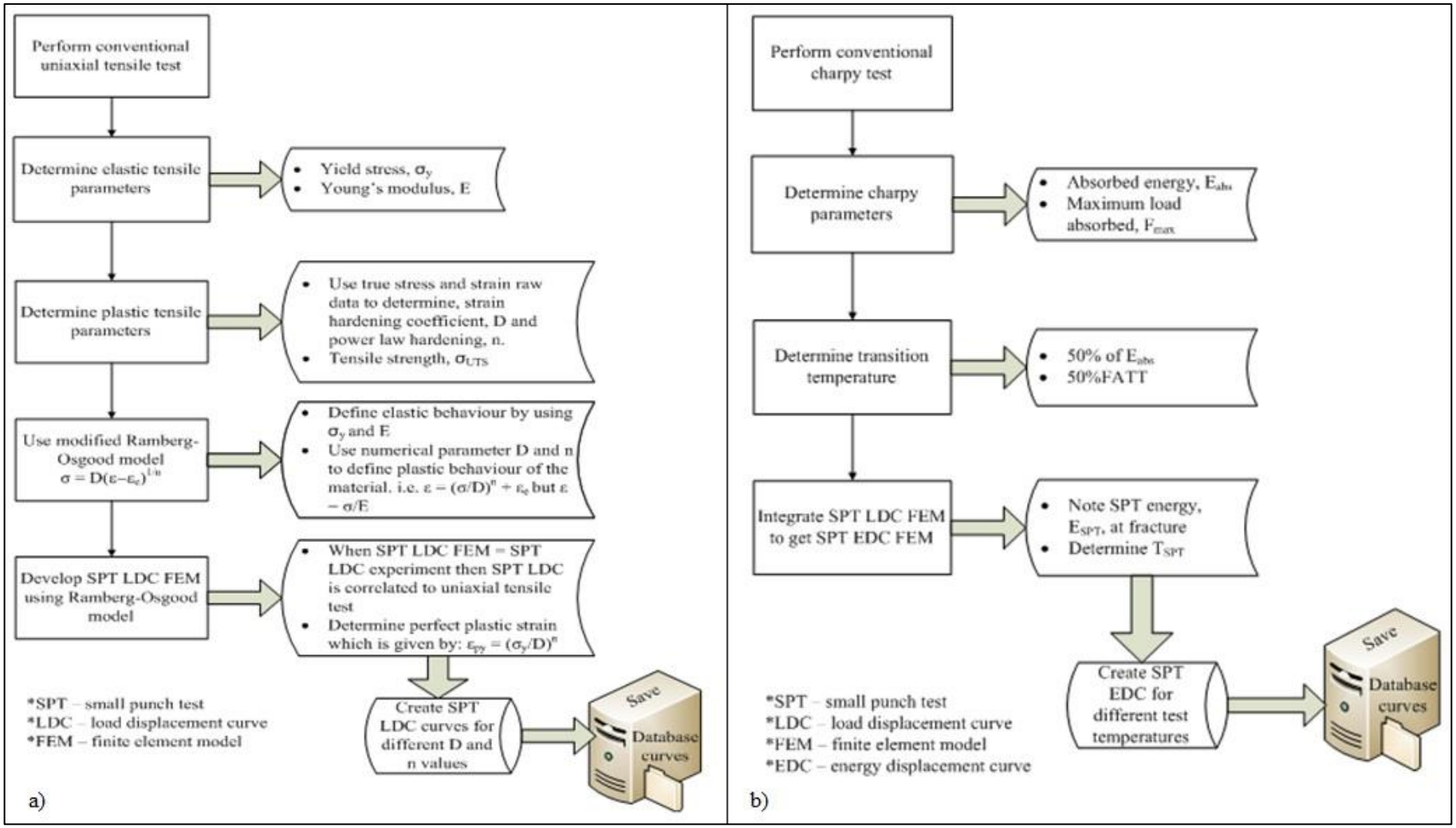

Figure 4-20 Approach to correlate: a) SPT LDC to uniaxial tensile test and b) E_{SP} to Charpy impact energy.

CHAPTER 5: RESULTS AND DISCUSSION

This chapter focuses on the test results of the standard mechanical test and the SPT. The test results are given in the sequence of the standard mechanical tests, followed by the SPT results and correlation between them. The details of the results are discussed at the end of each section and critical data (as shown in Figure 4-19 and Figure 4-20) required for correlation are summarised and evaluated against embrittlement.

5.1 Standard mechanical test

The standard mechanical test results are compared to pre-service exposure tests results [48] where possible, depending on the historical availability of such commissioning tests. NiCrMoV LP rotor steel was designed to operate at a nominal pressure of 10.77 bars and an operating temperature of 252°C. The total time of service exposure was 26 years.

5.1.1 Tensile test

Tensile test results are reported in two formats, namely tables and graph sketches. Figure 5-1 is a template for how the graph sketch should be interpreted. The following interpretation should be applied to all tensile test result figures unless stated otherwise:

- A: Title material designation, which is NiCrMoV,
- B: Sample identification, AR (only As-Received samples were used for the tensile test),
- C: Test temperature,
- D and E: Strain (in mm/mm or %) and Stress (in MPa), respectively,
- F and G: Number of samples (i.e. Sample 1 or Sample 2, etc.)

The title of the plotted graph will only show the material designation (NiCrMoV) whenever average raw data at different test temperatures are plotted. Strain gauge attached to samples during tests (up to 3.5% of each test) was to determine the Young's modulus (E) and 0.2% yield stress ($0.2\sigma_y$). This is done to improve the accuracy of the raw data of the elastic region, which is required to determine these two test parameters (E and $0.2\sigma_y$). Refer to Figure 5-2, Figure 5-3 and Figure 5-4 for details.

The plastic region of the tensile test is used for Ramberg-Osgood model parameters (D and n), as explained in Chapter 3, Section 3.7 and in Appendix-2. Raw data for true stress and

true strain is smoothened and plotted against the two samples at each test temperature (see Figure 5-5, Figure 5-6 and Figure 5-7). Table 5-1 summarises the tensile test showing and comparing the important tensile test parameters. The test data/parameters are plotted as Sample 1/Sample 2 for the commissioning test and the test temperatures carried out in this research.

5.1.1.1 Tensile test results

Refer to the figures and table below.

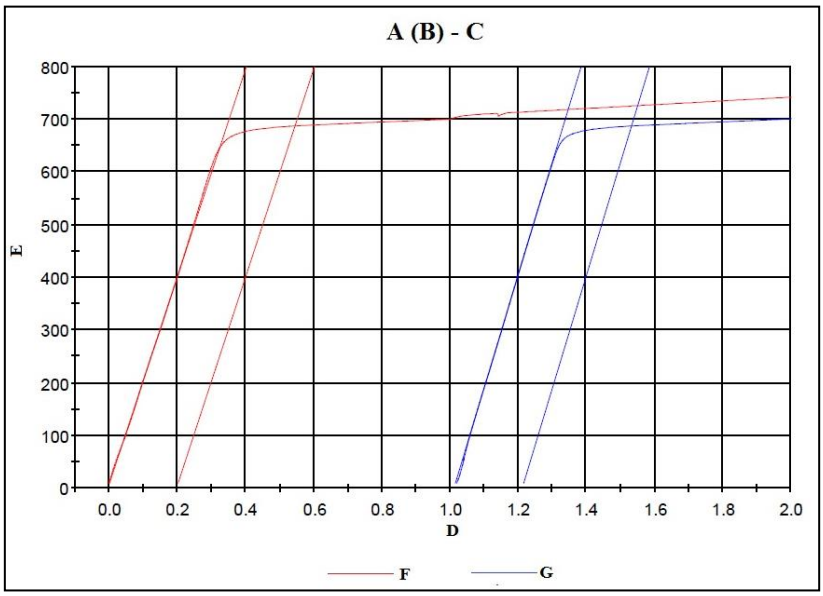

Figure 5-1: Tensile test template.

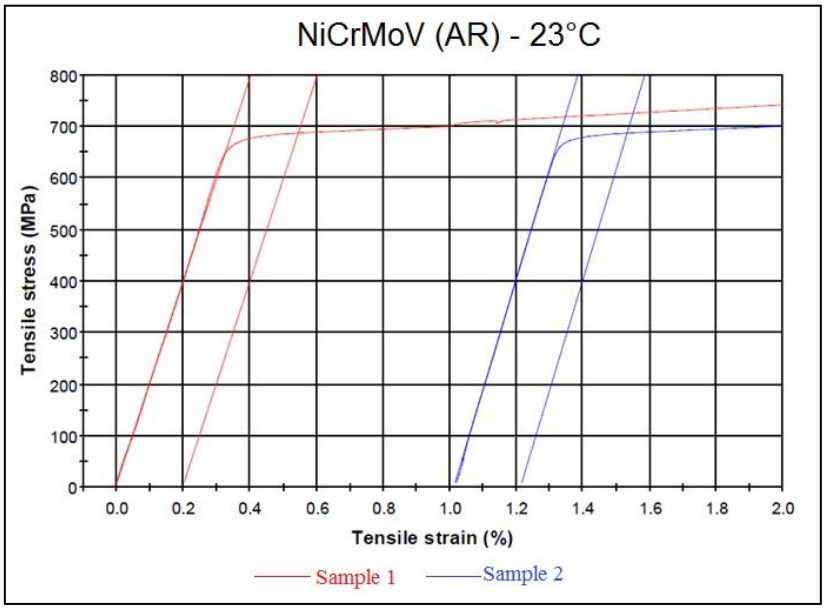

Figure 5-2: Tensile test showing method of determining E and 0.2σ_y at 23°C.

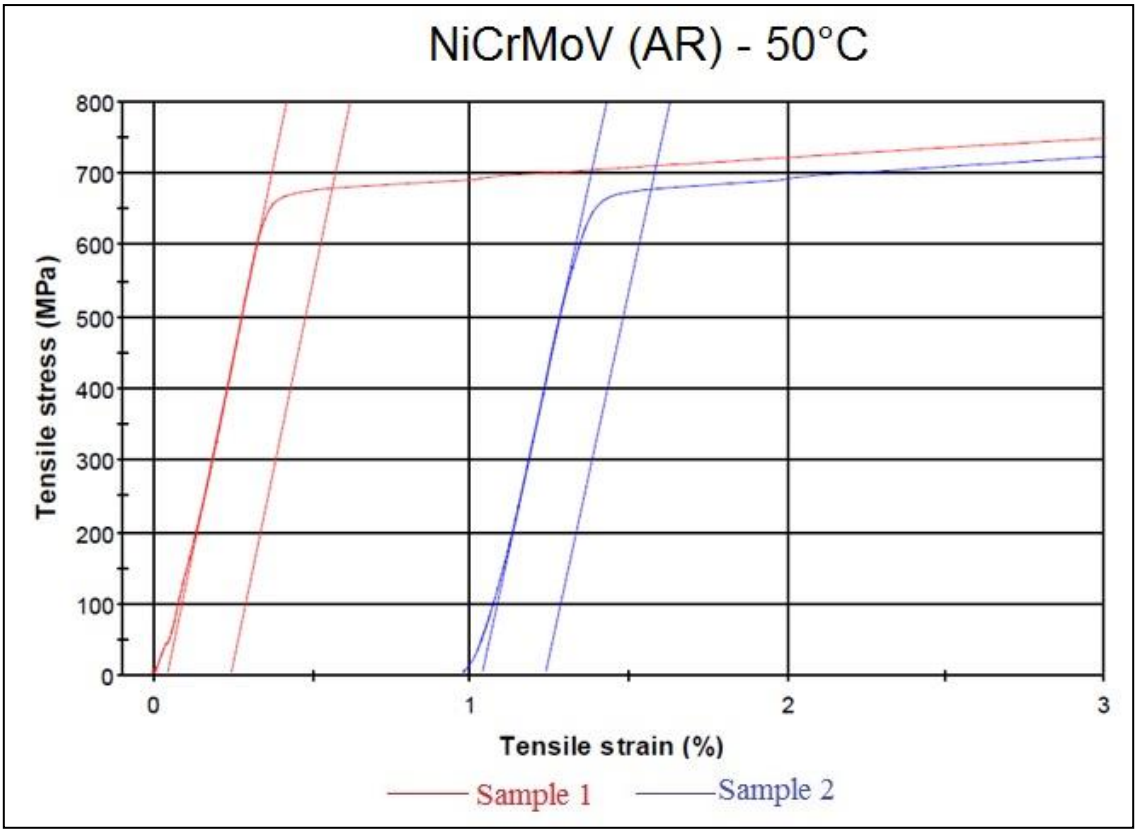

Figure 5-3: Tensile test showing method of determining E and $0.2\sigma_y$ at 50°C.

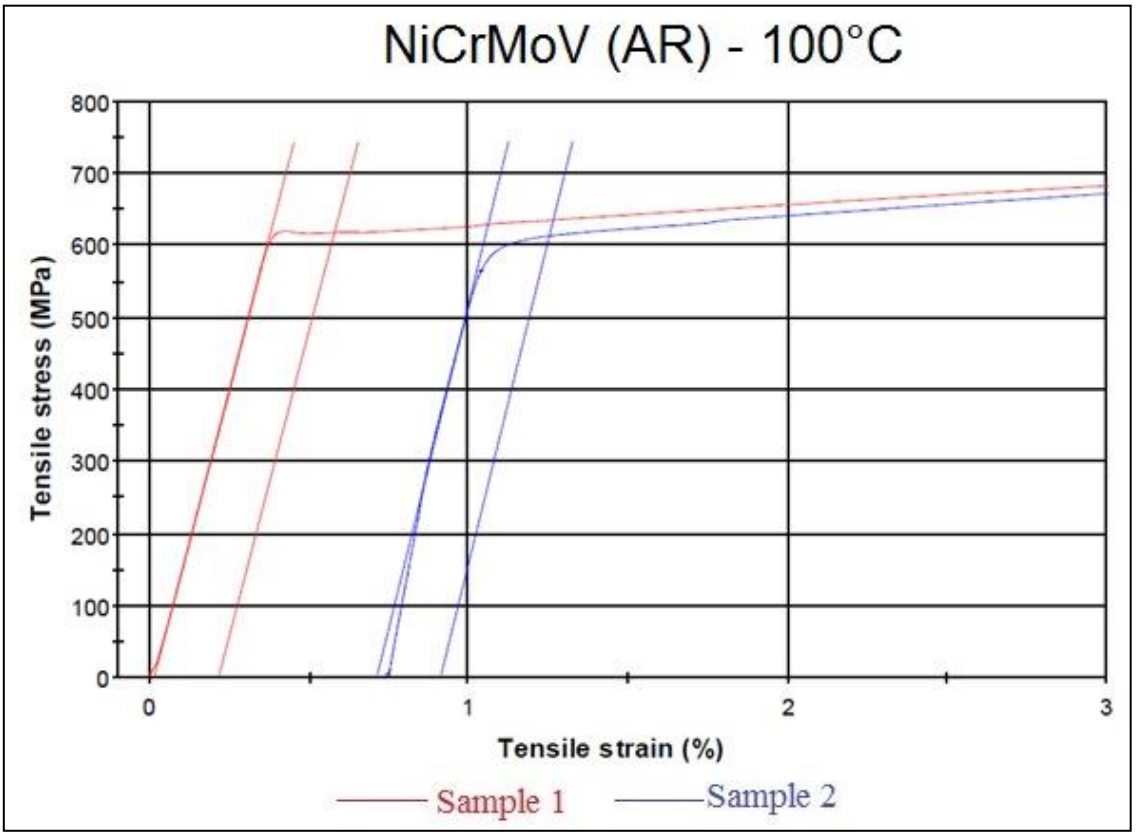

Figure 5-4: Tensile test showing method of determining E and $0.2\sigma_y$ at 100°C.

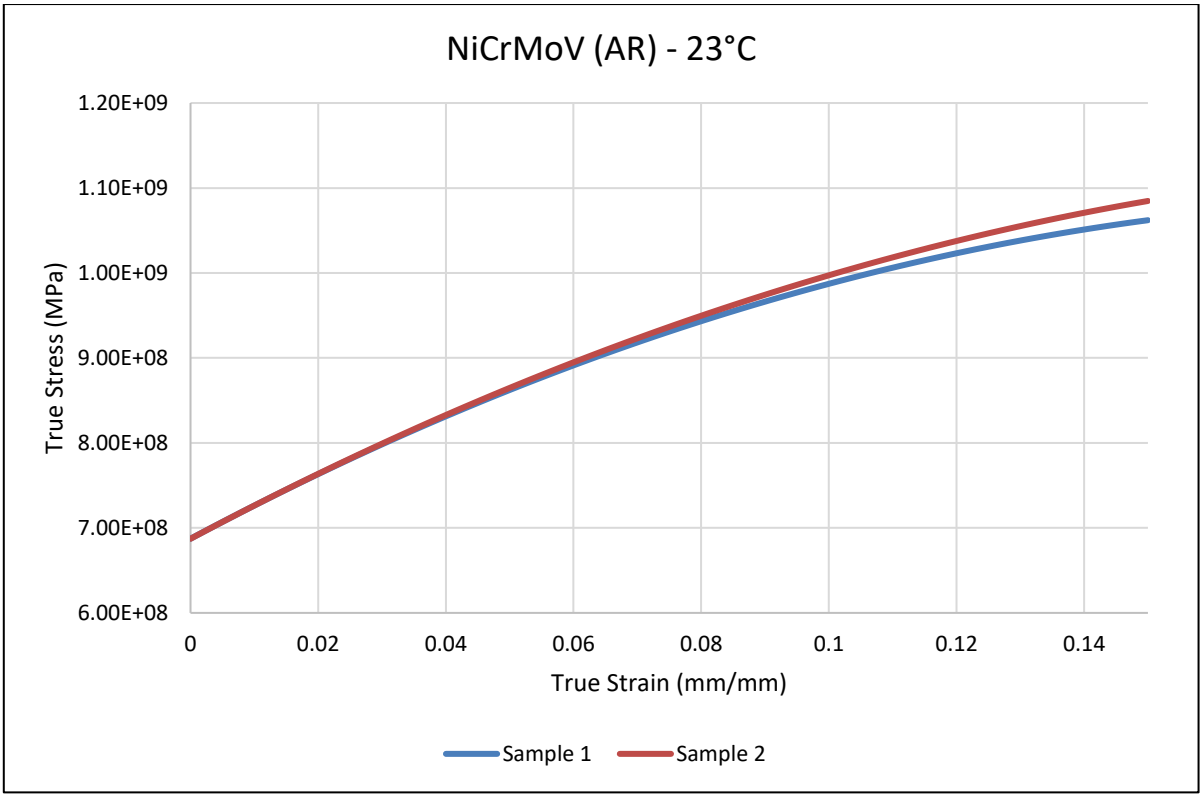

Figure 5-5: True stress vs true strain curve at 23°C.

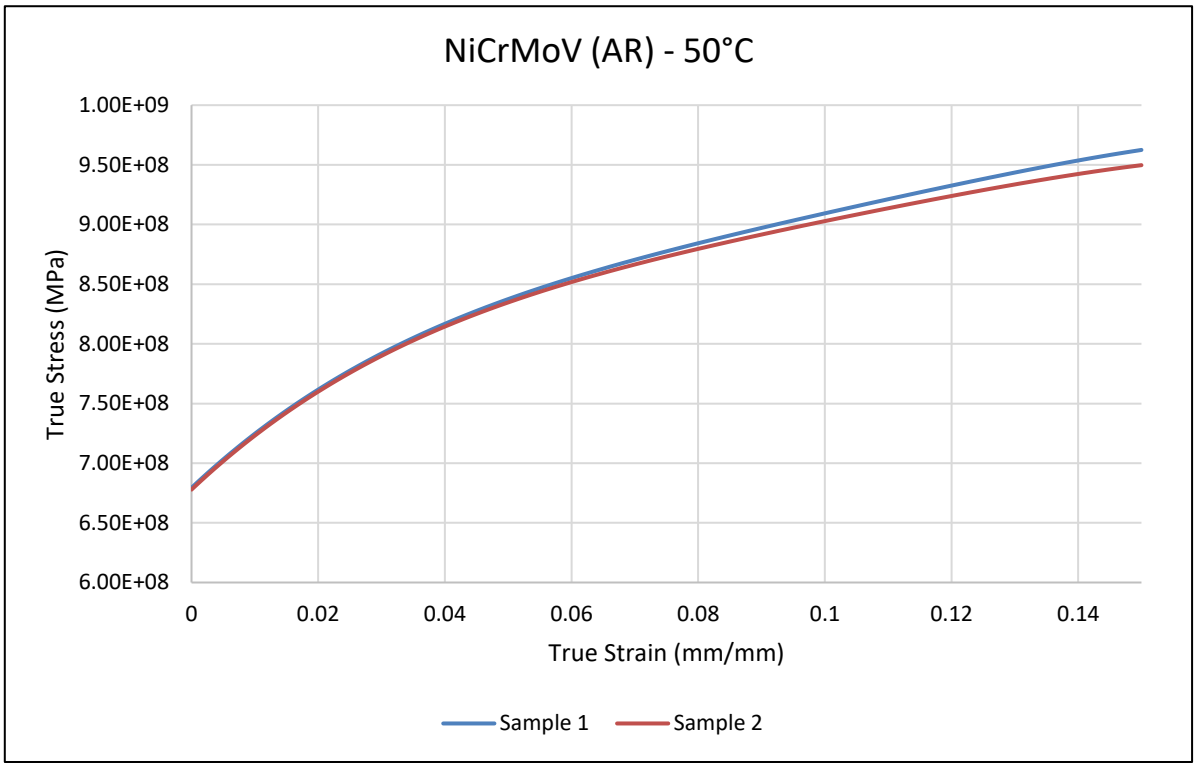

Figure 5-6: True stress vs true strain curve at 50°C.

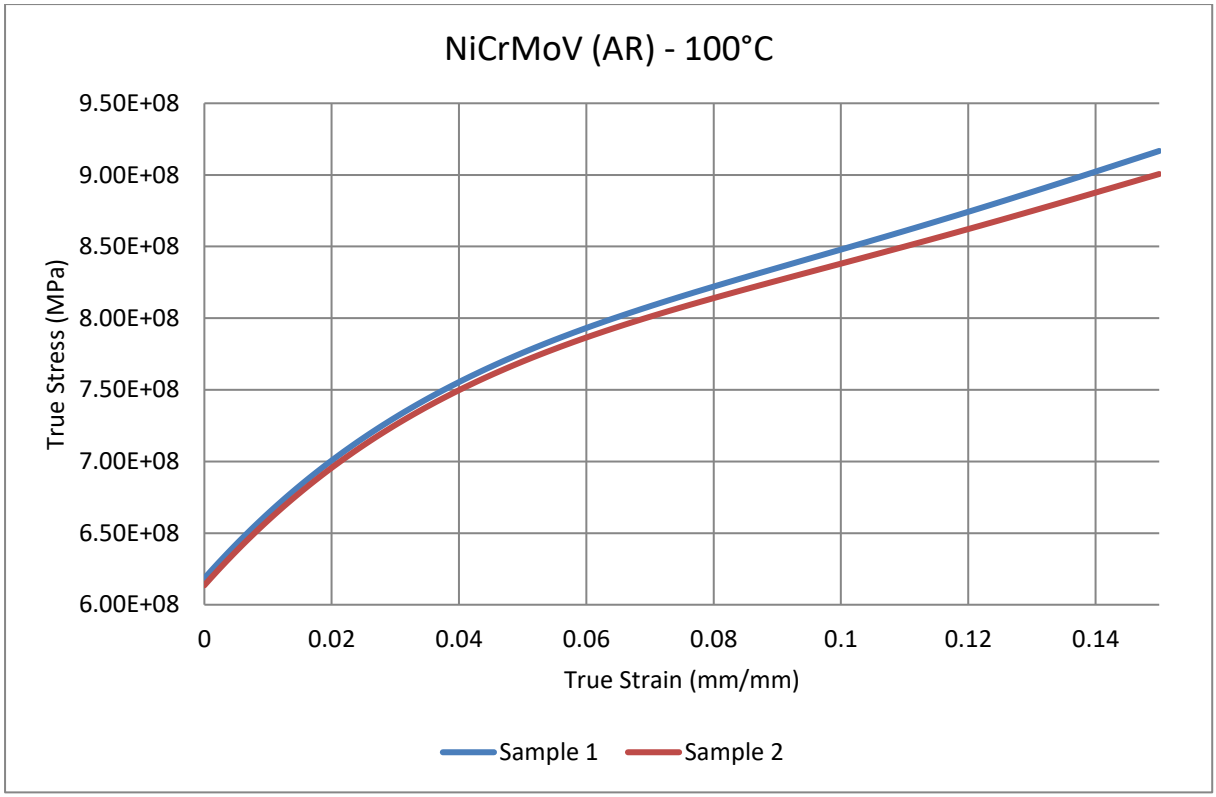

Figure 5-7: True stress vs true strain curve at 100°C.

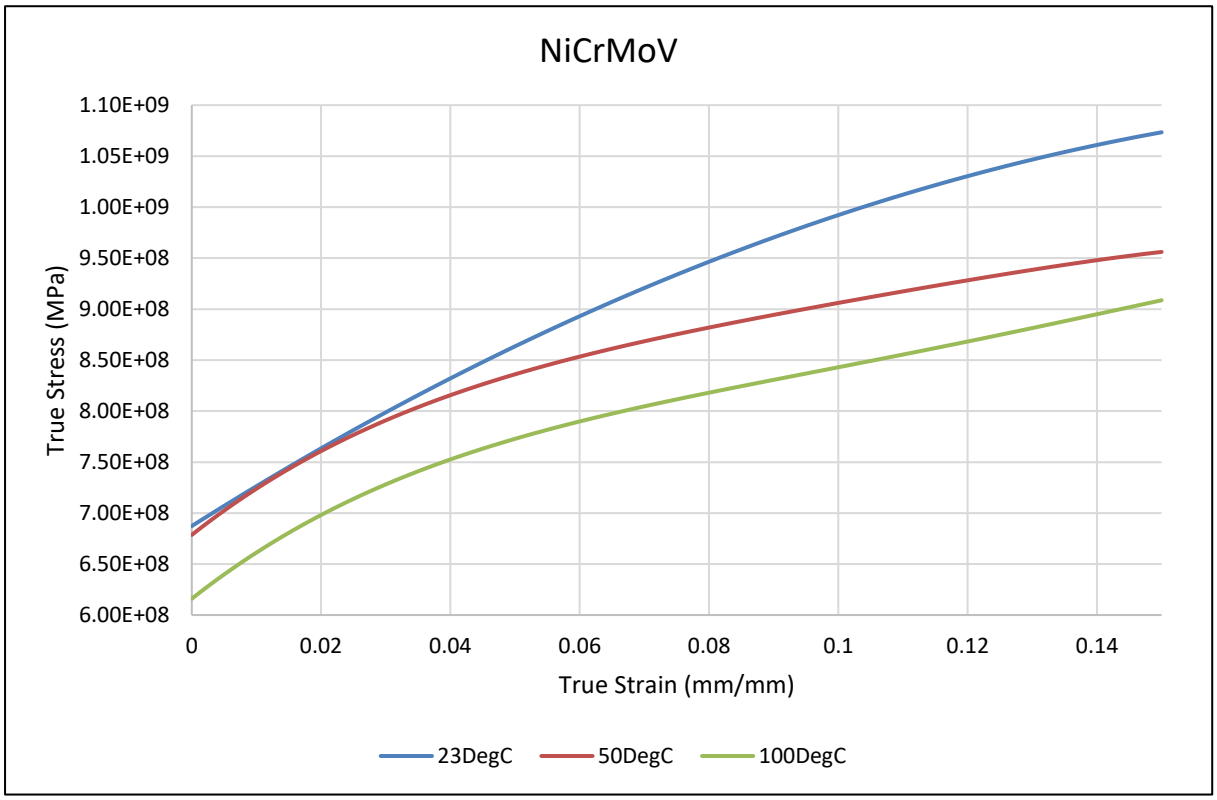

Figure 5-8: Average true stress vs true strain at different test temperatures.

Table 5-1: Tensile test results of virgin and exposed NiCrMoV turbine rotor.

Service	Test temp (°C)	$0.2\sigma_y$ (MPa)	UTS (MPa)	Elongation (%)	Reduction of area (%)	E (GPa)
Virgin	23	692.02/ 717.01	817.01/ 832.00	19.00/17.40	61.51/ 60.01	-
Exposed	23	687.31/ 687.23	825.87/ 825.58	20.35/ 18.61	63.96/ 63.10	197.44/ 214.30
	50	679.35/ 677.84	810.74/ 809.38	19.48/ 19.41	64.69/ 65.13	212.35/ 202.46
	100	654.22/ 663.89	777.56/786.57	17.36/ 18.79	62.98/ 66.33	186.70/165.03

5.1.1.2 Tensile test discussion

Table 5-2 was generated from Table 5-1 in order to illustrate the differences that occurred over the exposure life of this LP rotor steel. The discussion is divided into the three regions of the stress-strain curve, namely, the elastic, elastic-plastic and plastic region. The parameters within these three regions are compared and evaluated as shown in Table 5-2. 0.2% Proof Stress has dropped by about 2.51% while Young's modulus has increased by 2.85%. The elastic region of the exposed material seems to have both less 0.2% Proof Stress and strain as compared to the virgin material (assumed E = 200GPa as it was not supplied with history test reports).

Table 5-2: Tensile test comparison at room temperature.

Service	$0.2\sigma_y$		E		Elongation		Reduction of area		UTS	
	Elasticity				Plasticity				Elasticity/ Plasticity	
	Avg (MPa)	Chg (%)	Avg (GPa)	Chg (%)	Avg (%)	Chg (%)	Avg (%)	Chg (%)	Avg (MPa)	Chg (%)
Vgn	704.52	-2.51	200.00	2.85	18.20	6.57	60.76	4.36	824.51	0.15
Expd	687.27		205.87		19.48		63.53		825.73	

***Avg – Average, Chg – Change, Vgn – Virgin material and Expd – Exposed material.

The comparison of the plasticity determines if the material ductility is affected over the period of service exposure. The decrease in elongation or area reduction can symbolise material hardening due to temper embrittlement or other material degrading mechanisms. Elongation has increased by 6.57% and the reduction of the area has also increased by 4.46%, which indicates no sign of embrittlement from the ductility mechanical properties. The procedure of operating steam turbine rotors, which includes tempering during shutdowns and start-ups, is recommended by the Operating Equipment Manufacturer (OEM). This is done to minimise the risk of incurring turbine rotor temper embrittlement during cold shutdown. The tensile test of the ex-service has proven that the OEM's recommendations are part of ensuring the operation of full design life. The tensile strength (UTS), which can affect either the elastic or the plastic region, has an insignificant increase of 0.15%. The increase in UTS can be a sign of loss of ductility (elongation) and it can increase the yield stress in the process.

The Ramberg-Osgood model parameters were determined from the true stress-true strain curve (power trend line equation) as explained in Appendix-2 for all three test temperatures, refer to Table A2.1 under Appendix for details. These parameters/numerical values were determined at three dual yielding plastic strain values (as per raw data, ε_{py} = 0.01 and 0.002 for perfect plastic strain of low alloy) [20]. The first ε_{py} was determined using

$$\varepsilon_{py} = \left(\frac{\sigma_y}{D}\right)^n$$

Equation 5-1: Plastic strain for Ramberg-Osgood model.

The initial ε_{py} was determined using Equation 5-1 above. The MS Excel goal seek function was then used to determine new numerical values (D, n) when ε_{py} = 0.01 & 0.002. Table 5-3 shows the dual yielding strain values at each test temperature from the tensile raw data.

Table 5-3: Derived Ramberg-Osgood numerical values from tensile raw data.

Plastic strain	Test temp (°C)	Sample 1	Sample 2
ε_{py}	23	0.008	0.008
ε_{py}	50	0.006	0.008
ε_{py}	100	0.01	0.01

The main purpose of performing the tensile test was to validate both the SPT_{FEM} and the SPT rigs which will be applied during the tensile test – SPT correlation.

5.1.2 Charpy V-Notch (CVN) test

The Charpy results were reported for both virgin and service exposed material. The test results of prior service were supplied by the manufacturer [48] of the rotor and were performed during commissioning of the rotor.

5.1.2.1 CVN test results

The comparison of the virgin and exposed material was conducted to evaluate any sign of embrittlement in the material. The polynomial third order term was used to estimate both *DBTT* and *FATT* as shown in Figure 5-9. The test data supplied by Operating Equipment Manufacturer (OEM) in Quality Assurance Data Package (QADP) [48] was used to develop Figure 5-9.

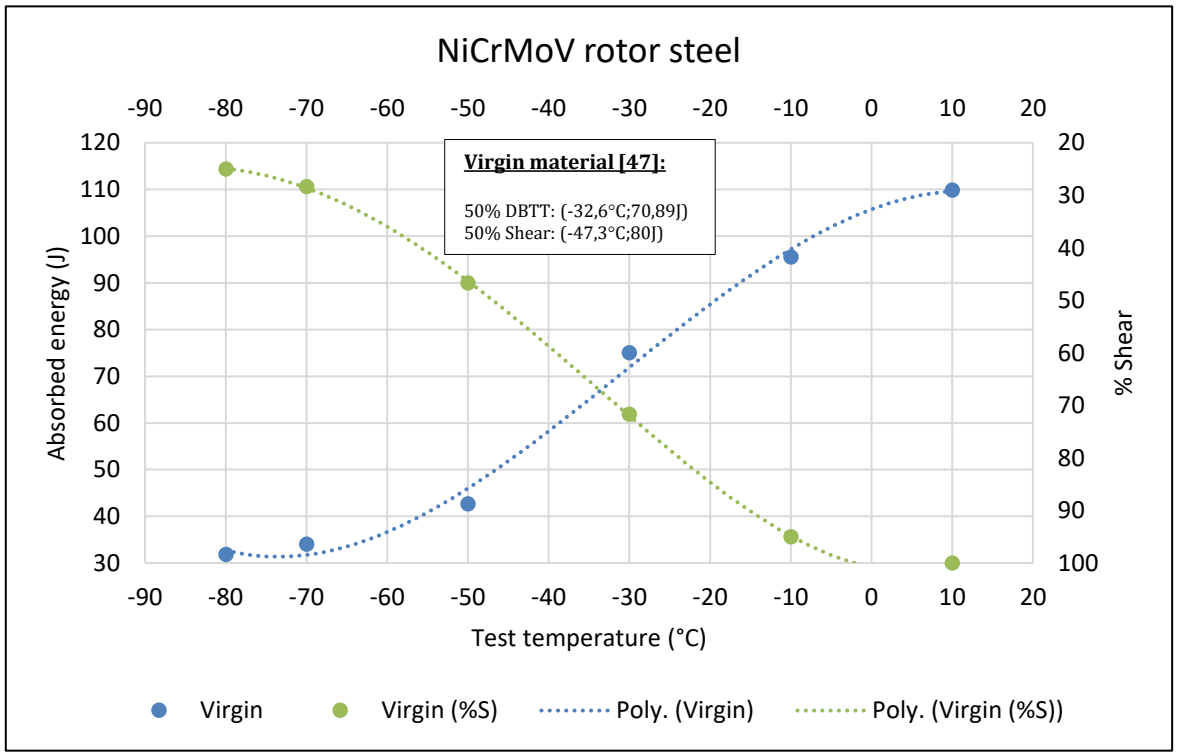

Figure 5-9: CVN test results for virgin NiCrMoV adopted from QADP [48]**.**

Table 5-4: CVN test results of virgin and exposed NiCrMoV turbine rotor.

Service	DBTT/FATT (°C)	**USE (J)	**LSE (J) @-80°C	Energy at DBTT/FATT (J)
Virgin	-32.6/-47.3	109.9@10°C	31.89	70.89/46.98
Exposed	-31.9/-33.6	156.33@23°C	6.78	81.55/67.39

** USE – Upper shelf energy and LSE – lower shelf energy.

These results are the averaged value of three samples tested at each test temperature as per ASTM E23. Figure 5-10 and Figure 5-11 illustrate the change in impact energy and transition temperature on both *DBTT* and *FATT*, respectively. The small punch transition temperature, T_{SP}, for low alloy steel (NiCrMoV) is provided by Foulds and Viswanathan [20] in Table 2-6 in the Literature Review. Table 5-5 provides the correlated values of T_{SP} for both virgin and service exposed materials at *FATT* and *DBTT*. The correlation is developed based on the energy absorbed and, therefore, the correlated *FATT* represent Charpy *DBTT*.

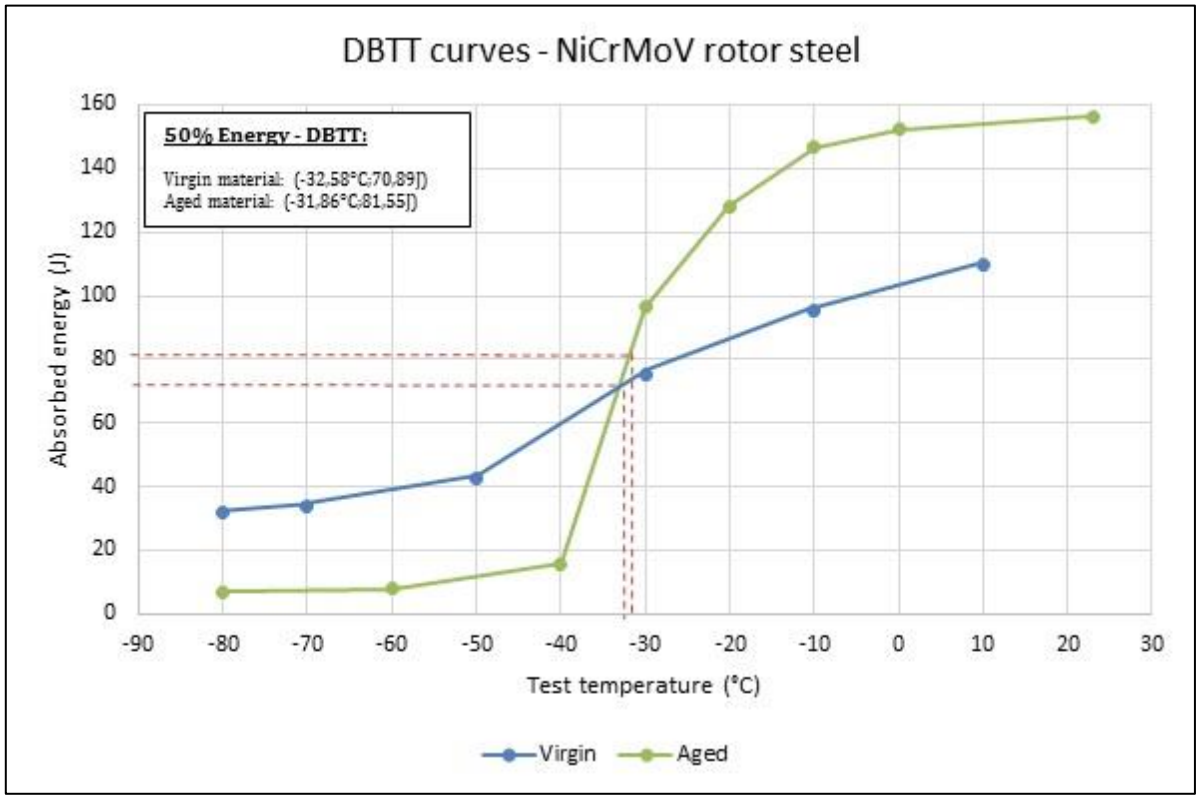

Figure 5-10: DBTT results of NiCrMoV rotor steel.

Table 5-5: T_{SP} correlated to FATT for low alloy steel (NiCrMoV) [20]**.**

FATT (°C) = 363.80 + 2.312T_{SP} (°C) [20]		**T_{SP} (°C)**
$FATT_{Virgin}$	-47,3	-177,8
$FATT_{Aged}$	-33,6	-171,9
$DBTT_{Virgin}$	-32,5	-171,4
$DBTT_{Aged}$	-31,9	-171,1

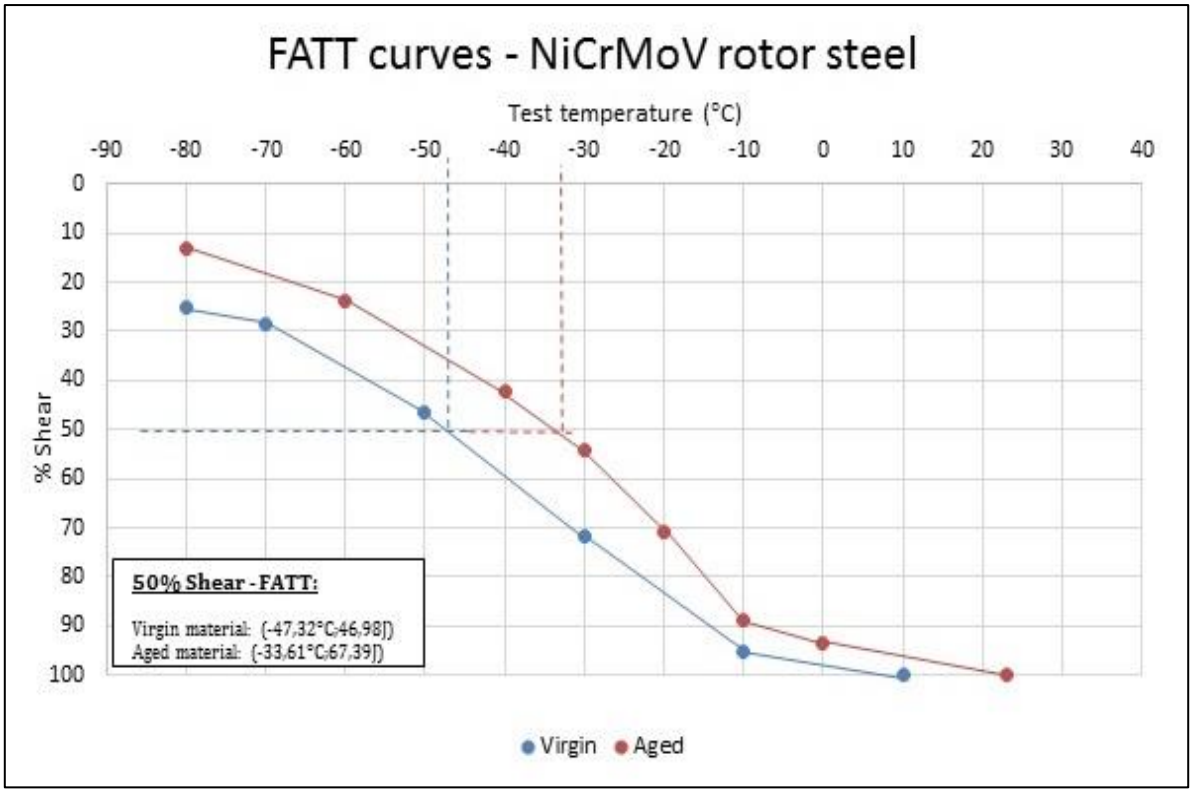

Figure 5-11: FATT results of NiCrMoV rotor steel.

Using developed empirical correlation between CVN impact energy and fracture toughness test for Lower Shelf Energy (LSE), K_{IC} was determined. The conversion of J_{IC} from K_{IC} was adopted from the ASTM E399 where the material ductility is regarded to be nil.

5.1.2.2 CVN impact energy – K_{IC} correlation

The known impact energy from experimental results was used to determine fracture toughness using the established correlation relationships in Table 5-6. The intent of these correlated K_{IC} (referred to as '*FATT* approach' in this study) was to compare these results to the experimental K_{IC} as well as the predicted EPRI approach K_{IC} in order to establish the error band between the predicted K_{IC}, and the experimental K_{IC}.

Table 5-6: CVN and K_{IC} correlation for transition temperature & lower shelf energy [2]**.**

Correlation		Property	LSE (-80°C)	DBTT (-31,9°C)	RT (23°C)	Comments
Units	K_{IC} (MPa√m)	CVN (J)	6,78	81,55	156.33	-
	J_{IC} (kJ·m^{-2})	*v*	0,3	0,3	0.3	-

Correlation		Property	LSE (-80°C)	DBTT (-31,9°C)	RT (23°C)	Comments
		σ (MPa)	-	-	687.3	-
Barsom-Rolf	$K_{IC}^2/E = 0.22(CVN)^{3/2}$	K_{IC}	0.88	5.69	9.27	CVN energy = 3 to 82J
		J_{IC}	3.53E-3	0.14	0.39	
	$K_{IC}^2/E = 2(CVN)^{3/2}$	K_{IC}	2.65	17.16	27.96	σy = 269 to 1696MPa static test
		J_{IC}	32.13E-3	1.34	3.57	

Table 2-7 in Chapter 2 shows the list of correlation established through experimental tests between CVN and fracture toughness. Barson-Rolf correlation was the only correlation applied to this study as the rest of the other correlations did not meet the requirements (i.e. comments as shown in Table 5-6). Figure 5-12 shows the difference in estimated K_{IC} values when considering CVN and tensile test data.

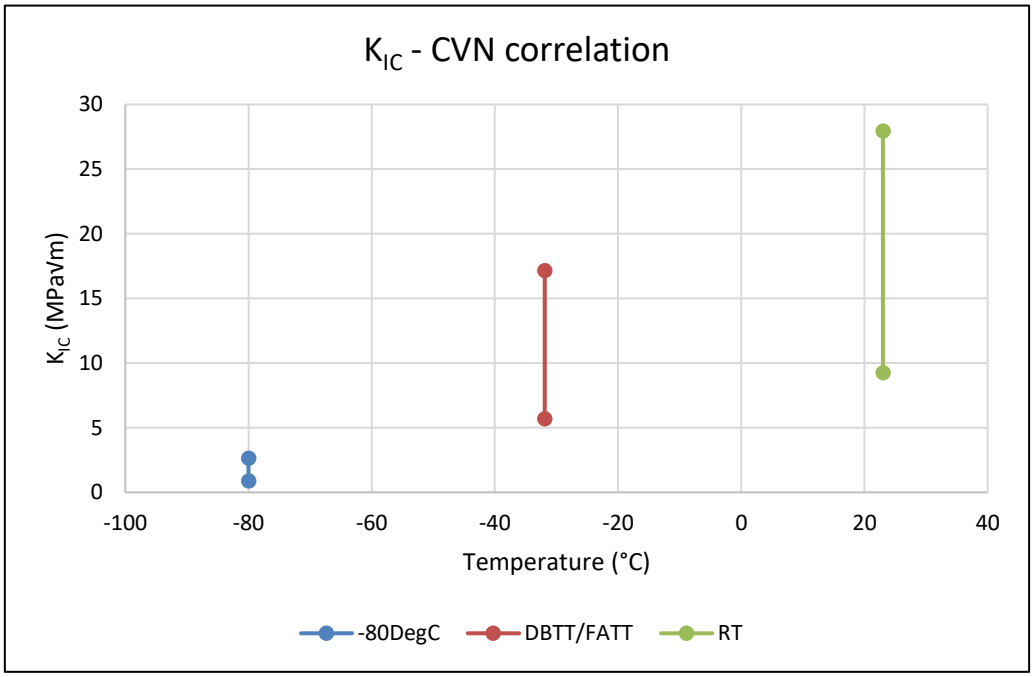

Figure 5-12: Estimated K_{IC} using CVN correlation.

5.1.2.3 CVN test discussion

a) Transition temperature results

The transition temperature signifies the temperature at which the material is vulnerable to embrittlement. The transition temperature (*DBTT* or *FATT*) occurs at a low impact energy at

which materials are not supposed to be operated, close to and/or below *DBTT/FATT*. The change in transition temperature was insignificant while the change in impact energy was significantly noticeable (refer to Table 5-7 for summarised results). *DBTT* is derived from impact energy against test temperatures and, therefore, human error in interpreting the results is very minimal. This is because the data is automatically stored via the hardware of the equipment used, which means the results are accurate. *FATT* is derived from fracture appearance, which is manually interpreted by looking at the fracture appearance area of fractured specimens. The material showed insignificant change at *DBTT,* which implies that the OEM manual was correctly applied during its service life. The difference noted in *FATT* is questionable based on what is stated above but it is still very low.

Table 5-7: CVN test summary.

Properties	Change in property	Comments
DBTT	0.7°C	Decrease in DBTT which is insignificant
FATT	13.7°C	Decrease in FATT which is significant
USE @DBTT	10.6J	Increase in impact absorbed energy
LSE @FATT	20.5J	Increase in impact absorbed energy

b) Impact energy results

With reference to Table 5-7, impact energy at transition and above seems to have increased, which can mean that the material has become a bit more ductile than before commissioning. It is regrettable that the opposite occurred, as seen in Figure 5-17, the impact energy below -32.6°C has decreased significantly, which can imply that the material is more brittle than it was below *DBTT* (e.g. impact energy difference at -60°C is approximately 32J).

c) Correlated K_{IC} using CVN impact energy

The estimated K_{IC} values seemed significantly small. The *FATT* approach is known to have an error band of up to 50%, which could be the reason for the achieved results. The ductile fracture toughness values were derived from the elastic behaviour equation as shown in the ASTM E399 (E was assumed to be 200 GPa, which is the known value for steel).

5.1.3 Fracture toughness

This test was performed to validate and compare the EPRI modelled K_{IC}. The modelled parameters were required to be confirmed through experimental fracture toughness.

5.1.3.1 Fracture toughness results

Fracture toughness pre-test requirements included fatigue load to initiate the crack and to grow the crack. Sample 1 was subjected to trial pre-test requirements and the fatigue parameters in Table 5-8 were reported.

Table 5-8: Crack growth caused by fatigue loading for NiCrMoV rotor steel.

Sample name	Fatigue load to initiate crack (kN)	Number of fatigue cycles to initiate crack	Fatigue load to grow crack (kN)	W/B (mm)
Sample 1	8-10	86280	10	25/12.5
Sample 2	8-10	82310	10	25/12.5
Sample 3	8-10	81590	10	25/12.5

Crack length, a, for each sample was grown to meet the requirement of $0.45W \leq a \leq 0.55W$ as per the ASTM E399 [15]. Table 5-9 shows the fracture toughness test results.

Table 5-9: Fracture toughness results of NiCrMoV rotor steel.

Sample name	Crack length, a (mm)	P_{MAX} (kN)	P_Q (kN)	*P_{MAX}/P_Q	K_Q (Mpa$\sqrt{m}$)
Sample 1	11.74	26.23	23.25	1.13	103.82
Sample 2	11.41	27.18	23.74	1.17	99.87
Sample 3	11.56	24.51	21.62	1.13	94.51

*P_{MAX}/P_Q of 1.10 was not met and therefore K_Q does not equal to K_{IC} as per ASTM E399.

Compliance of the results was evaluated using the compliance method(s) prescribed by the ASTM E399 and Table 5-10 shows non-compliance of the results.

Table 5-10: Fracture toughness test compliance.

Sample name	$2.5(K_Q/\sigma_y)^2$ (mm)	W-a (mm)	$2.5(K_Q/\sigma_y)^2 < (W-a)$
Sample 1	57.05	13.25	No, non-compliance

Sample name	$2.5(K_Q/\sigma_y)^2$ (mm)	W-a (mm)	$2.5(K_Q/\sigma_y)^2 < (W-a)$
Sample 2	52.79	13.59	No, non-compliance
Sample 3	47.28	13.44	No, non-compliance

5.1.3.2 Fracture toughness discussion

The ASTM E399 was followed to perform the fracture toughness test as shown above and regrettably the K_{IC} requirements were not met. The ASTM 1820 should have been used to carry out the experiment since the material tested was a non-linear (elastic-plastic) behaviour material. However, the results were used as K_Q because the load ratio (refer to Table 5-9) was out by a small margin of 2-6%. P_Q was used to validate the strain energy density of modelled compact tension, which is explained in detail in Section 5.2.

5.2 Small punch test

This sub-section entails the experimental results and discussion of the SPT. Figure 5-13 is a template of how the SPT LDC graph sketch should be interpreted. The following interpretation should be applied in all the SPT LDC result figures:

- A: Title material designation, which is always NiCrMoV in this research,
- B: Sample identification, AR (As-Received), DE (De-Embrittled, HD (Hardened),
- C: Test temperature (RT – room temperature, i.e. 23°C),
- D and E: Load (in N) and Displacement (in mm), respectively,
- Sn: Sample number (i.e. Sample 1, Sample 2, etc.)

5.2.1 SPT LDC experiment test

These results are reported in the sequence of material condition of AR, DE and HD LDCs at room and above room test temperatures (i.e. 23, 50 and 100°C). Seven LDCs at each temperature were generated in accordance with CWA15627 requirements for embrittlement tests. The average LDC was derived from seven SPT LDCs of each test temperature per material condition. These average LDCs were compared at each test temperature. The test temperature below room temperature was only performed for AR material specimens. These SPT LDCs below room temperature were plotted for average LDCs only. The discussion of the experimental SPT LDCs follows after the results (which were observed to be consistent for all three compared specimen conditions) given in Section 5.2.1.1.

5.2.1.1 SPT LDC experiment results

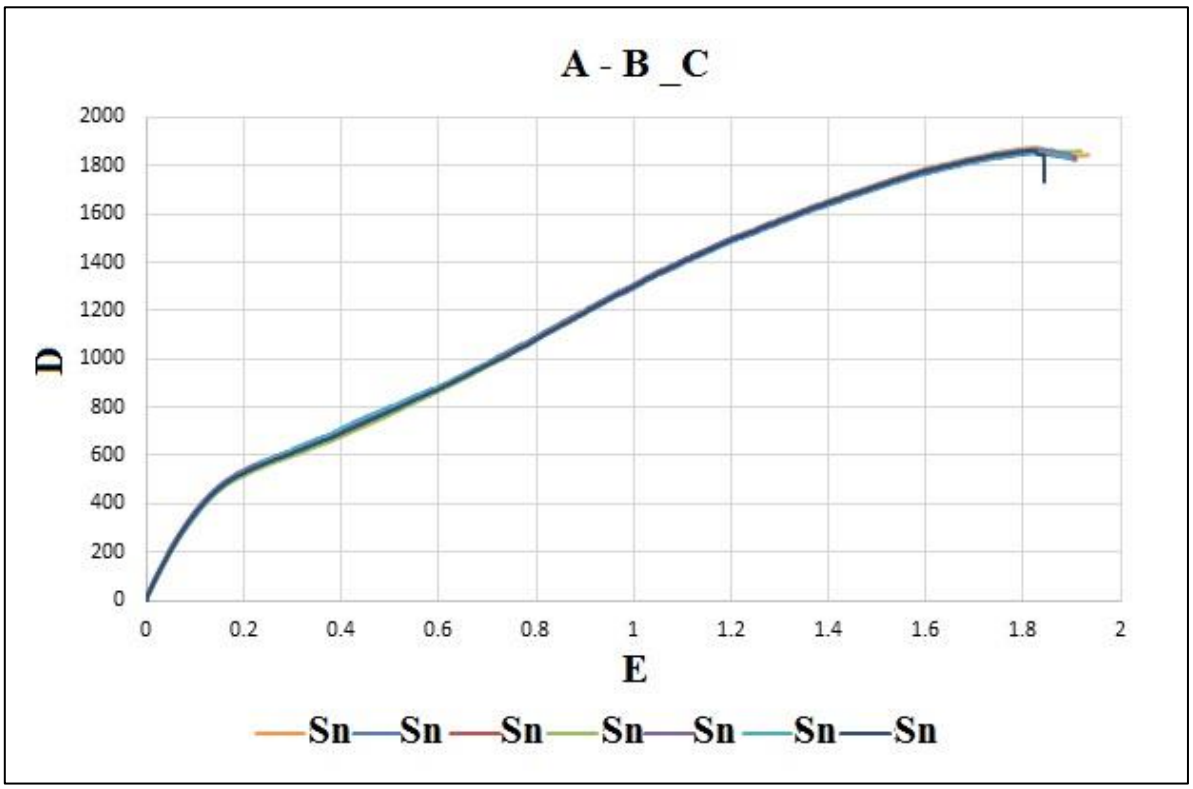

Figure 5-13: SPT LDC$_{EXP}$ template.

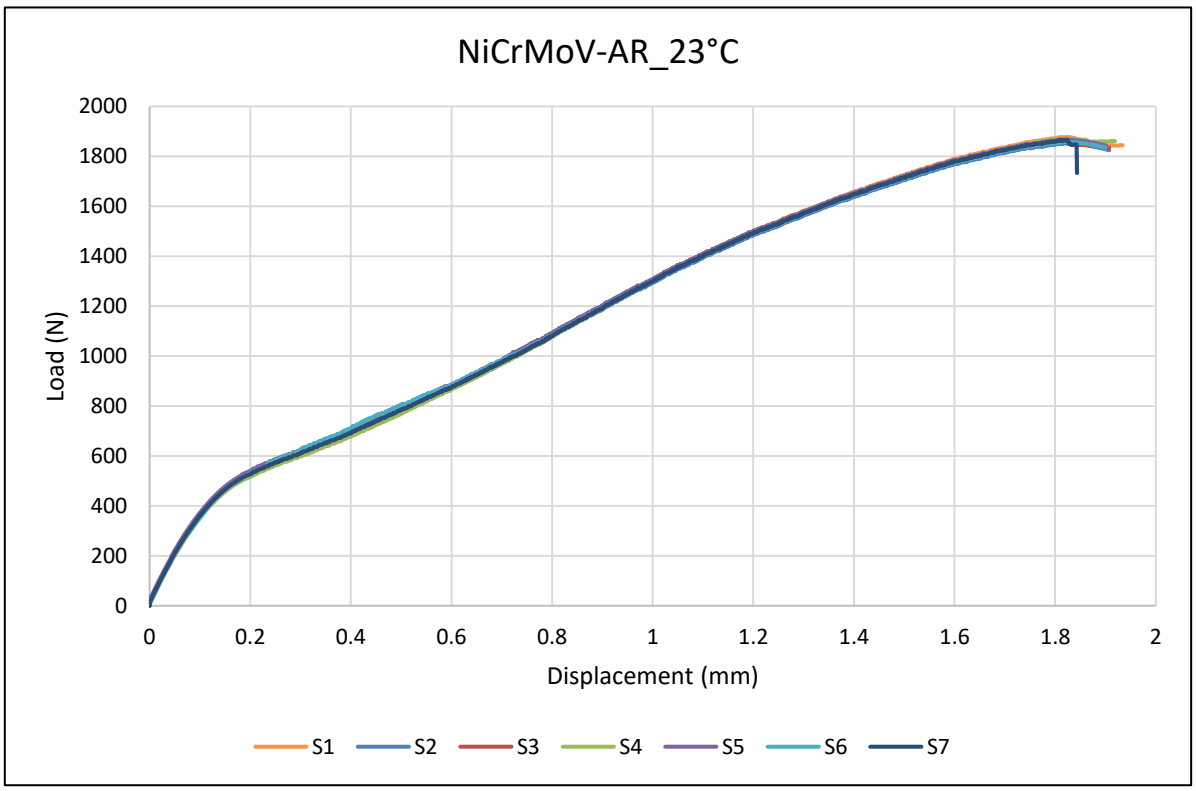

Figure 5-14: SPT LDC$_{EXP}$ – AR at 23°C.

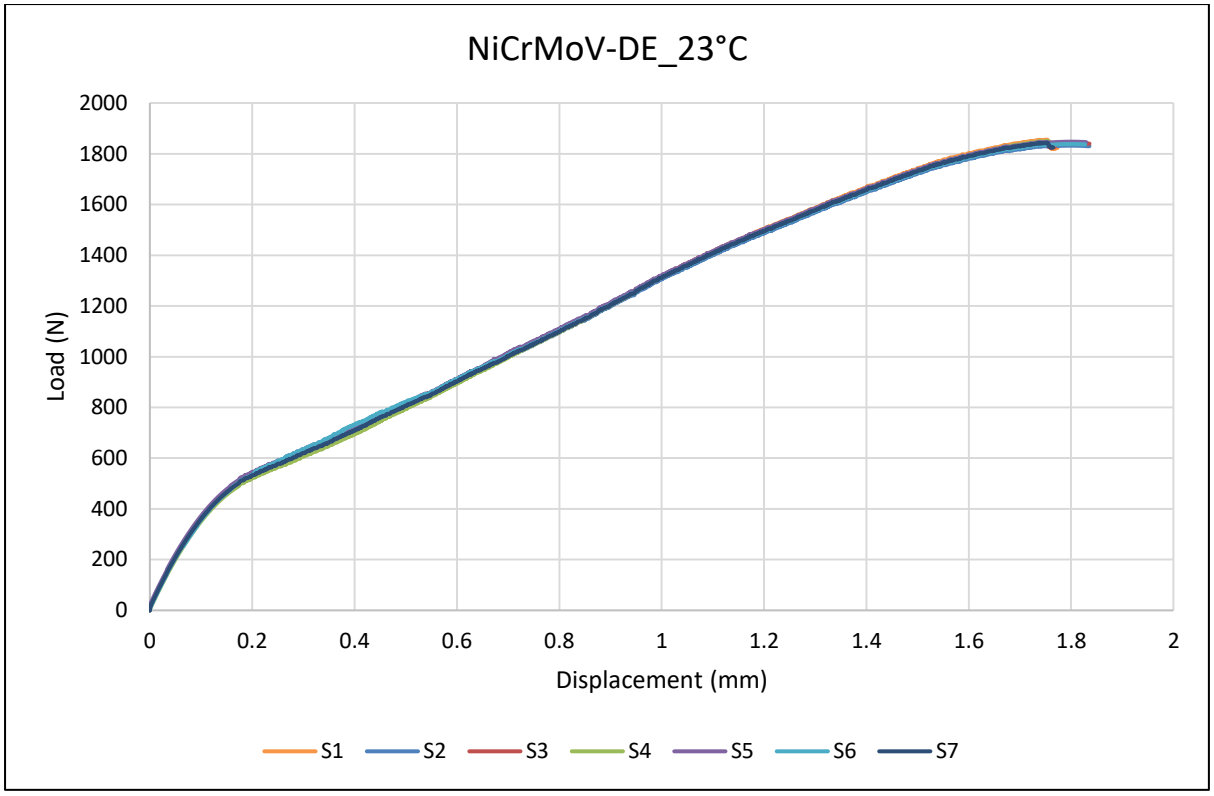

Figure 5-15: SPT LDC_{EXP} – DE at 23°C.

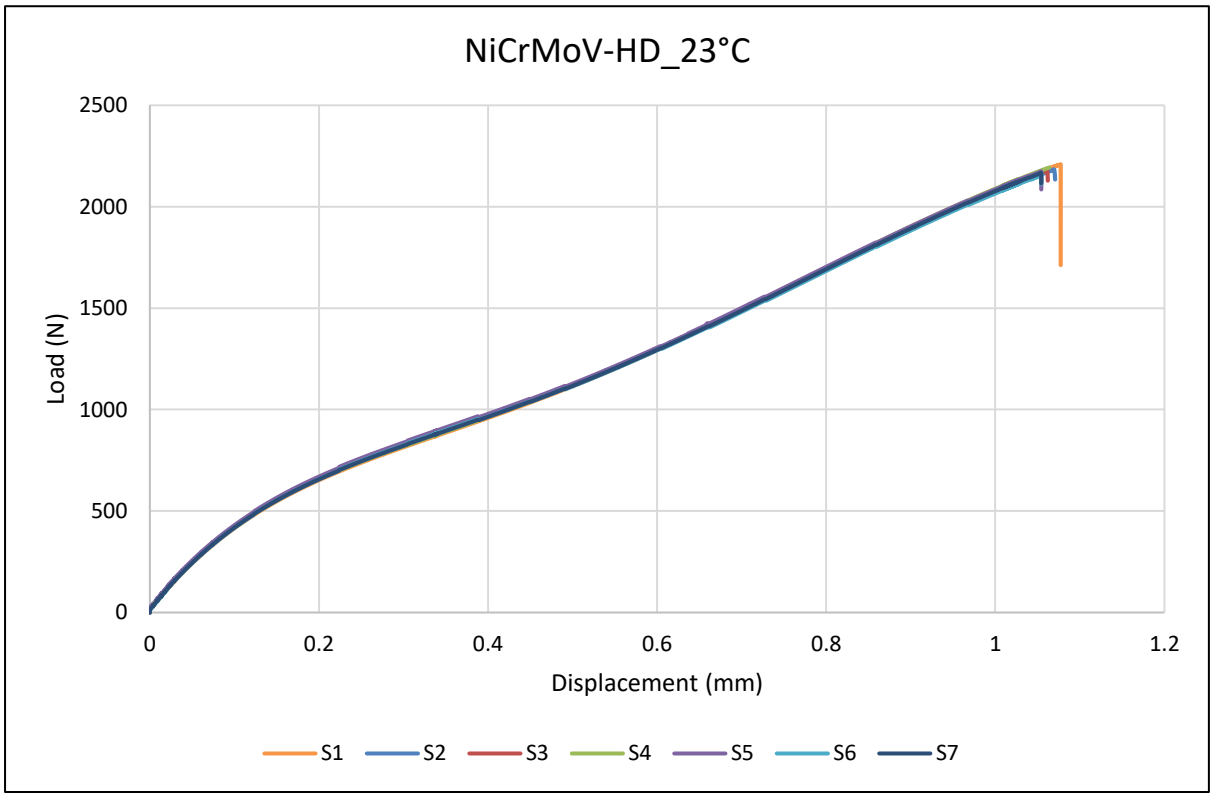

Figure 5-16: SPT LDC_{EXP} – HD at 23°C.

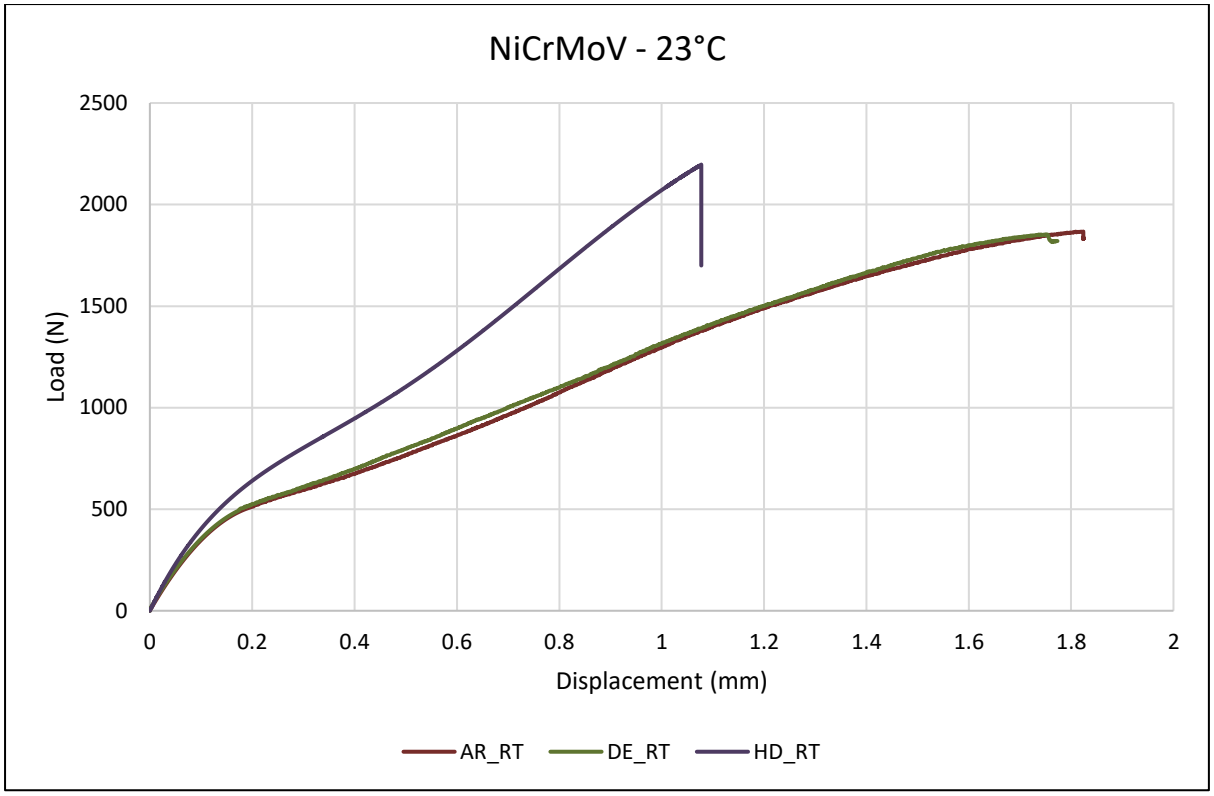

Figure 5-17: Comparison of SPT LDC_{EXP} –at 23°C.

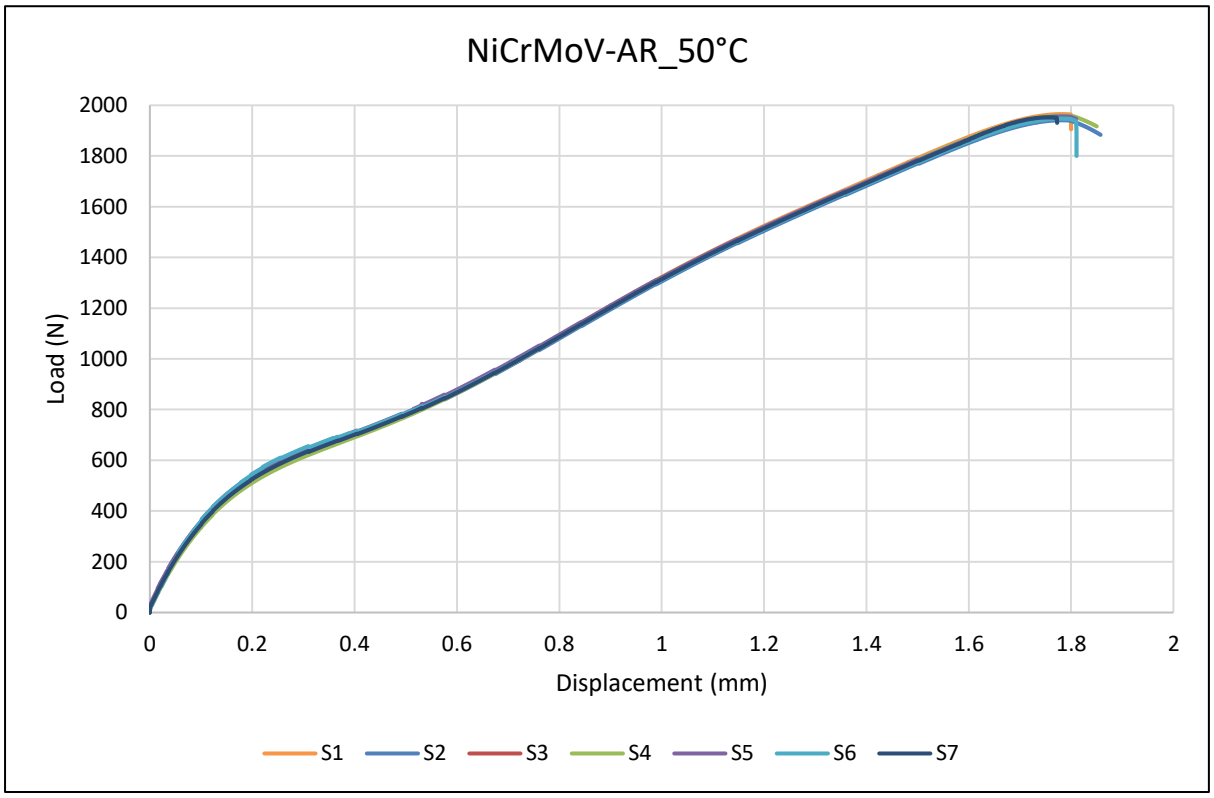

Figure 5-18: SPT LDC_{EXP} – AR at 50°C.

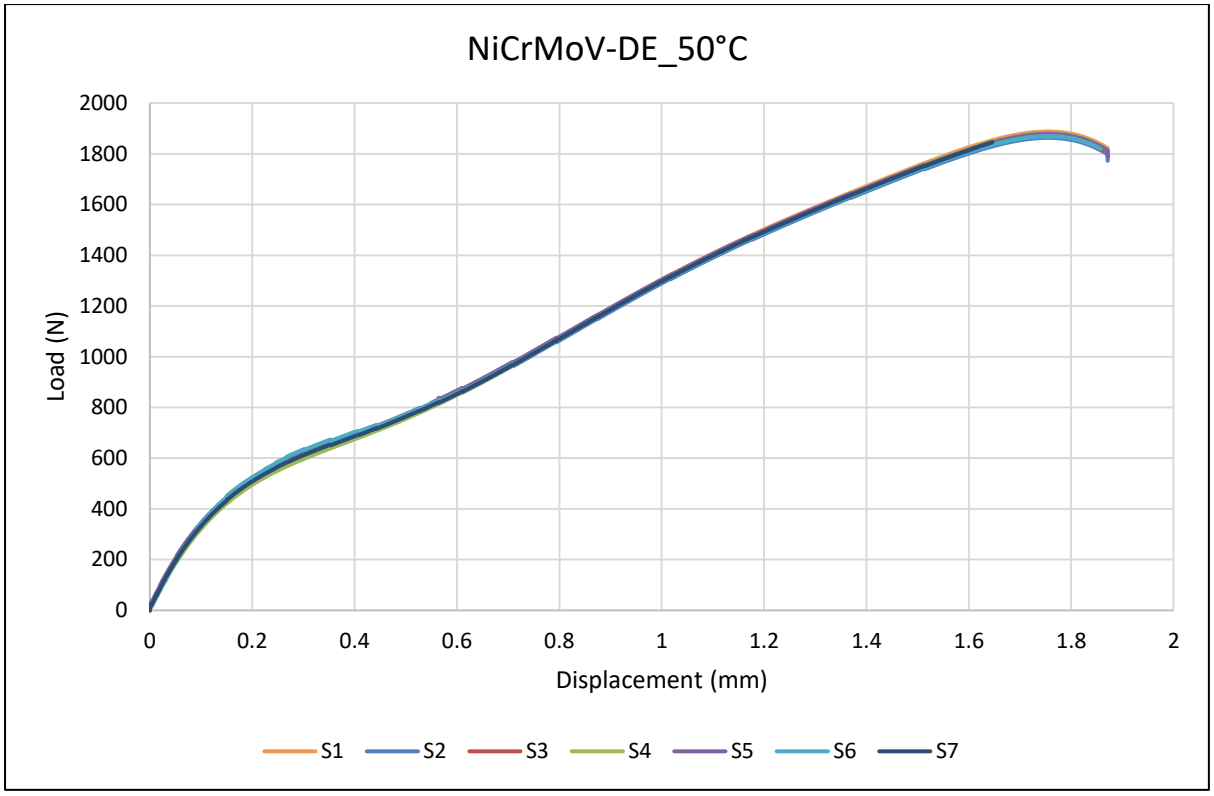

Figure 5-19: SPT LDC_{EXP} – AR at 50°C.

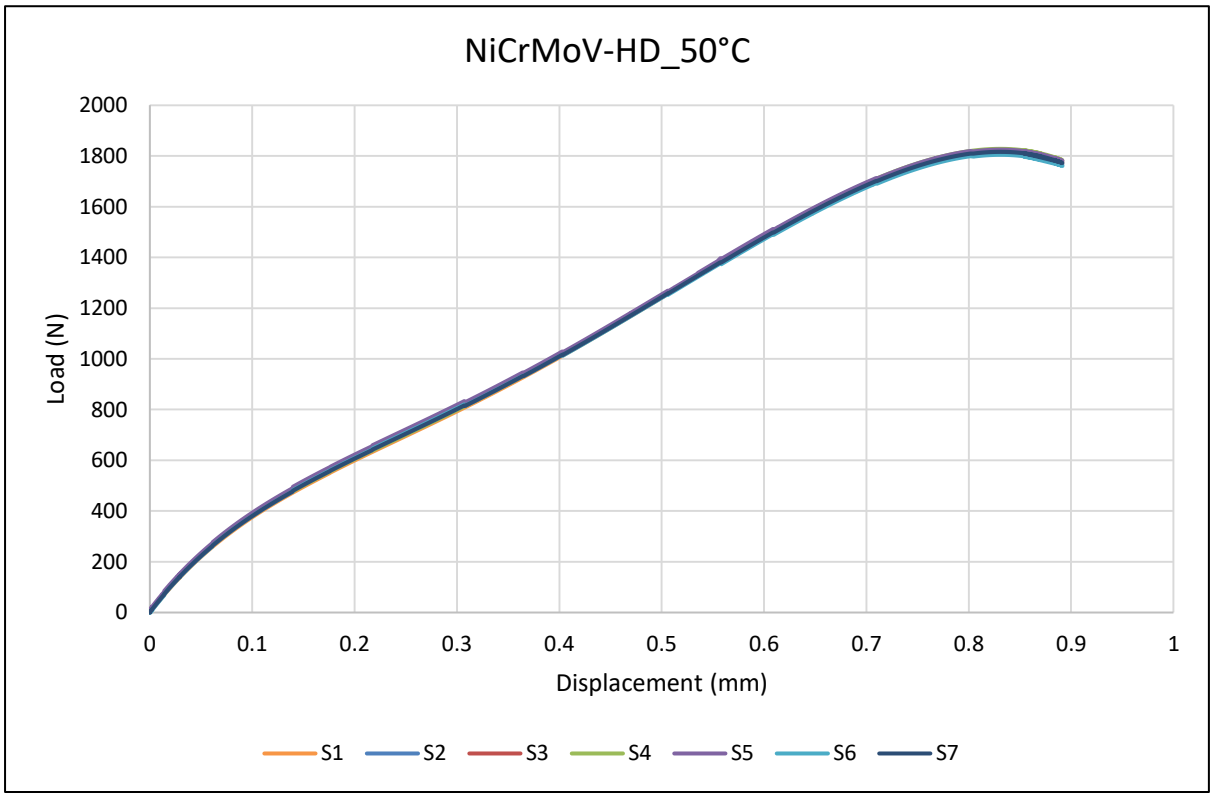

Figure 5-20: SPT LDC_{EXP} – HD at 50°C.

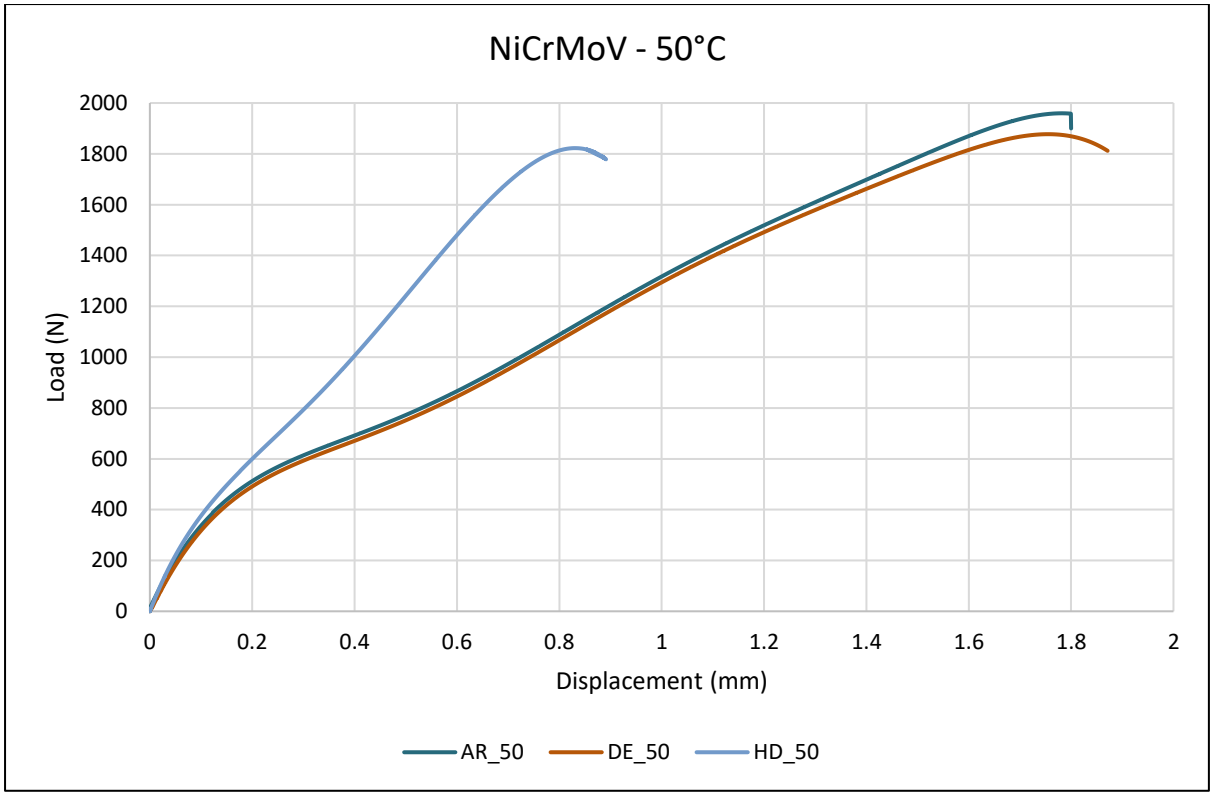

Figure 5-21: Comparison of SPT LDC_{EXP} - at 50°C.

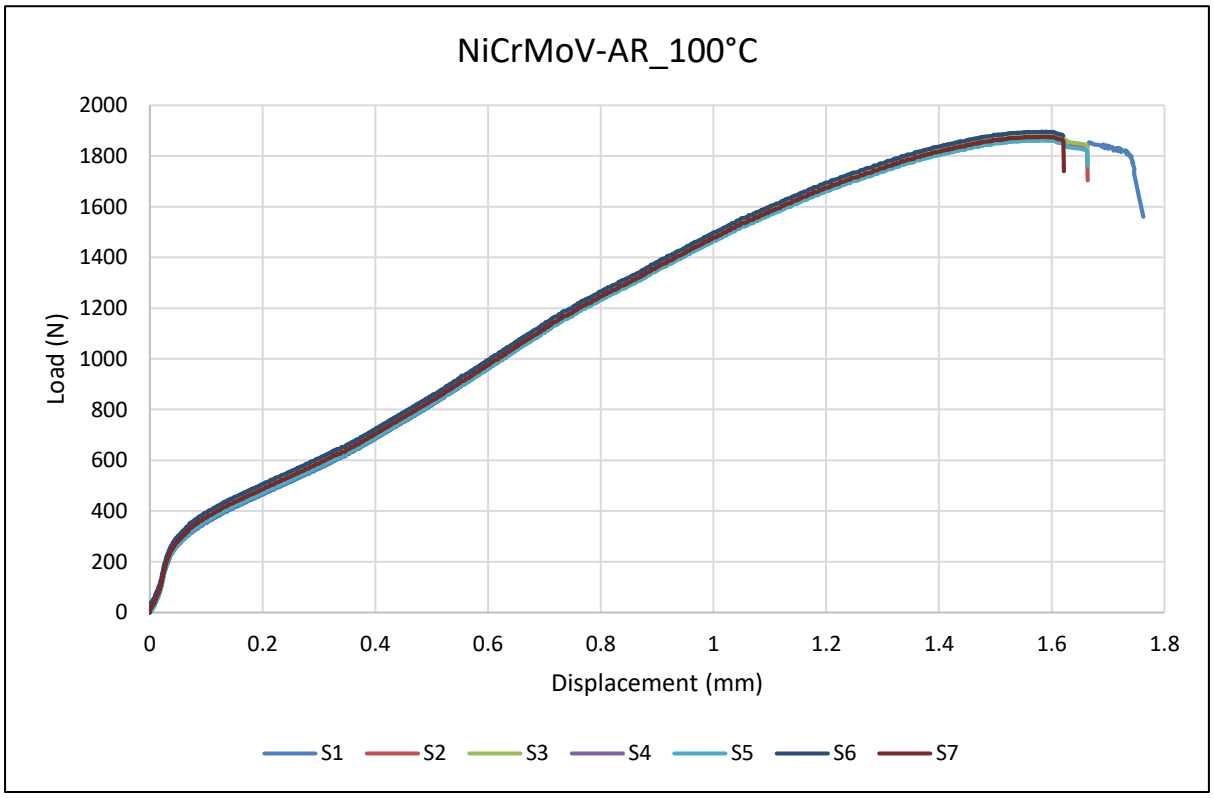

Figure 5-22: SPT LDC_{EXP} – AR at 100°C.

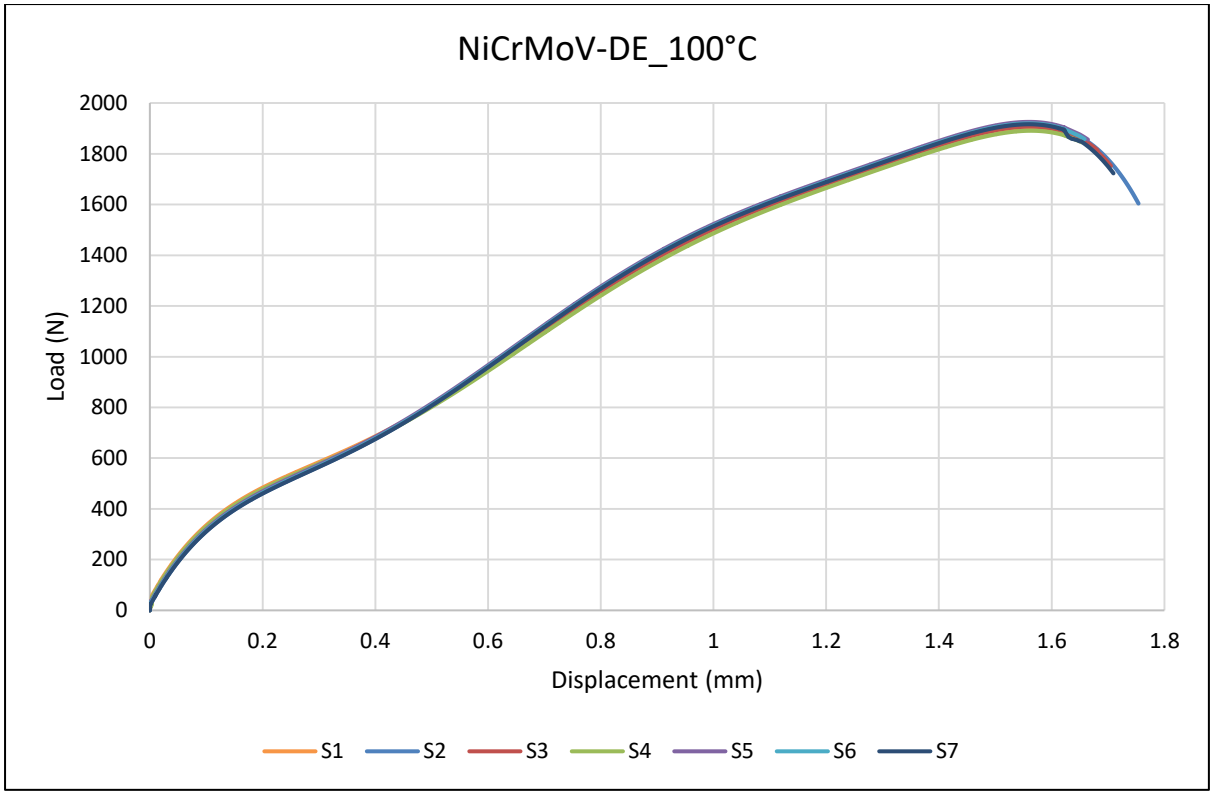

Figure 5-23: SPT LDC_{EXP} – DE at 100°C.

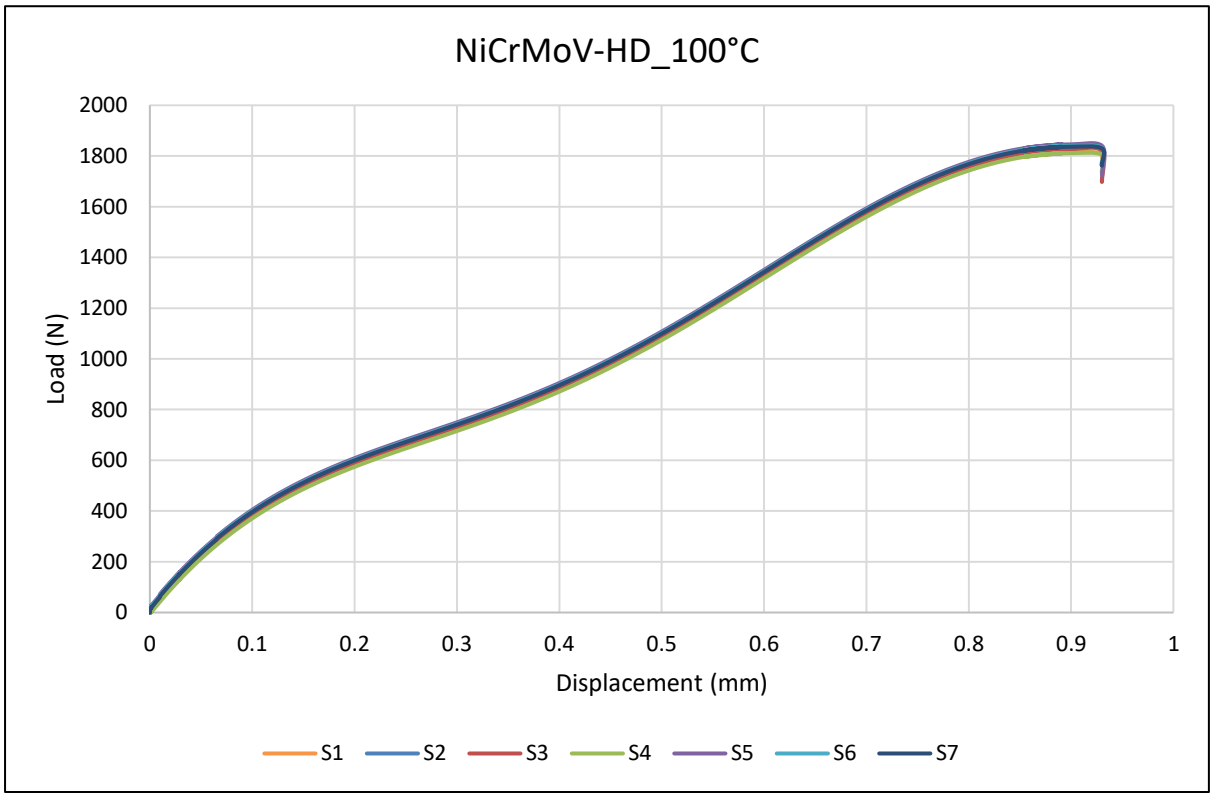

Figure 5-24: SPT LDC_{EXP} – HD at 100°C.

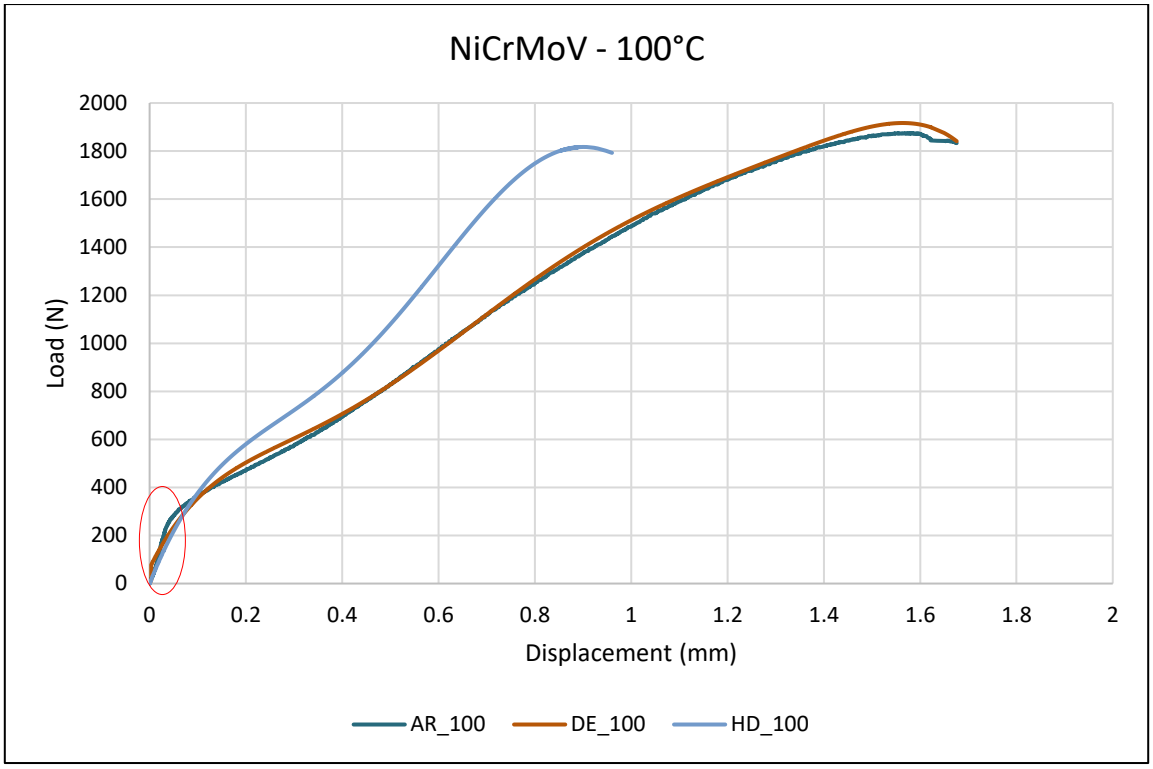

Figure 5-25: Comparison of SPT LDC_{EXP} (Incorrected linear portion) - at 100°C.

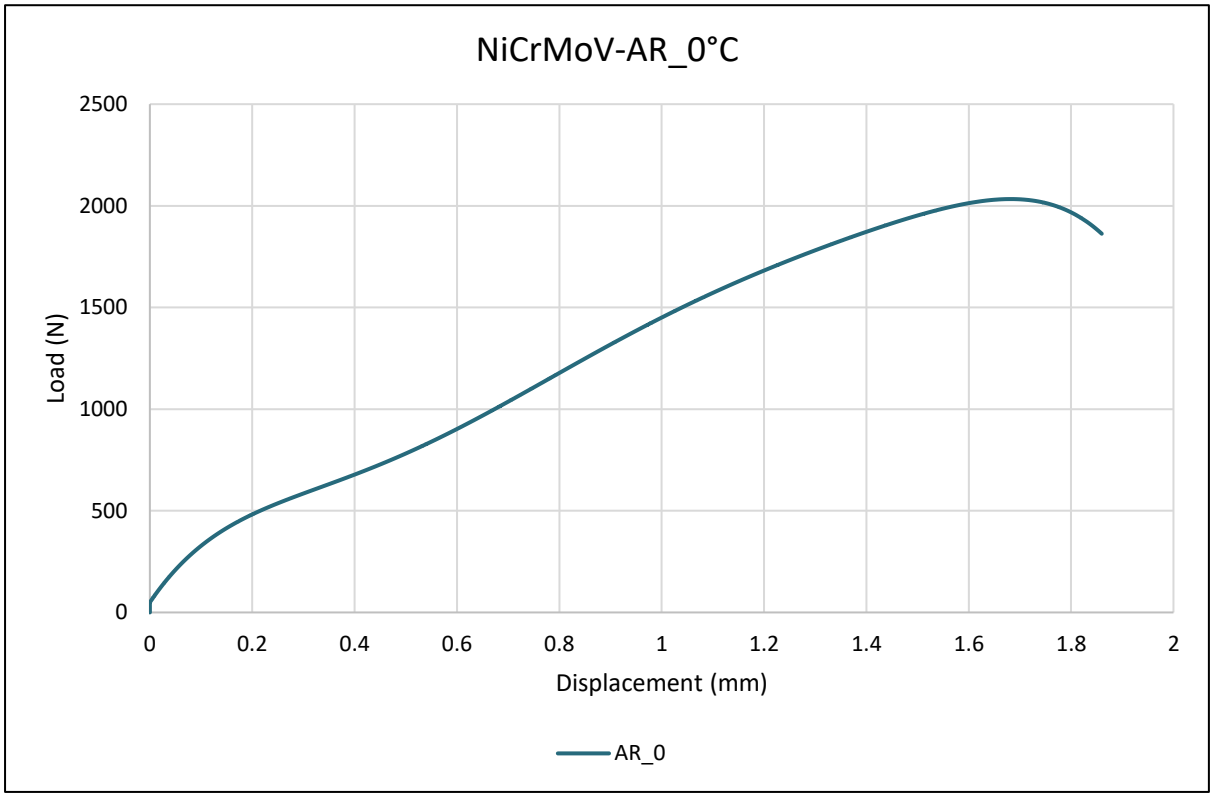

Figure 5-26: SPT LDC_{EXP} – AR at 0°C.

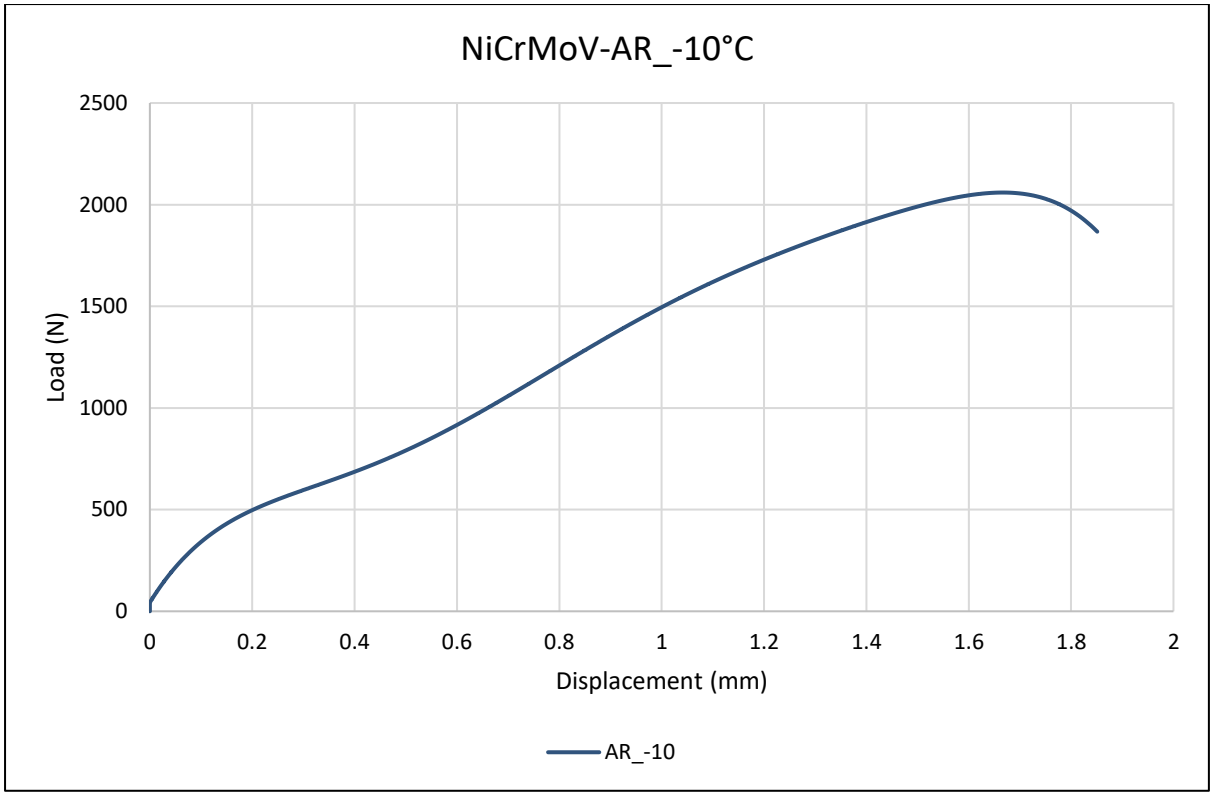

Figure 5-27: SPT LDC_{EXP} – AR at -10°C.

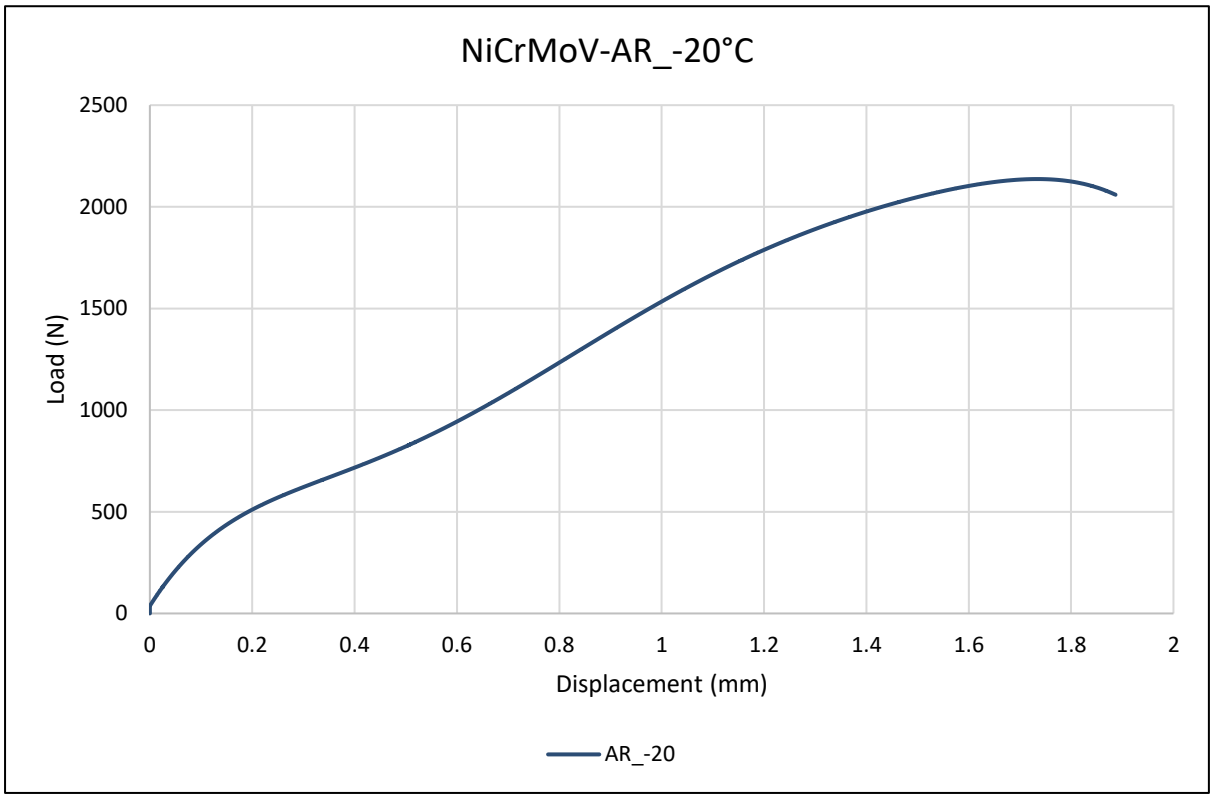

Figure 5-28: SPT LDC_{EXP} – AR at -20°C.

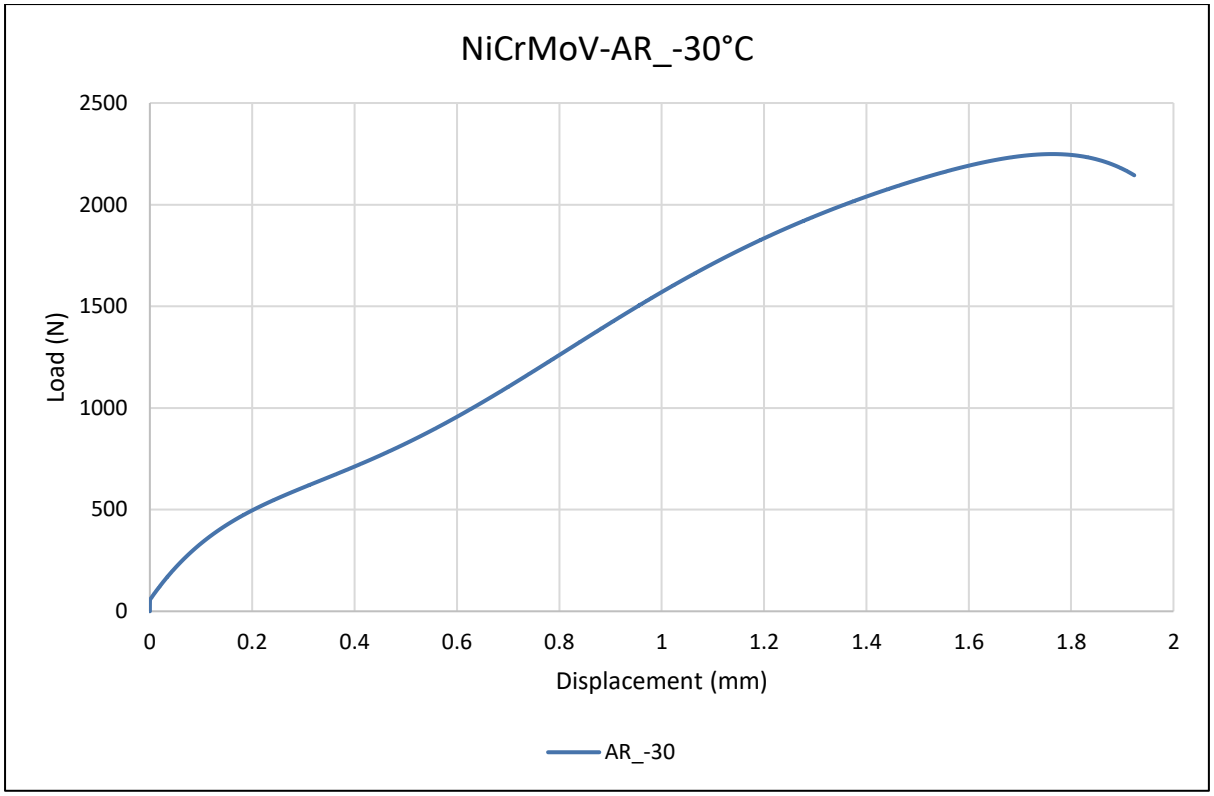

Figure 5-29: SPT LDC_{EXP} – AR at -30°C.

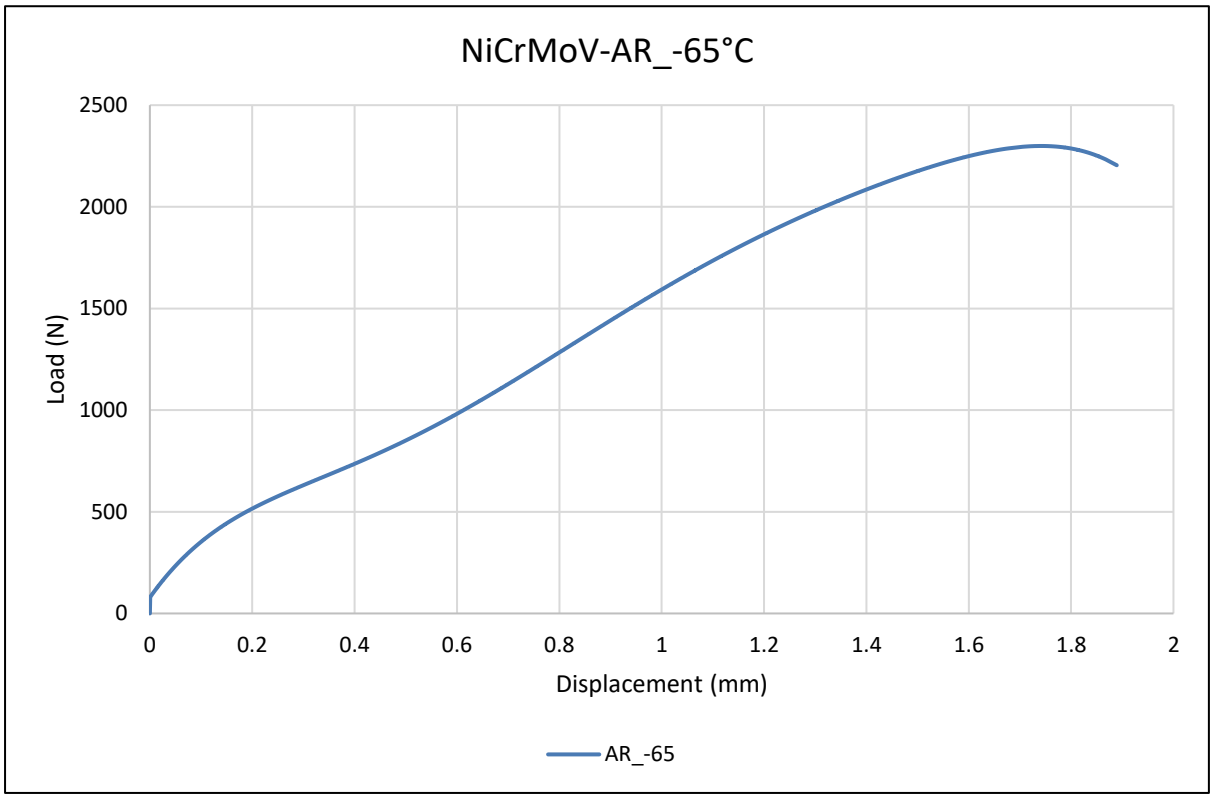

Figure 5-30: SPT LDC_{EXP} – AR at -65°C.

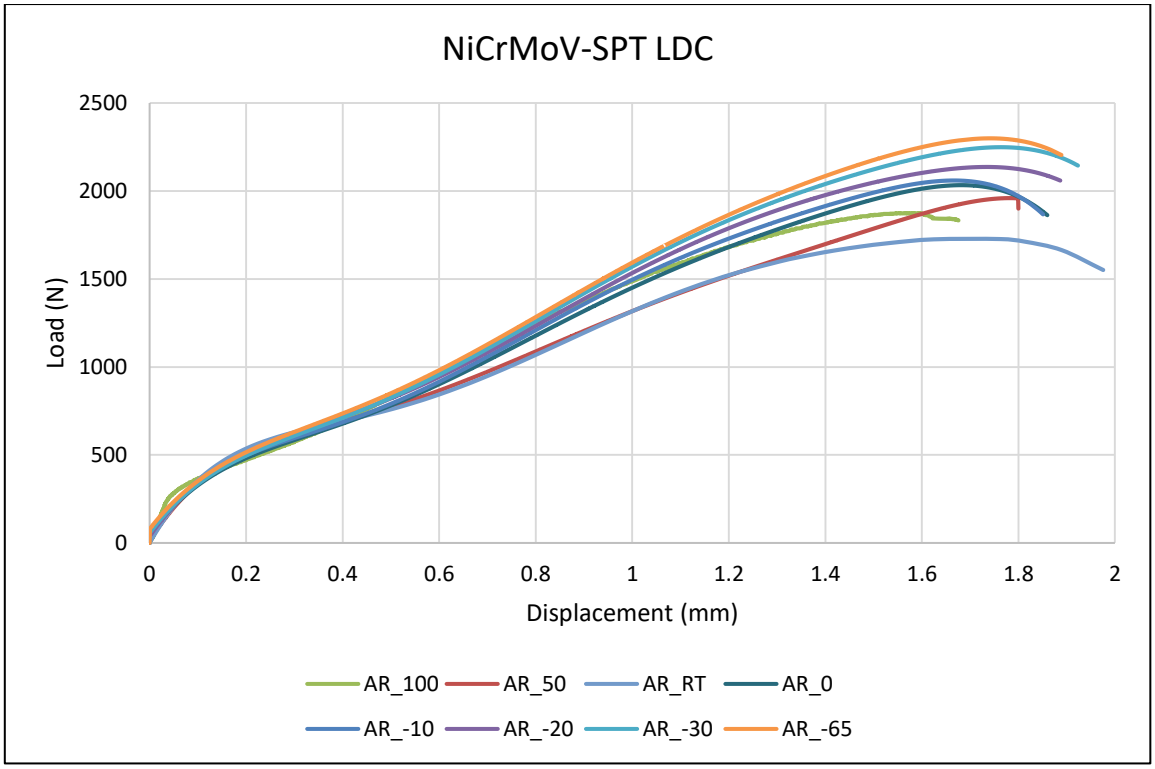

Figure 5-31: SPT LDC_{EXP} – at different test temperatures.

5.2.1.2 SPT LDC experiment discussion

The SPT results were consistent and prove to be valid because of the repeatability that was maintained at each test temperature. The difference between AR and DE (this can be seen in Figure 5-17, Figure 5-21 and Figure 5-25) samples at each test temperature was minimal, which implies that the AR material had no damage in it. It was evident that the HD samples had damage in them, which was indicated by the high hardness in terms of load and less ductility and less displacement (this can be seen in Figure 5-17, Figure 5-21 and Figure 5-25). Less displacement in HD samples illustrated that the material could not absorb more energy before it fractured than the AR and DE samples. The minimum obtainable test temperature was -65°C, this low temperature was not sufficient to determine the small punch transition temperature, T_{SP}. Figure 5-31 illustrates the impact of test temperature to load and displacement of the SPT samples. As the test temperature is lowered, the displacement decreases while the load increases. These results are in agreement with the expected low alloy steel SPT results (*FATT* - T_{SP} already established by Foulds [1] and EPRI [16]), which are shown by this relationship. Small punch energy, E_{SP} α test temperature (up to room temperature) and small punch load, P_{SP} α test temperature while the displacement reduced at lower temperatures. The SPT LDCs were smoothened using the polynomial 6th order term trendline equation, as illustrated in Figure 5-32 below.

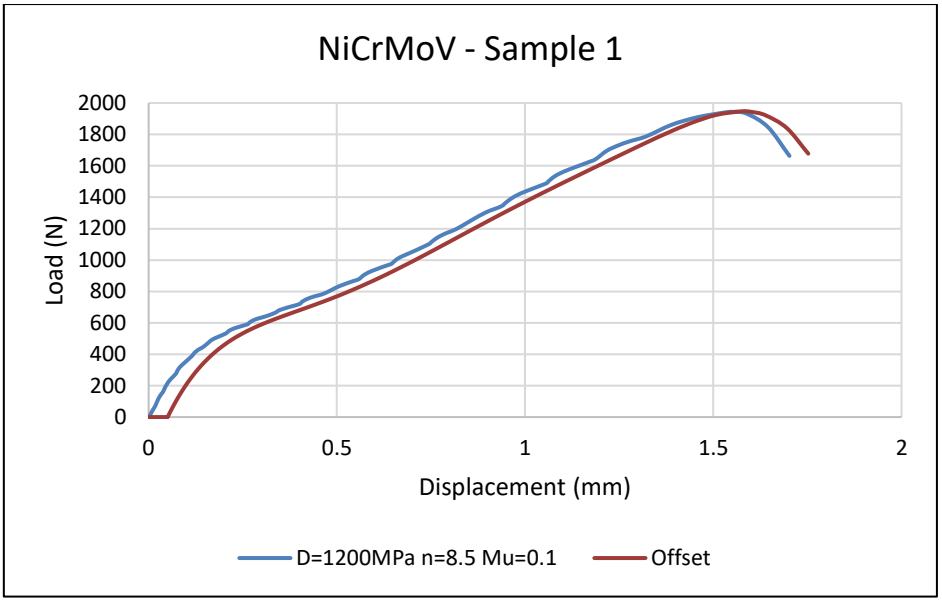

Figure 5-32: Smoothened LDC with an offset of 0.05 mm.

5.2.2 Modelling SPT LDC_{EXP}

The modelling of the SPT LDC (SPT LDC_{FEM}) at room temperature and above (23, 50 and 100°C) was validated using the tensile test true stress-true strain raw data as shown in Appendix-2: A2.2 and Table A2-1. The Ramberg-Osgood model parameters (*D* and *n*) determined from the tensile test were used to develop the SPT LDC_{FEM}, which were plotted with the averaged SPT LDC_{EXP} for the three test temperatures mentioned above. Parameters for the LDCs below room temperature were estimated using the validated models from the three test temperatures that had known tensile test data. The Ramberg-Osgood model parameters were changed to improve the SPT LDC_{FEM} in order to make it fit to the SPT LDC_{EXP} (i.e. SPT $LDC_{EXP} \neq$ SPT LDC_{FEM}). Stage 1 (elastic part) and Stage 2 (elastic-plastic part up to crack initiation point) are the only parts of the curve that have to fit, stages beyond this are not predictable as the crack introduces unstable behaviour of the material.

5.2.2.1 SPT LDC_{FEM} with different coefficient of friction

During the experimental SPT, friction between the punch (or ball) and sample is expected but it is not measurable during testing. It is important to include friction during modelling and standardise the friction based on the impact and repeatability that it has towards the SPT LDC_{EXP}. Figure 5-33 shows the SPT LDC_{FEM} with different coefficients of friction, μ (Mu). It was observed that coefficients of friction between 0.1 and 0.3 had a slight change in peak load (strength) and displacement (ductility). These two changes do not affect the part of the LDC that has to be estimated (Stages 1 and 2), refer Figure 5-33.

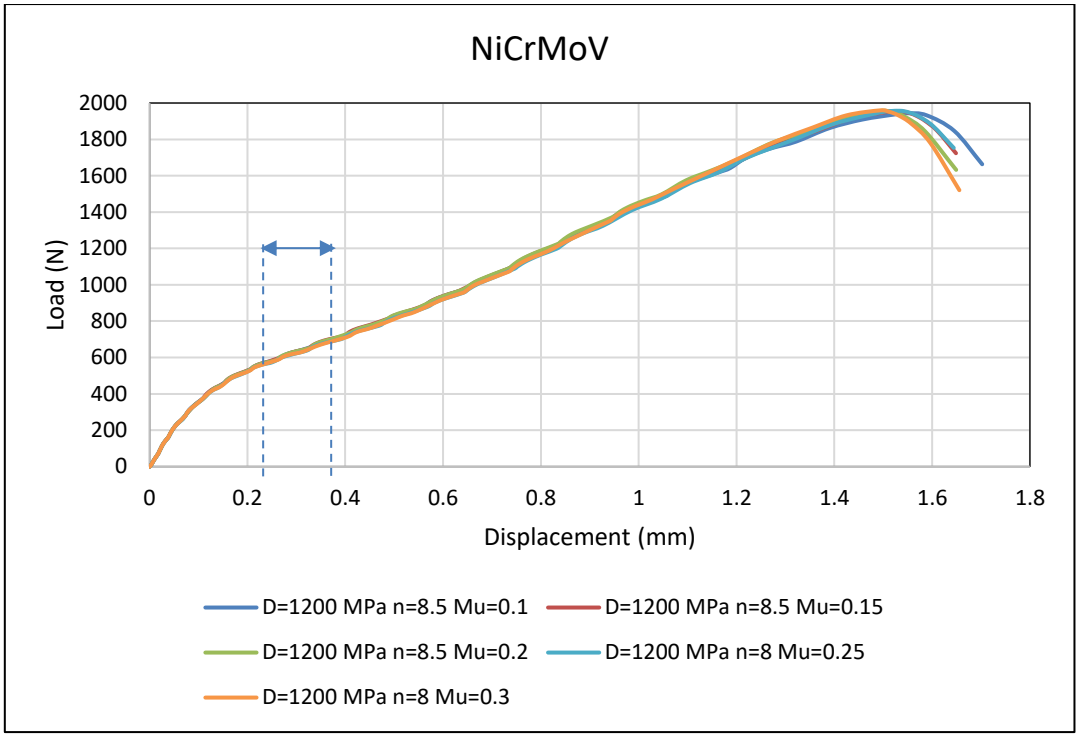

Figure 5-33: SPT LDC_{FEM} showing different coefficients of friction and the part of the LDC to be estimated.

5.2.2.2 SPT LDC_{FEM} fitted onto SPT LDC_{EXP}

The modelled LDC from known tensile test data were plotted against the experimental LDC at room and above room temperature. The SPT LDC_{EXP} for AR and DE specimens were plotted together for one SPT LDC_{FEM}. The tensile test data used were from the minimum number of two specimens tested and are shown in combined SPT LDCs as 'S1 for Specimen 1 and S2 for Specimen 2', *D* and *n* parameters, respectively. It was observed that the SPT LDC_{FEM} did not fit to the SPT LDC_{EXP} using the originally determined Ramberg-Osgood model parameters. The Ramberg-Osgood model parameters had to be improved to make the SPT LDC_{FEM} almost fit to the SPT LDC_{EXP}. The original Ramberg-Osgood model parameters were suspected to have a certain percentage of error due to scatter found in the tensile test true stress and strain raw data. Secondly, it was suspected that the Ramberg-Osgood model parameters were affected by the user's cut off point of raw data (the raw data was cut off at UTS) to avoid negative slope of the true stress and true strain data curve. Upon investigation of improving the Ramberg-Osgood model parameters from the tensile test raw data, it is advised to cut off the true stress-true strain curve at about 10% before the UTS, as this has a slight impact on the positive slope when fitting the power law curve as explained in Section 3.7.2.

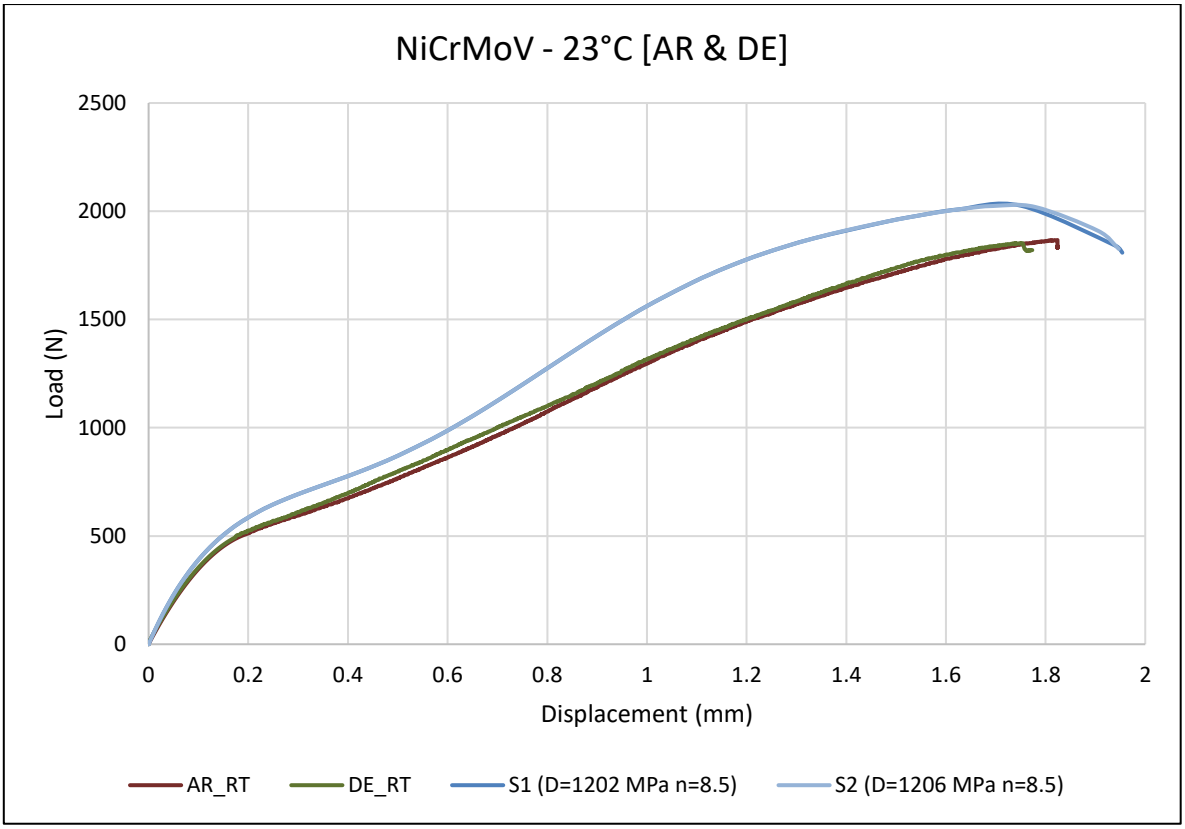

Figure 5-34: SPT LDC_{FEM} showing numerical values D & n from true stress and true strain compared to SPT LDC_{EXP} – AR at 23°C.

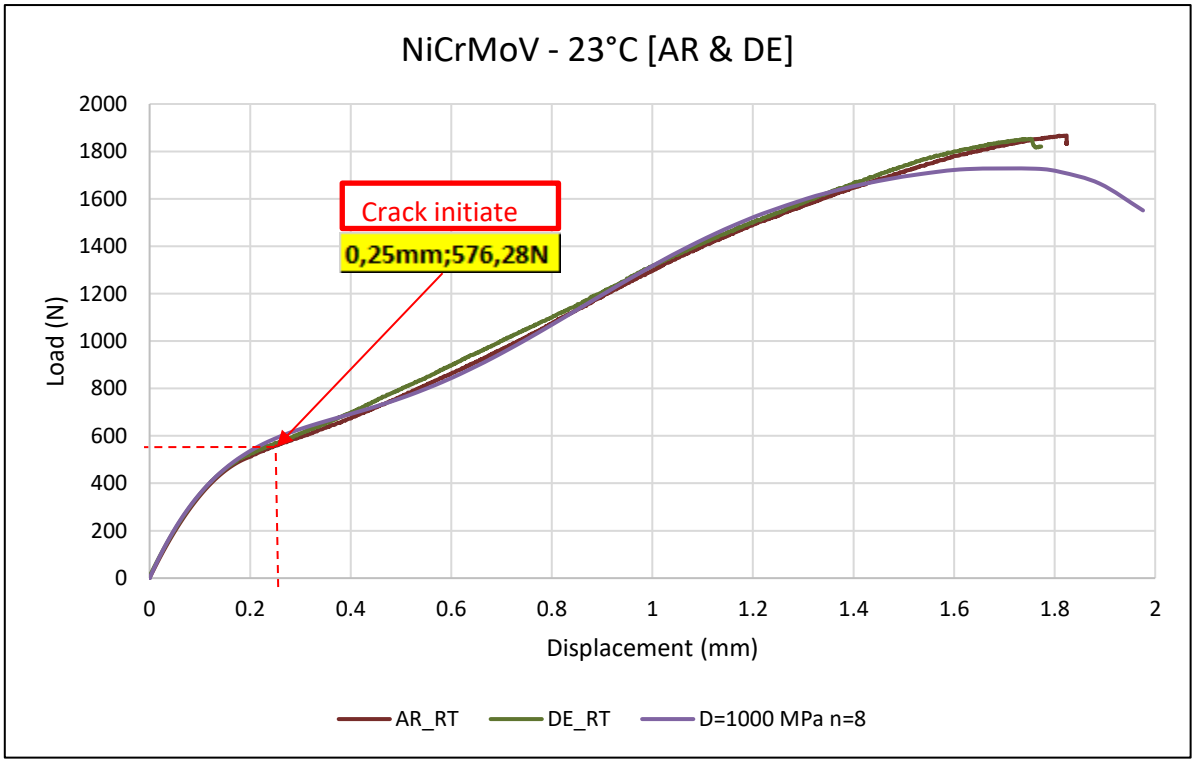

Figure 5-35: Improved SPT LDC_{FEM} to fit SPT LDC_{EXP} – AR & DE at 23°C.

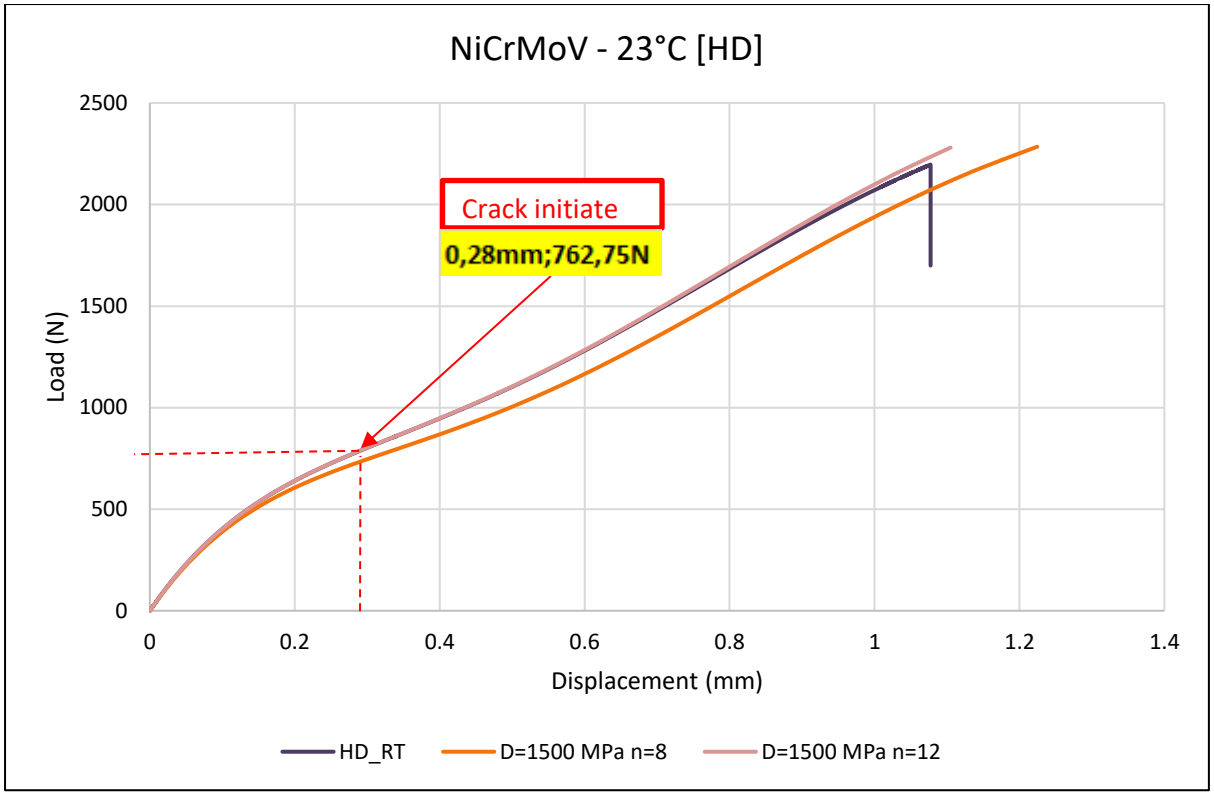

Figure 5-36: Improved SPT LDC_{FEM} to fit SPT LDC_{EXP} – HD at 23°C.

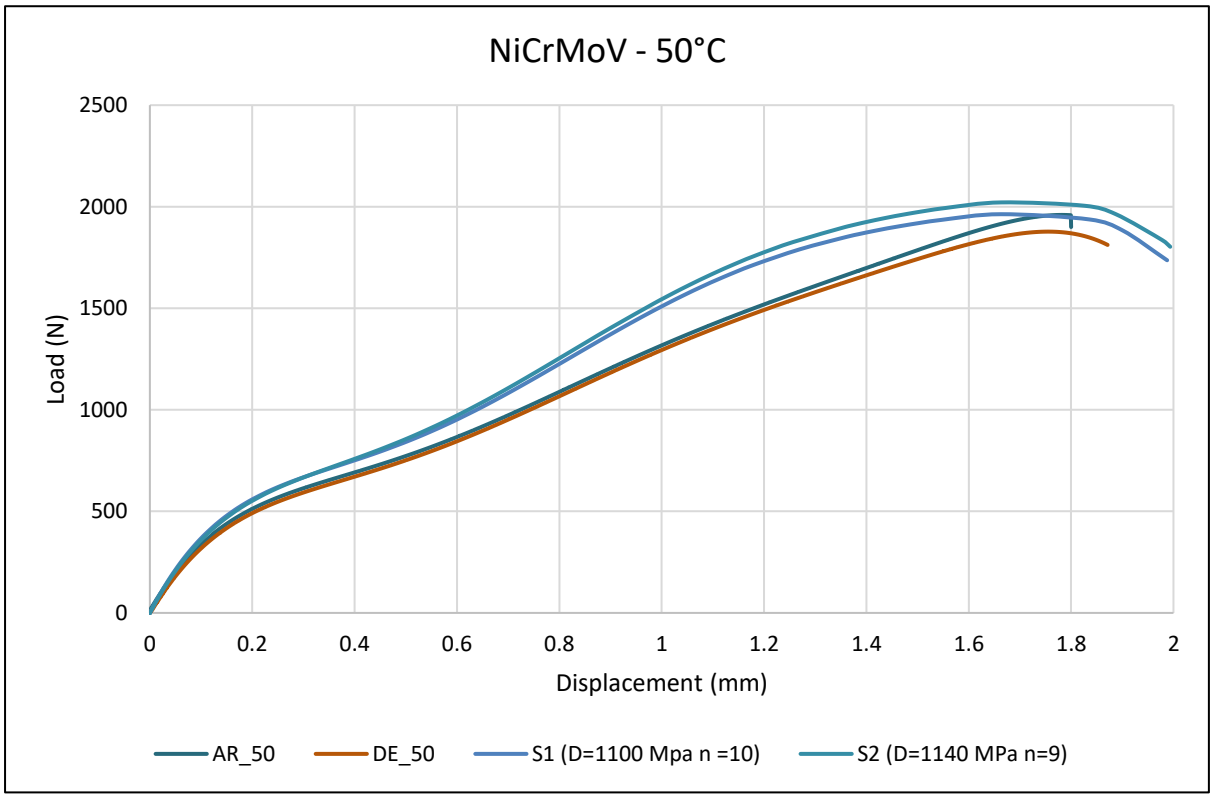

Figure 5-37: SPT LDC_{FEM} showing numerical value D & n from true stress and true strain compared to SPT LDC_{EXP} – AR & DE at 50°C.

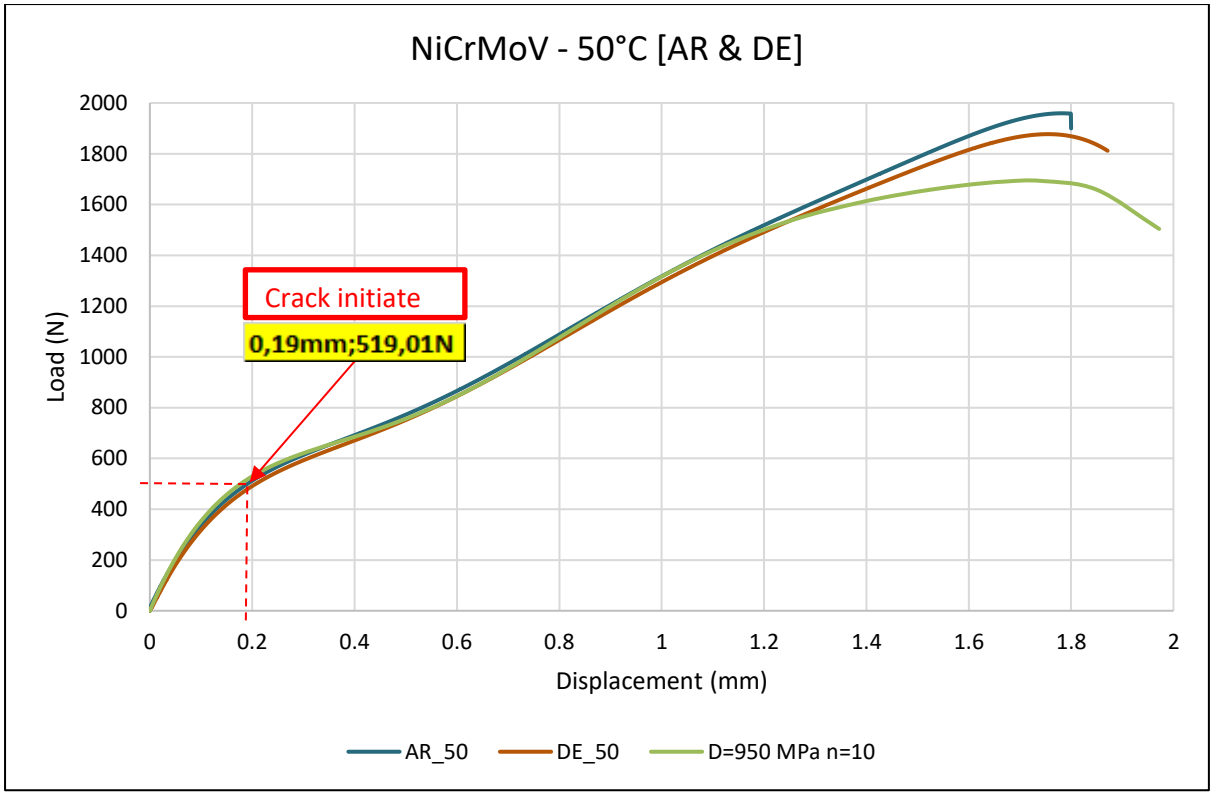

Figure 5-38: Improved SPT LDC_{FEM} to fit SPT LDC_{EXP} – AR & DE at 50°C.

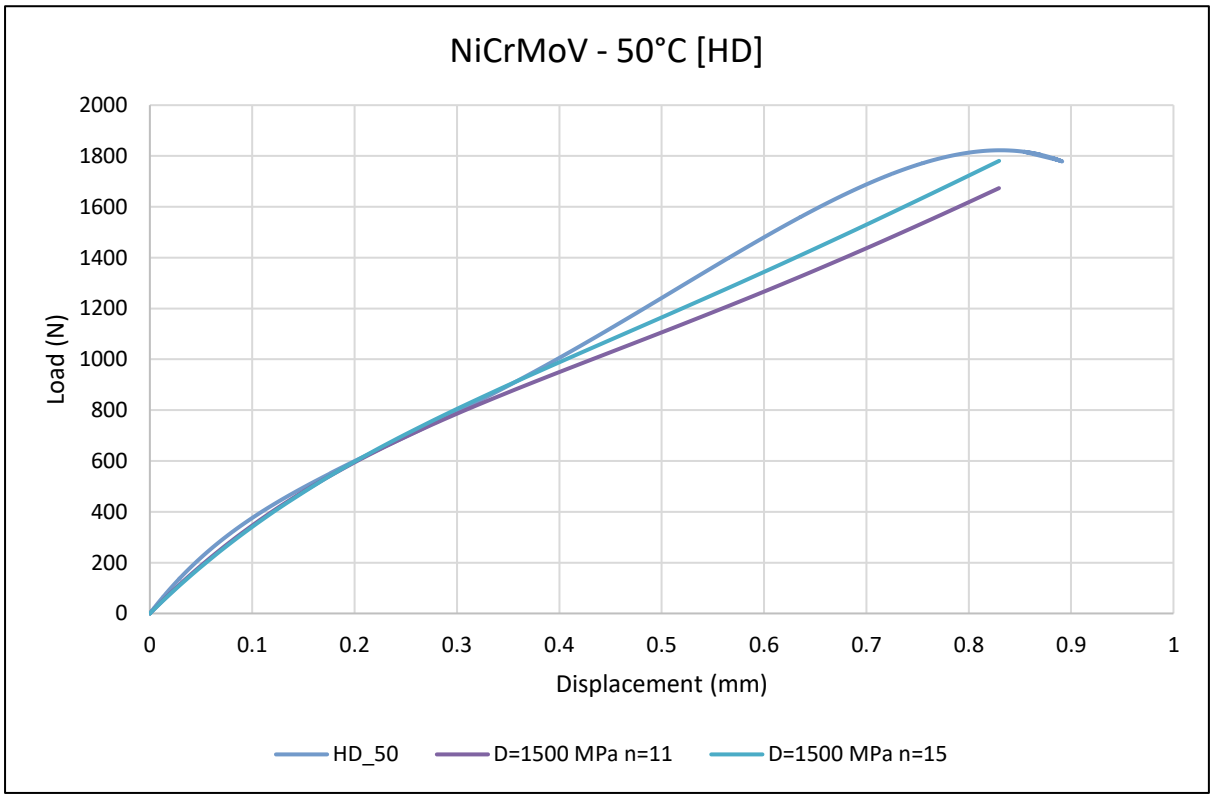

Figure 5-39: Improved SPT LDC_{FEM} to fit SPT LDC_{EXP} – HD at 50°C.

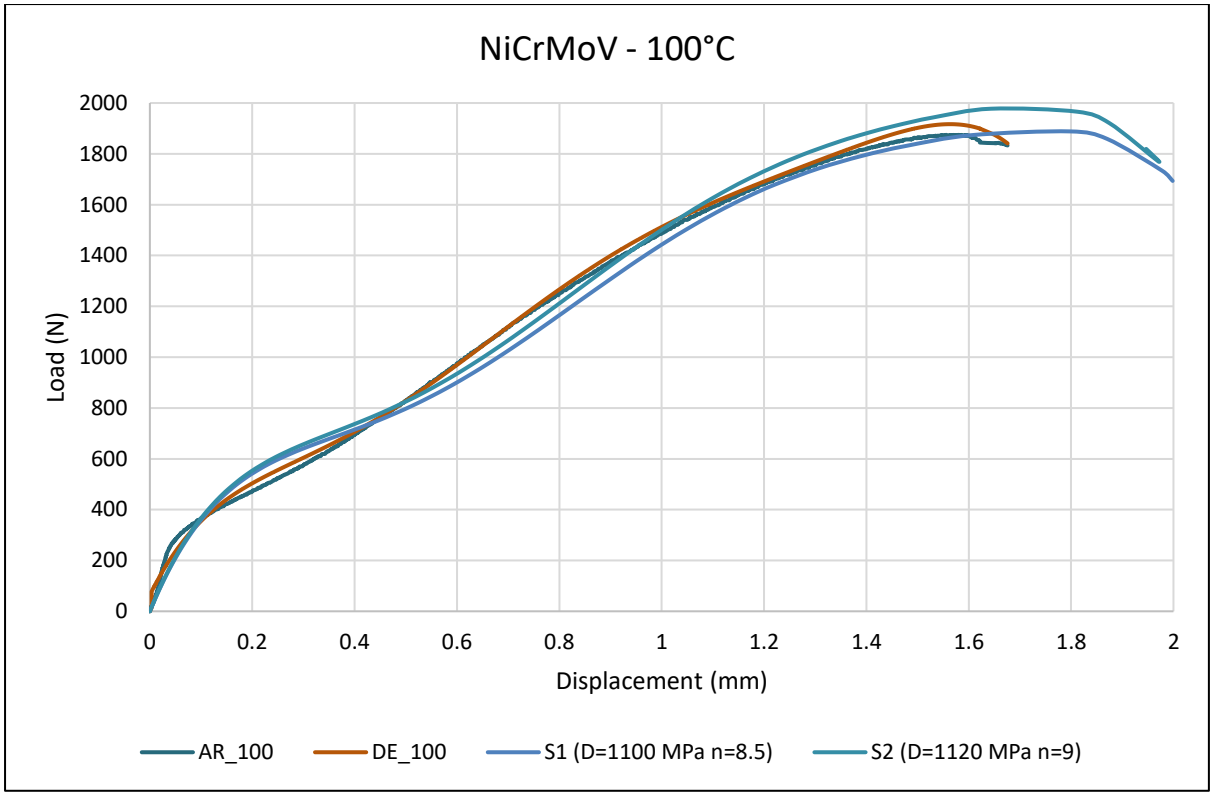

Figure 5-40: SPT LDC_{FEM} showing numerical value D & n from true stress and true strain compared to SPT LDC_{EXP} – AR & DE at 100°C.

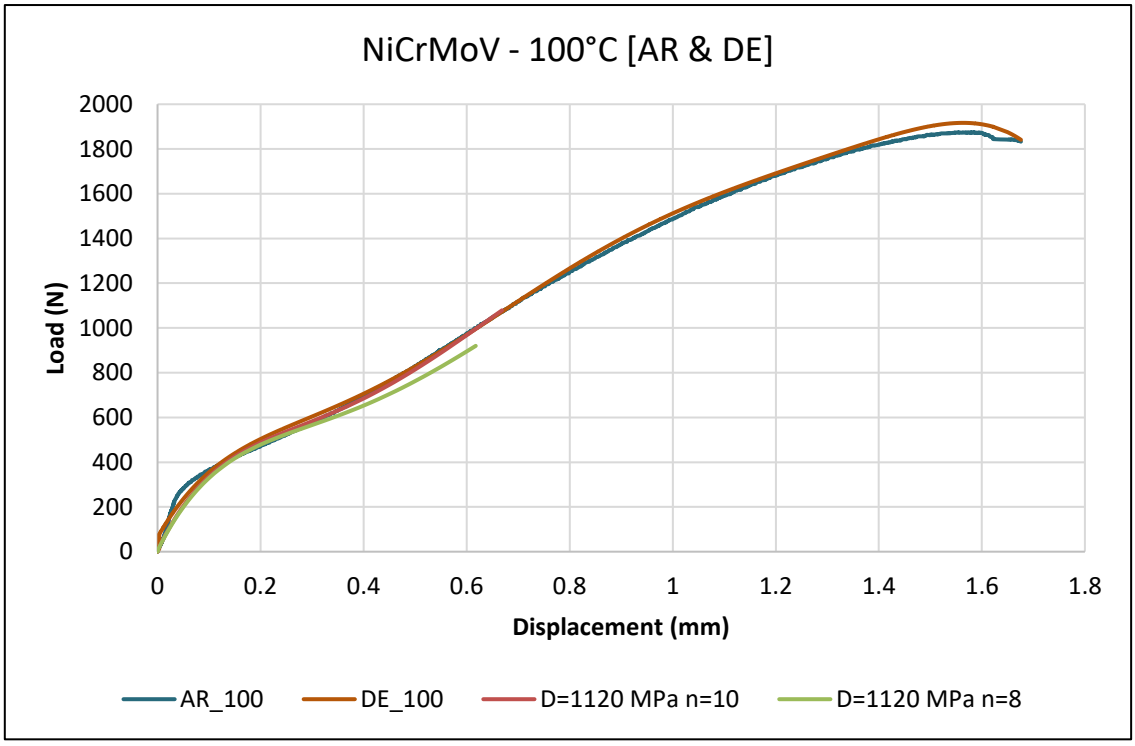

Figure 5-41: Improved SPT LDC_{FEM} to fit SPT LDC_{EXP} – AR & DE at 100°C.

5.2.2.3 Derived small punch energy (E_{SP})

The small punch energy curve is an integral of the small punch load displacement curve and is achieved using FEM. Superimposed LDC_{FEM} from LDC_{EXP} is used to determine small punch energy, E_{SP}.

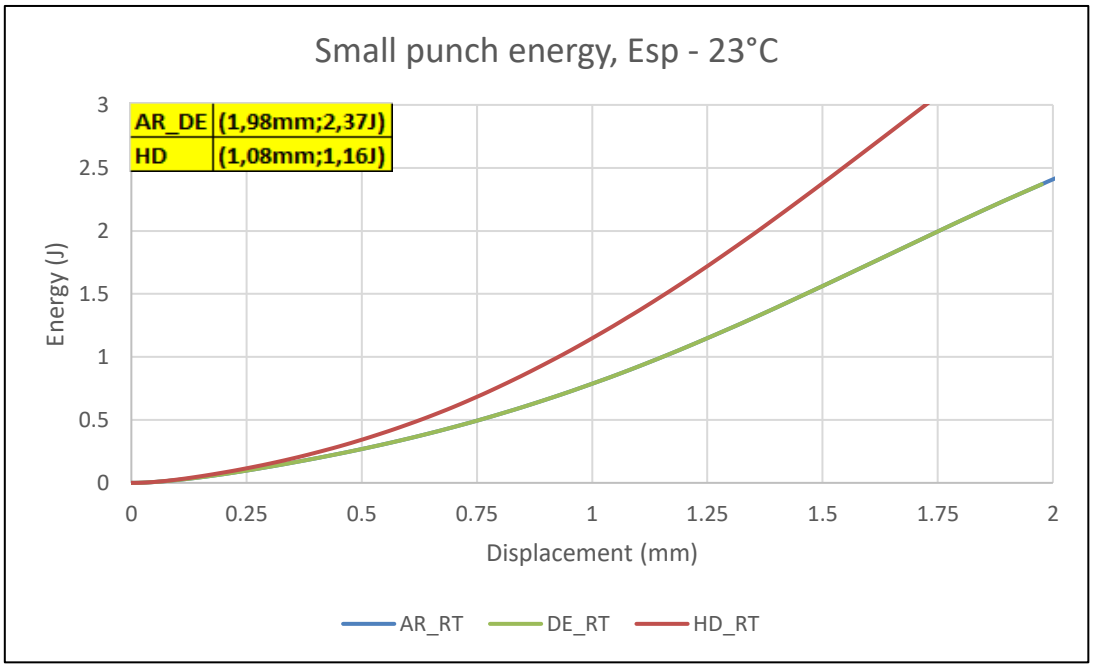

Figure 5-42: Small punch energy, E_{SP} for AR, DE & HD at 23°C.

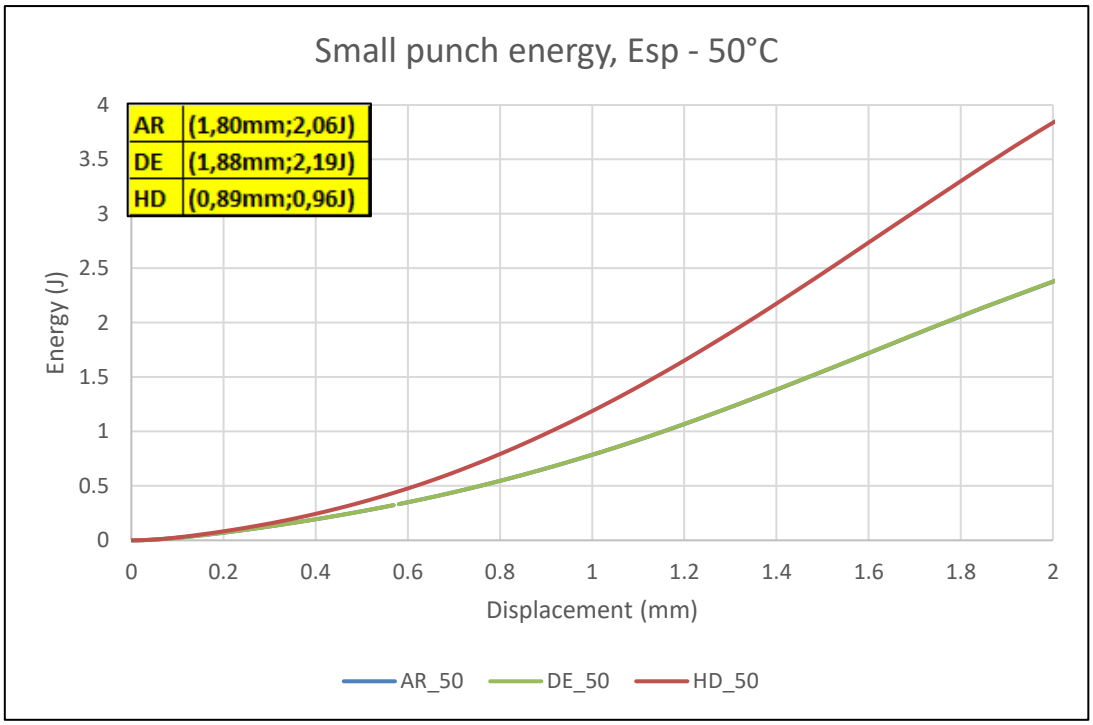

Figure 5-43: Small punch energy, E_{SP} for AR, DE & HD at 50°C.

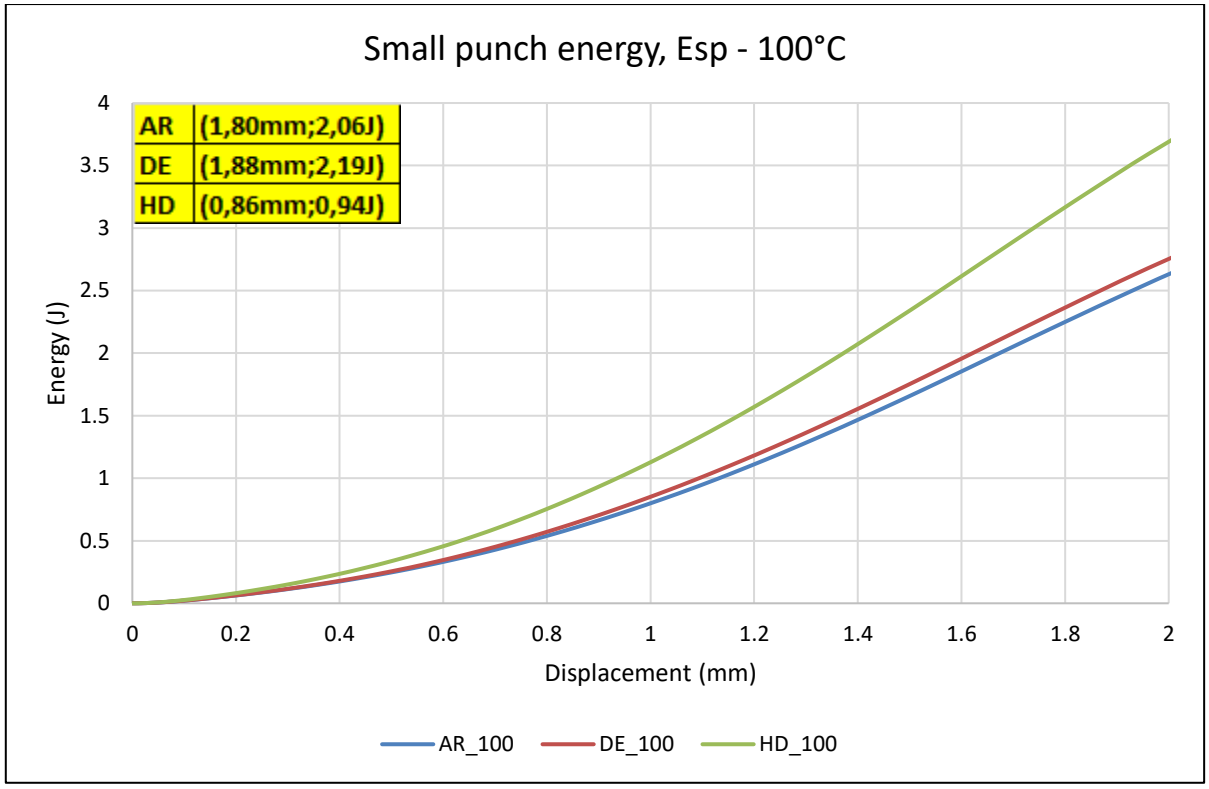

Figure 5-44: Small punch energy, E_{SP} for AR, DE & HD at 100°C.

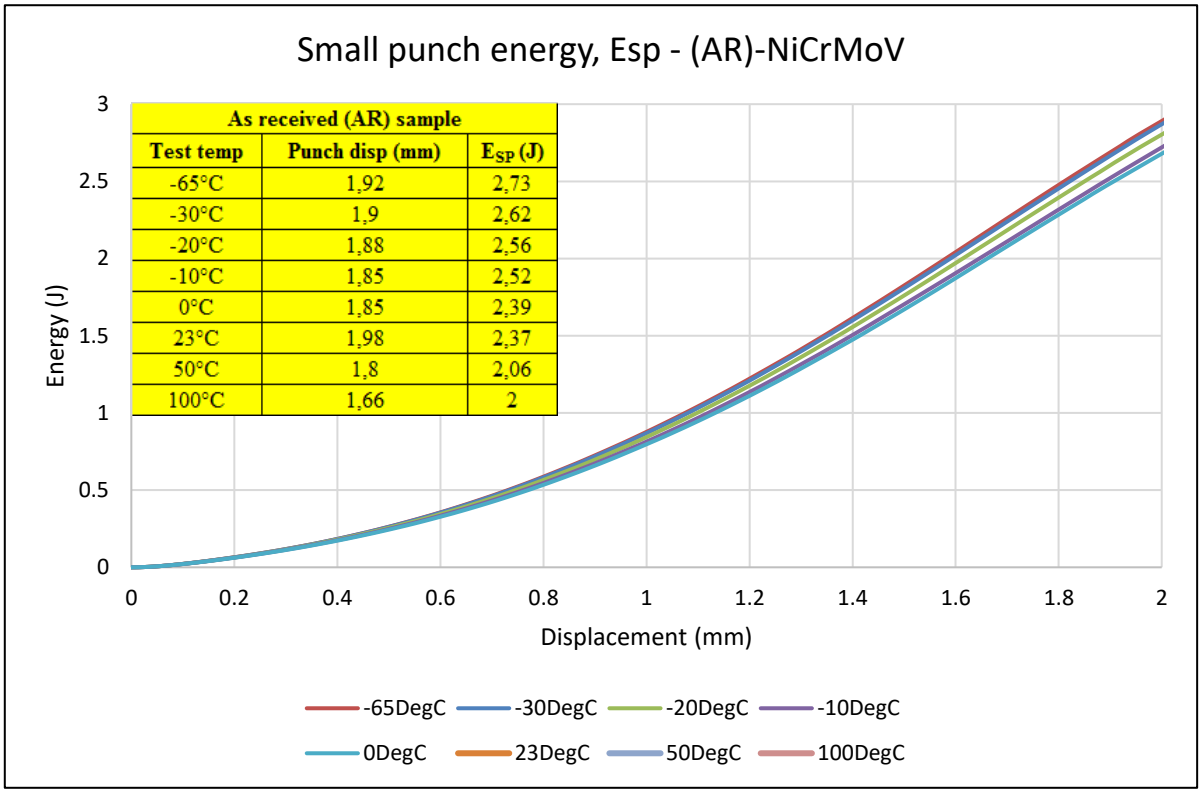

Figure 5-45: Small punch energy, E_{SP} for AR.

5.2.2.4 Modelling strain energy density (W_{SP})

According to the EPRI approach, the camera mounted on the bulge surface is supposed to identify the crack initiation during SPT. This process involves real-time recording of the video during SPT and the synchronisation of the video to SPT in order to estimate the location at which the crack initiated and the punch displacement at that point. Strain energy density is computed using FEM as small punch strain energy density (W_{SP}). This process was modified due to poor quality of images/videos that could not aid in identifying the point of crack initiation. The modification of this process is illustrated in Figure 5-46. This approach was also used to validate the compact tension model (CT_{FEM}).

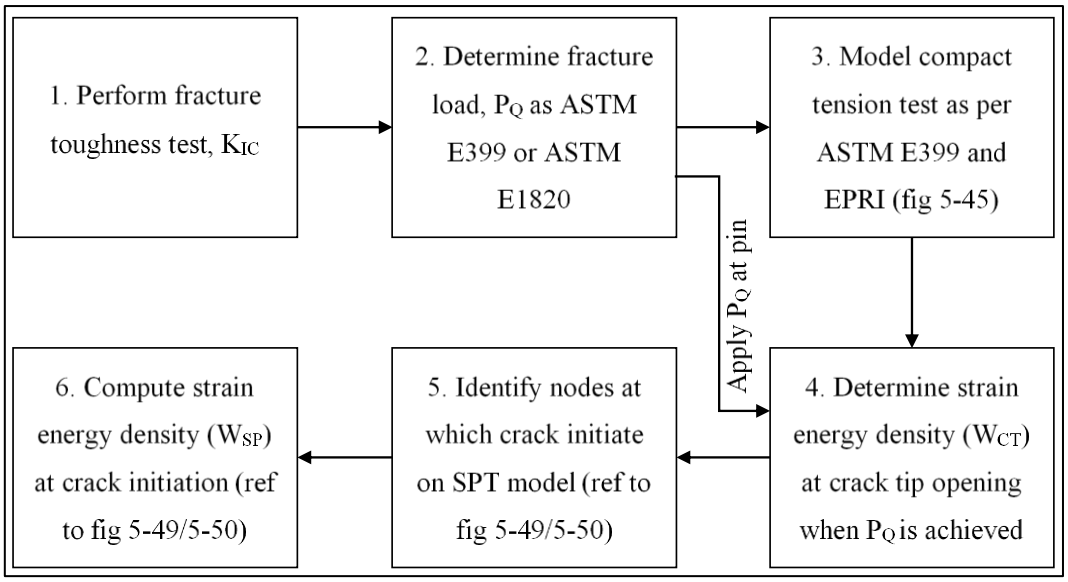

Figure 5-46: Approach to model strain energy density (W_{SP}).

Steps 1 and 2 in Figure 5-46 are covered in Section 5.1, Table 5-9.

5.2.2.5 Modelling compact tension test (Step 3)

The modelling was performed as in Appendix-2 and sketch dimensions were in accordance with the ASTM E399. W = 25 mm and B = 12.5 mm to maintain a/W = 0.5, note a is crack length. For room temperature estimation of K_Q as per experimental results, Table 5-8 and Table 5-9 were used to model the compact tension specimen. For other test temperatures, crack extension (for model), $a_{model} = 0.7a$, was adopted from EPRI [19]. The model is plane strain and had 2570 nodes and 2466 elements (i.e. 2416 linear quadrilateral elements (CPS4S) and 50 linear triangular elements (CPS3)). The half pin consisted of 88 linear quadrilateral elements (CPS4S). A crack tip radius of 0.025 mm was assumed and the minimum element size was about 0.02 mm (refer to Figure 5-47).

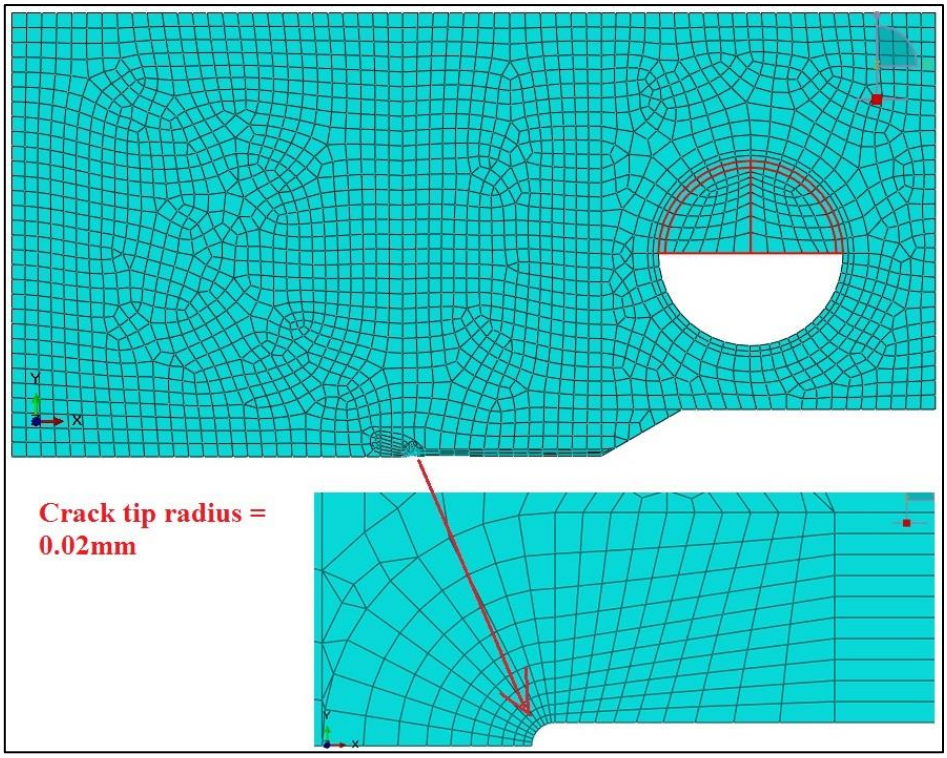

Figure 5-47: FEM for CT specimen used to compute strain energy density.

5.2.2.6 Compute strain energy density (W_{CT}) (Step 4)

The sum of reaction loads taken at the centre and edges of the horizontal diameter of the pin gives fracture load, $P_{Q\text{-FEM}}$. $P_{Q\text{-FEM}}$ is computed until the required room temperature experimental P_Q. W_{CT} at crack tip element is observed and computed ($P_{Q\text{-FEM}} = P_Q$).

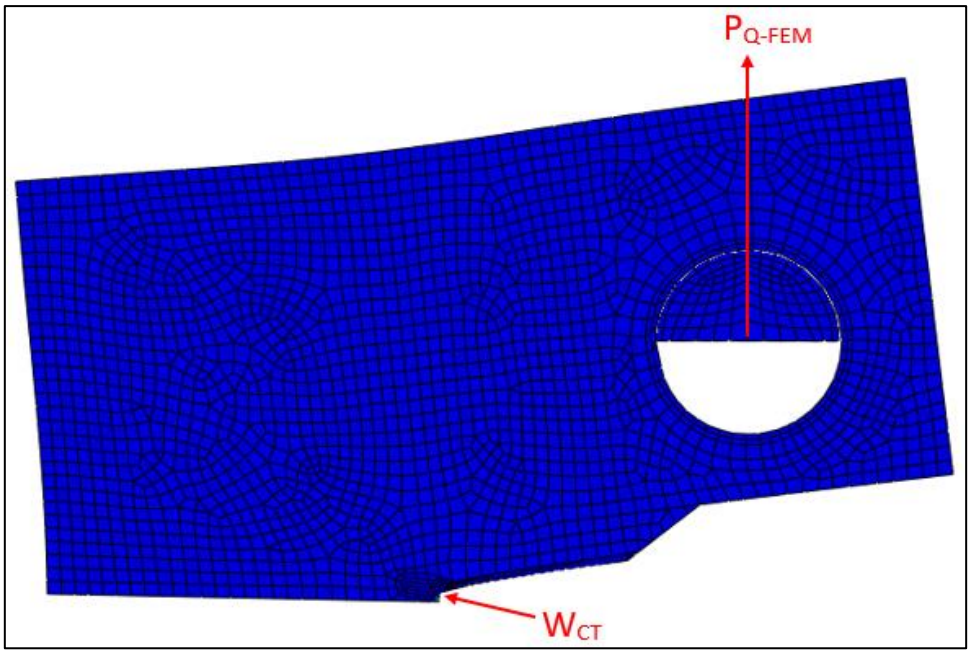

Figure 5-48: FEM CT specimen showing applied $P_{Q\text{-FEM}}$.

Table 5-11 gives computed W_{CT} data which were interpolated between the known fracture properties. The highlighted rows are experimental data P_Q and K_Q. J_Q is determined from the rearranged equation below:

$$J_Q = \frac{K_Q^2 \cdot (1 - v^2)}{E}$$

Equation 5-2: Ductile fracture toughness as per ASTM E399.

P_Q (or P_{EXP}) could not be computed from CT_{FEM}, P_{FEM} closest to P_Q had to be computed and thereafter applied for interpolation to compute W_{CT} that corresponds to P_Q. K_Q that corresponds to P_{FEM} was estimated using experimental fracture properties in Table 5-9.

Table 5-11: Fracture properties obtained from CT_{FEM} using raw data of fracture toughness performed at 23°C.

Sample no	P (kN)		W_{CT} (MJ/m^3)		K_Q (MPa√m)		J_Q (kJ/m^{-2})
	EXP	FEM	FEM	INT	EXP	ASTM E399	From K_Q
Sample 1	-	20.45	86.18	-	-	91.30	37.93
	21.62	-	-	98.47	94.51	-	40.64
	23.25	-	-	115.61	103.82	-	49.04
	23.74	-	-	120.77	105.99	-	51.11
	-	24.41	127.81	-	-	108.98	54.04
Sample 2	-	19.05	75.93	-	-	85.05	32.91
	21.62	-	-	92.81	96.53		42.40
	-	21.87	94.45		-	97.37	43.14
	23.25	-	-	113.91	103.82	-	49.04
	23.74	-	-	120.82	105.99	-	51.11
	-	25.54	146.2	-	-	114.03	59.16

Table 5-12 shows the error band between the experimental K_Q and the estimated $K_{Q\text{-FEM}}$ through using W_{CT}.

Table 5-12: Validation method for CT_{FEM}.

Average K_Q		
EXP	**ASTM E399 (CT_{FEM})**	**Error band**
101.44	100.14	1.28%
102.11	98.82	3.22%

5.2.2.7 Identify crack initiation and compute W_{SP} (Step 5-6)

W_{CT} at room test temperature was used to compute W_{SP} at room test temperature. The nodes at the bulge surface are observed where strain energy density develops. The test is continued up to punch displacement where $W_{SP} = W_{CT}$. The model is supposed to validate the crack initiation point that is captured by the video camera. The video camera used in this study did not have sufficient magnification pixels to identify this point (see the images taken in Figure 5-49 and Figure 5-50). The borescope video camera had four adjustable LED lights that produced poor images due to the reflections of light caused by the shiny polished SPT specimen.

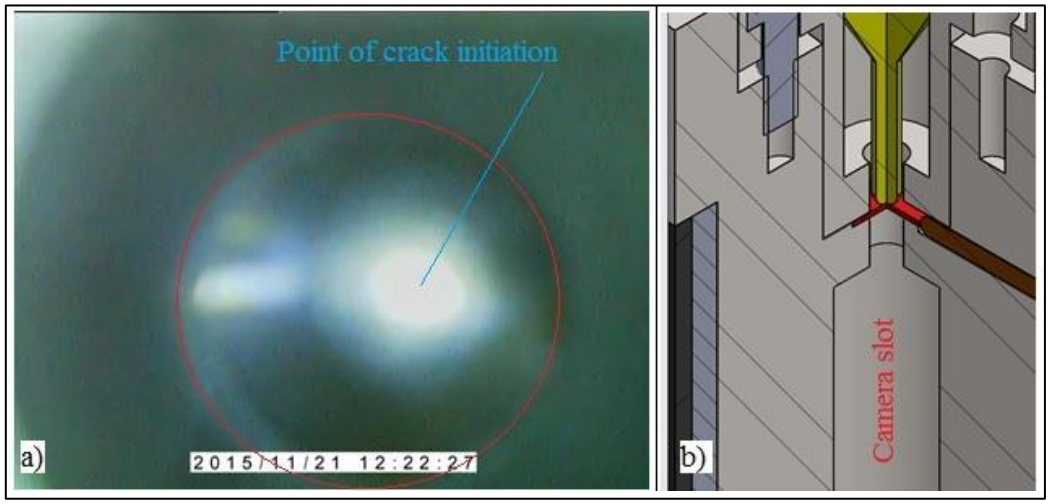

Figure 5-49: a) Photograph of SPT specimen showing an estimate point of crack initiation recorded by video camera and b) 3D CAD drawing showing the configuration of how the camera is mounted.

Figure 5-50: Two different specimens recorded with different LED lighting.

Figure 5-51 shows the SPT LDC_{FEM} with the bulge surface showing the strain energy density within each element. W_{CT} contour at the node 919 on the bulge surface illustrates the point at which the crack initiates. The distance from the centre of the sample at 23°C (0.25 mm) and the punch displacement (0.22 mm) were noted. The SPT at 50°C was analysed using the same method and its behaviour towards crack development can be seen in Figure 5-52. Details of properties (punch load and displacement, distance at which the crack initiates) required for computing W_{SP} are in Table 5-14 for all test temperatures.

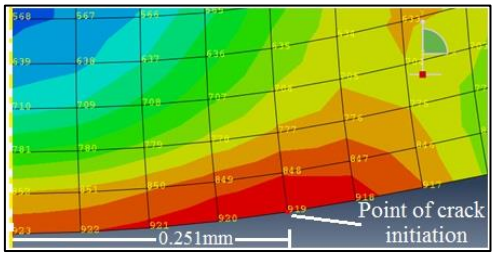

Figure 5-51: 2D Axisysmentry SPT_{FEM} showing crack initiation at 23°C.

This technique was applied to identify the load and displacement at the crack initiation point during the SPT LDC_{FEM} shown in Section5.2.2.2. Figure 5-53 and Figure 5-54 illustrate the strain energy density plotted against punch displacement for 23 and 50°C test temperatures. Figure 5-53 was extracted from three different nodes.

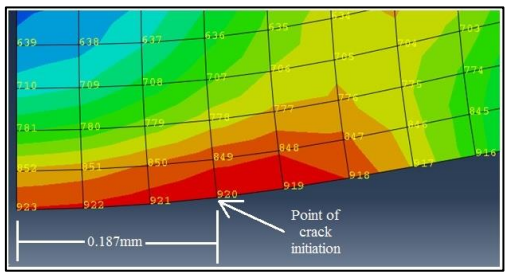

Figure 5-52: 2D Axisysmentry SPT_{FEM} showing crack initiation at 50°C.

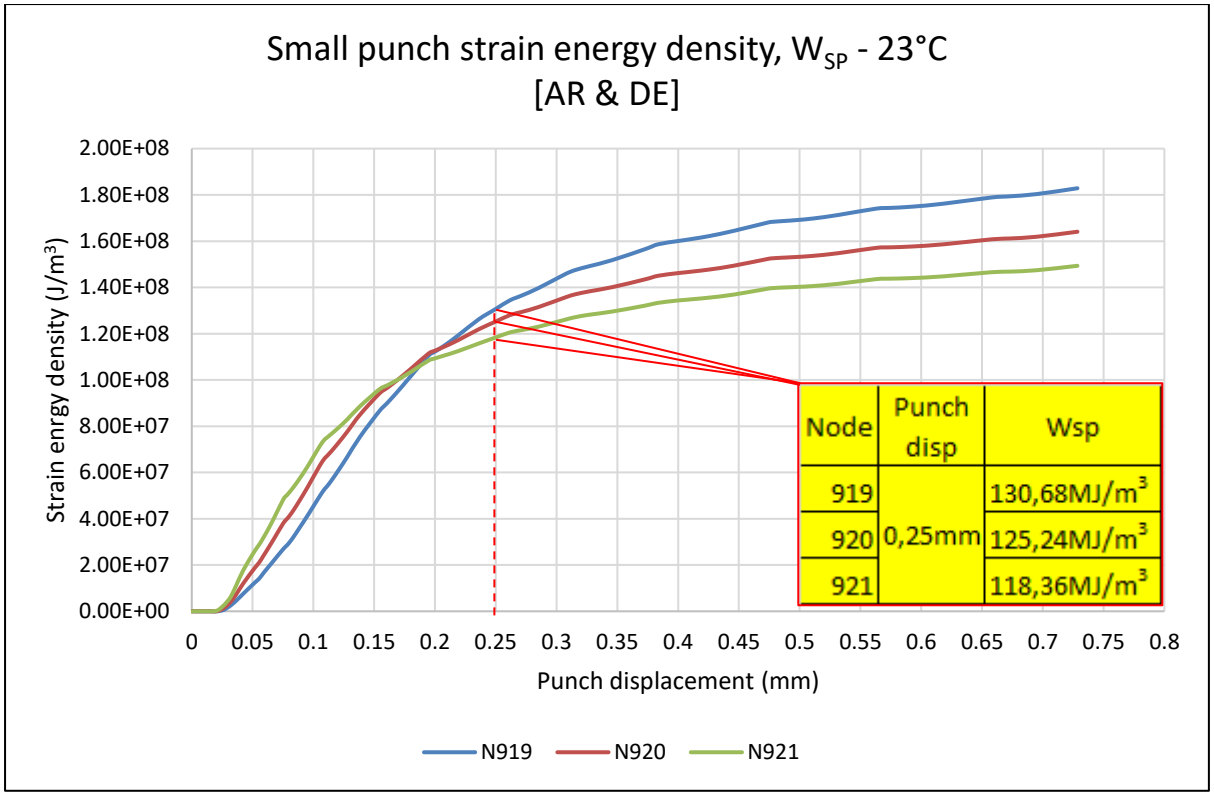

Figure 5-53: W_{SP} vs punch displacement for AR & DE at different nodes at 23°C.

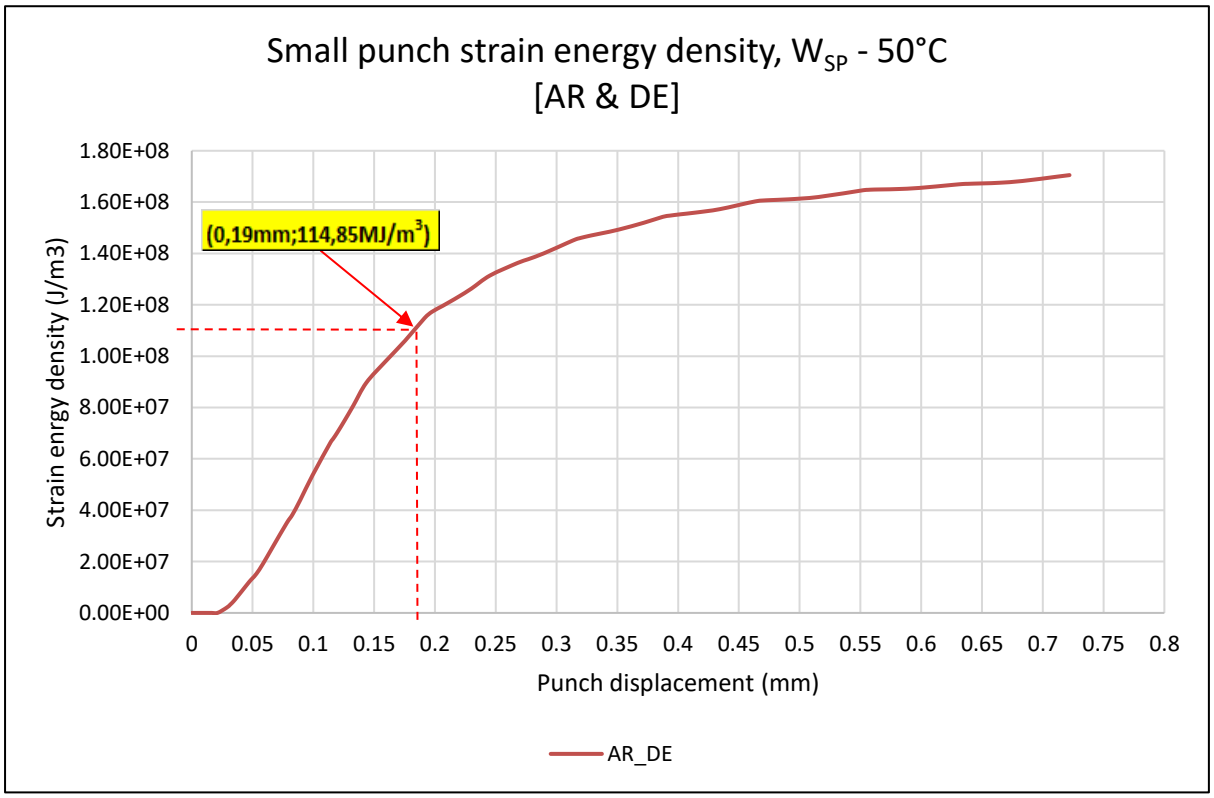

Figure 5-54: W_{SP} vs punch displacement for AR & DE at 50°C.

5.3 SPT correlation to standard mechanical tests

The correlation is carried out in the same sequence as that by which the mechanical test results were reported: tensile, CVN and fracture tests.

5.3.1 Correlation between the SPT and the tensile test

Two methods to estimate tensile properties were explained in Chapter 2. The first method makes use of elastic load (measured from Stage 1 of the SPT LDC) and peak load, dividing both loads by thickness (t and t_f) to get σ_y and UTS, respectively (refer to *FATT* approach in Section 2.3.2.2 and Figure 2-14 for the SPT LDC stages). This method was proven to have 10-20% scatter on estimated tensile test data on past studies and it was not investigated in this study.

This research focussed on an EPRI approach when it came to the correlation between the SPT and the tensile test. This approach requires database SPT LDCs to use as reference in order to estimate the SPT LDCs, which are modelled without any knowledge of tensile test behaviour.

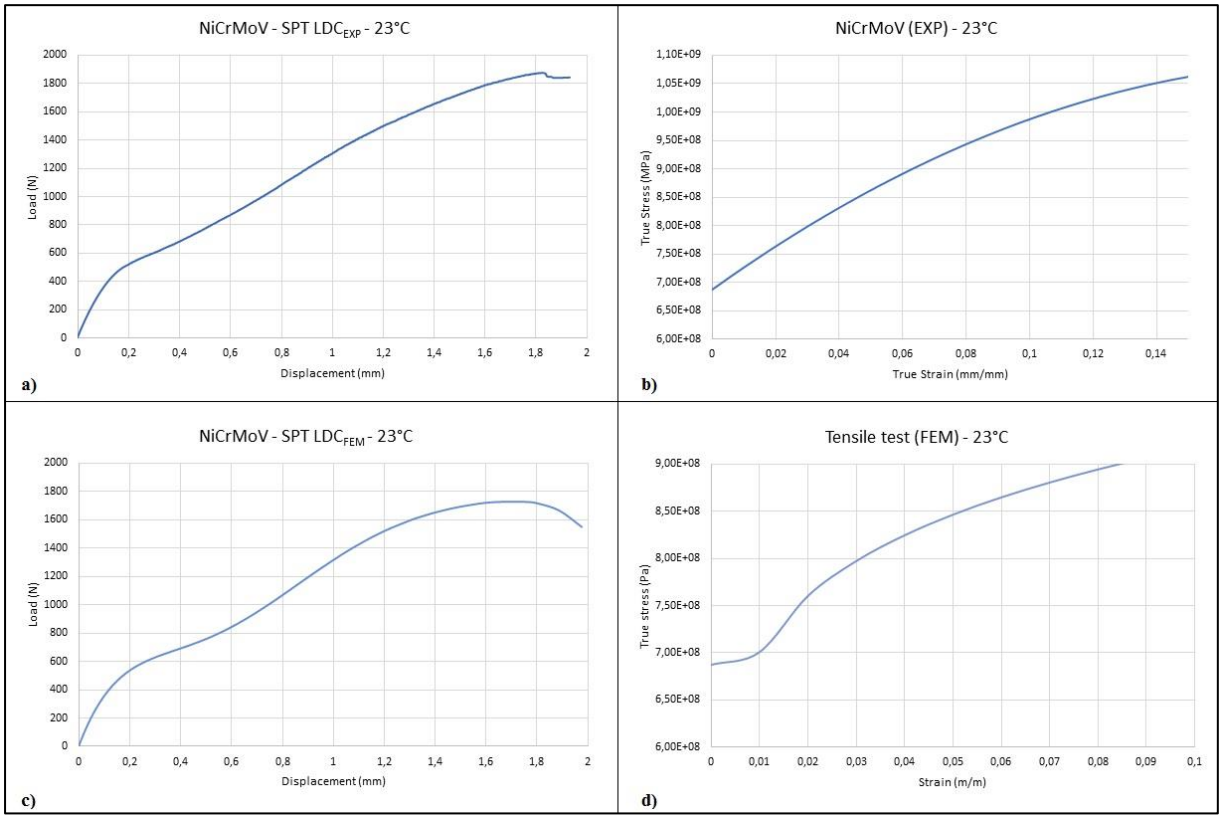

Figure 5-55: a) Experimental SPT LDC, b) experimental true stress – true strain curve, c) SPT LDC$_{FEM}$ and d) modelled true stress – true strain curve showing dual yielding at the beginning.

Figure 5-55 illustrates the approach of correlating the SPT to the tensile test, which comprises of: a) the SPT LDC_{EXP}, which represents b) experimental tensile test. The experimental tensile test raw data (using the Ramberg-Osgood model) is used to develop c) the SPT LDC_{FEM}, which d) the modelled tensile test is exported from. The plastic strain curves (shown in Figure 5-56) for the tensile test performed in room temperature showed behaviour similar to that which the EPRI paper [20] recommended for low alloy steel turbine material, i.e. ε_{py} 0.008 – 0.01.

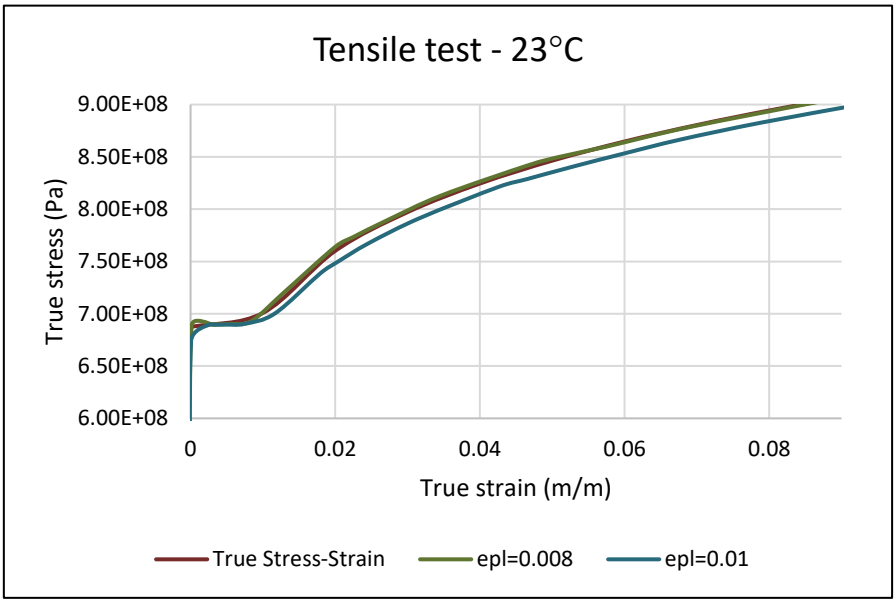

Figure 5-56: Tensile true stress – true strain for different dual plastic yielding at 23°C.

Equation 5-3 is used to determine plastic strain using yield stress and Ramberg-Osgood model parameters. Table 5-13 shows the summary of plastic strains at the test temperatures of the tensile test.

$$\varepsilon_{py} = \left(\frac{\sigma_y}{D}\right)^n$$

Equation 5-3: Plastic strain for Ramberg-Osgood model.

Table 5-13: Derived Ramberg-Osgood numerical values from tensile raw data.

Plastic strain	Test temp (°C)	Sample 1	Sample 2
ε_{py}	23	0.008	0.008
ε_{py}	50	0.006	0.008
ε_{py}	100	0.01	0.01

5.3.2 Correlation between the SPT and the CVN test

The small punch transition temperature could not be achieved through experimental work due to inabilities to test below -65°C. Table 5-5 illustrated the T_{SP} derived from the EPRI established T_{SP} - *FATT* correlation (refer to Table 2-6 in Chapter 2:. Figure 5-57 illustrates the energy curves between the SPT and the CVN test. T_{SP} was predicted using experimental Charpy *FATT*.

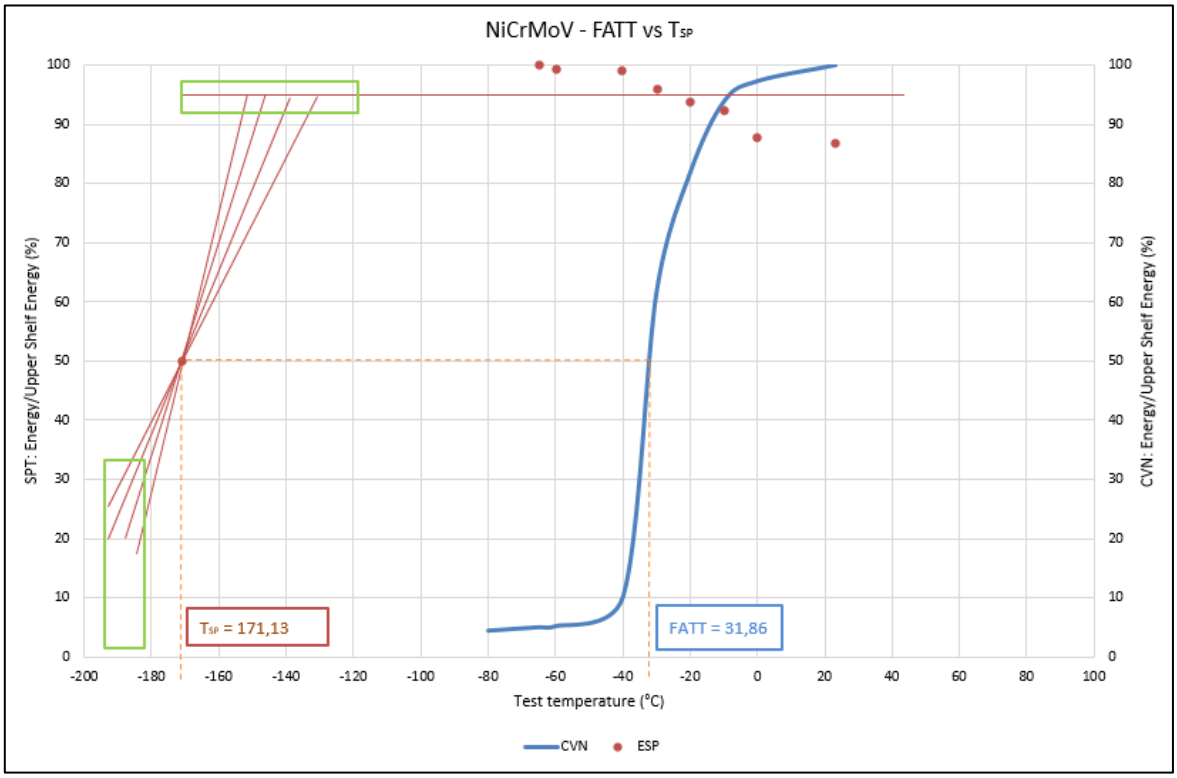

Figure 5-57: T_{SP} and FATT correlation achieved using NiCrMoV T_{SP} correlation [20].

5.3.3 Correlation between the SPT and the fracture toughness

The correlation between the SPT and the K_{IC} is achieved through strain energy density (W_{SP} = W_{CT}). Table 5-14 summarises the fracture properties that were estimated using FEM. The following, as shown in the table stands for:

- Dist, x – distance from the centre of the SPT specimen at which the crack initiated
- P-d – punch displacement corresponding to the crack initiation

Table 5-14: Estimated fracture properties using FEM for NiCrMoV at different test temperatures.

Sample ID	Test temp	Dist, x (mm)	P-d, x (mm)	W_{SP} (MJ/m^3)	W_{CT} (MJ/m^3)	P_Q(kN)	K_Q (MPa$\sqrt{m}$)	J_Q (kJ/m^{-2})
		SPT fracture criterion parameters			CT fracture criterion		ASTM E399	
AR	-65°C	0.19	0.27	157.55	-	-	-	-
AR	-40°C	0.19	0.22	150.86	150.86	25.59	114.25	59.39
AR	-20°C	0.19	0.25	164.65	-	-	-	-
AR	-10°C	0.18	0.21	134.63	-	-	-	-
AR	0°C	0.19	0.22	137.04	137.04	24.61	109.88	54.93
AR	23°C	0.25	0.24	110.39	110.39	22.87	100.76	46.27
DE		0.23	0.24	113.21	113.21	23.01	102.71	48.00
HD		0.19	0.28	243.32	243.32	32.23	143.89	94.20
AR	50°C	0.19	0.19	114.85	114.85	23.37	104.34	49.54
DE		0.19	0.20	114.96	114.96	23.45	104.69	49.87
HD		0.19	0.25	239.59	239.59	31.87	142.29	92.12
AR	100°C	0.18	0.15	117.27	117.27	-	-	-
DE		0.18	0.18	125.55	125.55	-	-	-

CHAPTER 6: CONCLUSION AND RECOMMENDATION

6.1 Conclusion

The purpose of this study was to develop the SPT rig(s), which can be used to test power plant materials as a life assessment technique using small specimens. Furthermore, the SPT technique was supposed to evaluate the embrittlement in these materials. This purpose was achieved and, in addition to this, the SPT data were successfully correlated to traditional mechanical tests involved in this study, which were tensile, CVN and fracture toughness tests. The conclusion is divided according to the main objectives and discussed below.

6.1.1 The SPT equipment and FEM

The SPT rigs were designed in accordance with the CEN Workshop Agreement (CWA 15627: 2007). The compliance of the SPT rigs was investigated through the following:

- Ability to produce repeatable LDCs for the same materials (AR, HD and DE) tested at the same temperatures with a minor error in load of ±20N for the same punch displacement,
- Further to comply, the SPT rigs with Stage 1 of the SPT LDC, which is a linear elastic region. Stage 1 consists of evaluating the behaviour of the linear elastic region, which is Young's modulus (E). A 5 mm thick specimen demonstrated that Young's modulus is in fact correct when compared to the SPT LDCFEM, as shown in Section 3.6.3,
- Data acquisition hardware and software required detailed attention in the block diagram design and programming and, thereafter, synchronisation of load with corresponding punch displacement occurred.

The SPT equipment includes the two rigs that were successfully designed and commissioned through multiple tests. The multiple tests were carried out as a method of verifying or qualifying the model parameter inputs (σ_y, D and n). The model parameters were confirmed to be accurate as compared to derived parameters from true stress-true strain raw data. It was, however, noted that the perfect dual plastic strain (ε_{py}) suggested by EPRI paper [20], which is 0.002 to 0.01, was found to be slightly higher by 0.008. When the model parameters were changed to 0.002 and 0.01, the yield strength changed within a ±5% error band, which was within the ±10% error band that the EPRI approach claims. The SPT LDC_{FEM} for unknown tensile test data (DE and HD samples) was evaluated assuming the ε_{py} of 0.002 and 0.01,

which then implies that the yield strength was estimated from the known database (AR samples) SPT LDC_{FEM}. The modelling of the CT specimen was verified by a traditional fracture toughness test carried out at room temperature. However, the test results did not comply with the ASTM E399 because the NiCrMoV steel being tested was an elastic-plastic material. The fracture toughness value, K_Q, was applied with its known parameters to qualify the model, thus W_{CT} was achieved through P_Q noted on the pin. The fracture criterion, W_{SP}, could not be estimated or identified using the available camera due to its poor pixel size. Hence, the CT_{FEM} was verified using K_Q.

6.1.2 Components susceptible to embrittlement and its types

The details of the components that are susceptible to embrittlement and techniques used to assess embrittlement have been covered in Chapter 2, Appendix-4 and Appendix-5. Most types of embrittlement were incurred during steel processing, service life and/or shutdown (e.g. temper embrittlement in turbine material during cold shutdown). In this study, mechanical tests were applied to evaluate embrittlement and the material was found to have no embrittlement in it. The SPT technique was then used to differentiate the effect of embrittlement between damaged (HD samples) and non-damaged (AR and DE samples) materials. The results were satisfactory and in agreement with the basic factors (absorbed energy, E_{SP}, and ductility as punch displacement) known to decrease when a material is embrittled.

6.1.3 The SPT correlation to standard mechanical tests

The correlation between the SPT and standard mechanical tests was achieved through an established correlation in the EPRI and *FATT* approach. The EPRI approach was adopted to correlate the SPT data with tensile test data (yield strength and elongation). The correlations between these two tests were derived from reference to the SPT LDC_{FEM} database, which was developed from known tensile test data at 23, 50 and 100°C. The SPT LDCs on HD samples were proof of loss of ductility of between 30 to 50% loss as compared to AR samples. It was evident that the NiCrMoV steel was still ductile and it was still as good as the virgin material with regards to tensile properties.

The CVN test was correlated to the SPT through absorbed energies at each test temperature. However, the SPTs were performed up to -60°C. These energies are used to determine the small punch transition temperature, T_{SP}, which gets correlated to *FATT*. In this study, T_{SP} was

achieved through developed EPRI T_{SP}-*FATT* correlation due to the constraints of performing at temperatures lower than -60°C.

The fracture toughness test, K_{IC}, would be determined using fracture load, P, at corresponding W_{CT}. The CT_{FEM} relied on W_{SP}, which equates to W_{CT}, and thereafter used fracture load in accordance with the ASTM E399. This correlation was achieved and the error band is expected to be within ±25%.

6.1.4 Life assessment using the SPT technique

Embrittlement is evaluated through the assessment of ductility and toughness of the material. Embrittlement is known to be one of the most failure-causing mechanisms of power plant components. The SPT technique has demonstrated with capability that it can be employed to evaluate embrittlement through investigating the ductility that can be directly extracted from the SPT data and/or the LDC. The SPT technique is able to assess the T_{SP}-*FATT*, which is determined through the energy absorbed. Life assessment is related to the critical crack that the material can withstand prior to fracture, i.e. fracture toughness. The SPT technique currently is able to estimate the fracture toughness with an error margin of 25% when using the EPRI approach used in this study. This technique is an advantage to utilities or other related industries such as the petrochemical industry as its test data can be used to estimate tensile, CVN and fracture toughness test data through correlation.

6.2 Recommendation for future work

The SPT rigs are currently independent and do not rely on the frame calibration and tensile tester's software/program. This is an advantage as the rigs can be used on any tensile testing machine without the effort of aligning and synchronising the rigs to the frame. It is, however, better to apply a much more user-friendly interface that will include the hardware used for logging load and displacement. The following are recommended tasks for future work to simplify the testing procedure and the acquisition of required raw data:

- A strain gauge that is compatible with the tensile testing machine (e.g. an Instron strain gauge for the 5kN Instron tensile testing machine), as this will mean that the Instron program can be used to run and acquire data as compared to the current method of acquiring raw data. The latter involves a basic knowledge of the LabVIEW program and conversion of data with correction where necessary to accommodate the 2 mm segment of which the magnetic strip consists.

- A better cooling automated system for the *DBTT* SPT rig. This may require the use of a solenoid valve or thermostatic valve and better insulation around the tubing and the rig's outer casing. This adjustment will ensure maintenance of the required testing temperature for longer and be able to test as low as -196°C.
- A higher magnification camera with a minimum of 50X magnification to be incorporated into the rigs. This type of camera will be able to identify the point of crack initiation on the bulge surface during the SPT. Acoustic emission (AE) sensors can be investigated further with reference to the work that the EPRI has already published as this will mean that the ±25% error band can be reduced. Another option to include is the use of digital image correlation techniques to detect the crack initiation.
- Do not use the recommended CWA chamfering during modelling as this complicates the model with stresses being experienced at sharp chamfering. Apply the EPRI rounding of 0.5 mm on the receiving die.
- Modelling scripts can be written in such a manner that the user can just change the Ramberg-Osgood parameters *D* and *n* and run the job to get the required results as an exported file (e.g. select a node and then get the tensile, strain energy density and energy displacement curve as an exported excel file).
- Sampling methods from in-service components need to be verified as there were two sampling methods covered in Section 2.2.4.2. These two methods were not assessed as the material tested was available ex-service.
- Metallurgical testing correlation with the SPT on a fractured surface can be looked at to identify metallurgical defects by looking at the microstructure.
- Superimposed LDCs were not optimised. The optimisation method adopted from the EPRI that is explained in the Literature Review needs to be explored. The optimisation will allow the user to have 100% curve fitting by manipulating the Ramberg-Osgood parameters *D* and *n*.
- Furthermore, to FEM, J-Integral method can be used on CT_{FEM} for elastic-plastic material, which means that J_{IC} can be determined without investigating the fracture load.

APPENDICES

Appendix-1 Design and manufacturing drawings of small punch test rigs

A1.1 SPT rig for DBTT test

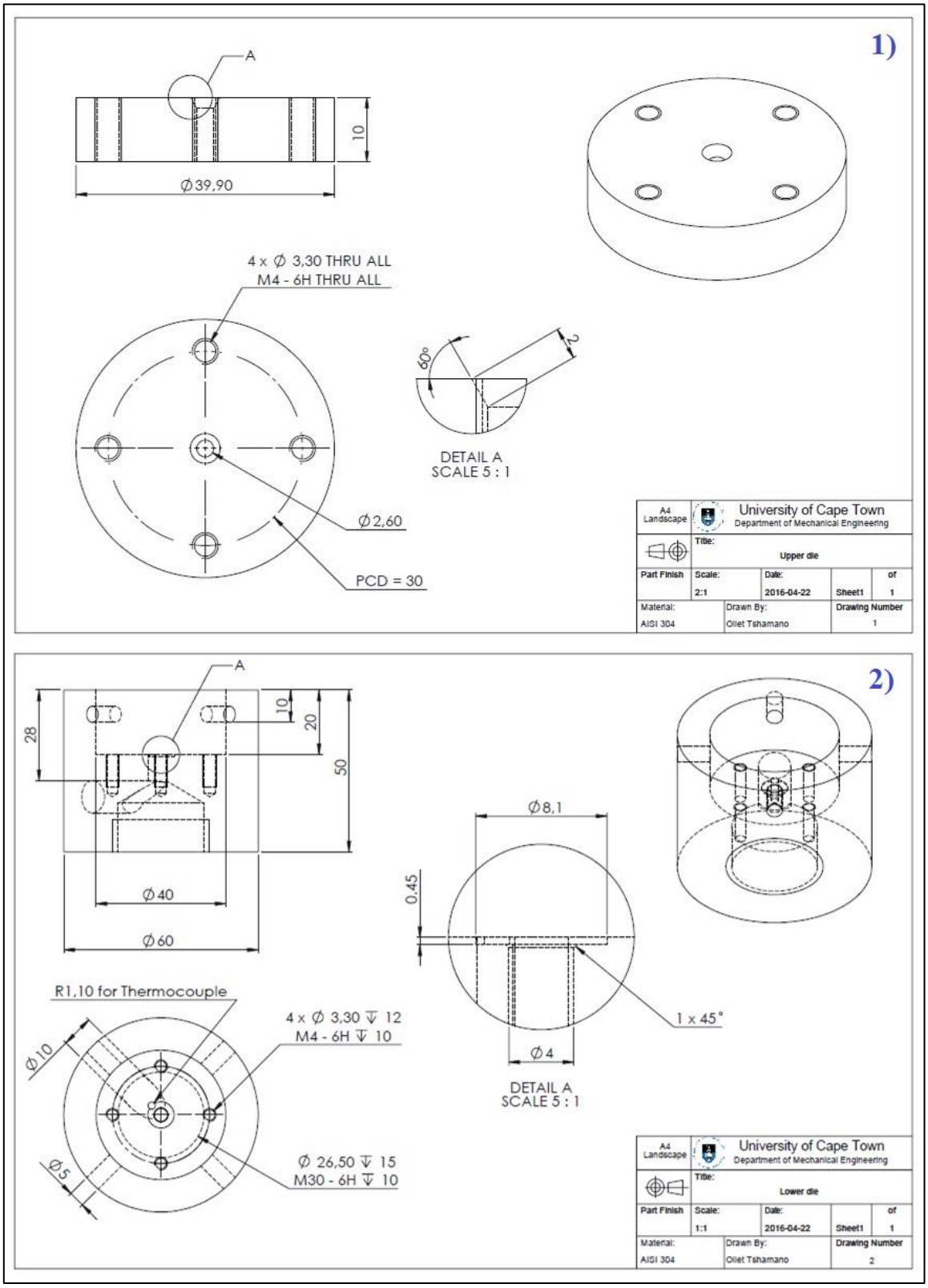

Figure A1-1: 1) Upper die and 2) lower/receiving die.

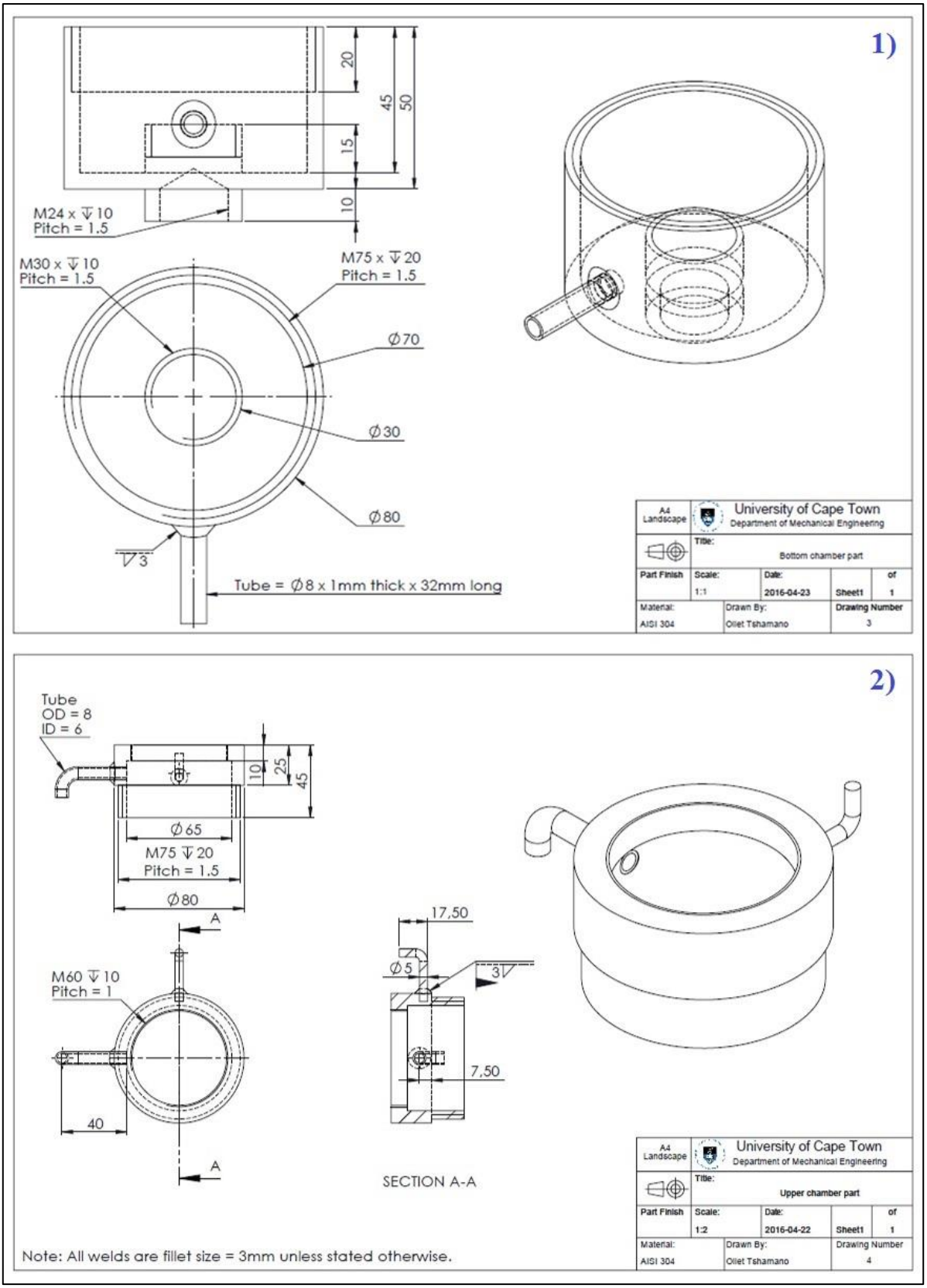

Figure A1-2: 1) Bottom chamber part and 2) upper chamber part

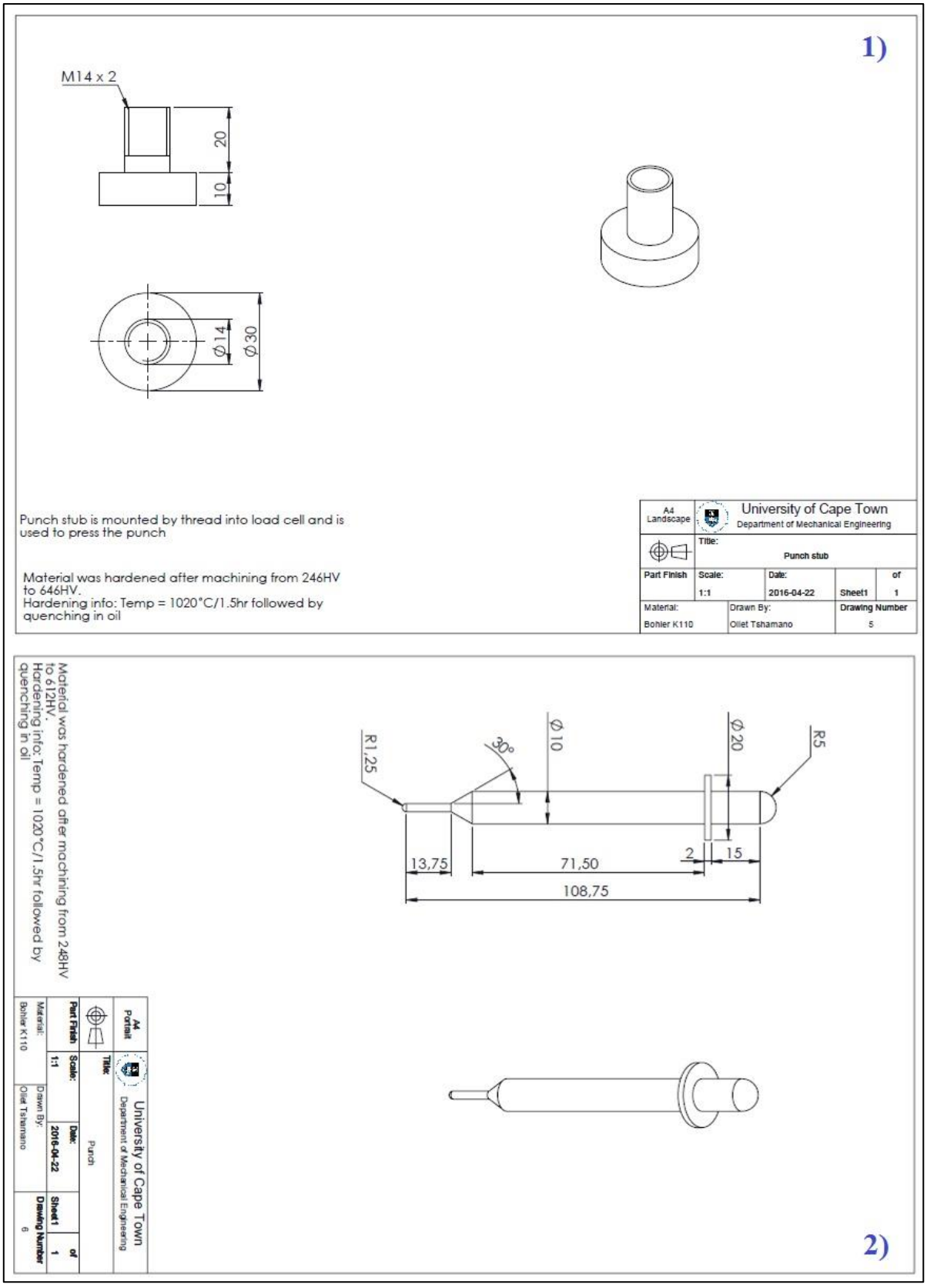

Figure A1-3: 1) Pressing stub and 2) punch.

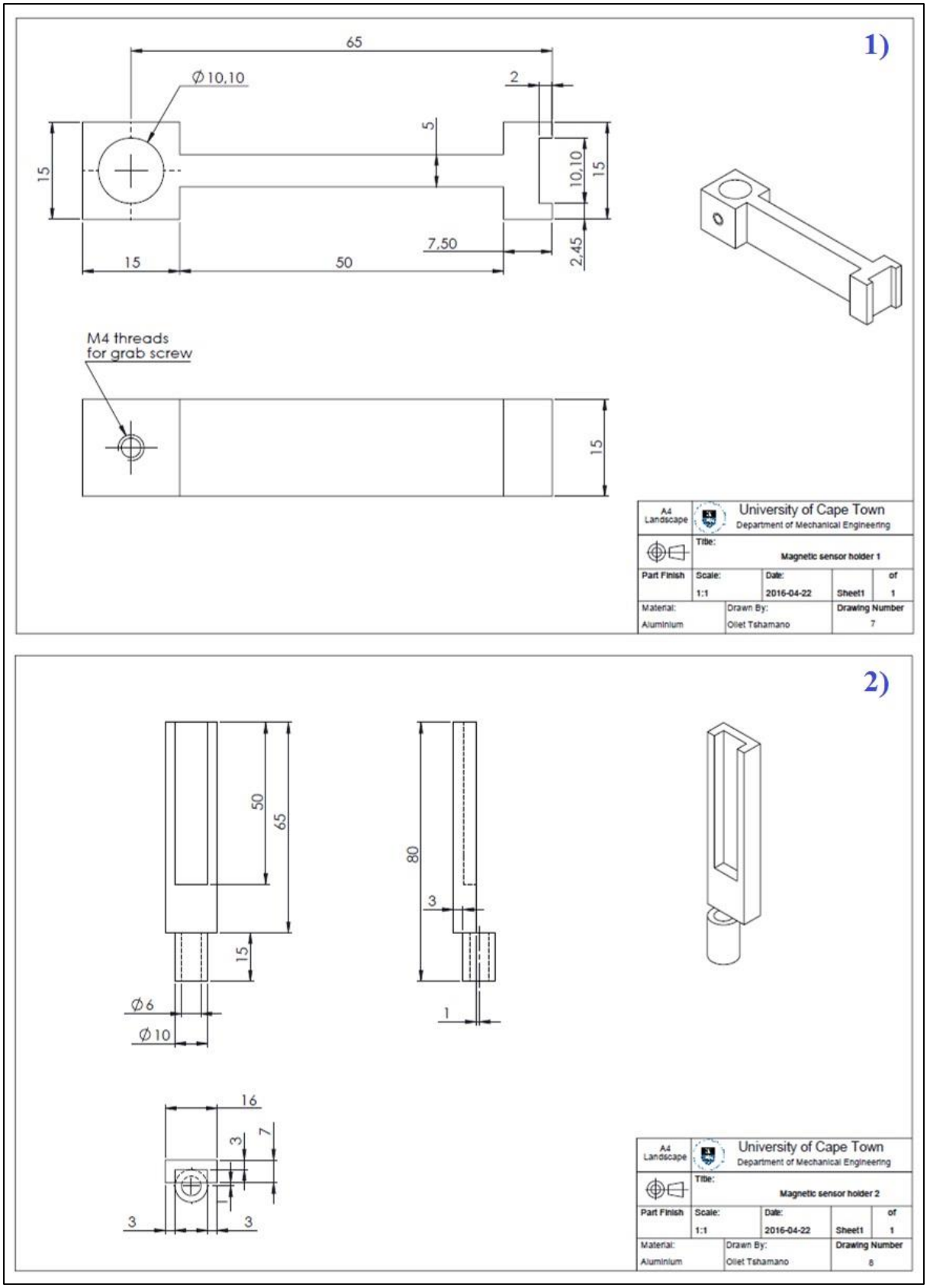

Figure A1-4: 1) Magnetic strip holder and 2) magnetic sensor holder.

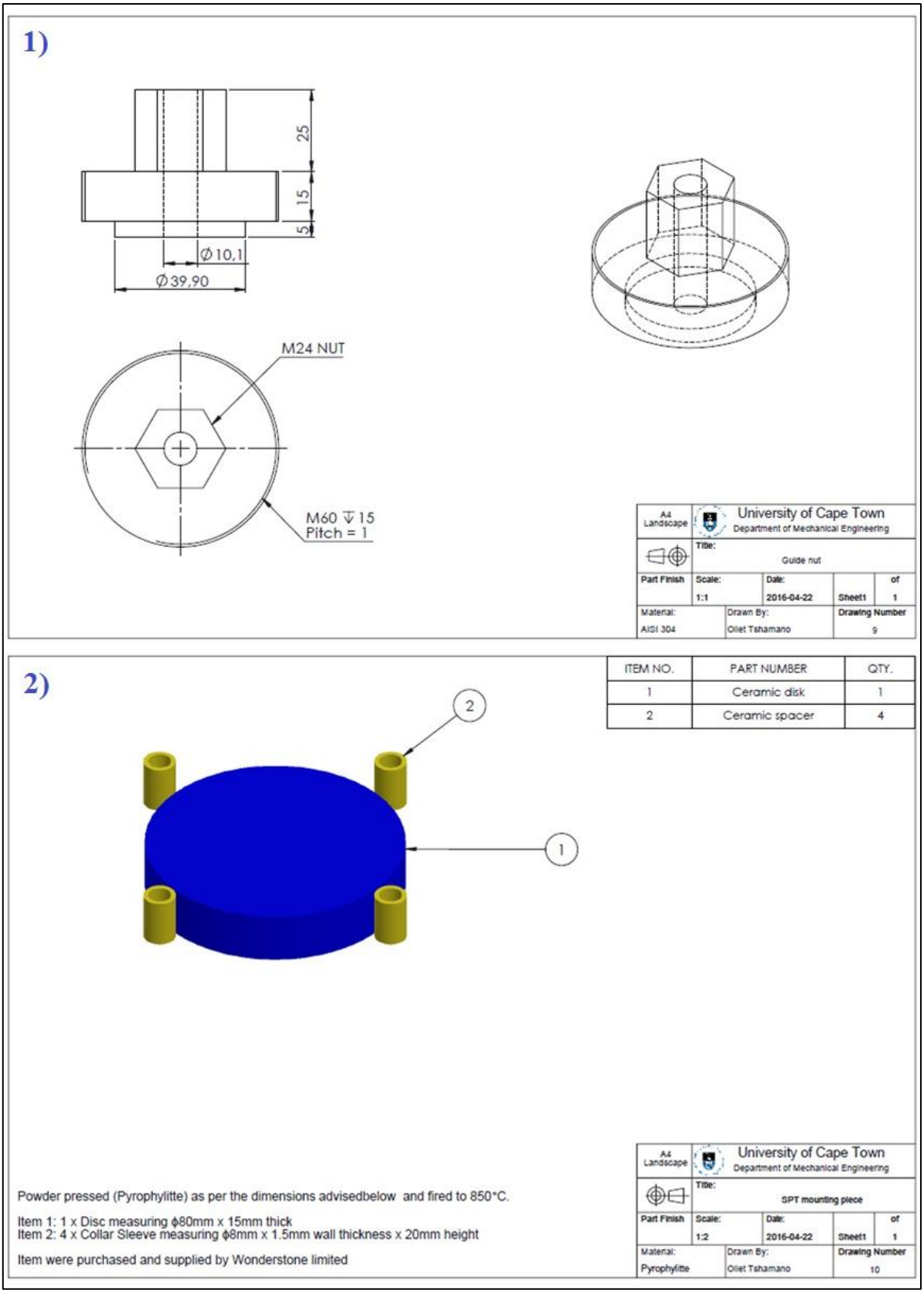

Figure A1-5: 1) Guide nut and 2) pyrophylitte disc and collars.

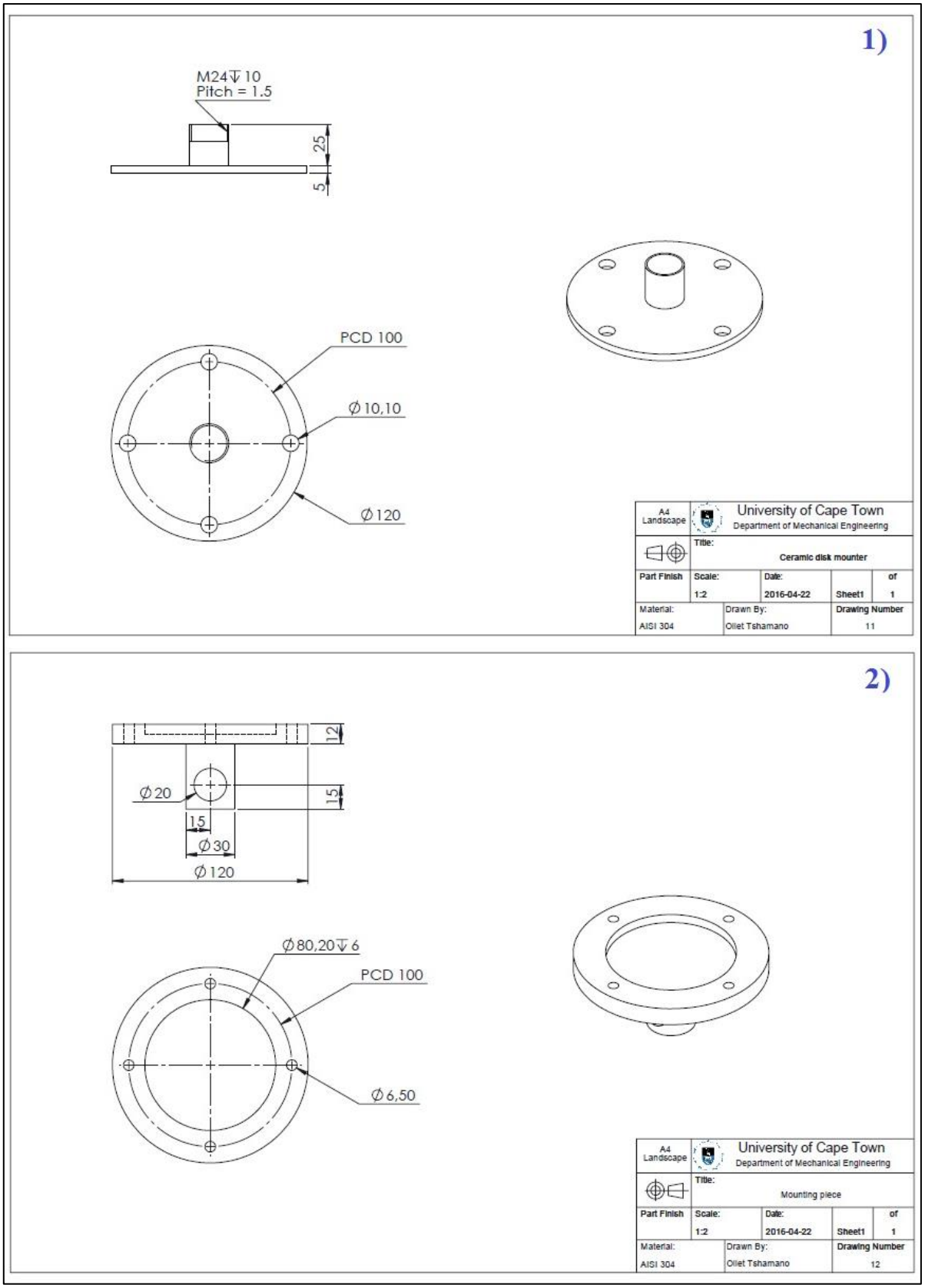

Figure A1-6: 1) Pyrophylitte holder and 2) mounting piece.

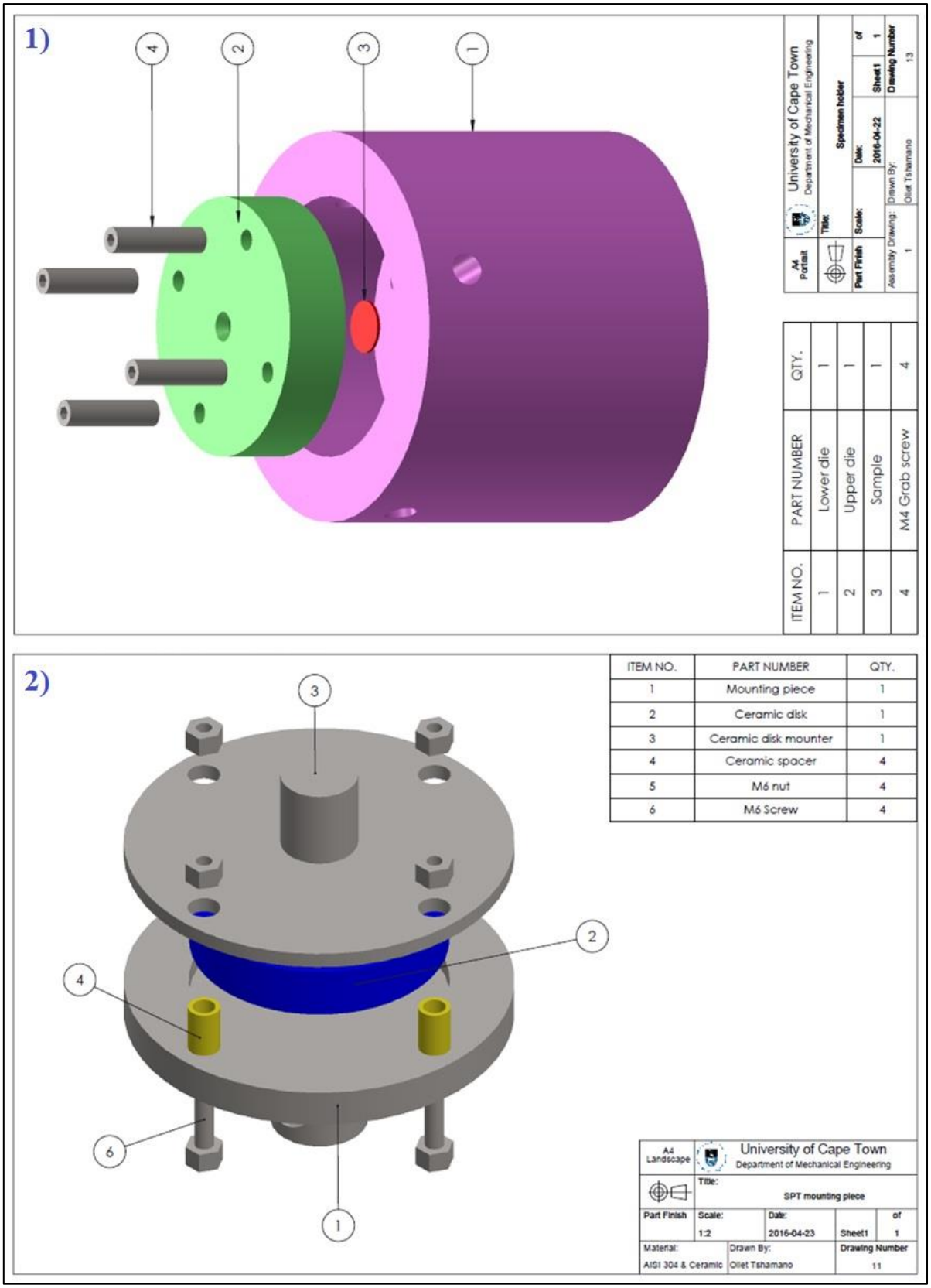

Figure A1-7: 1) Specimen holder and 2) SPT mounting piece.

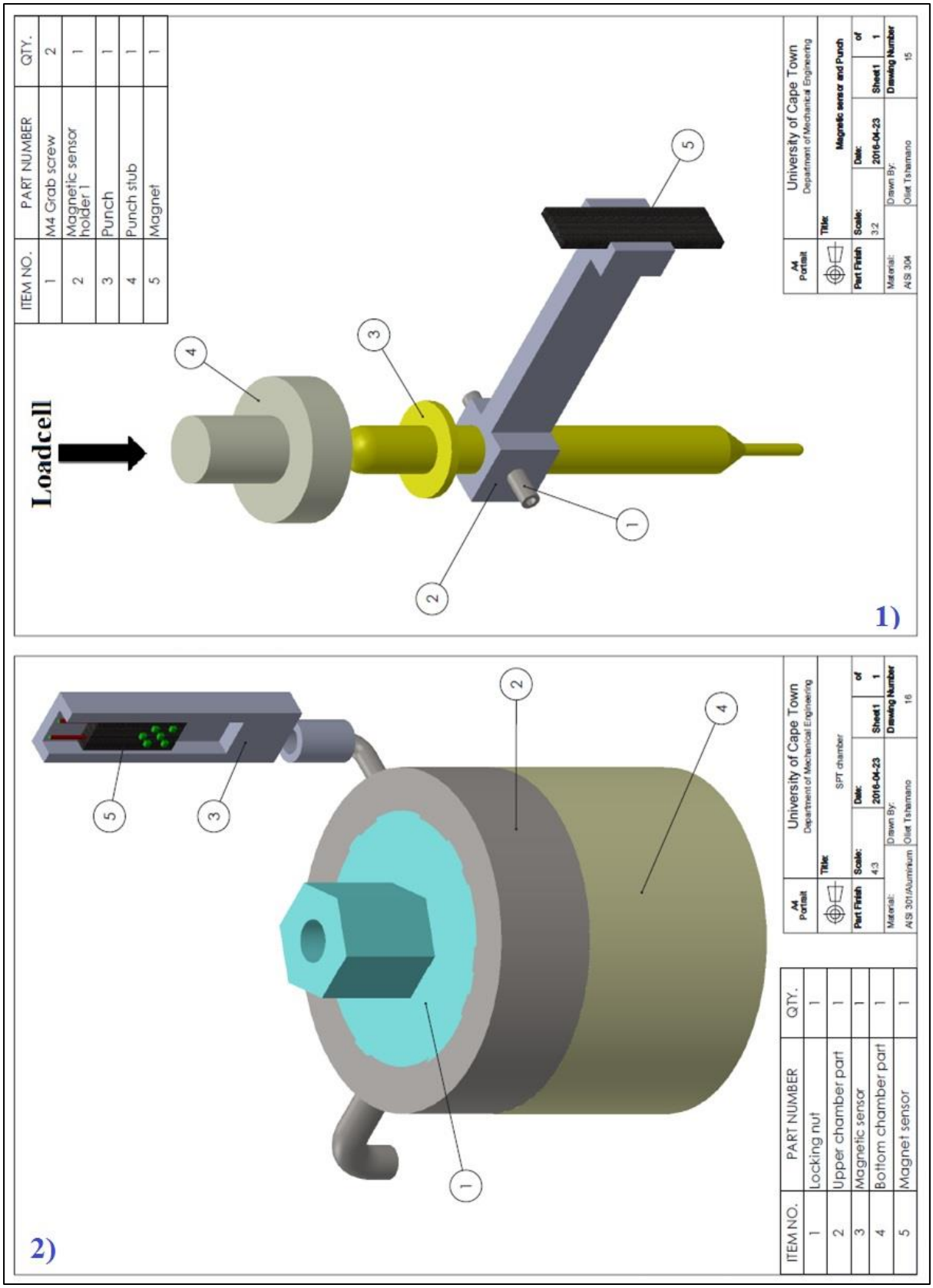

Figure A1-8: 1) Punch and magnet holder and 2) SPT chamber and magnetic sensor holder.

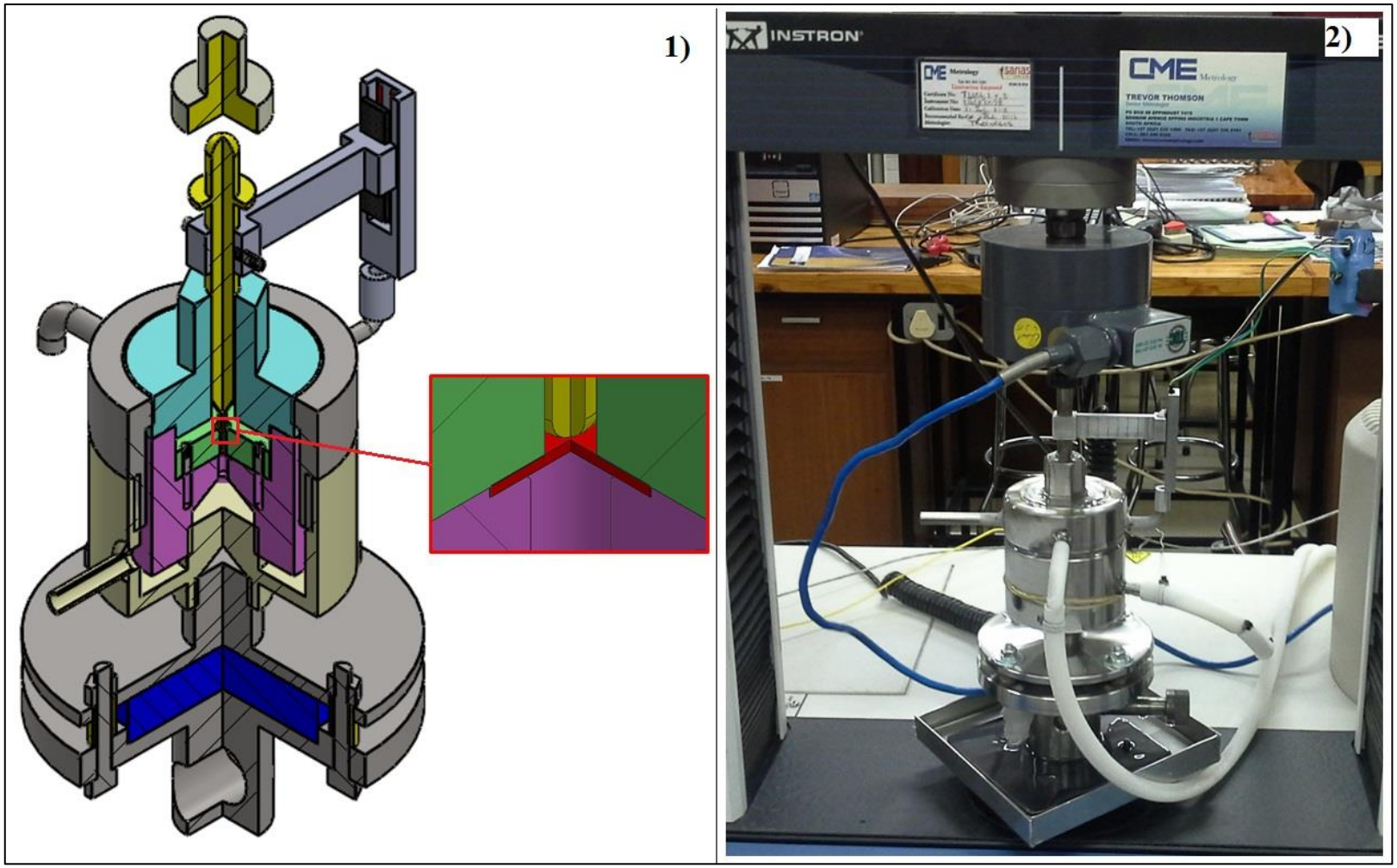

Figure A1-9: 1) SPT rig (CAD drawing) and 2) SPT rig (photograph) for DBTT test.

A1.2 SPT rig for room to elevated temperature

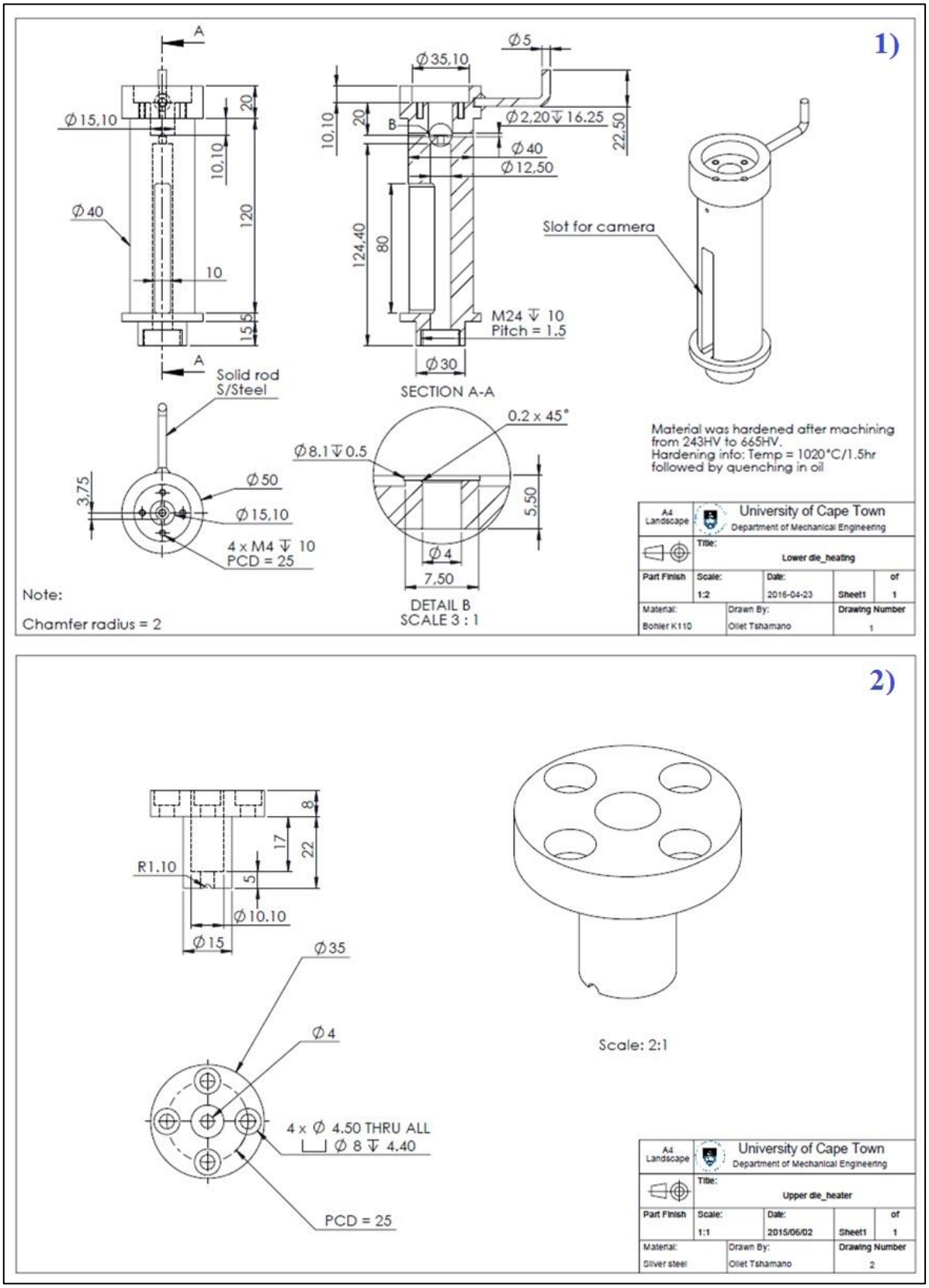

Figure A1-10: 1) Upper die and 2) lower/receiving die.

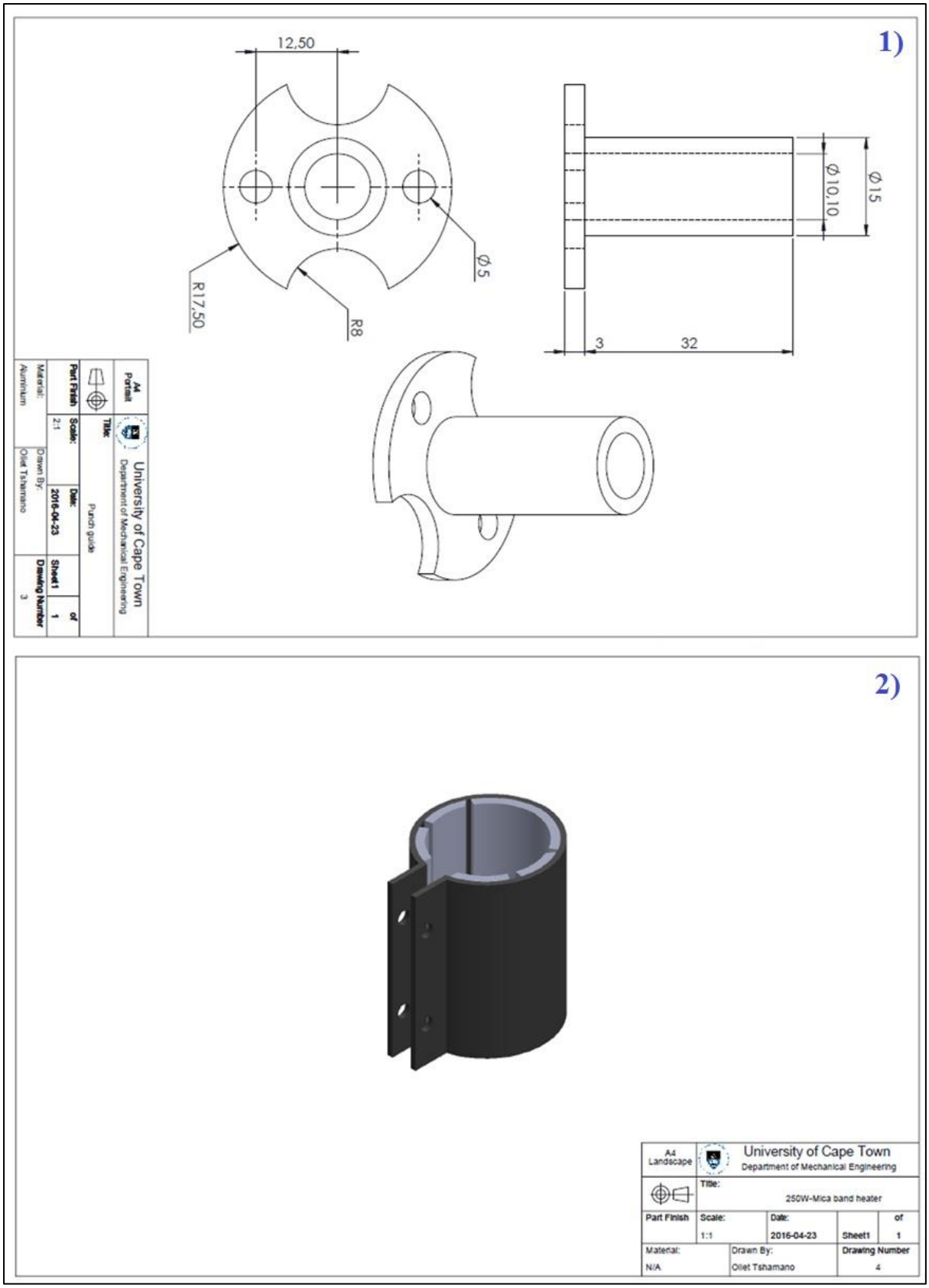

Figure A1-11: 1) Punch guide and 2) Mica band heater.

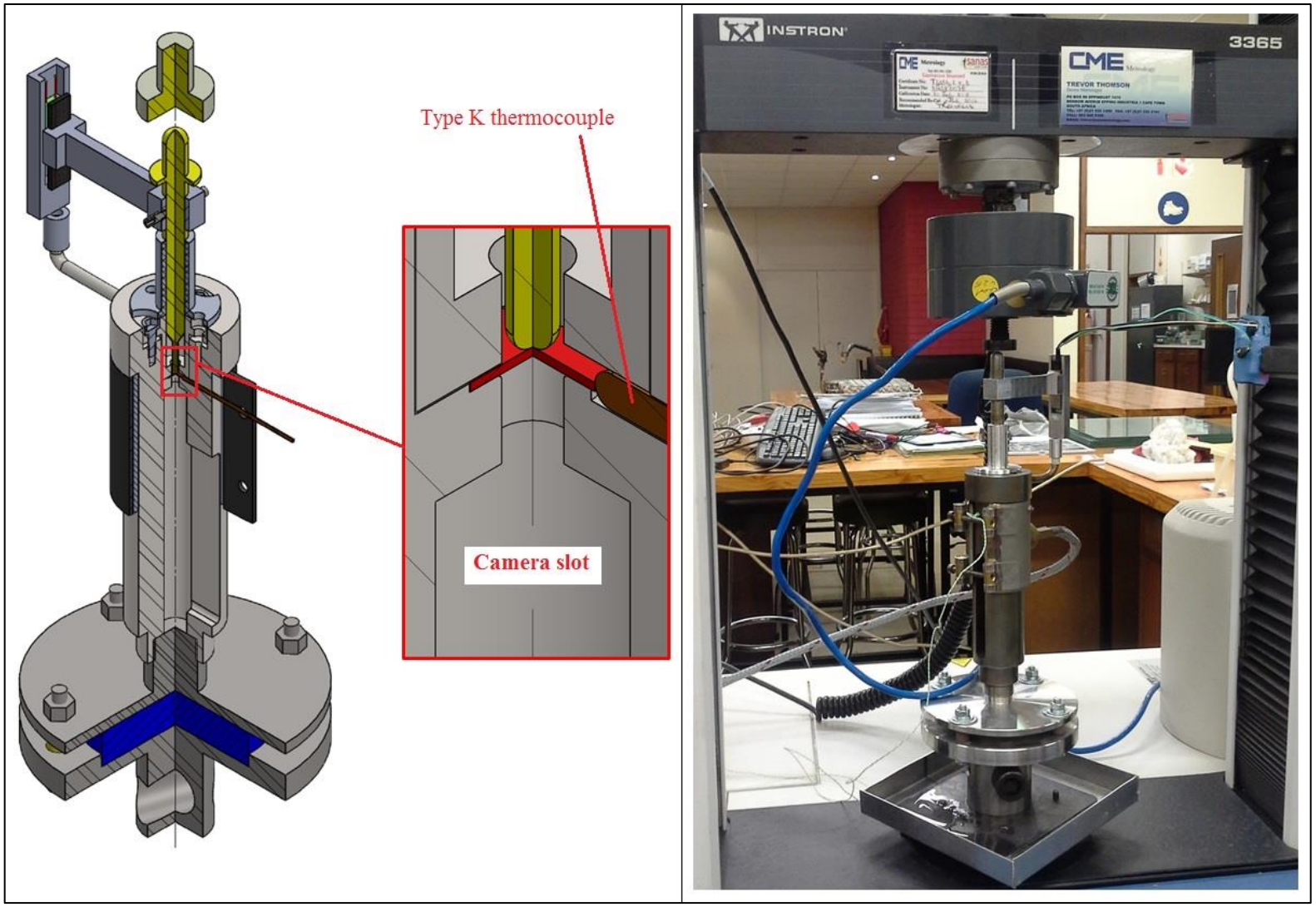

Figure A1-12: 1) SPT rig (CAD drawing) and 2) SPT rig (photograph) for room to elevated temperature.

Appendix-2 FEM instructions

There are three ways that were explored as to how to input tensile raw data to analyse the SPT LDC. Tensile test raw data is required to determine the Ramberg-Osgood model parameters *D* and *n*, which were explained in Section 2.3.3.1. The Ramberg-Osgood model uses the true stress and true strain values and engineering stress and strain can be converted as follows.

A2.1 Engineering stress-strain to true stress-true strain

This only applies when the tensile tester's software is unable to convert stress-strain data. Most of the tensile tester's software are advanced and can export the common output data that are necessary for analysis.

$$\sigma_T = \sigma_E(1 + \varepsilon_E)$$

Equation A2.1.1: true stress equation [49].

$$\varepsilon_T = ln(1 + \varepsilon_E)$$

Equation A2.1.2: true strain equation [49].

A2.2 Determining Ramberg-Osgood model parameters

True stress and true strain raw data can be plotted in a graph in order to apply a power equation trendline in MS Excel. Refer to Figure A2-1 below.

$$\sigma = D(\varepsilon - \varepsilon_e)^{1/n}$$

Equation A2.1.3: Ramberg-Osgood model [34].

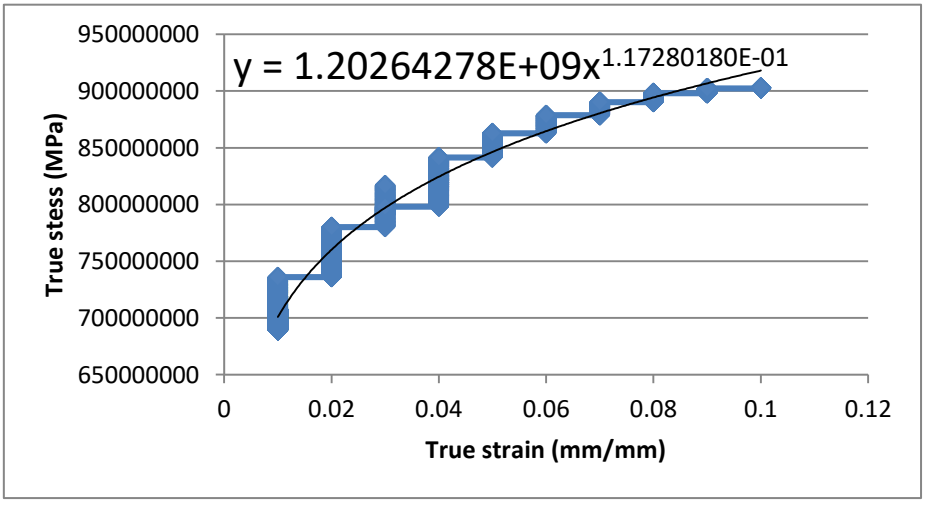

Figure A2-1: Ramberg-Osgood model parameter: D and n.

$\sigma = D(\varepsilon - \varepsilon_e)^{1/n}$

$\sigma = D(\varepsilon_{py})^{1/n}$

$y = C \cdot X^n$

D = 1202.64MPa and n = 1/0.11728018 = 8.5

A2.3 Creating a sketches/part(s) model in Abaqus

A2.3.1 Create a CAE file from the start-up window.

A2.3.2 Create a 2D deformable Axisysmentry parts (punch, sample and two dies) under the model using geometry dimensions.

Table A2-1: FEM sketch properties.

Sketch parts			
Part name	**Model space**	**Type**	**Dimensions**
Punch	Axisysmentry	Deformable	D = 2.5 x L = 10
Upper die	Axisysmentry	Deformable	OD = 30, ID = 2.6 and T = 5
Sample	Axisysmentry	Deformable	D = 8 and T = 0.5
Lower die	Axisysmentry	Deformable	OD = 30, ID = 2 and T = 5 [Sample seat: ID = 8.1, H = 0.4 and r = 0.5]

*** D – Diameter, L – Length, OD – Outside diameter, ID – Inside diameter, T – Thickness, H – Shoulder height and r – rounding radius.

A2.4 Assigning material property to parts

A2.4.1 Under module, drop-down to property or collapse the model tree on the left to property.

A2.4.2 Create two sets of materials and name one: ElastSteel (i.e. elastic steel) and the other: SampleSteel (i.e. sample steel).

A2.4.3 On each pop-up screen create under general, density and under mechanical elasticity with elastic properties as shown in Table A2-2.

A2.4.4 On SampleSteel, under mechanical, define plasticity using applied determined true stress-true strain data from the Ramberg-Osgood model (define hardening as isotropic).

A2.4.5 Use the example in A2-2 to determine the Ramberg-Osgood parameters. Rearrange the equation as shown in Equation A2.4.1 below and determine the true-strain at given

true-stress starting from 0.2σy at strain = 0. Plot data on XY data on MS excel with a small increment of stress (e.g. 50MPa) up to 10-20% high of UTS.

$$\varepsilon = \left(\frac{\sigma}{D}\right)^{n} + \frac{\sigma}{E}$$

Equation A2.4.1: Rearranged Ramberg-Osgood model [34].

Table A2-2: Define and assign material property.

Material property	**Create material**		**Create section**	**Assign material to parts**
Part name	General	Mechanical		
Punch	Density = 7850 kg/m3	Elastic (E = 200GPa and v = 0.3), name it: ElastSteel	Create two sections (solid and homogenous), name section 1: ElastSteel and select ElastSteel for material and name section 2: SampleSteel and select SampleSteel material	Assign ElastSteel material
Upper die		Elastic (E = 200GPa and v = 0.3), name it: ElastSteel		Assign ElastSteel material
Sample		Elastic (E = 200GPa and v = 0.3) and Plastic (σ_{true} vs ε_{true} from Ramberg-Osgood model), name it: SampleSteel		Assign SampleSteel material
Lower die		Elastic (E = 200GPa and v = 0.3), name it: ElastSteel		Assign ElastSteel material

- Other options to define material properties can be used; there are another two options that were investigated.

- Using the Abaqus written script (py file) that describes the model, see the example below in Figure A2-2.

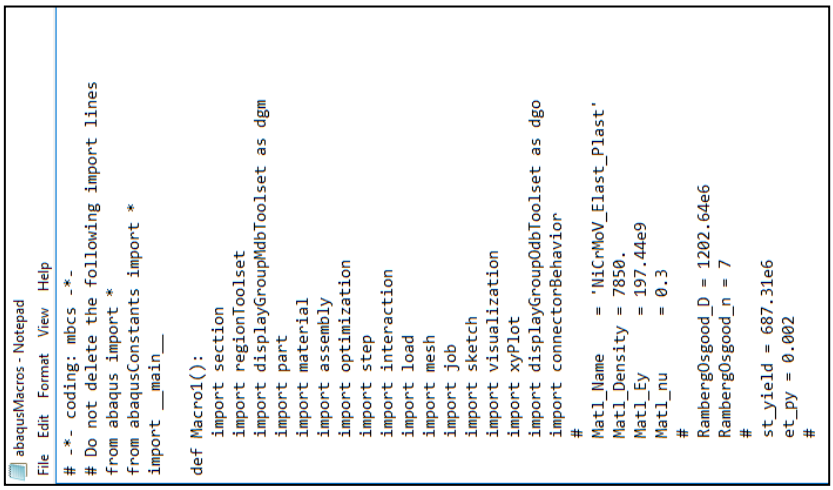

Figure A2-2: Abaqus macro script.

- The script allows the user to easily change parameters and reload to Abaqus with less effort as compared to manual input data from MS Excel.

A2.5 Assembly

A2.5.1 Under module drop-down, select assembly.

A2.5.2 Create instance and select mesh independent and apply for each part.

A2.5.3 Translate instance to assemble the parts, click on instance to select the part that is required to be assembled.

A2.5.4 Click the point on the part and translate it using vectors.

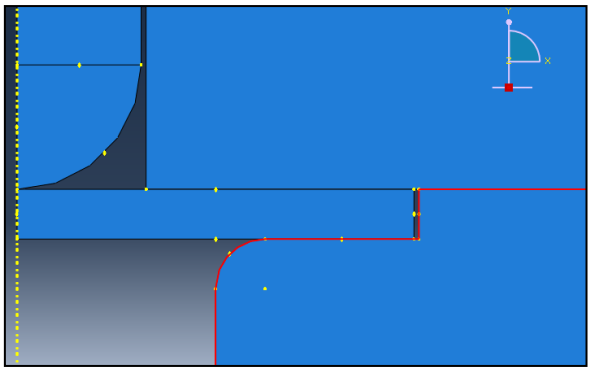

Figure A2-3: Assembled parts.

A2.6 Step

A2.6.1 Under module drop-down, select step.

A2.6.2 Create step (static, general) and refer to Figure A2-4 for details.

A2.6.3 Create field output and select outputs as shown in Figure A2-5.

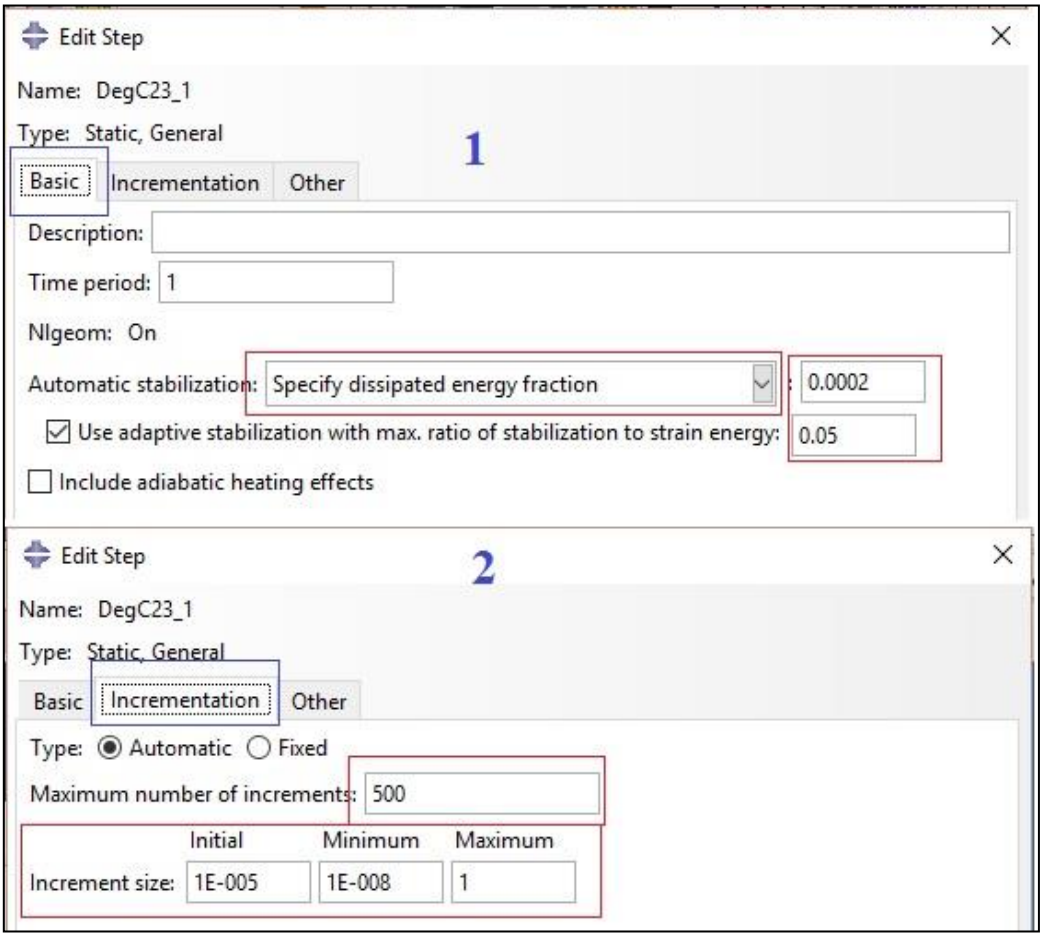

Figure A2-4: Create step.

A2.6.4 Create the history output for the whole model and punch load-displacement data. Refer to Figure A2-5 for details. This step is performed in order receive the output data required (e.g. von misses stress vs equivalent strain and/or punch displacement vs punch load) after each test run.

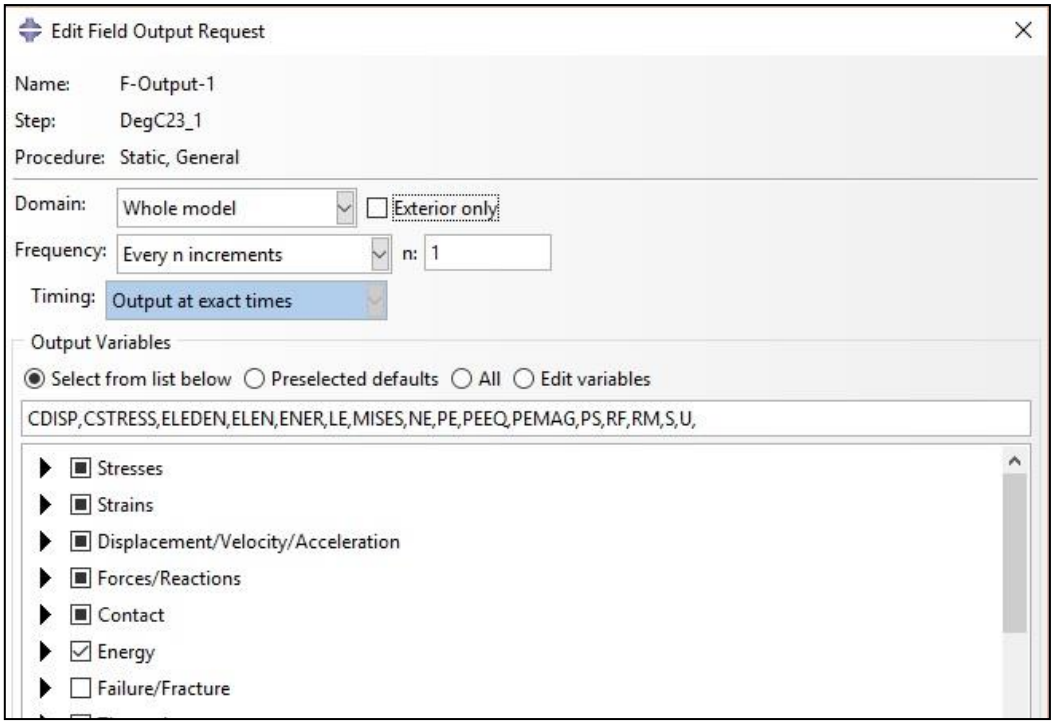

Figure A2-5: Create field output.

A2.7 Interaction

A2.7.1 Under module drop-down, select interaction.

A2.7.2 Create interaction property before interaction. On the pop-up screen, select contact, name it 'HardContact' and press continue.

A2.7.3 Click on the mechanical tab, select tangential behaviour and on the drop down arrow of the friction formulation, select penalty and add a friction coefficient of 0.1.

A2.7.4 Click on the mechanical tab again, select normal behaviour and on the drop down arrow of the pressure-overclosure, select hard contact and leave constraint as default.

A2.7.5 Click on create interaction and create three different surface to surface interactions by selecting the edges that are in contact between: 1) sample and punch, 2) sample and upper die and 3) sample and lower die. Each interaction must be named and saved separately and ensure that the sample is a slave at all times. Apply the 'HardContact' contact interaction property in all interactions created.

A2.7.6 Constraints may be applied at the top horizontal edge of the punch; this ensures that the reaction load (RF2) at this edge is vertical by using equation constraints with degree of freedom. In this research model, the constraint did not affect the results data.

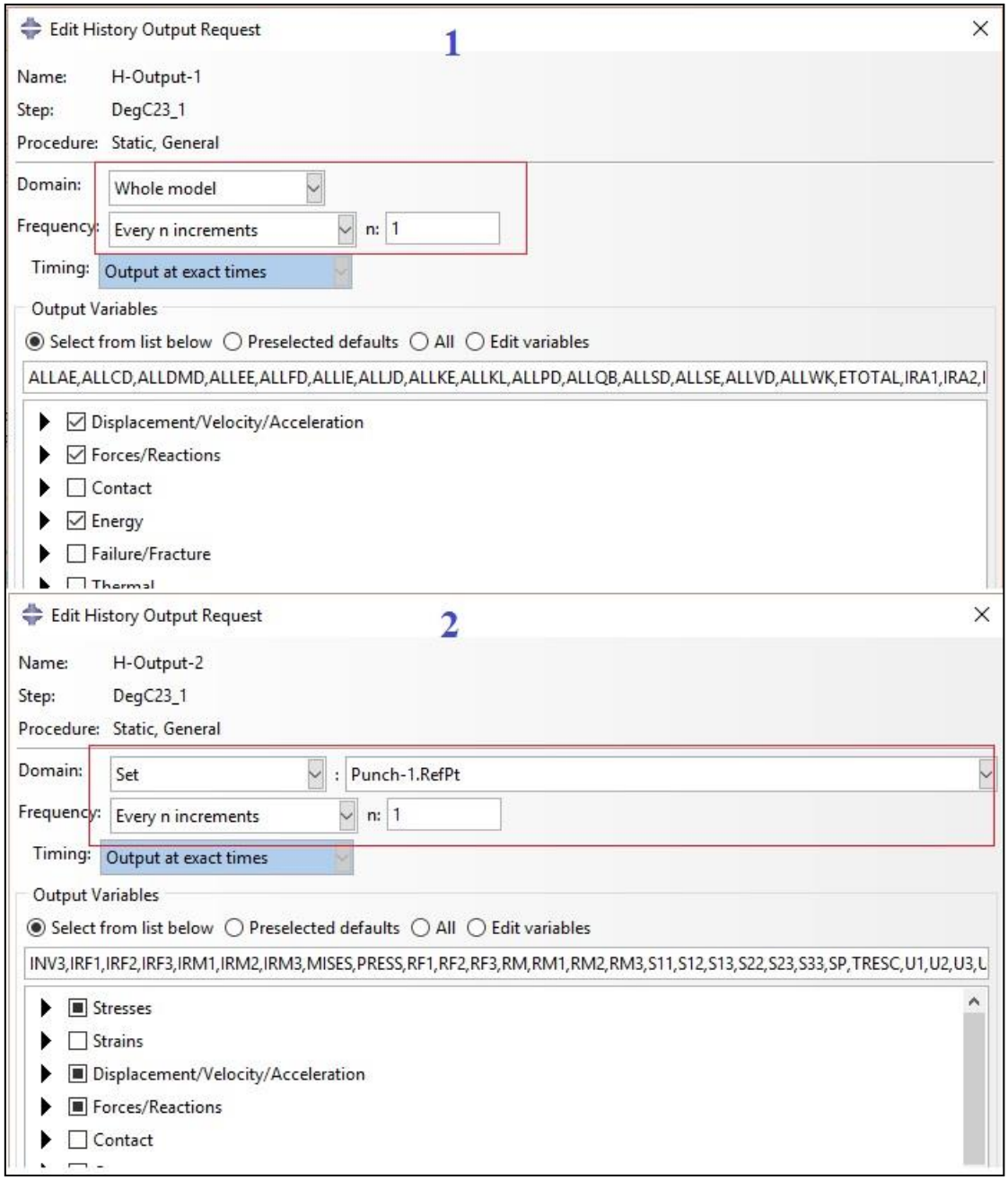

Figure A2-6: Create history output.

A2.8 Load

A2.8.1 Under module drop-down, select load.

A2.8.2 Create three boundary conditions for: 1) move punch, 2) fix bottom and 3) upper die.

A2.8.3 Create a boundary condition to move punch by selecting displacement/rotation step, mechanical category and on the drop down arrow select the model name (not initial).Click continue and select the top edge point as shown in Figure A2-7. Select Y-axis (U2) displacement and enter the displacement size (e.g. -3 mm, downward displacement).

A2.8.4 Create a boundary condition to fix the bottom die from moving when the punch moves against the sample. Select symmentry/antisymmentry/encastre on type of selected step and mechanical category. Select initial step under the step drop down arrow and click continue. Select the bottom edge as shown in Figure A2-8 and select encastre to fix all degrees of freedom to zero.

A2.8.5 Create a boundary condition to fix the upper die from moving when the punch moves against the sample. Select symmentry/antisymmentry/encastre on type of selected step and mechanical category. Select initial step under the step drop down arrow and click continue. Select the top edge as shown in Figure A2-9 and select encastre to fix all degrees of freedom to zero.

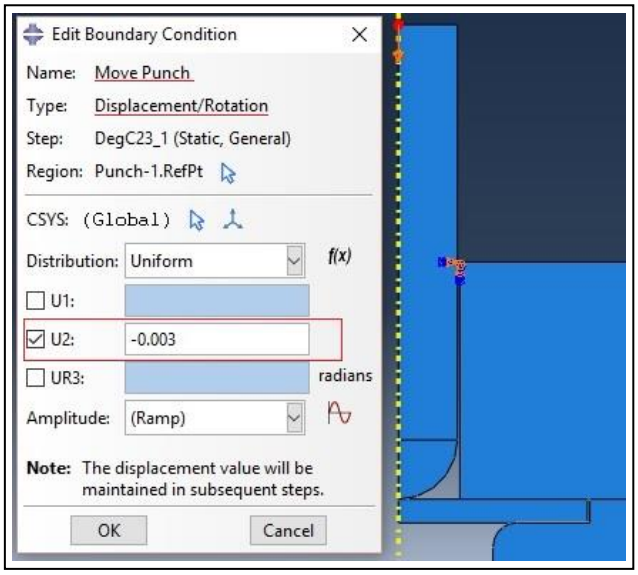

Figure A2-7: Boundary condition for moving punch displacement.

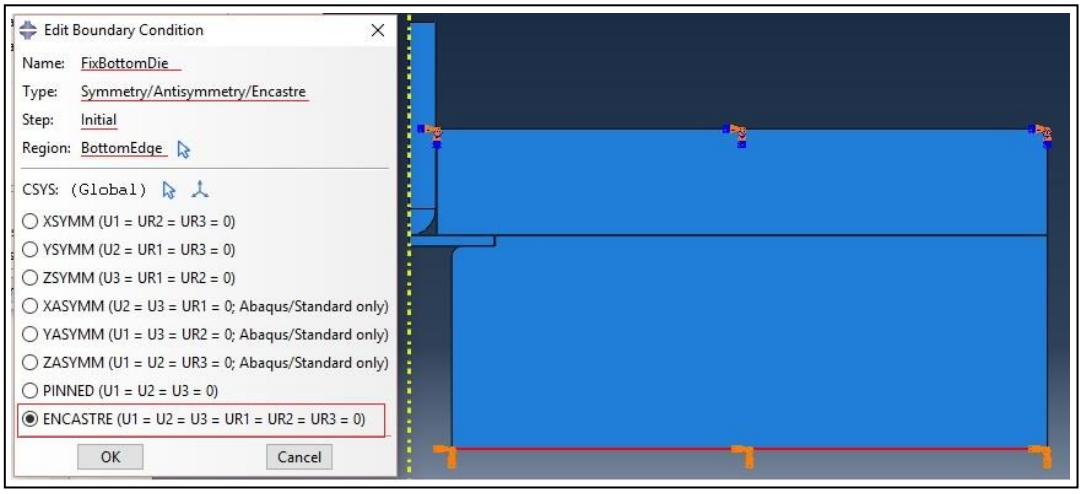

Figure A2-8: Boundary condition for fixing bottom die.

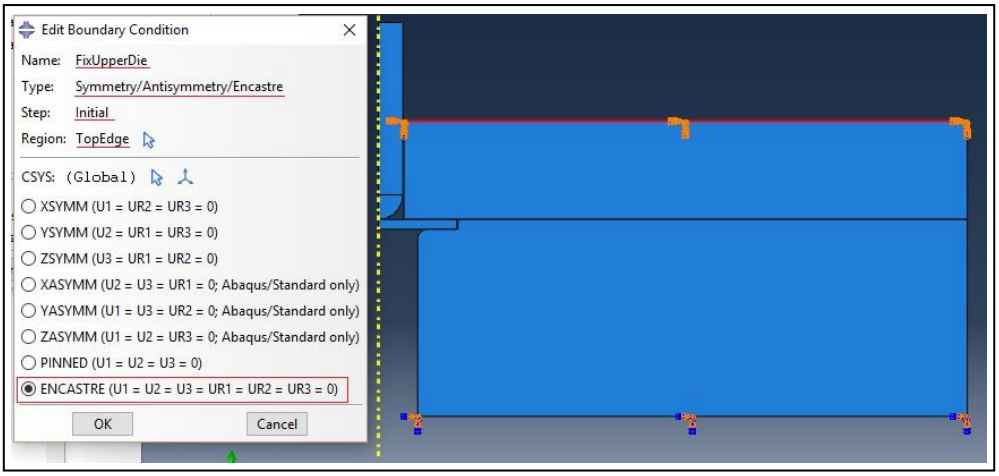

Figure A2-9: Boundary condition for fixing upper die.

A2.9 Mesh

A2.9.1 Under module drop-down, select mesh and on object, select part in order to mesh each part at a time.

A2.9.2 Select seed part when mesh elements are the same size and use seed edge for more refined mesh elements.

A2.9.3 Complete the meshing of parts as per Table A2-3.

Table A2-3: Mesh properties for parts.

Part	Seed	Assign mesh control	Assign element type	Number of elements/nodes
Punch	Edge (radius: number, elements = 40, single bias ratio = 5 and height: number, elements = 35)	As per partition for punch hemispherical head and seeding for punch height (quad element)	Standard linear without reduced integration (CAX4) under axisymmetric stress family	881 elements/958 nodes
Upper die	Edge (diameter: number, elements = 60, single bias ratio = 5 and thickness: number, elements = 10)	Element shape = quad, technique = free and algorithm = advancing front, use mapped meshing	Standard linear without reduced integration (CAX4) under axisymmetric stress family	600 elements/671 nodes
Sample	Edge (diameter: number, elements = 60,	Element shape = quad, technique = free and	Standard linear without reduced integration	840 elements/923

Part	Seed	Assign mesh control	Assign element type	Number of elements/nodes
	none bias and thickness: number, elements = 12)	algorithm = advancing front, use mapped meshing	(CAX4) under axisymmetric stress family	nodes
Lower die	Edge (rounding and seat: number, elements = 40, none bias for each	Element shape = quad-dominated, technique = free and algorithm = advancing front, use mapped meshing	Standard linear without reduced integration (CAX4) under axisymmetric stress family	CAX4 elements = 1635, CAX3 elements =54 and nodes = 1773

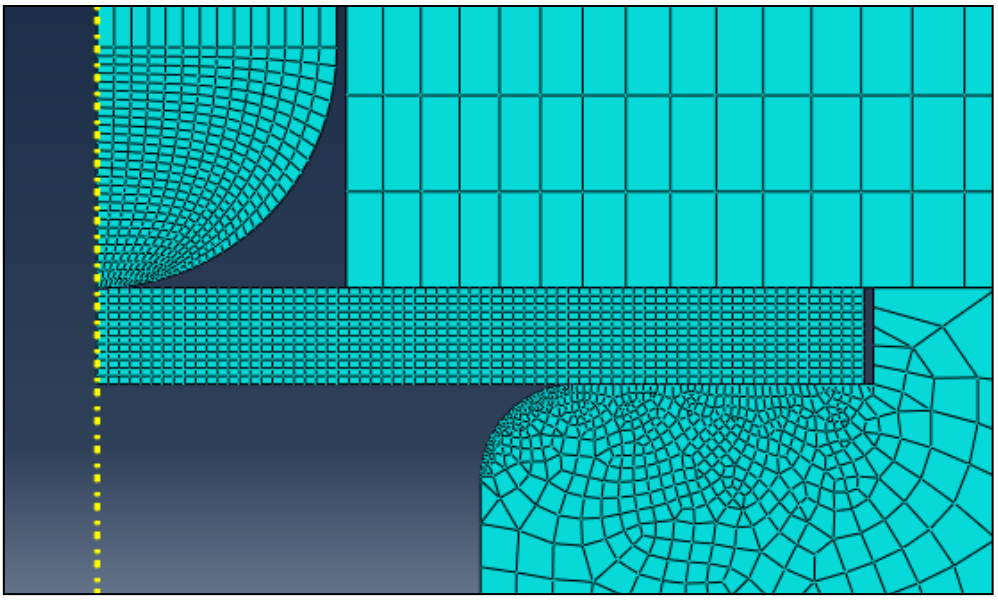

Figure A2-10: Meshed FEM SPT.

A2.9.4 Skip optimisation step and run the job. Export required test data such as load, displacement, stress, strain and strain energy density (refer to results for this data).

A2.10 Created database Ramberg-Osgood numerical values

Table A2-1: Numerical parameters of the Ramberg-Osgood model for NiCrMoV rotor steel.

Name	Test temp (°C)	D (MPa)	n	ε_{py}	E (GPa)	σ_y (MPa)
Sample – 1	23	1202.64	8.52	0.008	197.44	687.31
Sample – 2		1205.86	8.52	0.008	214.3	687.23
Sample – 1		1202.64	8.21	0.01	197.44	687.31
Sample – 2		1205.86	8.21	0.01	214.3	687.23
Sample – 1		1202.64	10.56	0.002	197.44	687.31
Sample – 2		1205.86	10.51	0.002	214.3	687.23
Sample – 1	50	1097.20	10.38	0.006	212.35	679.35
Sample – 2		1139.26	9.18	0.008	202.46	677.84
Sample – 1		1097.20	9.47	0.01	212.35	679.35
Sample – 2		1139.26	8.85	0.01	202.46	677.84
Sample – 1		1097.20	12.28	0.002	212.35	679.35
Sample – 2		1139.26	11.38	0.002	202.46	677.84
Sample – 1	100	1109.69	9.12	0.008	186.70	654.22
Sample – 2		1116.59	9.19	0.008	165.03	663.89
Sample – 1		1109.69	8.68	0.01	186.70	654.22
Sample – 2		1116.59	8.84	0.01	165.03	663.89
Sample – 1		1109.69	11.17	0.002	186.70	654.22
Sample – 2		1116.59	11.35	0.002	165.03	663.89

Appendix-3 Mechanical test specimen

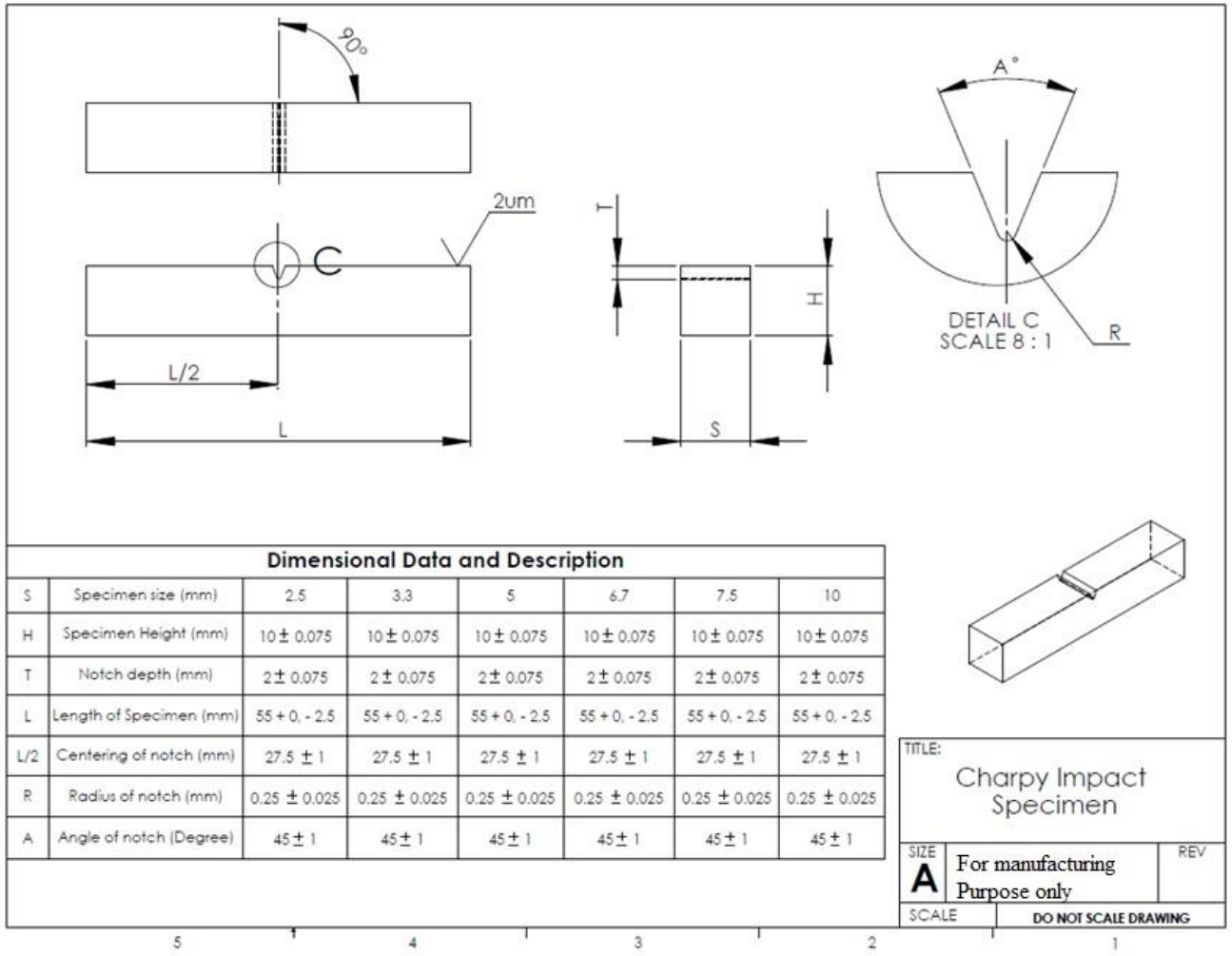

Dimensional Data and Description

S	Specimen size (mm)	2.5	3.3	5	6.7	7.5	10
H	Specimen Height (mm)	10 ± 0.075	10 ± 0.075	10 ± 0.075	10 ± 0.075	10 ± 0.075	10 ± 0.075
T	Notch depth (mm)	2 ± 0.075	2 ± 0.075	2 ± 0.075	2 ± 0.075	2 ± 0.075	2 ± 0.075
L	Length of Specimen (mm)	55 + 0, - 2.5	55 + 0, - 2.5	55 + 0, - 2.5	55 + 0, - 2.5	55 + 0, - 2.5	55 + 0, - 2.5
L/2	Centering of notch (mm)	27.5 ± 1	27.5 ± 1	27.5 ± 1	27.5 ± 1	27.5 ± 1	27.5 ± 1
R	Radius of notch (mm)	0.25 ± 0.025	0.25 ± 0.025	0.25 ± 0.025	0.25 ± 0.025	0.25 ± 0.025	0.25 ± 0.025
A	Angle of notch (Degree)	45 ± 1	45 ± 1	45 ± 1	45 ± 1	45 ± 1	45 ± 1

Figure A3-1: CVN specimen drawing.

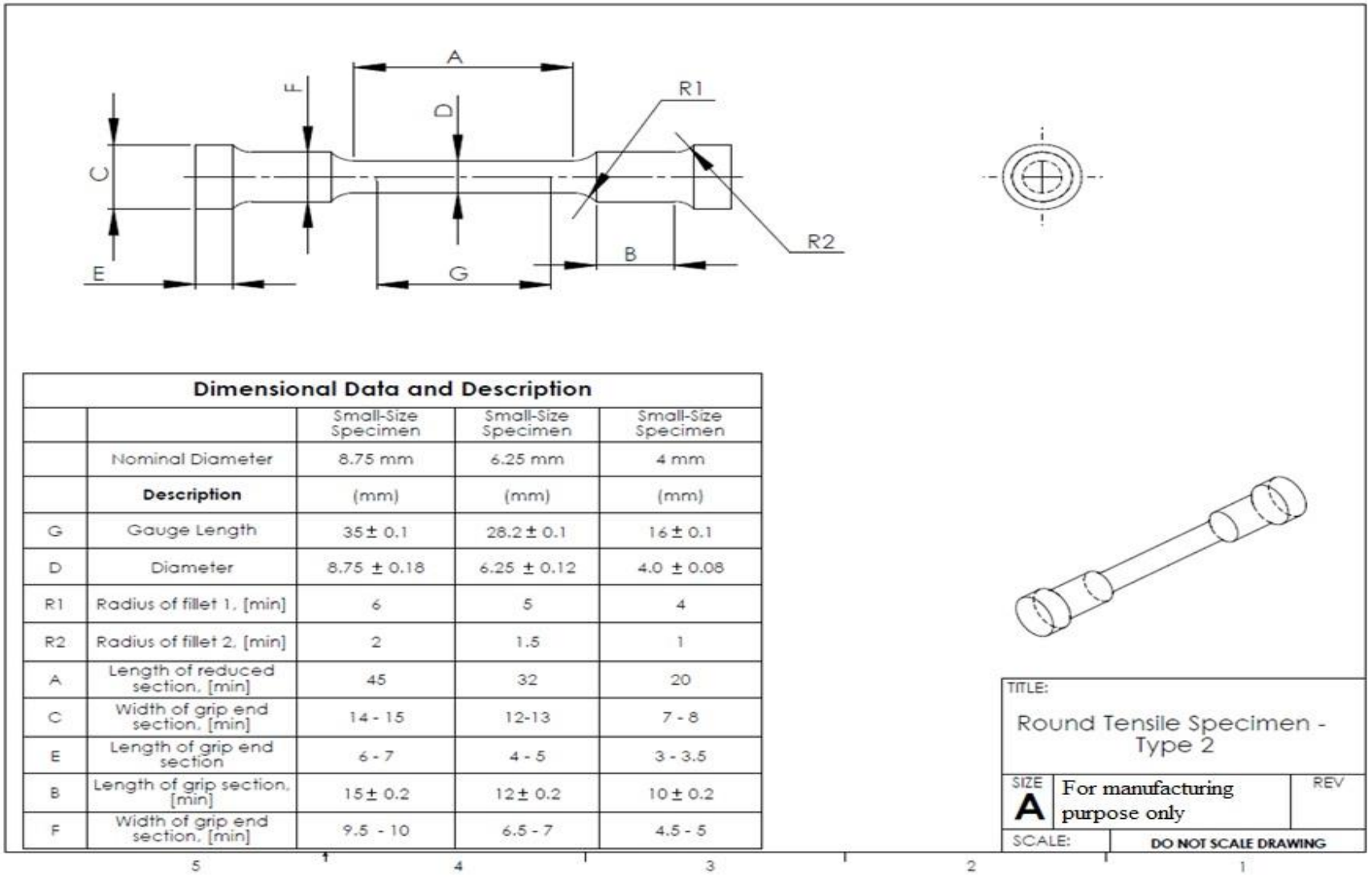

Dimensional Data and Description

		Small-Size Specimen	Small-Size Specimen	Small-Size Specimen
	Nominal Diameter	8.75 mm	6.25 mm	4 mm
	Description	(mm)	(mm)	(mm)
G	Gauge Length	35 ± 0.1	28.2 ± 0.1	16 ± 0.1
D	Diameter	8.75 ± 0.18	6.25 ± 0.12	4.0 ± 0.08
R1	Radius of fillet 1, [min]	6	5	4
R2	Radius of fillet 2, [min]	2	1.5	1
A	Length of reduced section, [min]	45	32	20
C	Width of grip end section, [min]	14 - 15	12-13	7 - 8
E	Length of grip end section	6 - 7	4 - 5	3 - 3.5
B	Length of grip section, [min]	15 ± 0.2	12 ± 0.2	10 ± 0.2
F	Width of grip end section, [min]	9.5 - 10	6.5 - 7	4.5 - 5

Figure A3-2: Normal room temperature tensile specimen drawing.

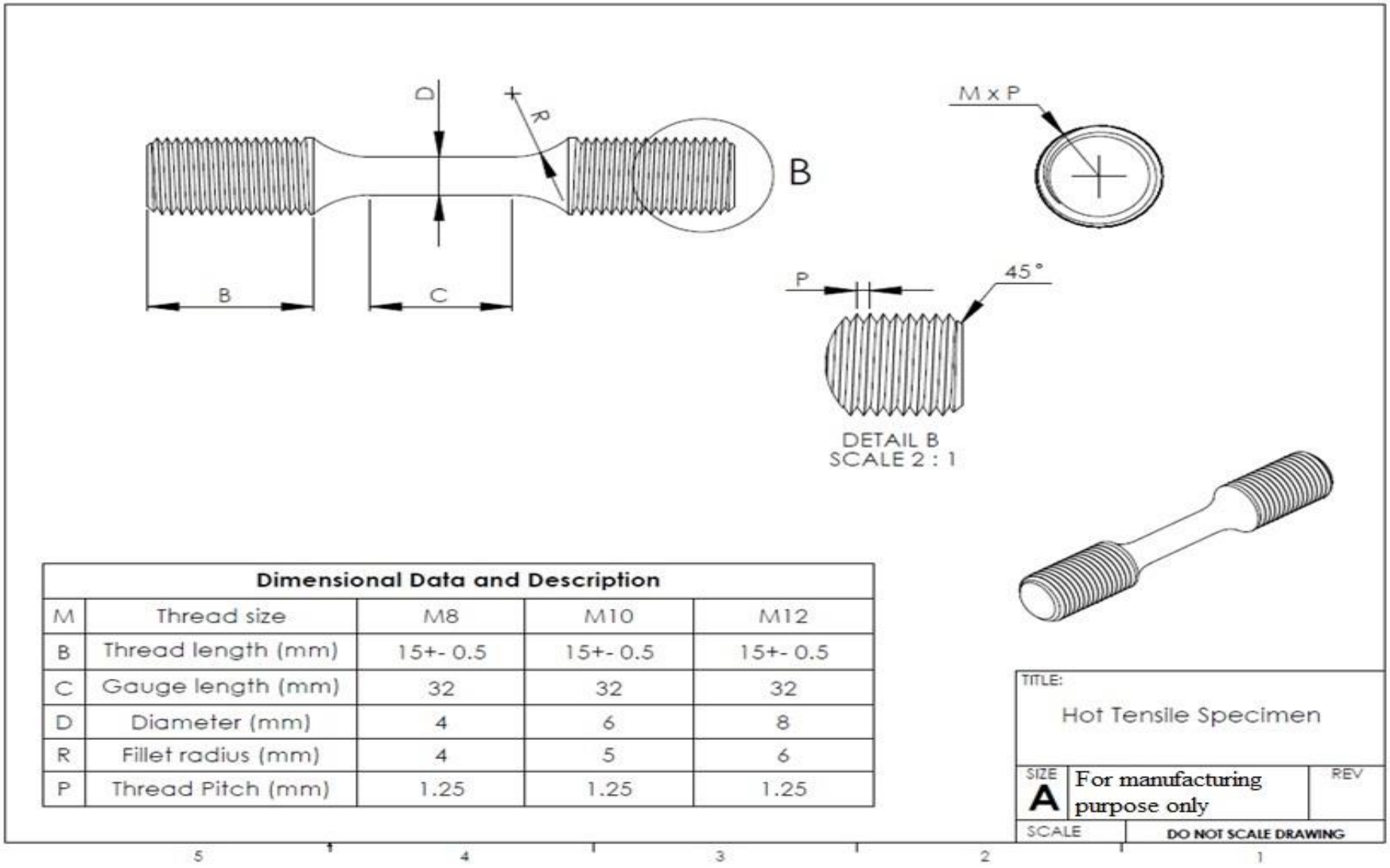

Dimensional Data and Description				
M	Thread size	M8	M10	M12
B	Thread length (mm)	15+- 0.5	15+- 0.5	15+- 0.5
C	Gauge length (mm)	32	32	32
D	Diameter (mm)	4	6	8
R	Fillet radius (mm)	4	5	6
P	Thread Pitch (mm)	1.25	1.25	1.25

Figure A3-3: Hot tensile specimen drawing.

Appendix-4 Types of power plant embrittlement

Table A4-1: Summary of embrittlement types, causes and susceptible materials [17],[38], [50]–[59],[31].

Types	Manufacturing causes	In-service causes	Materials/Components
Embrittlement due to phase change			
Graphitization of C-Mn and C-Mo steels	During welding process at HAZ at about 725°C	When operating between 427-550°C and during welding process at HAZ at about 725°C	C-Mn and C-Mo steels
Embrittlement of stainless steel			
Secondary hardening	Tempering of martensitic stainless steel at around 500°C resulting in the formation of large numbers of precipitates that reduce energy toughness	*	Martensitic stainless steel
475°C embrittlement	*	Martensitic and ferritic stainless steel embrittled with extended exposure to temperature between 400-510°C and at maximum at 475°C. The results are normally strengthening and hardening with decreasing of ductility and	Martensitic and ferritic stainless

Types		Manufacturing causes	In-service causes	Materials/Components
			toughness of these steels	
	Grain size	Grain growth on ferritic stainless steel that has no addition of second phase particles (Ti or Nb) which is normally added to this steel to limit grain growth. Coarse grains cause embrittlement by increasing FATT (result in loss of toughness) which is normally low on fine grains	*	Ferritic stainless steel
	Sigma phase	During welding process and post weld heat treatment (PWHT) on the weldments. Mostly found on austenitic stainless steel and can be found on both ferritic and martensitic stainless steel as well	Very hard (about 60 HRC), brittle and non-magnetic forms during thermal exposure between 550-900°C in austenitic stainless and nickel based super alloy	Ferritic, austenitic, martensitic and nickel based super alloys
Carbides effects				
	Carbon content	Carbon content is proportional to the fraction volume of pearlite (iron carbides or cementite (Fe_3C) and ferrite). Cementite or carbides is proportional to	*	C-steels

Types	Manufacturing causes	In-service causes	Materials/Components
	Charpy FATT and inversely proportional to impact energy		
Tempered martensite embrittlement (TME)	When martensitic steels are tempered at 200-400°C to improve toughness and ductility and maintain sufficient hardness	*	Low alloy CrMoV, martensitic steel
Thermal embrittlement	Solution treatment on maraging steels results in martensitic structure with fine precipitates (Tic and TiN), which increase tensile strength and reduce reduction area.	Carbides will grow when surface energy is reduced. Small precipitates are replaced by fewer large precipitates by diffusion. Diffusion tends to be faster in the grain boundaries than within grains which causes aging at grain boundaries (e.g. CrMo alloy steel)	Maraging steel Low alloy steel
Sensitization of austenitic steel	Alloying chemistry, heat treatment and tailoring the nature of grain boundaries can affect sensitization during austenitic steel processing	When exposed to temperatures within the range of 430-900°C, chromium carbides form at grain boundaries and deplete chromium along the grain boundary	Austenitic steel
Dissimilar metal welds	*	Carbides form at the weld interface and promote nucleation and growth of voids	Joining low alloy steel (e.g. CrMo) with austenitic stainless steel using nickel based filler

Types	Manufacturing causes	In-service causes	Materials/Components
Temper embrittlement	Occurs during slow cooling of big power plant components following tempering or PWHT. Impurities such as P, Sb, Sn and As diffuse at grain boundaries and reduce the critical flaw size	When operating low alloy, high strength alloy steel and stainless steel at a range between 345-550°C	LP rotors, generators, boiler headers, steam pipes, turbine casing, pressure vessels, turbine blades, fasteners, to HP-IP turbine rotors, alloy steels and combustion turbine disks
Environmental assisted			
Hydrogen embrittlement	Retained hydrogen during processing (melting, casting and pickling)	Inadequate control during welding (moisture, grease and other contaminants), picked hydrogen during in service of steel (may be due to corrosion in aqueous medium, excessive cathodic protection), introduced to steels during chemical milling or plating operations and present from an external molecular gas environment	Boiler evaporator tubes, 300 series austenitic stainless steel (primary system piping in nuclear power plant) depending on austenite stability, HAZ and weldments
Oxygen embrittlement	Oxygen in air is harmful and causes intermediate temperature embrittlement	Oxygen reacts with: (1) carbon to form a CO_2 gas bubble that initiates grain	Most metals such as iron, copper, nickel and nickel or cobalt based super alloy

Types	Manufacturing causes	In-service causes	Materials/Components
		boundary voids, (2) manganese sulphide to release sulphur, which results in embrittlement and (3) oxide to form fine oxide which provides sites for the nucleation of creep voids.	
Liquid embrittlement	It occurs above the melting point of alloys when stressed solid and embrittling elements have intimate contact	*	Alloy steels and weld metals
Neutron irradiation embrittlement	*	When atoms of reactor fuel split during the fission process, neutron particles are released. Neutron irradiation deteriorates material fracture toughness.	Nuclear plant critical components such as reactor pressure vessel, primary piping and valves that are exposed to neutron irradiation etc.

Appendix-5 Embrittlement management techniques

The literature review covered the techniques used to evaluate embrittlement in the power plant industry. The techniques are mechanical or metallurgical and Figure A5-1 below shows the embrittlement management options that are typically used in nuclear power plants.

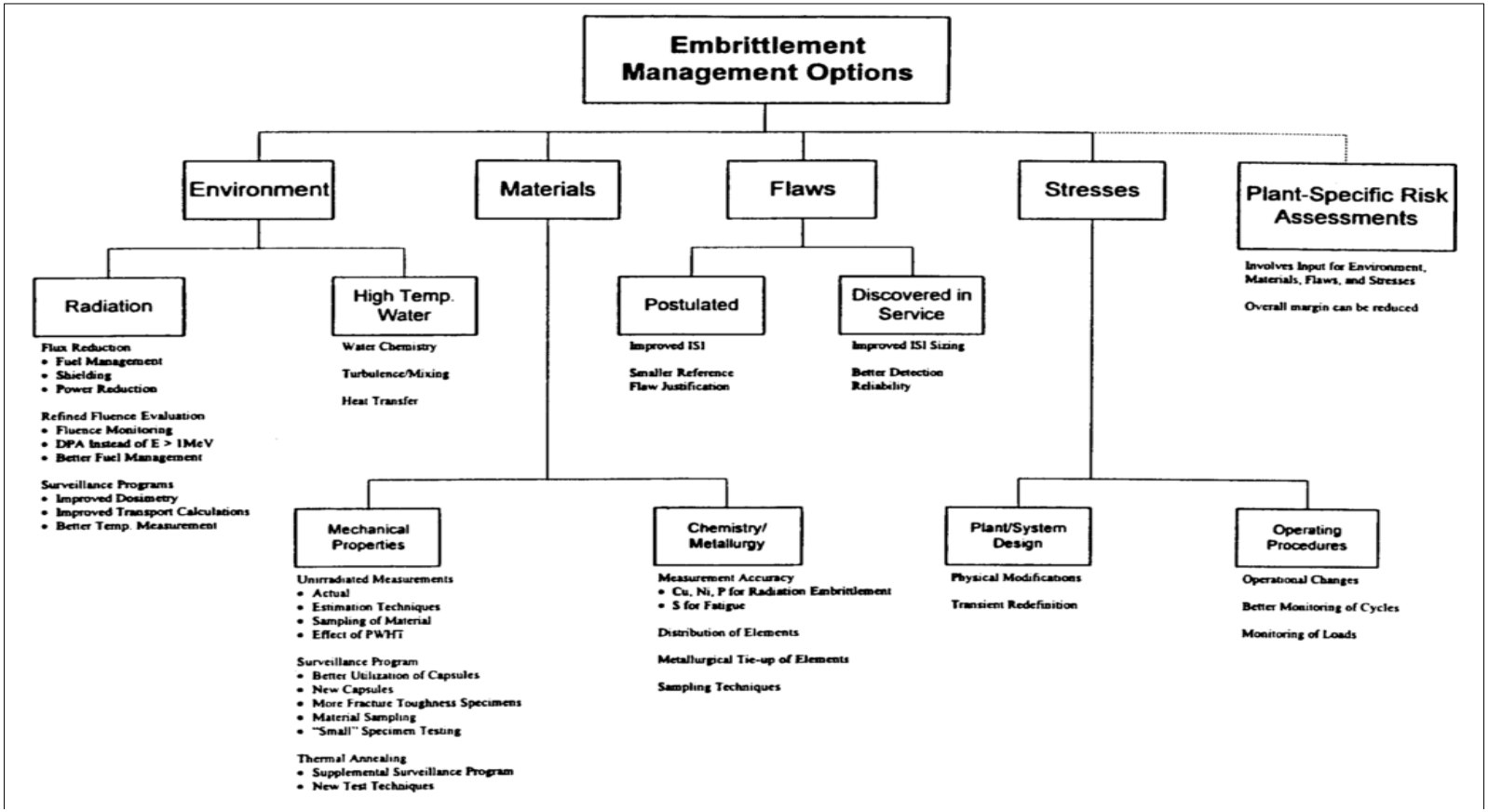

Figure A5-1: Embrittlement management option for nuclear power plant [7]

Appendix-6 Dry ice handling

Figure A5.1: Dry ice handing [60]**.**

BIBLIOGRAPHY

[1] J. R. Foulds, P. J. Woytowitz, T. K. Parnell, C. W. Jewett, and A. H. Kadarman, "Small Punch Testing for Fracture Toughness Measurement," 1995.

[2] "Embrittlement of Power Plant Steels," EPRI, Palo Alto, CA: 2013. 3002001474.

[3] "Generation plant mix." Eskom Holdings SOC Limited Integrated Report 2013, pp. 1–3, May-2014.

[4] SAPP, "SOUTHERN AFRICAN AFRICAN POWER POOL ANNUAL REPORT." 2014.

[5] "Evaluation of temper embrittlement in turbine rotor material," vol. 3, no. 3, 1991.

[6] "Small Punch Testing for Nuclear Reactor Embrittlement Assessment," EPRI; Palo Alto; CA: 1998. TR-111116.

[7] "Value of the Small Punch Test Method for Evaluating Fracture Toughness of Nuclear Pressure Vessels," EPRI, Palo Alto, CA: 1998. TR-111142.

[8] "Reactor Vessel Embrittlement Management Handbook," EPRI TR-101975-T1, Electric Power Research Institute, 1994.

[9] "Metallurgical Guidebook for Steam Turbine Rotors and Discs: Volume 1: Chemistry, Manufacturing, Service Degradation, Life Assessment, and Repair.," EPRI, Palo Alto, CA: 2009. 1017612.

[10] J. Foulds and R. Viswanathan, "Determination of the Toughness of In-Service Steam Turbine Disks Using Small Punch Testing," vol. 10, no. October, pp. 614–619, 2001.

[11] "Small Punch Testing of 3-3.5NiCrMoV Turbine Disk Steel for Toughness," EPRI, Palo Alto, CA:1999. TR-113646.

[12] T. L. Anderson, *Fracture Mechanics: Fundamentals and Applications*, Third Edit. CRC Press, 2005.

[13] W. D. Callister and D. G. Rethwisch, *MATERIAL SCIENCE AND ENGINEERING AN INTRODUCTION*, 8th ed. John Wiley & Sons, 2009.

[14] ASTM Int., "Standard Test Methods for Tension Testing of Metallic Materials 1," *Astm*, pp. 1–27, 2015.

[15] ASTM E399-09., "Standard Test Method for Linear-Elastic Plane-Strain Fracture Toughness K Ic of Metallic Materials."

[16] J. H. Allen, *Mechanics of Materials for DUMMIES*. Indiana: Wiley Publishing, Inc, 2011.

[17] ASTM E1820-01, "Measurement of Fracture Toughness 1," pp. 1–46, 2003.

[18] CEN WORKSHOP AGREEMENT, "Small Punch Test Method for Metallic Materials," CWA 15627:2007, DECEMBER 2007.

[19] "Small Punch Testing for Fracture Toughness: A Demonstration Project," EPRI, Palo Alto, CA: 2013. 3002000250.

[20] "Determination of Strength and Fracture Toughness by Small Punch Testing:

Micromechanical Approach," EPRI; Palo Alto; CA: 2011. 1023071.

[21] C. Rodríguez, E. Cárdenas, F. J. Belzunce, and C. Betegón, "Fracture Characterization of Steels by Means of the Small Punch Test," *Exp. Mech.*, vol. 53, no. 3, pp. 385–392, Jul. 2012.

[22] T. Linse, M. Kuna, J. Schuhknecht, and H. W. Viehrig, "Usage of the small-punch-test for the characterisation of reactor vessel steels in the brittle-ductile transition region," *Eng. Fract. Mech.*, vol. 75, no. 11, pp. 3520–3533, 2008.

[23] S. Rasche and M. Kuna, "Improved small punch testing and parameter identification of ductile to brittle materials," *Int. J. Press. Vessel. Pip.*, vol. 125, pp. 23–34, 2015.

[24] M. A. Contreras, C. Rodríguez, F. J. Belzunce, and C. Betegón, "Use of the small punch test to determine the ductile-to-brittle transition temperature of structural steels," *Fatigue Fract. Eng. Mater. Struct.*, vol. 31, no. 9, pp. 727–737, Oct. 2008.

[25] "Application of Small Punch Fracture Toughness of Turbine Materials," EPRI, Palo Alto, CA: 2015. 3002003324.

[26] J. Foulds, M. Wu, S. Srivastav, and C. Jewett, "Fracture and Tensile Properties of ASTM Cross-Comparison Exercise A 533B Steel by Small Punch Testing," pp. 557–574, 1998.

[27] R. Scheepers, "High Pressure Steam Turbine Discs Sampling," 2009.

[28] "A Guide to In-Service Steam Turbine-Generator Materials Evaluation by Small Punch Testing," EPRI, Palo Alto, CA: 2015. 3002007168.

[29] D. Omacht, "CRYSET: Equipment for Small Punch Testing for Tensile and Fracture Behaviour in Normal and Low Temperatures," Czech Republic, 2013.

[30] K. Turba, R. Hurst, and P. Hähner, "Evaluation of the ductile-brittle transition temperature in the NESC-I material using small punch testing," *Int. J. Press. Vessel. Pip.*, vol. 111–112, pp. 155–161, 2013.

[31] M. C. Kim, Y. J. Oh, and B. S. Lee, "Evaluation of ductile–brittle transition temperature before and after neutron irradiation for RPV steels using small punch tests," *Nucl. Eng. Des.*, vol. 235, no. 17–19, pp. 1799–1805, Aug. 2005.

[32] T. Linse, M. Kuna, and H. W. Viehrig, "Quantification of brittle-ductile failure behavior of ferritic reactor pressure vessel steels using the Small-Punch-Test and micromechanical damage models," *Mater. Sci. Eng. A*, vol. 614, pp. 136–147, 2014.

[33] K. Matocha, M. Filip, and Š. Stejskalová, "DETERMINATION OF CRITICAL TEMPERATURE OF BRITTLENESS TK0 BY SMALL PUNCH TESTS," 2012.

[34] J. R. Foulds, J. Peter, P. J. Woytowitz, T. K. Parnell, and C. W. Jewett, "Fracture Toughness by Small Punch Testing," *J. Test. Eval.*, vol. 23, no. 1, pp. 3–10, 1995.

[35] "Small Punch Fracture Toughness Evaluation of Combustion Turbine Materials," Palo Alto, CA: 2013. 3002001468.

[36] J. R. FOULDS, P. J. WOYTOWITZ, T. K. PARNELL, and C. W. JEWETT, "Fracture toughness by small punch testing," *J. Test. Eval.*, vol. 23, no. 1, pp. 3–10.

[37] ASTM E 23-12c, "Standard Test Methods for Notched Bar Impact Testing of Metallic Materials," 2013.

[38] A. Shekhter, S. Kim, D. G. Carr, A. B. L. Croker, and S. P. Ringer, “Assessment of temper embrittlement in an ex-service 1Cr-1Mo-0.25V power generating rotor by Charpy V-Notch testing, KIc fracture toughness and small punch test,” *Int. J. Press. Vessel. Pip.*, vol. 79, no. 8–10, pp. 611–615, 2002.

[39] “ABAQUS User documentation 6.14,” 2014. [Online]. Available: http://www.3ds.com/products-services/simulia/support/documentation/. [Accessed: 10-Jun-2014].

[40] J. Matlack, “Position/Presence/Proximity Modern LVDTs in New Applications in the Air, Ground, and Sea,” 2010. [Online]. Available: http://www.sensorsmag.com/sensors/position-presence-proximity/modern-lvdts-new-applications-air-ground-and-sea-7508. [Accessed: 24-Aug-2014].

[41] “Thermoelectric Handbook.” [Online]. Available: www.lairdtech.com. [Accessed: 28-Sep-2015].

[42] “NSE-5310 Miniature Position Encoder with Zero Reference and I^2C Output,” Victor, NY 14564.

[43] “USER INSTRUCTION MANUAL FOR LOADCELL TRANSMITTER MODEL TDC/I/0550 (SOFTWARE : VER2A).” [Online]. Available: http://www.loadcell.co.za/products_instrumentation.htm. [Accessed: 01-Oct-2015].

[44] “Thermocouple Data Logger.” [Online]. Available: https://www.picotech.com/data-logger/tc-08/thermocouple-data-logger. [Accessed: 03-Oct-2015].

[45] “USB TC-08 Specifications.” [Online]. Available: https://www.picotech.com/data-logger/tc-08/usb-tc-08-specifications. [Accessed: 02-Oct-2015].

[46] “User Manual: Inspection Camera with Recording LCD Monitor (Model No: 8803AL).” [Online]. Available: http://www.instruments.co.za/Borescopes.html. [Accessed: 12-Jun-2014].

[47] “LabVIEW System Design Software.” [Online]. Available: http://www.ni.com/labview/. [Accessed: 07-Aug-2015].

[48] ALSTHOM, “Koeberg Original Unit 1 LP3 QADP material certificates,” 1982.

[49] A. Saxena, J. Landes, and J. Bassani, *Nonlinear Fracture Mechanics: Elastic-plastic fracture*. 1988.

[50] J. R. Foulds, R. G. Lott, and R. Viswanathan, “SMALL PUNCH TESTING FOR IRRADIATION EMBRITTLEMENT.” 1995.

[51] P. ZAHUMENSKY and J. JANOVEC, “Some Aspects of Tempered Martensite Embrittlement in 3Cr-Mo-V,” vol. 34, pp. 536–540, 1994.

[52] P. Taylor, J. Lee, I. Kim, and A. Kimura, “Application of Small Punch Test to Evaluate Sigma- Phase Embrittlement of Pressure Vessel Cladding Material Application of Small Punch Test to Evaluate Sigma-Phase Embrittlement of Pressure Vessel Cladding Material,” no. July 2014, pp. 37–41.

[53] J. K. Sahu, U. Krupp, R. N. Ghosh, and H. Christ, “Effect of 475 ◦ C embrittlement on the mechanical properties of duplex stainless steel,” vol. 508, pp. 1–14, 2009.

[54] M. Akita, T. Kakiuchi, and Y. Uematsu, “Microstructural changes of high-chromium ferritic stainless steel subjected to cyclic loading in 475°C embrittlement region,”

Procedia Eng., vol. 10, pp. 100–105, 2011.

[55] T. Michler, C. San Marchi, J. Naumann, S. Weber, and M. Martin, "Hydrogen environment embrittlement of stable austenitic steels," *Int. J. Hydrogen Energy*, vol. 37, pp. 16231–16246, 2012.

[56] M. B. Djukic, V. S. Zeravcic, G. Bakic, a. Sedmak, and B. Rajicic, "Hydrogen Embrittlement of Low Carbon Structural Steel," *Procedia Mater. Sci.*, vol. 3, pp. 1167–1172, 2014.

[57] J. S. Cheon and I. S. Kim, "Evaluation of thermal aging embrittlement in CF8 duplex stainless steel by small punch test," *J. Nucl. Mater.*, vol. 278, no. 1, pp. 96–103, Feb. 2000.

[58] S.-H. Song, R. . Faulkner, P. E. . Flewitt, R. . Smith, and P. Marmy, "Temper embrittlement of a CrMo low-alloy steel evaluated by means of small punch testing," *Mater. Sci. Eng. A*, vol. 281, no. 1–2, pp. 75–81, Apr. 2000.

[59] M. A. Neri, R. Colás, and S. Valtierra, "Graphitization in High Carbon Commercial Steels," *J. Mater. Eng. Perform.*, vol. 7, no. February 1997, pp. 467–473, 1998.

[60] "Dry ice handling," 2016. [Online]. Available: http://www.sidewind.co.za/safety/. [Accessed: 28-Jan-2016].